DUAL-WAVELENGTH FIBER LASERS COVERING THE REGIONS OF 1.0, 1.5 AND 2.0 MICRON AND THEIR APPLICATIONS

SEYED MOHAMMAD REZA KHALIFEH SOLTANIAN

INSTITUTE OF GRADUATE STUDIES
UNIVERSITY OF MALAYA
KUALA LUMPUR

2016

DUAL-WAVELENGTH FIBER LASERS COVERING THE REGIONS OF 1.0, 1.5 AND 2.0 MICRON AND THEIR APPLICATIONS

SEYED MOHAMMAD REZA KHALIFEH SOLTANIAN

THESIS SUBMITTED IN FULFILLMENT OF THE
REQUIREMENT FOR THE DEGREE OF
DOCTOR OF PHILOSOPHY

INSTITUTE OF GRADUATE STUDIES
UNIVERSITY OF MALAYA
KUALA LUMPUR

2016

UNIVERSITI MALAYA

ORIGINAL LITERARY WORK DECLARATION

Name of Candidate: Seyed Mohammad Reza Khalifeh Soltanian

Registration/Matric No: HHE130007

Name of Degree: DOCTOR OF PHILOSOPHY

Title of Project Paper/Research Report/Dissertation/Thesis ("this Work"):

DUAL-WAVELENGTH FIBER LASERS COVERING THE REGIONS 1.0, 1.5 AND 2.0 MICRON AND THEIR APPLICATIONS

Field of Study: Photonics Engineering

I do solemnly and sincerely declare that:

(1) I am the sole author/writer of this Work;
(2) This Work is original;
(3) Any use of any work in which copyright exists was done by way of fair dealing and for permitted purposes and any excerpt or extract from, or reference to or reproduction of any copyright work has been disclosed expressly and sufficiently and the title of the Work and its authorship have been acknowledged in this Work;
(4) I do not have any actual knowledge nor do I ought reasonably to know that the making of this work constitutes an infringement of any copyright work;
(5) I hereby assign all and every rights in the copyright to this Work to the University of Malaya ("UM"), who henceforth shall be owner of the copyright in this Work and that any reproduction or use in any form or by any means whatsoever is prohibited without the written consent of UM having been first had and obtained;
(6) I am fully aware that if in the course of making this Work I have infringed any copyright whether intentionally or otherwise, I may be subject to legal action or any other action as may be determined by UM.

Candidate's Signature Date

Subscribed and solemnly declared before,

Witness's Signature Date

Name:
Designation:

ABSTRACT

This report describes the methods and processes of generating tunable dual-wavelength fiber lasers by using three different types of gain media covering three different regions of 1, 1.5 and 2 micron, and an investigation regarding their applications. The homogeneous gain media used in the 1, 1.5, and 2 micron region are ytterbium-doped fiber (YDF), erbium-doped fiber (EDF), and thulium-doped fiber (TDF) respectively.

Dual-wavelength fiber laser (DWFL) designs using a selective element, such as photonic crystal fiber (PCF), I discussed in the report in terms of their output power, side mode suppression ratio (SMSR) and tunability. Dual-wavelength fiber laser generation in three different homogeneous medium has been achieved and discussed. Strong mode competition induced by homogeneous broadening represents the main challenge for achieving stable multi-wavelength oscillation at room temperature. By controlling the spatial hole burning, spectral hole burning and polarization states of the modes in the ring laser cavity, new and novel approaches can be proposed to overcome the mode competition issue faced by homogeneous medium for generation of balanced dual-wavelength output. Moreover, modes propagation in PCF is investigated both experimentally and via modeling to attain a deep understanding about the physics behind the generation of DWFL. The modeling results of the field profiles for the fundamental quasi-TM modes are calculated with the vector beam propagation method (BPM).

The DWFLs have numerous applications in various fields including fiber sensors and communications. In this study, new designs of DWFLs for various applications are presented and demonstrated. The single longitudinal mode (SLM) properties of the generated DWFL are also investigated and demonstrated. Potential application of DWFL for terahertz rays, the generation of dual-wavelength Q-switched fiber laser, and also the generation of DWFL for microwave generation are presented. All these applications

result from the high stability and excellent quality of the fiber laser in terms of output powers and high value of SMSR.

ABSTRAK

Laporan ini menerangkan kaedah dan proses menjana harmonik laser serat dwi-panjang gelombang dengan menggunakan tiga jenis medium di tiga kawasan yang berbeza 1, 1,5 dan 2 mikron, dan kajian berhubung penggunaannya. Medium homogen digunakan dalam 1, 1.5, dan 2 mikron rantau ini adalah serat ytterbium-didopkan (YDF), erbium-didopkan serat (EDF), dan serat tulium-didopkan (TDF) masing-masing.

Dual-panjang gelombang gentian laser (DWFL) direka menggunakan elemen terpilih yang berbeza, seperti serat fotonik kristal (PCF), dibincangkan dalam laporan ini dari segi kuasa output, sebelah nisbah mereka mod penindasan (SMSR) dan harmonik . Penjanaan dwi-panjang gelombang serat laser dalam tiga medium homogen yang berbeza yang telah diperolehi dan dibincangkan. Persaingan mod kuat disebabkan oleh perluasan homogen merupakan cabaran utama untuk mencapai kestabilan pelbagai panjang gelombang ayunan pada suhu bilik. Dengan mengawal pembakaran ruang lubang, pembakaran lubang spektrum dan kutub-kutub polarisasi daripada mod dalam rongga laser cincin, pendekatan baru dan novel boleh dicadangkan untuk mengatasi isu persaingan mod yang dihadapi oleh medium homogen untuk penjanaan keluaran dwi-panjang gelombang yang seimbang. Selain itu, kaedah penyebaran dalam PCF disiasat dalam kedua-dua uji kaji dan melalui pemodelan untuk mencapai pemahaman yang mendalam tentang fizik disebalik penjanaan DWFL. Keputusan pemodelan profil medan untuk asas mod separa TM dikira dengan kaedah penyebaran sinaran vektor (BPM).

The DWFLs mempunyai pelbagai aplikasi dalam pelbagai bidang termasuk sensor gentian dan komunikasi. Dalam kajian ini, reka bentuk baru DWFLs untuk pelbagai permohonan dikemukakan dan ditunjukkan. Mod tunggal membujur (SLM) sifat-sifat yang DWFL dihasilkan juga disiasat dan ditunjukkan. Potensi penggunaan DWFL untuk sinar terahertz, penjanaan dwi-panjang gelombang Q-switched serat laser,

dan juga penjanaan DWFL untuk penjanaan gelombang mikro dibentangkan. Semua aplikasi ini disebabkan oleh kestabilan yang tinggi dan kualiti yang sangat baik daripada laser gentian dari segi kuasa output dan nilai tinggi SMSR.

ACKNOWLEDGEMENTS

First of all, I would like to express my appreciation to my supervisors, Prof. Datuk Dr. Harith Ahmad and Prof. Dr. Sulaiman Wadi Harun for the continuous support, motivation, patience and knowledge throughout my Ph.D. study. Their guidance helped me in all times of research and thesis writing.

My sincere gratitude also goes to Dr. Chong Wu Yi, Dr. Rozalina Zakaria, Dr. Mohd Zamani Zulkifli and Dr. Lim Kok Sing for their help and knowledge sharing. You all brought so many ideas to the lab despite the ups and downs that we encountered during our research.

To my wife, Leila, parents and sibling, thank you for your encouragement and support. Again, thank you to everyone who had helped me directly or indirectly with my research.

TABLE OF CONTENTS

CHAPTER 1: INTRODUCTION

CHAPTER 2: A REVIEW ON FIBER LASER PHOTONICS AND THEORETICAL BACKGROUND

CHAPTER 5: APPLICATIONS OF DUAL-WAVELENGTH FIBER LASERS

CHAPTER 6: CONCLUSION AND FUTURE OUTLOOK

LIST OF FIGURES

LIST OF TABLES

LIST OF SYMBOLS AND ABBREVIATIONS

A_{eff}	Effective area
L_{eff}	Effective length
B_2	Group velocity dispersion parameter
I	Light intensity
α	Nonlinear coefficient
n_2	Nonlinear refractive index
P_{th}	Threshold power
T	Transmittivity of light
λ	Wavelength
AC	Auto-correlator
AWG	Array Waveguide
ASE	Amplified Spontaneous Emission
Bi-EDF	Bismuth-Erbium Doped Fiber
BFA	Brillouin Fiber Laser
CW	Continuous Wave
DCF	Dispersion Compensation Fiber
DFB	Distributed Feedback
DSF	Dispersion Shifted Fiber
DWDM	Dense Wavelength Division Multiplexing
DWFL	Dual Wavelength Fiber Laser
EDF	Erbium Doped Fiber
EDFL	Erbium Doped Fiber Laser
EDFA	Erbium Doped Fiber Amplifier
FBG	Fiber Brag Grating
FWHM	Full Width Half Maximum

FWM	Four-Wave Mixing
GO	Graphene Oxide
GVD	Group Velocity Dispersion
HNLF	Highly Nonlinear Fiber
MCVD	Modified Chemical Vapor Deposition
MPE	Maximum Phonon Energy
NA	Numerical Aperture
NRP	Nonlinear Polarization Rotation
NALM	Nonlinear Amplifying Loop Mirror
NOLM	Nonlinear Optical Loop Mirror
OAN	Optical Access Network
OCS	Oscilloscope
OLT	Optical Line Terminal
OPO	Optical Parametric Oscillator
OSA	Optical Spectrum Analyzer
OSC	Oscilloscope
OSNR	Optical Signal to Noise Ratio
OTDM	Optical Time Division Multiplexing
PC	Polarization Controller
PCF	Photonic Crystal Fiber
PHB	Polarization Hole Burning
RFSA	Radio Frequency Spectrum Analyzer
SA	Saturable Absorber
SCPCF	Solid-Core Photonic Crystal Fiber
SLM	Single Longitudinal Mode
SMF	Single Mode Fiber

SNR	Signal to Noise Ratio
SOA	Semiconductor Optical Amplifier
SPM	Self-Phase Modulation
TBF	Tunable Bandpass Filter
TDF	Thulium Doped Fiber
TDFL	Thulium Doped Fiber Laser
TDM	Time Division Multiplexing
WAN	Wireless Access Network
WDM	Wavelength Division Multiplexing
YDF	Ytterbium Doped Fiber
XPM	Cross Phase Modulation

CHAPTER 1: INTRODUCTION

1.1 Fiber Lasers

Development of fiber optic technology was initiated with the invention of the laser in the 1960s. Copper is acknowledged as the most suitable medium for guiding electrons, and analogously optical fiber became recognized as the optimal medium for guiding light. Transmission of light within optical fibers is based on the principle of total internal reflection, which occurs under conditions of the refractive index of the fiber core being slightly higher than that of the cladding. Fiber lasers are constructed with a gain medium of optical fiber doped with rare-earth elements such as ytterbium, erbium, thulium and neodymium, and these lasers have inherent advantages over traditional solid-state lasers. One major advantage of fiber lasers lies in the flexible structure of the constituent optical fiber, which allows the laser to be directed easily to a focusing element with consequent significance for laser welding, laser cutting, and folding of metals and polymers. Optical fibers achieve higher optical quality and reliability than solid-state lasers while providing a far more compact physical size. In general, there are four different modes of laser operation: continuous wave, Q-switching, mode locking, and Q-switched mode-locking. High energy pulsed lasing can be achieved by Q-switching, and finds important applications in the fields of laser processing, medicine, environmental sensing, range finding, telecommunications, reflectometry, remote sensing and material processing. Mode locking techniques are primarily applied for generation of very short duration pulses, and particularly pulses with pulse width within the picosecond and femtosecond regions. Generation of such pulses is significant for various fields, including telecommunications, range finding, biomedical research, manufacturing, and material processing. Single-frequency operation on the other hand is important for coherent beam combining of laser outputs, nonlinear frequency conversion and many other applications such as high-resolution spectroscopy, interferometry, optical fiber communications, optical data storage, optical sensors, temperature measurement, atmospheric pollution monitoring, wind speed measurements via Doppler LIDAR, optical metrology, and applications requiring a very low intensity noise.

All laser operation modes described above can be achieved by employing appropriate saturable absorbers in the fiber laser cavity, whereby the laser cavity design and the saturable absorption properties of the saturable absorber are primarily taken into account. However, it must be noted that the saturable absorbers work in a different way for either the pulse or the SLM generation; a saturable absorber operates in time domain for pulse generation and frequency domain for SLM generation.

Unlike most other types of lasers, the laser cavity in fiber lasers is constructed monolithically by fusion splicing different types of fiber; fiber Bragg gratings replace conventional dielectric mirrors to provide optical feedback. Another type is the single longitudinal mode operation of ultra-narrow distributed feedback lasers (DFB) where a phase-shifted Bragg grating overlaps the gain medium. Fiber lasers are pumped by semiconductor laser diodes or by other fiber lasers. Q-switched pulsed fiber lasers offer a compact, electrically efficient alternative to Nd:YAG technology (Hecht, 2015).

1.2 Optical Fiber Technology in Telecommunication System

Telecommunication is actually a term coming from two words, which are ‘tele’ and ‘communis’. The word ‘tele’ comes from French’s word meaning at distance, while ‘communis’ comes from Latin’s word, meaning to share. In physical practice, the word telecommunication is simply an activity of delivering information over significant distance through electromagnetic means.

During the old times, smoke signals, Chappe telegraphs, signal flags and beacons were involved in the old long distance optical communications. During the time, the Ancient China's soldiers (Tang Dynasty Era during year 620s) were enforced to keep alert of the smoke signal, from tower to tower to get the information of any enemy attack. The smoke signal had to be lit to inform any security information at any particular tower. By doing so, no tower could be detained by the enemy without being realized by the other towers. One more example is the 'optical telegraph' invented by Claude Chappe in 1790s. The design was called as Chappe telegraphs with semaphores mounted on towers, to give information to the next tower and operated by human's power.

In 1880, the first optical wireless telephone system known as Photophone had been introduced and patented by Alexander Graham Bell (MIMS III, 1980). However, the information technology by using a modulated light for conversation was seemed to be not so practical to be applied for practical purposes as the transmission of his design could be easily interfered by clouds, fog, rain and snow. The idea of light guided by glass is actually arose in 1840s, when Daniel Colladon and Jacques Baabinet were first demonstrating the total internal reflection of light in jet of water. It seemed like the light was trapped in it, as long as the reflection of light was not overpass its critical angle. The idea was further improved by John Baird and Clarence Hansell in 1920s by demonstrating the light guided by transparent rod for facsimile systems.

The optical fiber technology was making a huge progress when the lamps were invented. This is possible since the light can be switched on and off in a very fast duration, thus can be used as a blinker light to pave the way for optical fiber technology growth. A major breakthrough of the technology undeniably was led by the invention of laser in the 1960s, which had triggered numerous developments in the field of optical fiber communication systems. Despite its initial high value of 20 dB/km (Kao & Hockham, 1966), fiber losses in the long run dropped to less than 0.2 dB/km (Kato, Hirano, Onishi,

& Nishimura, 1999). This was caused by the rapid development in fiber fabrication technology in the 1970s.

In the late 1970s, single mode fiber (SMF) operated at the wavelength of 800nm was commercially available for long distance applications with the signal coming from gallium aluminum-arsenide laser diodes. It was called the first window for optical fiber communication. For the second window, the information spacing was increased significantly by shifting the operating wavelength to 1300 nm region which was called the O-band region. It offers a lower loss of less than 1 dB/km and a minimum dispersion which is good for modulated signal. The optical fiber in the third window system operated at 1550 nm region and can be called as C-band region. In this region, the signal experienced even lower loss of less than 0.2 dB/km (Miya, Terunuma, Hosaka, & Miyashita, 1979; Murata & Inagaki, 1981).

1.3 DWDM Communication Systems

Single-longitudinal mode lasers operating in C-band region was successfully designed in 1990 to cope with the increasing demand of capacity bared by the communication systems. However, the signal has to be amplified in order to preserve the data transfer after a few kilometres (typically around 60 km) of its propagation along the fiber. In the earlier stage, the repeater was used to regenerate the signal. The process of converting the data from optical to electrical has to be done. Then, it will be amplified electrically before being converted back to the optical signal. It is a process of optical-electrical-optical conversion, which becomes a tedious effort to work with.

The invention of optical amplifiers helped in significant growth of the optical fiber technology in subsequent years. The optical amplification process is possible during these years by virtue of erbium doped fiber amplifiers (EDFAs) with the optical amplification naturally in 1550 nm region. This allows the transmission of signal without being converted to the electrical signals. The data rates were around 2.5 Gbit/s. The rapid growth of the technology, subsequently, increased the bandwidth demand, thus introducing the wavelength division multiplexing (WDM) technology. The WDM technology clearly increases the information carrying capacity of a single fiber. The time domain multiplexing (TDM) system was also introduced to enhance the bit rate of the existing channels with the data rates of 10 Gbit/s. The TDM system however has a dispersion problem when it comes to the higher bit rate transfer (Agrawal, 2012; Inoue, Nakanishi, Oda, & Toba, 1994; Kawanishi et al., 1996) and makes it less preferred. The optical time domain multiplexing (OTDM) system was then introduced to improve the previous TDM system. The bits rates transfer from 80 Gbit/s to 320 Gbit/s have been reported during that time (Kaman & Bowers, 2000; Marcenac, Ellis, & Moodie, 1998; Moodie et al., 1995; Raybon et al., 2000; Toliver, Deng, Glesk, & Prucnal, 1999). A transmission as fast as 640 Gbit/s was then reported by Nakazawa in 1998 (Nakazawa, Yoshida, Yamamoto, Yamada, & Sahara, 1998).

To cope with the wavelength demand as the channel for transmitting data, the dense wavelength division multiplexing (DWDM) was then introduced. The improvement was necessary to transmit large number of relatively closely spaced channels along an optical fiber. Instead of 8 Channels provided by the conventional WDM systems, the DWDM system would typically provide 40 channels with 100 GHz spacing, or 80 channels of 50 GHz spacing. The WDM and DWDM are however working with the same principle by having a combination of multiple signal wavelengths, only in a single optical fiber. The only difference is their inter channel spacing, number of channels involved and the ability to do the optical amplification with combination of many channels.

1.4 Single Wavelength Fiber Lasers

Single wavelength fiber lasers have become more attractive nowadays, after the first invention of a fiber laser at 1060 nm by Elias Snitzer (Snitzer, 1961) in 1961 by using a flash lamp as a laser pump source. The invention influenced the world in profound ways due to its contribution especially in the field of material processing (Steen, Watkins, & Mazumder, 2010), spectroscopy (Ito et al., 1996; Sanders, 2002), LIDAR (Koroshetz, 2005), telecommunications including internet (Kaminow, Li, & Willner, 2010), interferometry, medical imaging technology (Oraevsky, Jacques, & Esenaliev, 1998; Tearney et al., 2000) and high power illuminator for directed energy weapon system (Perram, Marciniak, & Goda, 2004). These various applications are possible by virtue of the fiber-based laser itself, which gives many advantages as compared to the other type of lasers. They include fiber compatibility, low intensity noise, high output power, its compactness, high optical quality and narrow linewidth. Since the growth of optical fiber technology, there have been a lot of studies in many aspects to make use of it. Despite extensive studies on its applications, studies on improving the signal quality guided by the fiberglass material are also involved. In achieving this aim, a few gain media have been identified that can be used as the optical amplifier for amplification in the optical telecommunication systems. They include erbium doped fiber amplifier (EDFA) and neodymium doped fiber amplifier (NDFA) for amplification in 1550 nm and 1060 nm respectively which was later found to be really useful in generating single wavelength fiber laser. This fiber compatibility is important, as the light is already being coupled to the fiber and can provide the best quality of single wavelength fiber laser outputs.

Without any external coupling from the bulk laser, the fiber laser system emits low intensity noise, giving a high quality beam which is really useful for sensing purposes. The single wavelength fiber laser also can generate high output power. This can be done by using a long length of gain medium (as long as several kilometres) to achieve a high optical gain. This is useful for the high power applications including cutting and welding technology. The size is not a problem since the fiber can be spooled to a compact size, and therefore they are much smaller as compared to the other type of lasers such as solid state lasers, dye lasers and gas lasers.

The single wavelength fiber laser also emits a narrow line-width output which is comparable to the other type of lasers such as semiconductor lasers. This is due to the fact that single wavelength fiber lasers emit low phase noise and high spectral purity. A narrow linewidth laser is important in order to get a highly coherent output that can be used as sensors for long distance applications (Geng, Spiegelberg, & Jiang, 2005; Smith, Zarinetchi, & Ezekiel, 1991).

A lot of devices were proposed and experimented in order to generate single wavelength fiber laser. These were fiber Bragg grating (FBG) (Kashyap, 1999), tunable bandpass filter (TBF) and arrayed waveguide grating (AWG) as the wavelength selective element. The generation of single wavelength fiber laser can be done typically by using a linear cavity and ring cavity configurations. A more attractive criterion that comes from the fiber based is that the single wavelength fiber laser can be tuned or switched into a few other wavelength options. By using the TBF, the wavelength selection can be done within the operating wavelength of the TBF. On the other hand the FBG can be compressed, stretched or cascaded together for variety wavelength options. The AWG on the other hand, can be made switchable by connecting it to the optical channel selector (OCS).

1.5 Dual-Wavelength Fiber Lasers

Multi-wavelength fiber lasers and Dual-Wavelength Fiber Lasers (DWFLs) are well known to be useful for applications such as in the field of optical fiber sensors (Bolognini, Soto, & Pasquale, 2009; Y.-G. Han, Tran, Kim, & Lee, 2005; P.-C. Peng, Tseng, & Chi, 2004; Talaverano, Abad, Jarabo, & Lopez-Amo, 2001) which can be used for long haul sensing system and also for optical spectroscopy (Marshall, Stewart, & Whitenett, 2006). The sensing system is actually done by taking a wavelength as a reference and another signal which has almost the same wavelength is used as the sensor indicator for any slight changes which gives a shifting effect to the second wavelength of the fiber laser output. Most of the experiments are done by using FBGs as the wavelength selective elements. The optical spectroscopy application on the other hand, uses the multi-wavelength fiber laser or DWFL for observing the wavelength absorption in order to determine the atom identity. This is due to the fact that the wavelength of light is being absorbed is related to the specific energy transition by a specific atom.

Other applications are for microwaves photonics systems (Capmany et al., 2005; M. Soltanian, Ahmad, Pua, & Harun, 2014; Jie Sun, Dai, Chen, Zhang, & Xie, 2006; Yao, Chen, Dai, & Xie, 2006) and optical wavelength division multiplexing systems (WDM) (X. Feng, Li, et al., 2011; J. Pan, 1993). The microwave generation is basically using the dual-wavelength beating technique in order to generate the microwave signals. The technique is easy to setup and can be easily sensed by using a photo-detector. The technique also becomes useful due to its advantage of noise reduction in the system. The DWFL and multi-wavelength fiber laser, on the other hand, can act as the selectable wavelength laser source in the WDM systems which made them useful for these applications. Other useful applications are for optical component testing, optics instrumentation and characterization of photonics component such as for chromatic dispersion measurement (Maran, Slavík, LaRochelle, & Karásek, 2004). However the technology nowadays move forward to the generation of dual-wavelength fiber lasers (DWFLs) since DWFLs are attractive for advance applications that need only two synchronize wavelengths for many applications. Despite the usefulness of the multi-wavelength fiber laser, the DWFLs are more attractive due to their potential to work as a high precision strain and temperature sensors, for wavelength conversion application (Qureshi et al., 2007; Uchida, Takeoka, Nakata, & Kannari, 1998) to convert the signal from one communication band to another without using any active devices to make an optical- electrical-optical conversion thus can be effectively used to fulfil the communication demand with a low cost borne by the network providers, and also for terahertz generation (Alouini, Brunel, Bretenaker, Vallet, & Le Floch, 1998; Jeon, Kim, et al., 2010b; M. R. K. Soltanian, Amiri, Alavi, & Ahmad, 2015) signal that is quite notable in the new industrial process quality controls and for security monitoring applications. These three applications however need many efforts in order to generate the single longitudinal mode (SLM) DWFLs that exhibit a high spectral purity.

A lot of methods have been used to generate the multi-wavelength fiber lasers and DWFLs. The gain media typically used in order to generate DWFLs in C-band region for telecommunication window are erbium doped fiber amplifiers (EDFAs). However, the generation of DWFL is quite cumbersome for the researchers to mull over. This is due to the mode competition caused by the cross-gain saturation and strong homogeneous line broadening faced by the homogeneous gain media such as ytterbium doped fibers (YDFs), erbium doped fibers (EDFs) and thulium doped fibers (TDFs). Various means have been utilized to generate DWFL such as by cooling the EDF with liquid nitrogen (N. Park & Wysocki, 1996; Shinji Yamashita & Hotate, 1996) and by using an elliptical EDF (Das & Lit, 2002). For the first method, the EDF is cooled to 77 K by using liquid nitrogen to reduce its homogeneous line-width, as narrow as 1 nm. Thus a stable multi-wavelength fiber laser can be easily generated. On the other hand, the elliptical EDF helps in generating multi-wavelength fiber lasers and DWFLs by using the principle of anisotropic gain behavior of the elliptical core EDF. This is done by having the same output lasing threshold of the multi-wavelength lasers, by adjusting the polarization controller (PC) to control the polarization state of the pump along the cavity axis. This subsequently generates a stable multi-wavelength fiber laser source. Another method is by using a polarization maintaining FBG (PMFBG) for wavelength selection (S. Feng, Xu, Lu, Ning, & Jian, 2009) and a frequency shifter in the cavity (Bellemare, Rochette, & LaRochelle, 2000). In the paper, the DWFL is easily generated by using the PMFBG due to the polarization hole burning enhancement. This is an important effect since it is helping in increasing the inhomogeneous broadening effects thus providing a stable dual-wavelength oscillation in the cavity design. The technique also uses the PC to control the polarization state in the cavity, thus helps to balance the lasing of the DWFL. For the latter case, a frequency shifter is inserted in the cavity to prevent only a single frequency oscillation which is caused by a single steady state lasing in order to generate a stable DWFL. The other alternative ways are by using DFB fiber laser source with a separate resonance cavity (Jie Sun et al., 2006) and four wave mixing effect (FWM) as a stabilizer (Mable P Fok & Chester Shu, 2007). The first method succeeded in generating the DWFL by the virtue of the spatially separated of two lasing wavelength and avoiding the mode competition to occur in the cavity. While the latter is using a highly nonlinear bismuth-oxide fiber to generate the FWM effect which shows a significant stability improvement compare to the cavity without the highly nonlinear fiber. The other methods are by using the optical injection Fabry-Perot laser (C.-H. Yeh et al., 2009) and by using dual-ring fiber laser (Yeh, Shih, Chen, Lee, & Chi, 2007). For the second method, the cavity is controlled separately by using two different PCs to achieve a stable DWFL. Generation of DWFLs also has been reported by using semiconductor optical amplifiers (SOAs) as another type of gain medium (X. Chen, Deng, & Yao, 2006; Tanaka, Inamoto, Yokosuka, Somatomo, & Takahashi, 2007). However, SOAs does not provide the best solution in terms of lower output power and higher noise compared to using EDFs.

1.6 Objectives

The aim of the research presented in this thesis has been planned thoroughly and highlighted. The research work focus on the unsolved problem faced by the current device in the optical communication systems, subsequently to improve the weakness of the current design.

1.6.1 The Generation of Tunable Dual-Wavelength Fiber Lasers

The first motivation of the thesis is to design the tunable dual-wavelength fiber lasers. It is known that the YDF, EDF and TDF are good amplifier in the 1, 1.5 and 2 micron regions respectively. However, they have their own limitation of difficulty to provide dual-wavelength or multi-wavelength output due to the close to homogeneous broadening effects of the gain medium. A novel approach of using short length photonic crystal fiber (PCF) as the wavelength selective element, with a cavity loss control method has been designed and reported by our group. The design is effective to overcome the limitation of mode competition inherited in the homogeneous media to provide a balanced dual-wavelength output power source. Some other few designs are also proposed by using the same technique but using different wavelength selective elements.

1.6.2 Applications of Dual-Wavelength Fiber Lasers

The second objective is the main objective to see the significance of the new DWFL designs. This is done by proposing a few new applications that can be provided by the design invented. It has been proven by the research study that the DWFLs have a lot of functions and all of them are presented in Chapter 4 and 5 including for DWFL Q-switching, microwaves generation for future optical to microwaves communication systems and single longitudinal mode DWFL for possible application in Terahertz generation.

1.7 Thesis Overview

There are six chapters in the thesis. Chapter 1 revolves around a brief understanding of optical fiber technology and its relation with the telecommunication system. Chapter 2 on the other hand, provides the theoretical background for the generation of fiber laser. It also provides the basic equations for spontaneous and stimulated emission from basic atomic rate equations for three different gain media which are YDF, EDF and TDF. The explanation is then followed by the difference of broadening effect between both of them. A brief explanation on the PCF and its characteristics especially the PCF used in this thesis is also investigated and discussed in this chapter.

Chapter 3 demonstrates the generation of tunable DWFL. PCF as a wavelength selective element used comprises of a tunable band-pass filter (TBF), fiber Bragg gratings (FBGs) with add/drop micro-ring resonator. The working principle of generating DWFL in three different media is discussed in this chapter. The demonstration of the fiber laser generation is done by using a closely to homogeneous broadening of the YDF, EDF and TDF as the gain media. The stability of output power and difference of SMSR for each design is then being discussed in this chapter. Moreover, generating dual-wavelength coherent source from mode-locked laser is also explained.

The experimental setup, procedures, experimental results taken, and data analyses for generation of Q-switched DWFL are covered in Chapter 4. There are several material such as graphene, graphene oxide, Bismuth telluride (Bi_2Te_3) and Selenium Bismuth (Bi_2Se_3) used in this work as the saturable absorber for Q-switching operation in various setup configurations. An analytical comparison is undertaken on the Q-switching output performance using the different wavelength selective elements. Furthermore, a Q-switched EDFL based on graphene oxide as the saturable absorber embedded into PCF with capillary effect is also introduced and presented in this chapter.

Chapter 5 presents research work on application of the DWFL by the virtue of new findings that have been explained in Chapter 3 and 4. A few applications demonstrated in this research are considered as new and novel, since it is invented by using some new designs of the DWFL. A few new applications presented in this chapter are tunable dual-wavelength single longitudinal mode fiber laser, and also the DWFL for the generation of tunable microwaves signals for the next generation of wireless and all-optical communication system and DWFL for generation of terahertz radiation.

Finally, Chapter 6 concludes the thesis with a summary of the main contributions from the research work. Recommendations for future works in the field are also discussed as the extension of the works done in this research.

CHAPTER 2: A REVIEW ON FIBER LASER PHOTONICS AND THEORETICAL BACKGROUND

2.1 Introduction

This chapter begins with a brief overview of the historical and theoretical background on ytterbium doped fiber (YDF), erbium doped fiber (EDF) and thulium doped fiber (TDF) as the gain medium used in this work. The theoretical part includes the basic equations for spontaneous and stimulated emission and will cover the basic atomic rate equation of YDF, EDF and TDF as an important aspect of optical amplification in laser generation. Experimental analysis of gain measurement for EDF is also presented in this chapter. The basic processes of the optical amplifiers and fiber laser are therefore discussed in this chapter. Subsequently, laser transition processes in a fiber gain media, specifically in erbium doped fibers (EDFs) are discussed in this chapter. This is followed by a discussion on the broadening effect on the homogeneous and inhomogeneous media. The chapter will be end up by explanation and discussion on PCF used in this work. Modes propagation inside the PCF is explained and discussed both experimentally and theoretically.

2.2 Interaction of photons with atoms

Optical amplification comprises of three basic processes, optical absorption, spontaneous emission, and stimulated emission processes. These three processes are elaborated in this section.

I. Optical Absorption: Consider a case where an atom is in its steady state condition and suddenly a photon is passing by. If the photon energy coincides with one particular band-gap energy of the atom, the photon may get ‘absorbed’ by the atom. This causes the energy of the atom to increase, as the atom is excited to an upper energy level. This photon-induced process is called ‘optical absorption’.

II. Spontaneous Emission: This is a term to describe the process when the randomly excited atom from the upper state returns spontaneously to its ground state level without any given signal as the trigger, and thereby releasing energy in the form of photon. This is as shown in Figure 2.1(a). This is why it is called spontaneous emission, as the atom will decay ‘spontaneously’ to its initial state. However, since the de-excitation happens spontaneously, the photons travel in all direction with slightly different frequencies, leading to a variety of wavelength emissions in addition to contributing to noise. This signal is known as amplified spontaneous emission (ASE) and will be discussed in the following chapters.

III. Stimulated Emission: Stimulated emission is important in order to achieve optical amplification to form a laser system, which is characterized by a property called ‘coherence’, meaning that the output optical signal has the same frequency, wavelength and energy. To achieve this, an atom must be excited to a higher energy level denoted as E_2 from its ground level denote as E_1 by supplying energy in form of light such as with arc lamps, flash lamps or semiconductor laser diodes. In this condition, the excited atoms are not stable and prefer to occupy the ground state level which a much in stable state. Suppose an external photon with energy equal to the energy difference of the excited state and ground state level was introduced in the system, the excited electron in E_2 tends to de-excite, and the relaxation process causes a release of a photon with the same energy, frequency and direction to the incoming photon. This is what we call as stimulated emission and can be illustrated in Figure 2.1(b). This process is crucial for signal amplification in C-band optical communication systems.

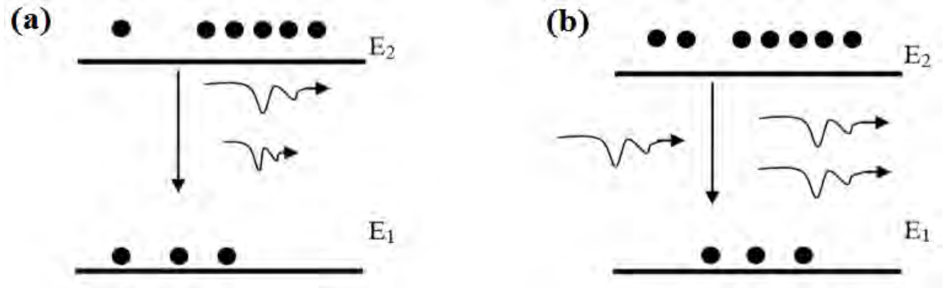

Figure 2.1: The processes of (a) spontaneous emission and (b) stimulated emission.

2.3 Types of Gain Media

There are several types of gain media used for optical amplification for realizing fiber lasers, such as YDF, EDF, TDF, semiconductor optical amplifier (SOA), Brillouin fiber amplifier (BFA) and Raman fiber amplifier (RFA). For our purposes, we focused on the study of only YDF, EDF and TDF amplifiers, as these three provides different region of lasing in generating fiber lasers as will be discussed later in this chapter.

2.3.1 Ytterbium doped fiber

Ytterbium (Yb) is a chemical element belonging to the group of rare earth metals. In laser technology, it has acquired a prominent role in the form of the trivalent ion Yb^{3+}, which is used as a laser-active dopant in a variety of host materials, including both crystals and glasses. It is often used for high-power lasers and for wavelength-tunable solid-state lasers (Hanna et al., 1988; Rüdiger Paschotta, Nilsson, Tropper, & Hanna, 1997).

2.3.1.1 Special Properties of Ytterbium-doped Gain Media

Ytterbium-doped laser crystals and glasses have a number of interesting properties, which differ from those of, e.g., neodymium-doped gain media:

- They have a very simple electronic level structure, with only one excited state manifold ($^2F_{5/2}$) within reach from the ground-state manifold ($^2F_{7/2}$) with near-infrared or visible photons. Pumping and amplification involve transitions between different sublevels of the ground-state and excited-state manifolds (see Figure 2.2) (G. Liu & Jacquier, 2006).

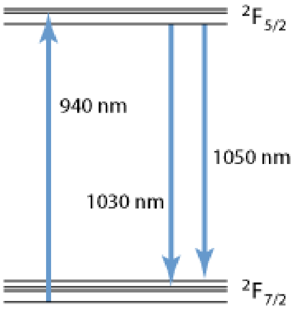

Figure 2.2: Energy levels of Yb^{3+} ions in Yb:YAG, and the usual pump and laser transitions.

- The quantum defect is always small, potentially allowing for very high power efficiencies of lasers and reducing thermal effects in high-power lasers. However, complications can arise from the pronounced quasi-three-level behavior (see section 2.2.2).
- The simple electronic structure excludes excited-state absorption and also a variety of detrimental quenching processes.
- The gain bandwidth of the laser transitions is typically fairly large, compared with, e.g., neodymium-doped crystals. This allows for wide wavelength tuning ranges or for generating ultra short pulses in mode-locked lasers.
- The upper-state lifetimes are relatively long (typically of the order of 1–2 ms), which is beneficial for Q switching.

2.3.1.2 The quasi-three level energy system

The small quantum defect also has a usually unwanted consequence: the significant quasi-three-level behavior, particularly at short wavelengths. This requires such lasers to be operated with relatively high pump intensities and makes it more difficult to realize fully the potential for high power efficiency. Another difficulty arises for the resonator designs of end-pumped ytterbium lasers: a resonator mirror for injecting the pump light must have a high reflectivity at the laser wavelength and a high transmission at the only slightly shorter pump wavelength. Dichroic mirrors with such properties for closely lying wavelengths are difficult to make (Maddaloni, Bellini, & De Natale, 2013). Figure 2.3 shows the ytterbium transition cross sections of a germane silicate glass. Efficient pumping is possible around a wavelength of 910 nm or near 975 nm. In the latter case, the pump line-width must be small, and only ≈ 50% excitation level can be achieved due to stimulated emission, but the absorption length and the quantum defect are smaller than for 910-nm pumping. Strong three-level behavior occurs for lasing around 1030 nm, whereas nearly four-level behavior is observed beyond 1080 nm, where there is very little re-absorption. For ytterbium-doped crystals (e.g. Yb:YAG), there is often a choice between different lasing transitions, where those with shorter wavelengths exhibit more pronounced three-level characteristics.

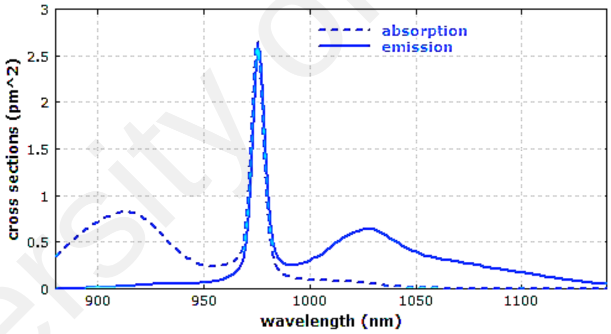

Figure 2.3: Absorption and emission cross sections of ytterbium-doped germanosilicate glass, as used in the cores of ytterbium-doped fibres. (Data from spectroscopic measurements by R. Paschotta)

2.3.2 Erbium doped fiber

Erbium doped fiber (EDF) has emerged as a strong candidate for employment as the gain medium in a fiber ring laser, with particular desirable properties such as large gain bandwidth of typically tens of nanometers due to lack of sharpness in its energy level. Exciting the constituent Erbium ions allows EDF to provide amplification of signals around 1550 nm wavelength without introducing any effects of gain narrowing (Becker, Olsson, & Simpson, 1999; Mahad, Supa’at, & Sahmah, 2009), which is highly attractive for optical communication. Although there are many other types of gain media such as semiconductor optical amplifier (SOA), Brillouin fiber amplifier (BFA) and Raman fiber amplifier (RFA), EDF is preferable over these gain media and widely used as the gain medium for optical amplification in generating fiber lasers, with its behavior and characteristics well documented.

Erbium belongs to the Lanthanides group, also known as rare earth elements and comprises fifteen Lanthanides (atomic numbers from 57 until 71) (Emsley, 2011). The elements in this group have 5s and 5f outermost electrons accounting for laser transitions, with the ability to provide the population inversion condition that is necessary in the generation of lasers. These Lanthanides typically appear in an ionic form of a trivalent state $(Ln)^{3+}$ with the atomic form of $(Xe)\ 4f^{N}\ 6s^{2}$ or $(Xe)\ 4f^{N-1}\ 5d^{1}\ 6s^{2}$ (Becker et al., 1999). The trivalent state forms upon elimination of three electrons; two of which originate from the 6s orbital and the other from either the 4f or 5d orbitals. In the case of erbium, the three electrons originate from the 6s and 4f orbitals.

Amplification via EDFA occurs with the transition of an electron from the meta-stable state, denoted as $^{4}I_{13/2}$, to the ground state level, denoted as $^{4}I_{15/2}$, from the 4f state. The meta-stable state has a 10 ms lifetime, which is a sufficient amount of time for optical amplification to occur. The commercially available EDFA for modern applications typically employs either a 980 nm or 1480 nm semiconductor laser diode as the pump, which is also known as a pump laser diode.

2.3.2.1 The quasi-three level energy system

A model of a quasi-three level energy system is used, as discussed in detail in Ref. (Desurvire, Giles, Simpson, & Zyskind, 1991), in order to understand the atomic rate equation of an EDF. Figure 2.3 shows the schematic diagram of the EDF three-level energy system, with levels denoted as E_1, E_2 and E_3.

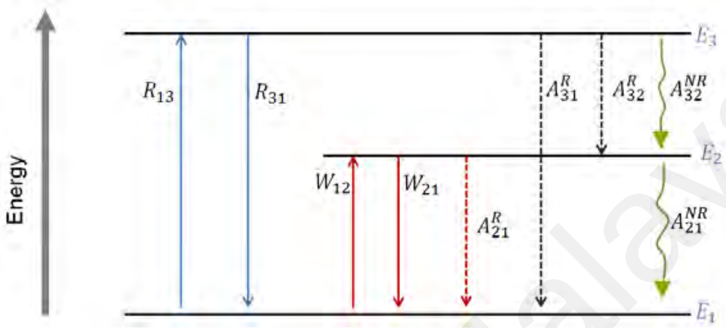

Figure 2.4: Illustration of three-level energy system for EDF (Desurvire et al., 1991).

E_1 indicates the ground state level, whereby atoms occupying this energy level have zero energy. E_2 and E_3 indicate the metastable state and pumping levels respectively, such that $E_3 > E_2 > E_1$. τ represents the transient lifetime of the metastable state E_2. The denotations of the other symbols in the figure are as shown in Table 2.1.

Table 2.1: The symbols in the atomic rate equation and their respective denotations

Symbols	Denotations
R_{13}	Rate of pumping from E_1 to E_3
R_{31}	Rate of stimulated emission from E_3 to E_1
W_{12}	Absorption rates
W_{21}	Stimulated emission rates
A_{21}^{R}	Spontaneous radiative decay/emission rate from E_2 to E_1

A_{31}^{R}	Spontaneous radiative decay/emission rate from E_3 to E_1
A_{32}^{R}	Spontaneous radiative decay/emission rate from E_3 to E_2
A_{32}^{NR}	Spontaneous non-radiative decay/emission rate from E_3 to E_2
A_{21}^{NR}	Spontaneous non-radiative decay/emission rate from E_2 to E_1

For the case of unstable excitation at level E_3, the unstable electrons will undergo either radiative or non-radiative decay immediately following their excitation. Assuming that the non-radiative transition from E_3 to E_2, denoted as A_{32}^{NR}, is the largest contributor of decay from level E_3, it can be expressed $A_{32}^{NR} \gg A_3^{R}$, where $A_3^{R} = A_{32}^{R} + A_{31}^{R}$ and the emission from level E_3 to E_2 is denoted as A_{32}^{NR} for simplicity.

However, a different process takes place in the case of the transition from E_2 to E_1, whereby the most dominant transition is the spontaneous radiative emission A_{21}^{R} rather than the spontaneous nonradiative emission A_{21}^{NR} i.e. $A_{21}^{R} \gg A_{21}^{NR}$. For the fluorescence lifetime τ, $A_{21}^{R} = \frac{1}{\tau}$. Assigning N_1, N_2 and N_3 as the number of ions at level E_1, E_2 and E_3, respectively and ρ as the laser ion density with relation $\rho = N_1 + N_2 + N_3$, the atomic rate equations for the three-level energy system be expressed as (Desurvire et al., 1991);

$$\frac{dN_1}{dt} = -R_{13}N_1 + R_{31}N_3 - W_{12}N_1 + W_{21}N_2 + A_{21}N_2 \tag{2.1}$$

$$\frac{dN_2}{dt} = W_{12}N_1 - W_{21}N_2 - A_{21}N_2 + A_{32}N_3 \tag{2.2}$$

$$\frac{dN_3}{dt} = R_{13}N_1 - R_{31}N_3 - A_{32}N_3 \tag{2.3}$$

Initially, the ion population is assumed to be constant and this state is called the steady state condition. This condition is only satisfied when $\frac{dN_i}{dt} = 0$, where $i = 1, 2$ and 3 indicate the different energy levels.

Defining $a = (R_{31} + A_{32})$ and $b = (W_{21} + A_{21})$ allows equations (2.2) and (2.3) to be expressed as

$$W_{12}N_1 - bN_2 + A_{32}N_3 = 0 \qquad 2.4$$

$$R_{13}N_1 - aN_3 = 0 \qquad 2.5$$

The equation $\rho = N_1 + N_2 + N_3$ can be re-expressed as $N_3 = \rho - N_1 - N_2$ to allow equations (2.4) and (2.5) to give the solution for N_1 and N_2 ;

$$N_1 = \rho \frac{ab}{b(a + R_{13}) + aW_{12} + R_{12}A_{32}} \qquad 2.6$$

$$N_2 = \rho \frac{R_{13}A_{32} + aW_{12}}{b(a + R_{13}) + aW_{12} + R_{13}A_{32}} \qquad 2.7$$

Using the definitions for a and b along with factorising A_{21} and A_{23} results in

$$N_1 = \rho \frac{(1 + W_{21}\tau)(1 + \frac{R_{13}}{A_{32}})}{(1 + W_{21}\tau)\left(1 + \frac{R_{13} + R_{31}}{A_{32}}\right) + W_{12}\tau\left(1 + \frac{R_{31}}{A_{32}}\right) + R_{13}\tau} \qquad 2.8$$

$$N_2 = \rho \frac{R_{13}\tau + W_{12}\tau(1 + \frac{R_{13}}{A_{32}})}{(1 + W_{21}\tau)\left(1 + \frac{R_{13} + R_{31}}{A_{32}}\right) + W_{12}\tau\left(1 + \frac{R_{31}}{A_{32}}\right) + R_{13}\tau} \qquad 2.9$$

Assuming $A_{32} \gg R_{13}$ and $A_{32} \gg R_{31}$, it can be deduced that $\frac{R_{13,31}}{A_{32}} \approx 0$. From the initial assumption that non-radiative decay rate is dominant, equations (2.8) and (2.9) become

$$N_1 = \rho \frac{1 + W_{21}\tau}{1 + R\tau + W_{12}\tau + W_{21}\tau} \qquad 2.10$$

$$N_2 = \rho \frac{R\tau + W_{12}\tau}{1 + R\tau + W_{21}\tau + W_{12}\tau} \qquad 2.11$$

where $R = R_{13}$. From equation (2.10) and (2.11), it can be inferred that $N_3 = \rho - N_1 - N_2 = 0$. This means that the pump level population is neglected by the major contribution of the non-radiative decay (A_{32}) from energy level of E_3 to E_2, which is the metastable level. These equations provide the basic conditions for occurrence of amplified stimulated emission, which is the key enabler for the generation of lasers. The next subsection covers experimental analysis of the EDFA gain measurement.

2.3.2.2 Experimental analysis of the EDFA gain measurement

A simple experimental setup is constructed, as shown in Figure 2.5, in order to measure the saturation power for the EDFA as the gain medium. The setup consists of a 980 nm laser diode, a 980/1550 nm wavelength division multiplexer (WDM) and a 3 m EDF. An optical attenuator is used to control the input power entering the amplifiers. The gain measurements for the EDF are then carried out and analysed.

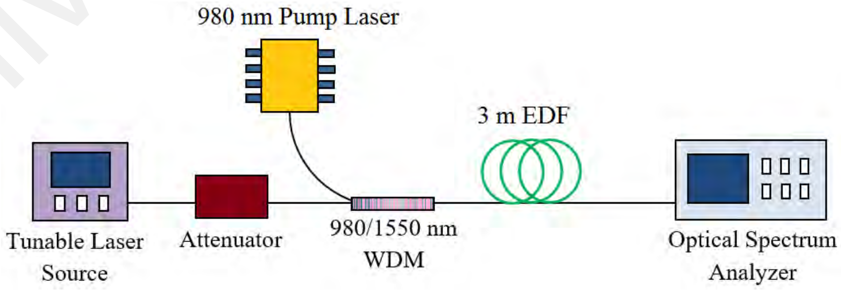

Figure 2.5: Experimental setup for gain measurement of EDFA

The saturation input power for the EDFA is determined by measuring the input power level when it has a 3dB gain attenuation from the maximum gain (Desurvire et al., 1991). Figure 2.6 shows the gain value against signal power, with saturation power for

EDFA observed at approximately -5 dBm from this graph. The experimental result agrees with the theoretical assumption, which states that for a higher injected signal power there will be a corresponding lower gain obtained (Desurvire et al., 1991). Thus, the expectation is that the depletion of the active region, which is responsible for the gain, will increase when the injected input power is higher than the saturation power (A. E. Siegman, 1986).

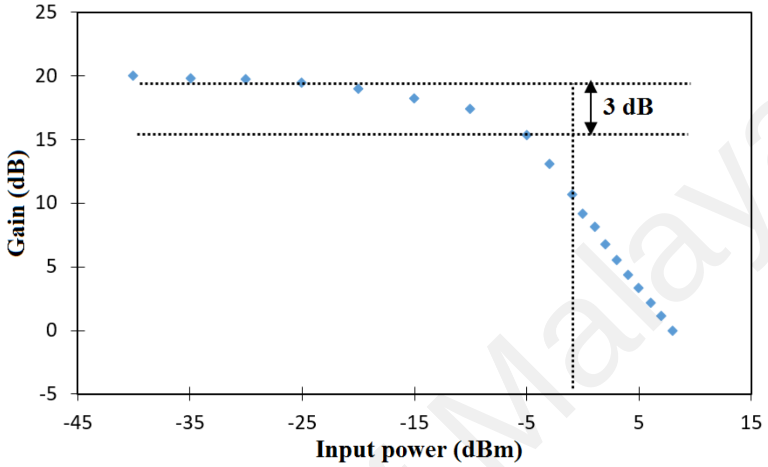

Figure 2.6: Experimental result for gain measurement of the EDFA

2.3.3 Thulium doped fiber

Interest in the Thulium-doped fiber laser (TDFL) originates from its emission band in the range of 1400-2700nm lying between the bands of Er^{3+} and Tm^{3+} ions. Since the advent of double-cladding configuration of fiber and the recent technological development of high-power laser diodes, output power (performance) of Tm^{3+}-doped fiber lasers has scaled exponentially. Up to date, the maximum output achieved in Tm^{3+}-doped fiber lasers has been comparable with that from Yb^{3+}-doped fiber lasers. Laser beam in the 2 micron wavelength range has wide applications. First, it is a good candidate in laser microsurgery due to high absorption of water in this spectral region thus can provide high-quality laser tissue cutting and welding. In addition, this wavelength-range laser has potential applications in environment monitoring, LIDAR, optical-parametric-oscillation (OPO) pump sources, and so on. (Esterowitz, 1990; Henderson et al., 1993; Myslinski et al., 1993; Stoneman & Esterowitz, 1990).

For obtaining laser emission in the mid-infrared wavelength region, the Thulium-doped fiber (TDF) is an excellent candidate due to several unique advantages it possesses. First, the TDF has a strong absorption spectrum that has good overlap with the emission band of commercially available AlGaAs laser diodes, which have been significantly developed and are being developed at an unprecedented speed. Second, the specific energy-level structure of Tm^{3+} ions provides the TDFL with a special advantageous energy transfer process; the $^3H_4 + ^3H_6 \rightarrow ^3F_4 + ^3F_4$ cross relaxation process. In this process, two excited state ions can be obtained with depletion of just one absorbed pump photon. With an appropriately high doping level, the cross relaxation process can offer a quantum efficiency close to two, which greatly improves the efficiency of the TDFL. Thirdly, the TDF has a very broad emission band, spanning over more than 400 nm. This feature offers the TDFL especially high-degree of wavelength tunability, which is very useful in applications such as spectroscopy, atmospheric sensing and so on.

For laser ions, the combination of the energy gaps between the excited level and the one just below it and the maximum phonon energy (MPE) plays an important role in the non-radiative relaxation rate, which in turn has a significant influence on the laser efficiency originated from the excited states. For Tm^{3+} ions, different host materials show a great difference in the maximum phonon energy (MPE) value. Two most common host materials used for Tm^{3+} fibers are silica and fluoride glass. Their MPE differs about several times, being 1100 cm^{-1} (silicate) and 550 cm^{-1} (fluorides), respectively (Sorokina & Vodopyanov, 2003). Large MPE of the silicate glass fiber limits its infrared transparency range less than 2.2 μm and improves its multi-phonon relaxation rates. Therefore, fluoride fibers are preferred as the host material for Tm^{3+} ions to achieve comparatively longer-wavelength emission. In TDFLs, the $^3F_4 \rightarrow ^3H_6$ transition is usually exploited to achieve the ~2 μm high-power laser output. This transition can produce a very wide emission band, providing a broad tuning range for lasers and a wide optical bandwidth for amplifiers. However, the relaxation of the $^3F_4$ level is predominantly non-radiative. The measured lifetime of the $^3F_4$ level for Tm^{3+} doped silica fiber is just 0.2 ms (Hanna, Percival, Smart, & Tropper, 1990) showing a high non-radiative rate thus low quantum efficiency. Therefore, TDFLs usually have high laser thresholds. On the contrary, fluoride based TDFLs have comparatively lower thresholds due to a low MPE. The high non-radiative rate, however, does not impair laser slope efficiency; because stimulated emission will dominate non-radiative relaxation once the laser has been raised above threshold. Due to high damage threshold and the very effective modified chemical vapor deposition (MCVD) technique for fiber fabrication, silica based TDFs are usually chosen to construct high-power 2 μm fiber lasers.

TDFs can be either core pumped or cladding pumped. In the past, the fiber laser was usually core pumped. The fiber core areas are generally <100 μm which limit the power scalability because this method depend on expensive high-beam-quality pump sources. Since the invention of double cladding fiber configuration with a larger cladding area >10000 μm together with a high numerical aperture (NA) of 0.3-0.55, output power of Tm^{3+}-doped fiber lasers can be greatly improved by use of high-power diode-arrays as pumping sources. In the design of fibers for cladding pumping, the core of the fiber is usually made small (such as less than 5 microns) to guide a single-transverse mode (LP_{01}). The cladding generally has a much larger cross section (several-hundred-micron diameter) for high-power launching, and the shape of the cladding can be flexible with novel consideration. The shape of the inner cladding of the fiber has a great impact on the absorption efficiency of launched pump light. In the past, the inner cladding used to be circularly symmetric, which can be drawn with ease and is compatible with the pigtail fiber of the pump laser diode. However, the circular symmetry will make large portion of the pump light to be skew light, greatly reducing the absorption efficiency of doping ions. In order to improve the utility efficiency of pump sources, and take the pump light shape into account (compatible with the inner cladding shape), various double cladding fiber structures are invented, by using these double cladding fibers, the pump efficiency is significantly enhanced.

Figure 2.7 shows the absorption spectrum of a Thulium-doped silica fiber (Agger, Povlsen, & Varming, 2004). As shown in the figure, the fiber has strong absorption near 790 nm, which has good overlap with the emission band of present fully developed AlGaAs diode lasers. This feature of the TDFL makes the pump process comparatively easier and less expensive, offering an exciting potential for power scaling in the 2 μm wavelength range. Besides 790 nm pumping, we can also use 1200 nm and 1550 nm pumping schemes for the TDFL.

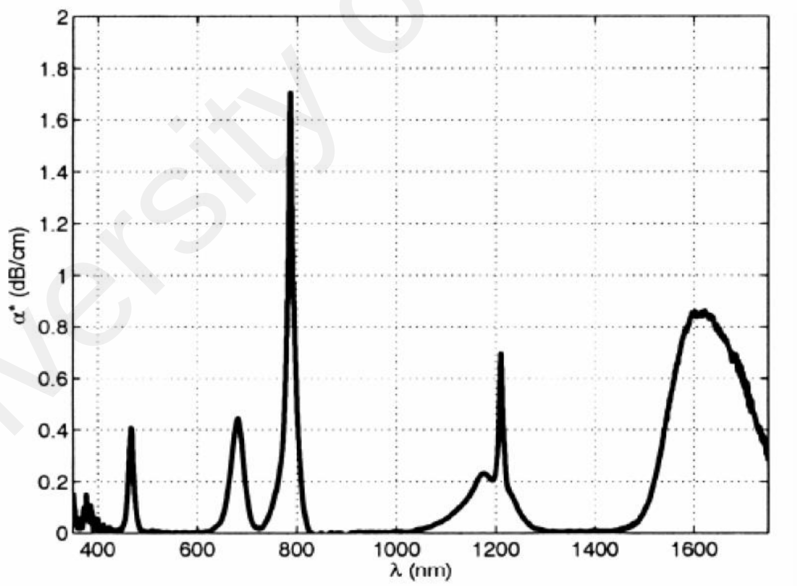

Figure 2.7: Absorption spectrum of a silica-based TDF (Agger et al., 2004).

Figure 2.8 shows the simplified energy-level diagram of Tm^{3+} ions. As shown in the diagram, the pump light at ~790 nm excites Tm^{3+} ions from $^3H_6$ to $^3H_4$, which then non-radiatively decay to the upper laser level of $^3F_4$ with a fluorescence lifetime of 0.55 ms (Gandy, Ginther, & Weller, 1967). The transition from $^3F_4 \rightarrow {}^3H_6$ will radiates photons at wavelength of ~2 µm. Due to large Stark splitting of the lower laser level (the ground state level), the TDFL is a quasi-four-level system.

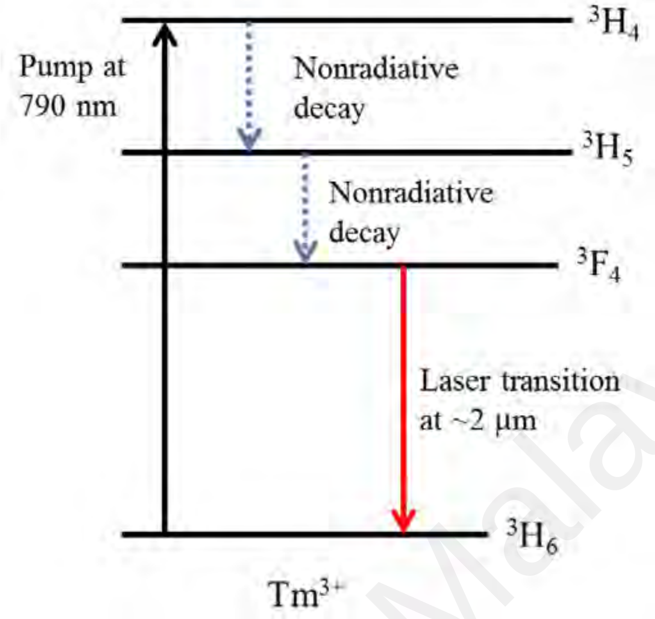

Figure 2.8: The simplified energy-level diagram of Tm^{3+} ions.

2.4 Homogeneous and Inhomogeneous Broadening Gain Media

There are two types of atomic transition for spectral broadening in an active gain media, namely, homogeneous and inhomogeneous spectral broadening, corresponding to homogeneous and inhomogeneous gain media, respectively. Homogeneous spectral broadening is explicitly exhibited by most rare earth doped fibers such as erbium doped fibers (EDFs) (X. Feng, Wai, Tam, Lu, & Guan, 2011; Junqiang Sun, Qiu, & Huang, 2000; C. Yeh et al., 2009), ytterbium doped fibers (YDFs) (Guan & Marciante, 2007; L. Pan, Utkin, & Fedosejevs, 2009; Zongjiu & Liu, 2010) and thulium doped fibers (TDFs) (Oh, Morse, Weber, Kilian, & Reinhart, 1994; W. Peng et al., 2013; X. Wang et al., 2013), while inhomogeneous spectral broadening can be seen in devices such as the semiconductor optical amplifiers (SOAs). This does not mean that both of the gain media only exhibit homogeneous and inhomogeneous spectral broadening, but rather these two gain media exhibit gain profiles which are either dominantly homogeneously broadened or in-homogeneously broadened.

Here, the shapes of the atomic line-width transitions, which are either Lorentzian or Gaussian, will be discussed in relation to either the homogeneous or inhomogeneous gain media. This will allow for a numerical interpretation for these two spectral line-widths. In the next subsection, the characteristics of these two broadening phenomena are studied through experimental work which will be explained further.

2.4.1 Homogeneous Gain Medium

The gain media which will be used in the work are YDF, EDF and TDF due to their commercial availability. In general, all rare earth doped fibres exhibit homogeneous broadening transition. As the present work will involve all the three mentioned types of gain media, these would be the primary method in investigating homogenously broadened gain media (Bellemare, 2003). Now, atomic transitions in EDFs, for example, are caused by stimulated emission from the $^4I_{13/2}$ level to the $^4I_{15/2}$ level, when pumped by either a 980 nm or 1480 nm laser diode. This transition, however, experience Stark broadening, induced by Stark effect (Desurvire et al., 1991), which splits the energy levels into an upper and lower manifold, denoted as g_1 and g_2 respectively. This splitting of energy levels into upper and lower levels allows for an increase in the number of atomic transitions thereby causing a broadening of the laser transition. As mentioned previously, the characteristic of every transition is also different and not homogeneous. However, in the case of EDF, it can be viewed as homogeneous due to the fact that the energy sublevels are strongly coupled by the thermalization effect, which results in homogeneous broadening. Homogenous broadened transition has a Lorentzian line shape, and therefore causes a narrowing of the transition line-width as depicted in Figure 2.9. The broadening also has an unambiguous dependence of the resonance frequency to the signal frequency, and due to the response of each individual ion in the collection, the signal is broadened equally and homogeneously (A. Siegman). Hence, the atomic transition will exhibit exactly the same line-shape if the right conditions are provided by the cavity and surroundings. The Lorentzian gain coefficient, $\gamma(\upsilon)$, can be expressed as (Saleh, Teich, 1991);

$$\gamma(\upsilon) = \gamma(\upsilon_0)\frac{(\Delta\upsilon/2)^2}{(\upsilon-\upsilon_0)^2+(\Delta\upsilon/2)^2} \qquad 2.12$$

where $\gamma(\upsilon_0)$ is the gain coefficient at the central frequency, υ_0 and $\Delta\upsilon$ is the emission line-width. The homogeneous broadening effect therefore leads to a uniform saturation of the gain across the whole gain spectrum, independent of frequency, with the lasing frequency selected from the conditions within the cavity. This effect is depicted in Figures 2.10(a) and 2.12(a), while Figure 2.10 (b) and Figure 2.12 (b) are shown to depict the effect of inhomogeneous broadening to the gain curve for comparison.

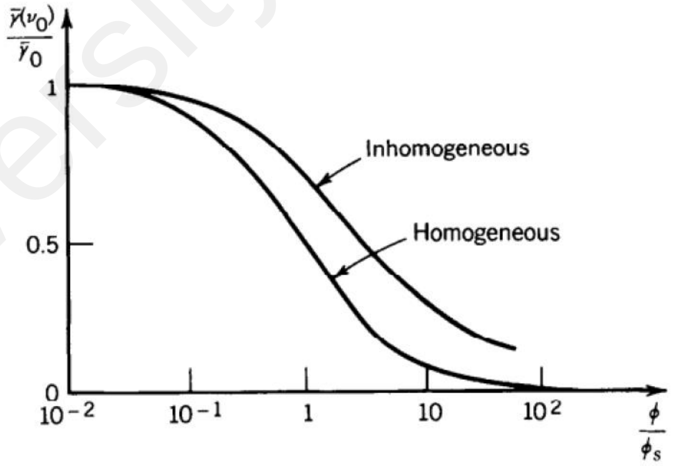

Figure 2.9: The Lorentzian and Gaussian line shape on normalized saturated gain coefficient versus normalized photon flux density (Saleh et al., 1991).

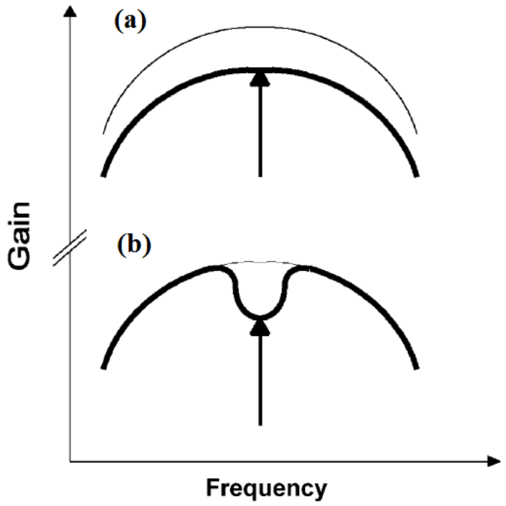

Figure 2.10: The effect of saturating signal on the gain curve for (a) Homogeneous and (b) Inhomogeneous spectral broadening (Bellemare, 2003).

2.4.2 Inhomogeneous Gain Medium

SOAs exhibit both of homogenous and inhomogeneous broadening effect. However, as has been proven by many research and experiments, the emission has a relatively large portion of in-homogeneously broadened transitions as compared to homogeneous broadening transitions (Tanaka et al., 2007; M. Tang et al., 2011). SOA was found to have an emission spectrum that is largely inhomogeneous broadened (Piprek, Hutchinson, Henness, Masanovic, & Coldren, 2004; Vlachos, Bintjas, Pleros, & Avramopoulos, 2004; C. Yang, 2007; Zilkie et al., 2007) as has been studied by many research groups (Sadao Adachi, 1982, 1989; S Adachi, Kawaguchi, Takahei, & Noguchi, 1981; Broberg & Lindgren, 1984; Fiedler & Schlachetzki, 1987; Henry, Johnson, Logan, & Clarke, 1985; E. H. Li, 2000). In contrast to homogeneously broadened transition, atoms in inhomogeneous broadening materials act in a different manner due to the fact that they have different orientations and lattice location (Connelly, 2007), in addition to quantum well imperfections. This is manifested in the independent saturation of different frequencies for each mode in the steady state condition. Consequently, multi-longitudinal modes fiber laser can be established in in-homogeneously broadened lasers. In-homogeneously broadened gain media differ from homogeneously broadened gain media in that they exhibit a phenomenon known as the hole-burning effect, which occurs at the centre of the saturating signal emitted by in-homogeneous gain medium. This is because the saturating signal will only affect the transition of atoms with similar frequencies. This then only allows a relatively small number of atoms to be homogeneously broadened and therefore having a reduced gain, while leaving other atoms free. The aggregation of these atoms then is an in-homogeneously broadened transition, as illustrated in Figure 2.11.

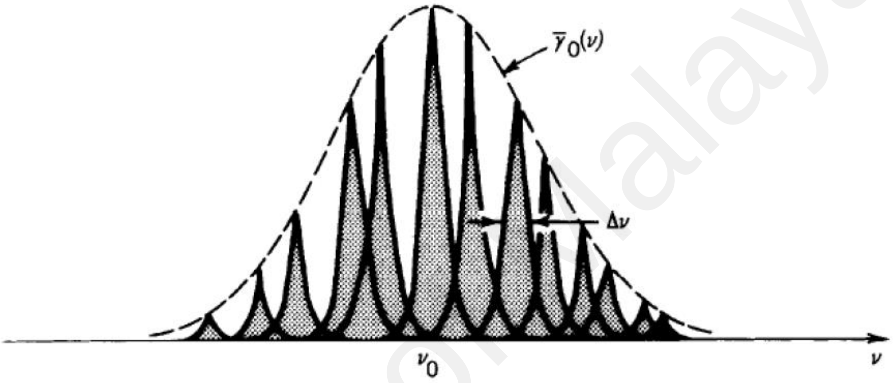

Figure 2.11: The line shape of in-homogeneous broadened gain medium (Saleh et al., 1991).

As SOAs generally is in-homogeneously broadened, they exhibit an in-homogeneously broadened line shape, as shown in Figure 2.11. It also can be seen from the same figure that the inhomogeneous gain coefficient saturates slower than homogeneous gain coefficient. The Gaussian gain coefficient, can be expressed as (Saleh et al., 1991):

$$\gamma_\beta(\upsilon) = \frac{b(\Delta\upsilon/2\pi)}{(\upsilon-\upsilon_\beta-\upsilon_0)^2+(\Delta\upsilon_s/2)^2} \qquad 2.13$$

where β is the subset of frequency, υ_β, $\Delta\upsilon$ is the emission line-width, $\Delta\upsilon_s$ is the Lorentzian shape of width and υ_0 is the central frequency. *b* is a constant and is defined as, $b = N_0\left(\lambda^2/8\pi\tau_{sp}\right)$, with τ_{sp} is the spontaneous lifetime, N_0 the steady state population difference and λ the wavelength of light in the medium. The hole-burning effect was also explained by Siegman (A. Siegman) as an indispensable phenomenon in in-homogeneously broadened gain media when a strong signal is injected into the gain medium and causing saturation of only a sub-group of atoms with similar resonance frequencies as the signal. Other transitions at more distant frequencies will not be affected. This physical explanation can be clearly seen as illustrated in figure 2.12 (b).

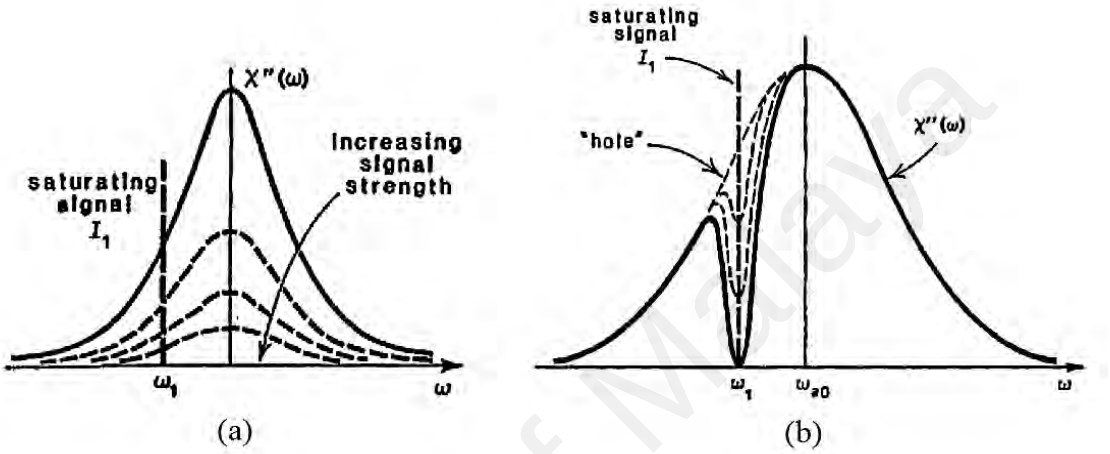

Figure 2.12: The saturation condition for (a) homogeneous and (b) in-homogeneous profile (A. E. Siegman, 1986).

2.5 Optical Fiber Lasers

LASER is an acronym for light amplification by stimulated emission of radiation. It is a device which allows for the generation of amplified light provided that three conditions are satisfied. First, the device must contain a laser medium such as atoms or molecules which acts as the active medium for amplification. Secondly, the device must contain an optical cavity which allows for circulation of photons inside the cavity, and therefore, causes cavity population inversion. This enables the laser beam to propagate back and forth in the cavity, increasing the gain until saturation, before being extracted to obtain the output. The third condition is that the device must include a pumping method to excite the active medium and cause stimulated emission to take place inside the cavity. A simple configuration of a laser is shown in figure 2.13.

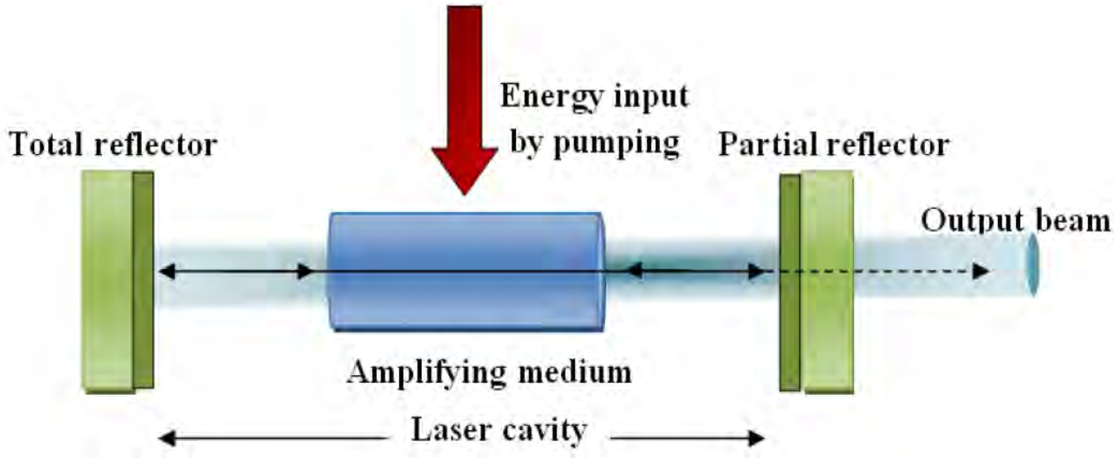

Figure 2.13: A simple free space laser cavity design

As was discussed previously, one of the most important aspects to be considered before a laser can be realized is population inversion. Population inversion occurs while a system (such as a group of atoms or molecules) exists in a state in which more members of the system are in higher, excited states than in lower, unexcited energy states. When the gain of the laser is higher than the cavity loss the lasing will start.

There are several types of lasers, such as solid state lasers, gas lasers, semiconductor lasers, dye lasers and optical fiber lasers. Optical fibber lasers are generally designed by inserting an active gain medium such as the EDFA or SOA into an optical cavity whose output is looped back to the input port the gain medium. This is illustrated in figure 2.14. The laser is generated from the amplification of the optical gain medium output which has reached the lasing threshold, by reconnecting the output to the input via a WDM (see figure 2.14). The process continues until it reaches its highest output power when the gain saturation is reached. The condition is called as a steady state condition, where the fiber laser cannot produce any larger amount of output power.

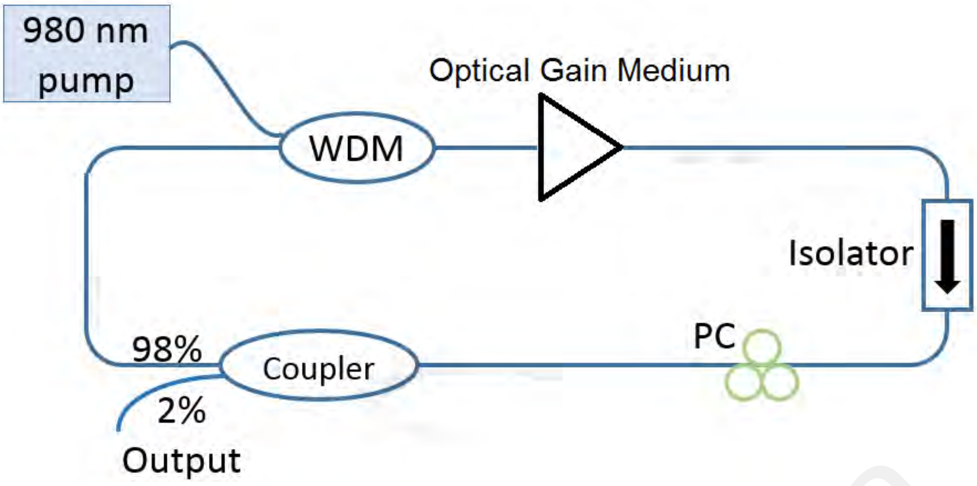

Figure 2.14: A configuration of a basic optical fiber laser

2.6 Characteristic of Fiber Lasers

The SMSR on the other hand is necessary to evaluate the degree of noise in the fiber laser. The SMSR can be defined as the intensity difference between the main longitudinal mode and the maximum side mode, and can be written as (Mynbaev & Scheiner, 2001):

$$SMSR(dB) = 10\log\left(\frac{I_{main}}{I_{side}}\right) = I_{main}(dBm) - I_{side}(dBm) \qquad 2.14$$

A high value of SMSR indicates a good performance of a fiber laser. A conventional laser diode has a typical SMSR value of 40 dB. Therefore, in order to build a well performing laser, the SMSR value is required to be as high as possible, preferably with a minimum value of 40 dB. This is important in order to reduce the crosstalk in the WDM networks when they function as transmitters. The tunability of a laser allows for the selection of wavelengths provided by the fiber laser. The wider the range, the better the fiber laser is and can be used for a number of applications, such as in DWDM communication system as a transmitter, in spectroscopy and as sensors, especially temperature and displacement sensors. Stability is the measure of fluctuation of the output power with time. It is important to see whether a fiber laser is stable enough and operate for a long period of time. This is important, as a stable output power fiber laser is required for transmission purposes in communication systems to prevent extra cost.

2.7 Photonics Crystal Fiber

The improvement of fiber drawing techniques led to the development of micro-structured fiber, commonly referred to as Photonic Crystal Fiber (PCF). This fiber design offered an increased modal confinement and unique dispersion tailoring qualities not available to standard step index fiber (Knight, Birks, Russell, & Atkin, 1996).

The development of photonic crystal fibers and the exploration of the great variety of possible applications have attracted huge interest. The field, which constitutes a part of the wider field of photonic bandgap structures while incorporating other ideas as well, can be considered as one of the most active fields of current optics research. This is partly because these fibers offer many degrees of freedom in their design to achieve a variety of peculiar properties, which make them interesting for a wide range of applications.

A photonic crystal fiber (also called holey fiber, hole-assisted fiber, microstructure fiber, or micro-structured fiber) is an optical fiber which obtains its waveguide properties not from a spatially varying glass composition but from an arrangement of very tiny and closely spaced air holes which go through the whole length of fiber. Such air holes can be obtained by using a preform with (larger) holes, made e.g. by stacking capillary and/or solid tubes (stacked tube technique) and inserting them into a larger tube. Usually, this preform is then first drawn to a cane with a diameter of e.g. 1 mm, and thereafter into a fiber with the final diameter of e.g. 125 µm. Particularly soft glasses and polymers (plastics) also allow the fabrication of preforms for photonic crystal fibers by extrusion (Ebendorff-Heidepriem, Warren-Smith, & Monro, 2009; Kumar et al., 2002). There is a great variety of hole arrangements, leading to PCFs with very different properties. All these PCFs can be considered as specialty fibers.

The simplest (and most often used) type of photonic crystal fiber has a triangular pattern of air holes, with one hole missing (see figure 2.15), i.e. with a solid core surrounded by an array of air holes. The guiding properties of this type of PCF can be roughly understood with an effective index model: the region with the missing hole has a higher effective refractive index, similar to the core in a conventional fiber. There are also so-called photonic bandgap fibers (PBG fibers) (Cregan et al., 1999) with a totally different guiding mechanism, based on a photonic bandgap of the cladding region. The latter mechanism even allows guidance in a hollow core (i.e. in a low-index region) (see figure 2.16), such that most of the power propagates in the central hole (→ hollow-core fibers). Such air-guiding hollow-core photonic crystal fibers (or air core bandgap fibers) can have a very low nonlinearity and a high damage threshold. They typically guide light only in a relatively narrow wavelength region with a width of e.g. 100–200 nm and can be used e.g. for pulse compression with high optical intensities, as most of the power propagates in the hollow core.

Most PCFs are made of pure fused silica (→ silica fibers), which is compatible with the above-mentioned fabrication techniques. However, various PCFs made of other materials have been demonstrated, most notably of heavy metal soft glasses and of polymers (plastic optical fibers), sometimes used even for terahertz radiation (H. Han, Park, Cho, & Kim, 2002; M. R. K. Soltanian, Sadegh Amiri, Alavi, & Ahmad, 2015). Solid core PCFs guide via total internal reflection. However due to the silica core effectively being surrounded by air cladding, the refractive index contrast is much higher than for standard optical fiber. Figure 2.15 (a) shows a PCF end facet showing the periodic microstructure of the of the air-hole cladding. This allows for a higher modal confinement and a smaller guided mode. From equation 2.15 this then yields a much higher effective nonlinearity. The γ is the effective fiber nonlinearity and is defined as:

$$\gamma = \frac{2\pi n_2}{\lambda A_{eff}} \qquad 2.15$$

where A_{eff} is the effective mode area, n_2 is the nonlinear refractive index and λ is the pump wavelength. This effective fiber nonlinearity arises due to the guided mode of an optical waveguide or fiber experiencing a different nonlinear refractive index than simply that of the base material. From equation 2.15 it is evident that a material with a high nonlinear refractive index and a small guided mode area would exhibit a high effective nonlinear refractive index. The high index contrast between the core and the cladding of PCF means that they can support guided modes with a higher degree of core confinement and thus an increased effective nonlinear refractive index. To optimize this phase matching process the fiber would ideally have a flat dispersion profile over a wide range of wavelengths and ideally the pump wavelength should be situated in the anomalous dispersion regime, as a non-zero value of $2P\gamma$, where P is the peak pump power, allows sideband generation in the anomalous dispersion regime of fiber via a process known as modulation instability (MI) (Dudley & Taylor, 2010).

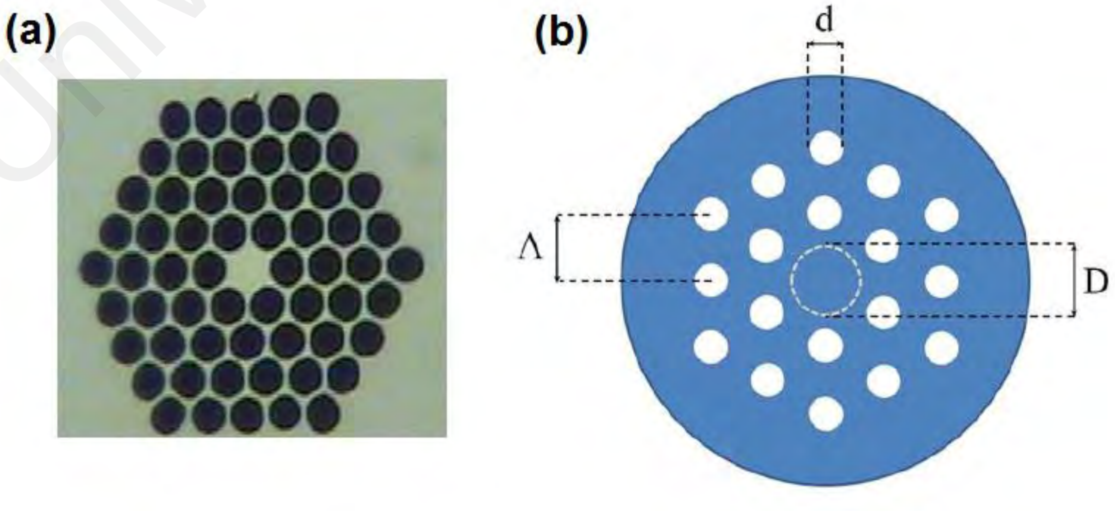

Figure 2.15: (a) Photonic crystal fiber end facet. (b) Schematic of PCF end facet.

2.7.1 CGCRI photonic crystal fibers

A fiber with sample names PCF-19A was fabricated by the Central Glass & Ceramic Research Institute (CGCRI) and investigated in this work. The fiber consisted of a three air-ring cladding structure and had a zero dispersion wavelength in the region of 987 nm. This would allow solitary wave propagation to occur within the PCF structures when pumped by laser sources such as Nd:YAG or ytterbium doped fiber laser systems. The fiber named as PCF19A had circularly symmetric core to reduce birefringent. The purposes of this investigation were to observe the threshold for the separate spectral broadening mechanisms in short lengths of PCF at pump wavelengths either side of the zero dispersion wavelength. These were then compared with the theoretical spectra numerically modeled by collaborators at CGCRI. The experimental framework provided by this study aided micro-structured fiber development at CGCRI by validating their nonlinear guiding model and allow them to accurately model fiber nonlinearity in advance of fabrication and tailor fiber design characteristics to yield a desired output spectra.

2.7.2 PCF-19A

2.7.2.1 Fiber characteristics

Figure 2.16 shows the fiber facet image of PCF-19A. The image was taken using a microscope calibrated with a USAF 1951 resolution chart. The fiber had a hexagonal shaped core with a size of 4.37 µm, an air hole diameter size of 5.06 µm and pitch of 5.52 µm.

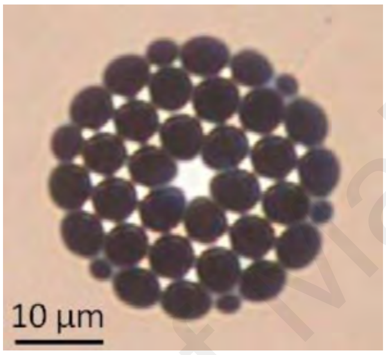

Figure 2.16: PCF-19A facet image

Linear characterization of the fiber was performed at CGCRI. This characterization included theoretical prediction of the dispersion profile and experimental measurement of the wavelength dependent loss. The theoretical dispersion profile would subsequently be used to calculate the higher order dispersion terms required to accurately model the nonlinear pulse propagation in the fiber. Figure 2.17 (a) shows the theoretically predicted dispersion profile of the fiber from 800-1800 nm. The zero dispersion wavelength of PCF19-A was calculated to be 987 nm. Figure 2.17 (b) shows the wavelength dependent loss in dB/km between 800 nm and 1800 nm. The large attenuation measured at 1400 nm, 1215 nm and 910 nm are due to large OH absorption.

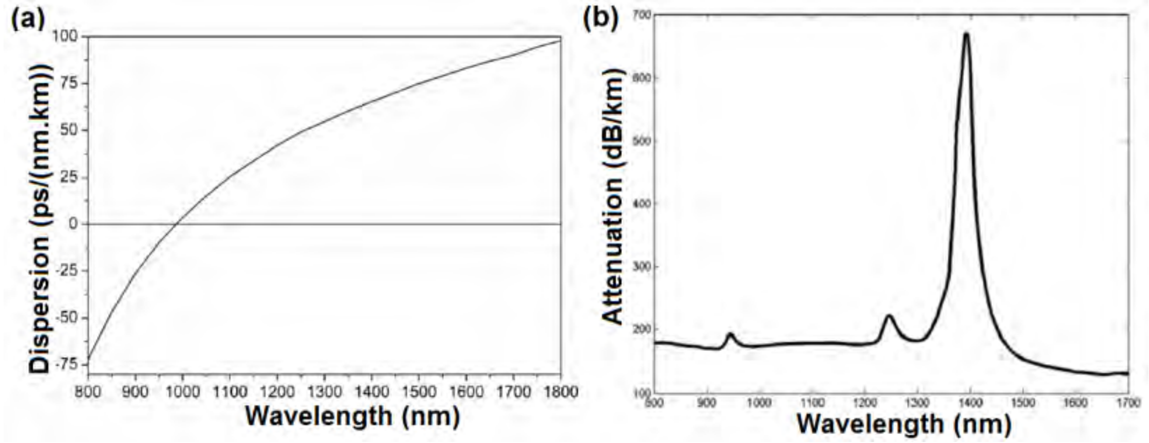

Figure 2.17: (a) Theoretical dispersion profile and (b) Attenuation of PCF-19A

The evolution of the spectral broadening of femtosecond pulses after propagation along 15, 20 and 30 cm fiber lengths were investigated for pump wavelengths of 900, 980 and 1060 nm.

2.7.2.2 Modes propagation inside PCF

The unique properties of PCF, such as wide range single mode operation, dispersion flexibility and large mode area, have been investigated recently (Russell, 2006), and the inherent flexibility in particular indicates the suitability of PCF for use as an interferometer. Interferometers employing PCF (Choi, Kim, & Lee, 2007; Jiangbing Du, Dai, Lei, Tong, & Shu, 2010) also can be wavelength-selective filters (WG Chen et al., 2009) due to the wavelength-dependent characteristics afforded by PCF. A constructed compact interferometer using a 10 cm length of few-mode PCF spliced on each end to SMF is shown for one side in the image labeled “spliced area” within Fig.3.21. Manually splicing the PCF and SMF fiber at two points in series led to an inevitable collapse of the PCF air holes and creation of a very simple Mach-Zehnder interferometer (MZI). The length of the PCF was directly related to fringe spacing, and in this case a free spectral range (FSR) was 0.2 nm, as observed in the transmission spectrum of the MZI displayed in Fig. 2.19. Figure 2.19 shows the transmission spectrum of the PCF-MZI after utilizing a wide band white light source. The polarization characterization of an MZI based on the state of polarization (SOP) and power measurement at the interferometer output has been carefully investigated in (Mabrouki, Gadonna, & Le Naour, 1996).

The fundamental and cladding modes accumulate a phase difference along the PCF, which acts as an MZI due to different phase velocities, and this phase difference depends on the length of PCF and the wavelength of the guided light. Since the phase difference and the phase velocities are wavelength dependent, the optical power transmitted by the interferometer will be minimum at certain wavelengths and maximum at other specific wavelengths. The superimposition of fundamental modes, which resulted in excited core and cladding modes in the few modes PCF-MZI section, are shown in Fig. 2.18 (a-1), (b-1) and (c-1) for modes m = 0, 11, and 26 respectively. These three different polarization states images were captured by SPIRICON OPHIR Photonics mode beam profiler model SP503U-1550 while a SLM laser generated output of a wavelength of 1550 nm. Figure 2.18 (a-2), (a-3), (b-2), (b-3), (c-2) and (c-3) show the modeling results of the field profiles for the fundamental quasi-TM modes calculated by RSoft Photonic Design Software which utilizes beam propagation method (BPM) and a generalized mode solver based on the Finite Element Method (FEM).

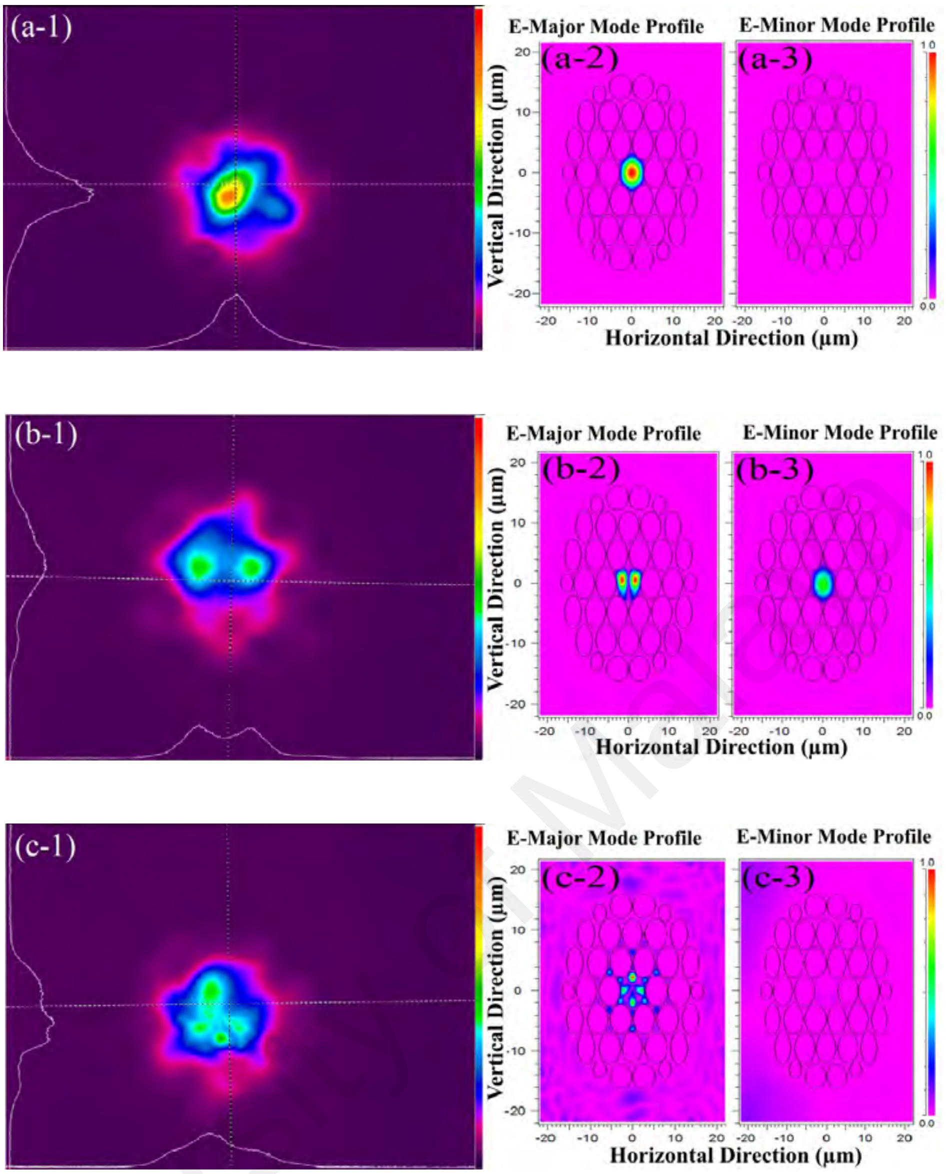

Figure 2.18: (a-1), (b-1) and (c-1) Image captured by photonics mode beam profiler for three polarization states variations via PC adjustments while a SLM laser source launched in a wavelength of 1550 nm. (a-2), (a-3), (b-2), (b-3), (c-2) and (c-3) are modeled field profiles for the fundamental quasi-TM modes corresponding to the experimental results for the modes with mode number of m = 0, 11 and 26 respectively.

Fields that propagates through a waveguide will not be exactly TE or TM modes; they will also have a field distribution in the direction perpendicular to the direction in which they are polarized. If electrical fields are considered as an example, the TM modes are normally in the y direction, (E-Major, corresponding to major components of the electric field) yet has a small amount of energy in the x direction (E-Minor, corresponding to minor components of the electric field). The modeled results were in agreement with the experimental results for the modes with the mode number of m = 0, 11 and 26, and these agreed results showed that the fundamental mode undergoes diffraction and couples into several higher order modes after diffraction. The guided mode with m = 0 is called the fundamental mode and those modes with m = 1, 2, … are higher-order modes, as explained in detail in (Jia-Ming, 2005). A portion of the fundamental core mode of PCF subsequently could become coupled to a single mode or several cladding modes of the PCF. A variety of optical paths corresponding to the different arms of the MZI emerged as a consequence of the effective refractive index of the cladding being smaller than that of the core. The effective refractive indices, n_{eff}, corresponding to mode number are tabulated in Table 2.2. The imaginary part of the effective refractive index, which describes confinement losses not associated with absorption, varies with hole size, the number of rings of holes, and wavelength, and give the minimum number of rings of holes required for a specific loss for given parameters (W. Song et al., 2007; White, McPhedran, de Sterke, Botten, & Steel, 2001).

Table 2.2: Effective refractive indices corresponding to mode numbers

Mode Number (m)	**Effective Refractive Index (n_{eff})**	
	Real	**Imaginary**
0	1.445051	-1.429e-018
11	1.444998	9.036e-008
26	1.441989	3.008e-005

The separation between consecutive peaks of a two-mode interferometer is given by $\Delta\lambda=\lambda^2/L\Delta n_{eff}$, where λ represents the source wavelength, L is the length of the PCF between the two splices, and Δn_{eff} symbolizes the effective refractive indices difference between the core and cladding modes calculated in Table 2.2. The Calculated FSR based on the achieved n_{eff} from Table I for three different modes are shown in Table 2.3.

Table 2.3: The FSR corresponding to mode numbers

Mode Number (m)	**Calculated FSR (nm)**
11	0.1847
26	0.1851

A constructed compact interferometer using a 10 cm length of few-mode PCF spliced on each end to SMF is shown for one side in the image labeled "spliced area" within figure 3.21. Manually splicing the PCF and SMF fiber at two points in series led to an inevitable collapse of the PCF air holes and creation of a very simple Mach-Zehnder interferometer (MZI). The length of the PCF was directly related to fringe spacing, and in this case the free spectral range (FSR) was about 0.2 nm, as observed in the transmission spectrum of the MZI displayed in figure 2.19. Figure 2.19 shows the transmission spectrum of the PCF-MZI after receiving output from a wide band white light source. The calculated FSR spacing shown in Table 2.3 are in agreement with the experimental FSR spacing achieved shown in figure 2.19.

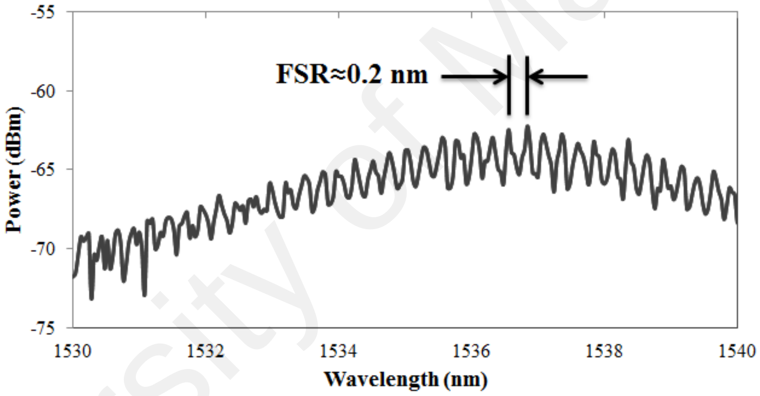

Figure 2.19: Transmission spectrum of the Mach-Zehnder interferometer.

The polarization characterization of an MZI based on the state of polarization (SOP) and power measurement at the interferometer output has been carefully investigated in (Mabrouki et al., 1996). The effects of changing various coupling constant (*k*), differential loss and deviation from average effective index n_{eff}, on group delay transfer, magnitude response and phase delay (φ) of asymmetric MZI like PCF-MZI has been theoretically investigated in (Roeloffzen et al., 2013).

CHAPTER 3: DEVELOPMENT OF STABLE DUAL-WAVELENGTH FIBER LASERS

3.1 Introduction

The generation of dual-wavelength fiber lasers (DWFLs) is basically the continuation of single wavelength fiber lasers that is done by adding one more wavelength selective element to ensure only two frequencies oscillating simultaneously inside the cavity. DWFLs have become light sources that are needed especially for certain applications such as an application for sensor (D. Liu, Ngo, Tjin, & Dong, 2007; Shengchun Liu, Yin, Zhang, & Chen, 2009; Pinto et al., 2010; Shimose, Okamoto, Maruyama, Aizawa, & Nagai, 1991), wavelength converter (Qureshi et al., 2007; Tomkos et al., 1998; Uchida et al., 1998), the generation of microwave (X. Chen et al., 2006; S. Pan & Yao, 2009; Pradhan, Town, & Grant, 2006; M. Soltanian et al., 2014; Jie Sun et al., 2006; F. Wang, Zhang, Zhang, & Xu, 2010) and Terahertz wave (Alouini et al., 1998; Gong et al., 2007; M. R. K. Soltanian, Sadegh Amiri, et al., 2015; M. Tang & Wang, 2010). As has been mentioned previously, the process in order to obtain a dual-wavelength fiber laser by using YDF, EDF and TDF is quite challenging. This is due to the homogenous line broadening effect of rare earth doped fiber as the active gain medium, causing mode competition that hinder the process to get dual-wavelength output power simultaneously (Gong et al., 2005; Jiang, Shum, Lin, Tjin, & Jiang, 2011; X. Liu & Lu, 2005; Pua, Ahmad, Harun, & De La Rue, 2012). Several techniques have been realized to overcome this problem and have been discussed in detail in Chapter 1. This include the cooling of the gain media using liquid nitrogen (N. Park & Wysocki, 1996; Shinji Yamashita & Hotate, 1996), polarization hole burning process (S. Feng, Xu, et al., 2008; Junqiang Sun et al., 2000), hybrid with inhomogeneous line broadening gain medium (Daru Chen, Qin, & He, 2007; S. Pan, Zhao, & Lou, 2008b), by using an elliptical gain media (Das & Lit, 2002), by using a polarization maintaining FBG for wavelength selection (S. Feng, Xu, Lu, Mao, et al., 2009; S. Feng, Xu, Lu, Ning, et al., 2009; B. Lin et al., 2010), by using a frequency shifter in the cavity (Bellemare et al., 2000), by using DFB fiber laser source with a separate resonance cavity (Jie Sun et al., 2006), four wave mixing effect (FWM) as a stabilizer (Mable P Fok & Chester Shu, 2007), and last but not least is by using the optical injection Fabry-Perot laser (C.-H. Yeh et al., 2009). Even though they seem effective in solving the mode competition issues, most of them are really difficult to handle and needed a complicated setup in order to generate the dual-wavelength outputs. Most of the methods are incapable of generating tunable dual-wavelength output laser source which makes our design a novel architecture as compared to the others.

In this chapter, several new techniques to generate dual-wavelength fiber lasers in three different regions of 1, 1.5 and 2 μm are presented. The gain media used are the YDF, EDF and TDF which all inhibit homogeneous profile, respectively. Issues related to mode competition, due to the homogeneous gain medium, are also addressed in discussing these techniques.

3.2 Dual-Wavelength Fiber Lasers in 1 μm region

In this part, I demonstrated for the first time to the best of my knowledge, a simple YDF laser with a short length photonic crystal fiber (PCF) and tunable band-pass filter (TBPF) incorporated in our ring cavity setup to obtain sets of stable and narrow spacing DWFL output. By carefully adjusting the polarization state of the cavity and TBPF, we successfully achieved a narrow spacing dual-wavelength operation using a simple laser ring PCF based setup. Our proposed setup also shows a highly stable operation behavior, and has a potential to be further exploited for DWFL optimization in 1-micron region source.

3.2.1 Experimental Setup

The configuration of the DWFL system using a PCF based Mach-Zehnder interferometer (MZI) is illustrated in Figure 3.2. The DWFL consist of 974 nm laser diode, a 980/1060 nm wavelength division multiplexing, a 70 cm YDF gain medium, a tunable band-pass filter (TBPF) with 1nm bandwidth, a polarization controller (PC), an isolator, a short-length of 10 cm PCF and a 90/10 optical coupler. The laser is first pumped with 974 nm center wavelength laser diode with maximum output power of 600 mW and launch power of 182 mW (Oclaro Model LC96A74P-20R), connected to a 980/1060 nm wavelength division multiplexing (WDM) coupler. One port of the WDM was fusion spliced to a 70 cm YDF gain medium (DF1100 Fibercore) which has peak absorption of 1300 dB/m at 977 nm and another port was coupled to the 90/10 optical coupler via its 90% port. The YDF output was then connected to an isolator to ensure unidirectional laser ring operation. The isolator output was then attached to the PCF-based Mach-Zehnder interferometer (MZI). A constructed compact interferometer using an L=10 cm few mode PCF was spliced into two segment of SMF. Figure 3.22 (b) illustrates the PCF- based MZI, these two spliced points were located in series and resulted in a simple Mach-Zehnder interferometer, whereby the length of the PCF was directly related to fringe spacing. The cross section of PCF is shown in the inset of Figure 3.2, which has a solid core of 4.37 μm in diameter, and surrounded by air holes with 5.06 μm diameter and separation of 5.52 μm between holes. Splicing of PCF and SMF fiber was done using Fujikura 45 PM splicer.

The TBF consists of an angled-tuned etalon filter. The 3 dB bandwidth of the TBF is about 0.8 nm with 0.05 nm tuning resolution. The maximum insertion loss of the TBF is about 3 dB with typical insertion loss of 1.5 dB, and the back reflection is about -50 dB. These characteristics make the TBF a reliable wavelength selector. A schematic diagram of the fiber-coupled TBF is shown in Figure 3.1. The beam from a single mode fiber (SMF) passes through a collimator, and next travels through a free space region where it encounters a Fabry-Perot etalon that acts as a filter. The propagating beam is then re-coupled into the second collimator before entering the second SMF. The Fabry-Perot etalon filter is mounted on a rotational stage. The incident angle of the propagating beam can be adjusted by rotating the Fabry-Perot etalon, thus allowing for the selection of particular wavelength. In this regards, any desired wavelength within the operation region of the TBF can be selected by tuning the high precision micrometer of the TBF that in turn will rotate the Fabry-Perot etalon.

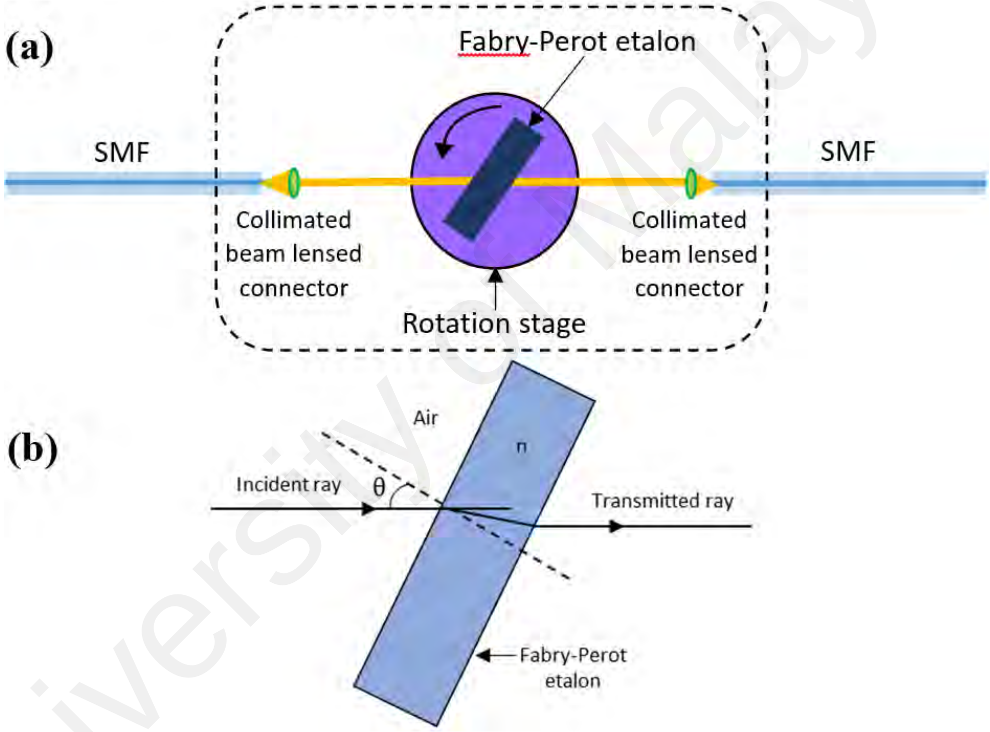

Figure 3.1: (a) An illustrative layout of the fiber coupled angle-tuned Fabry-Perot etalon and (b) propagation of light through the Fabry-Perot etalon

Figure 3.1 (b) shows the illustration of the propagating light into the Fabry-Perot etalon filter. The working principle of the TBF is adapted from the concept of Fabry-Perot interferometer as explained by Frankel *et. al* (Frenkel & Lin, 1989). Changing the incident angle of the beam allows wavelength selection, and this can be obtained by the following expression (Frenkel & Lin, 1989)

$$\lambda = \left(\frac{2nL}{m}\right)(\cos\theta) \qquad 3.1$$

where L is the thickness of the etalon filter, m is an integer, n is the refractive index of the etalon, λ is the wavelength of interest and θ is the angle between the incident beam and the normal axis.

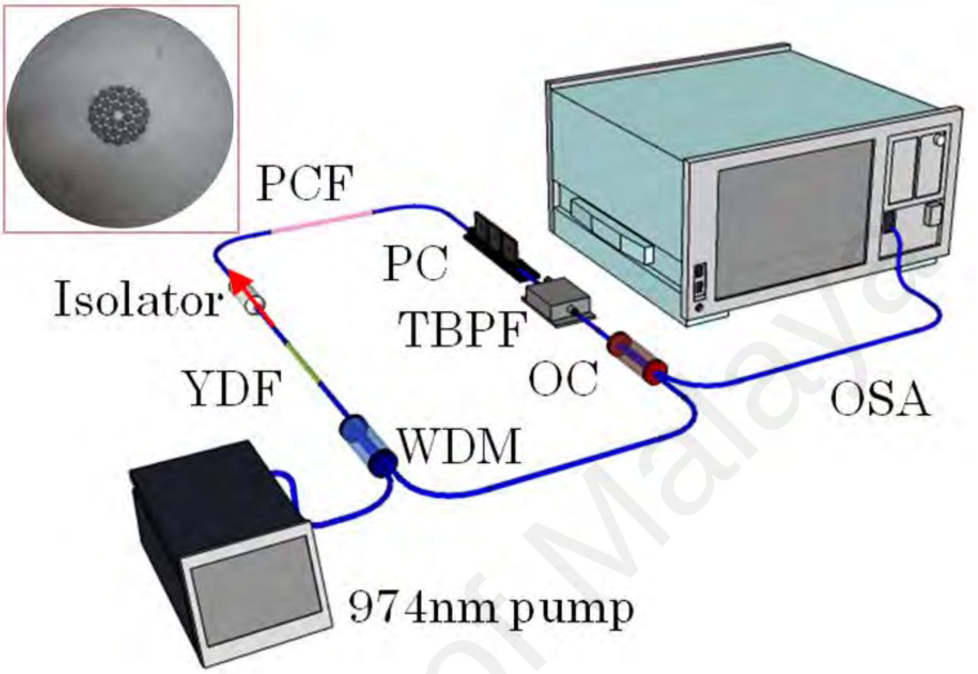

Figure 3.2: DWFL based system setup, *Inset*: cross section of PCF

The output of the PCF was connected to the polarization controller (PC) that controlled the polarization state of the laser cavity and the PC output was attached to the tunable band pass filter (TBPF). TBPF output is then connected to the input of 90/10 fused biconical optical coupler (OC). The 10% end of coupler was then connected to the input port of an optical spectrum analyzer (OSA) of type YOKOGAWA AQ6373 with a resolution of 0.02 nm. Figure 3.3 shows the transmission spectrum of the PCF-based MZI filter with unpolarized amplified spontaneous emission (ASE) source. The aggressive interference pattern, seen clearly in the red line of Fig. 2, was responsible for the narrow lasing when the ring laser was closed. Lasing usually occurred at the interferences peaks, and by finely controlling the system polarization state, the lasing wavelength is able to switch from one to the other and creates single or multi-wavelength laser output.

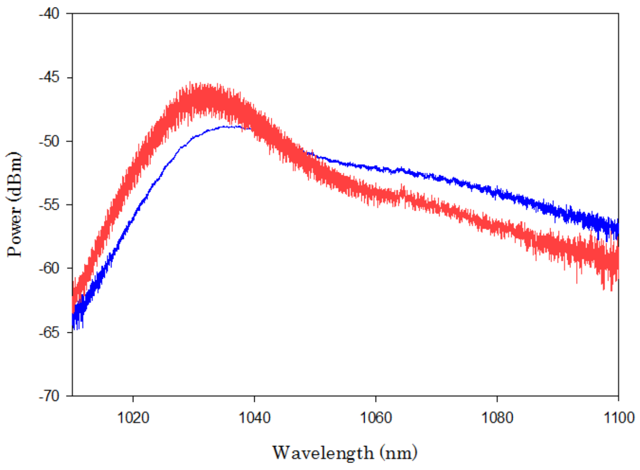

Figure 3.3: ASE spectrum with PCF (red) and without PCF (blue)

The first collapse region diffracts the fundamental mode which is passing by and therefore the core and cladding modes are excited in the few modes PCF section. Some part of the fundamental core mode of PCF can be coupled to a single or several cladding modes of the PCF. Phase shifting in the same physical length of L is a product of different effective refractive index of core and cladding modes. As the effective refractive index of the cladding is smaller than core the different optical paths corresponding to arms of the Mach-Zehnder interferometer can be achieved. The fundamental and cladding modes accumulate a phase difference along the PCF due to different phase velocities. This phase difference depends on the length of PCF and the wavelength of the guided light. By reaching the modes to the other collapsed area of PCF, the cladding modes re-coupled to the core mode. Since the phase difference and the phase velocities are wavelength dependent, the optical power transmitted by the interferometer will be minimum at certain wavelengths and maximum at the others. The separation between consecutive peaks of a two-mode interferometer is given by

$$\Delta\lambda = \lambda^2 / \Delta n_{eff} L \tag{3.2}$$

where Δn_{eff} is the effective refractive indices difference between the core and cladding modes and L is the interferometer length. The core and the cladding of the PCF play the role of arms of a Mach–Zehnder interferometer, while the collapsed points act as couplers splitting or combining light powers in the arms of the interferometer.

3.2.2 Results and Discussions

In the experiment, the pumping power for our YDF from the laser diode is set to 202.0 mW. The emission laser lines directly depend on the spectral transmission peaks produced by the photonic crystal fiber. In our case, we performed the spectral shifting by adjusting the PC and TBPF incorporated in the laser setup. The adjustment of the PC will rotates the polarization states of the laser so that the PCF allows to pass by and consequently continuous adjustment of the DWFL within the ring cavity is achieved. In order to obtain a narrow spacing dual wavelength laser it is necessary to adjust the tunable band-pass filter and then followed by tuning the polarization controller. The tunable band-pass filter has a wide range of tuning wavelength starting from 1018nm to 1070nm. In this experiment, the TBPF is adjusted until the single wavelength is set to 1040nm. The PC is tuned to achieve dual wavelength at the same power, some time we also need to fine retuning the TBPF to obtain dual wavelength laser. We obtained 2 sets of stable narrow spacing dual-wavelength that are 0.03nm and 0.07nm by using a simple design of dual wavelength fiber laser (DWFL) with a short cavity length of 6m as shown in Figure 3.4 (a). The observed side mode suppression ratio (SMSR) for both sets of dual-wavelength is 50dB. The high SMSR is contributed by TBPF in the ring cavity allow spectrum within 1nm wavelength range to pass through thus reducing the generation of amplified spontaneous emission (ASE).

The advantage of this proposed set up is the flexibility of TBPF in tuning the laser wavelength in difference wavelength region within the tuning range of the TBPF and hence the capability to adjust the narrow spacing dual wavelength fiber laser by adjusting the PC. Therefore in order to obtain dual wavelength in other wavelength region, the

TBPF is tuned to achieve single peak laser at center wavelength of 1064nm, then the PC is fine adjusted until dual wavelength laser achieved with almost same peak power level. Moreover, the spectral separation between these two lines can be varied by finely readjusting the polarization controller. Figure 3.4 (b) show 3 sets of stable narrow spacing dual-wavelengths that are 0.1nm, 0.2nm and 0.40nm at other wavelength region. The observed side mode suppression ratio (SMSR), measured by Yokogawa AQ6370B OSA with the resolution of 0.02 nm, for all sets of dual-wavelength is increasing from 37 dB to 49dB with the decreasing spacing wavelength from 0.40nm to 0.1nm. The higher resolution OSA will give more accurate measurement of SMSR.

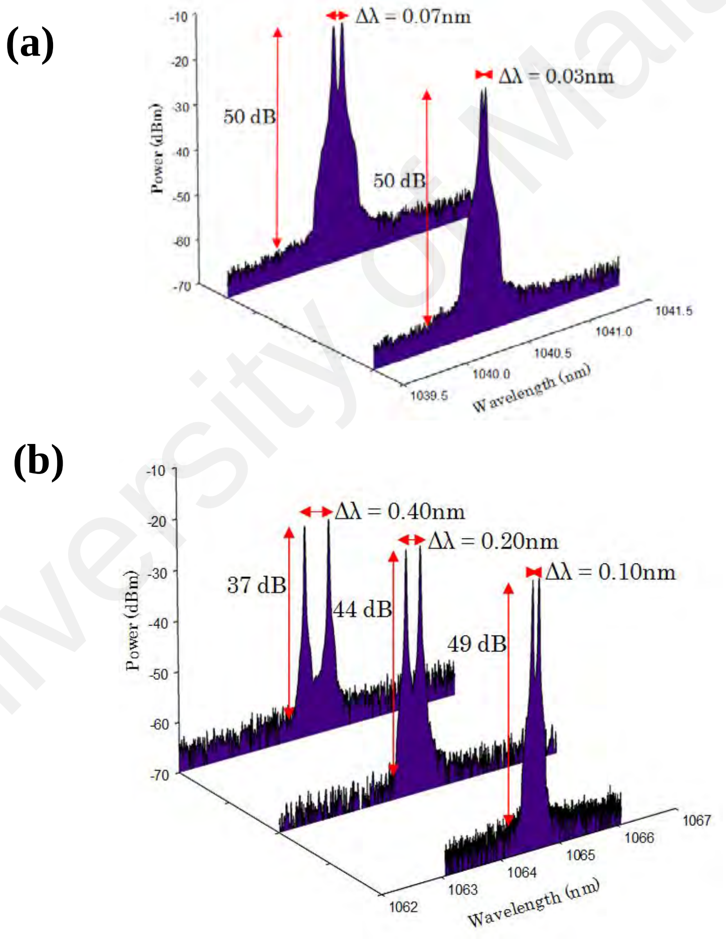

Figure 3.4: Spectral separation of tunable dual-wavelength in (a) 1040 nm region, (b) 1060 nm region

It is worth mentioning that all the dual-wavelength set were stability tested over time. Figure 3.5 and Figure 3.6 show the dual-wavelength stability scan for each set in the period of 15 minutes at 1040nm and 1064nm wavelength region respectively. They showed a maximum fluctuation of ~0.8 dB, which is shown on the right side of Figure 3.5 and wavelength fluctuation of less than 0.01 nm. We can say that the dual-wavelength demonstrated in this paper is highly stable in the experiment done at room temperature. We proved that the homogeneous broadening effect of YDF has been suppressed to a very low level.

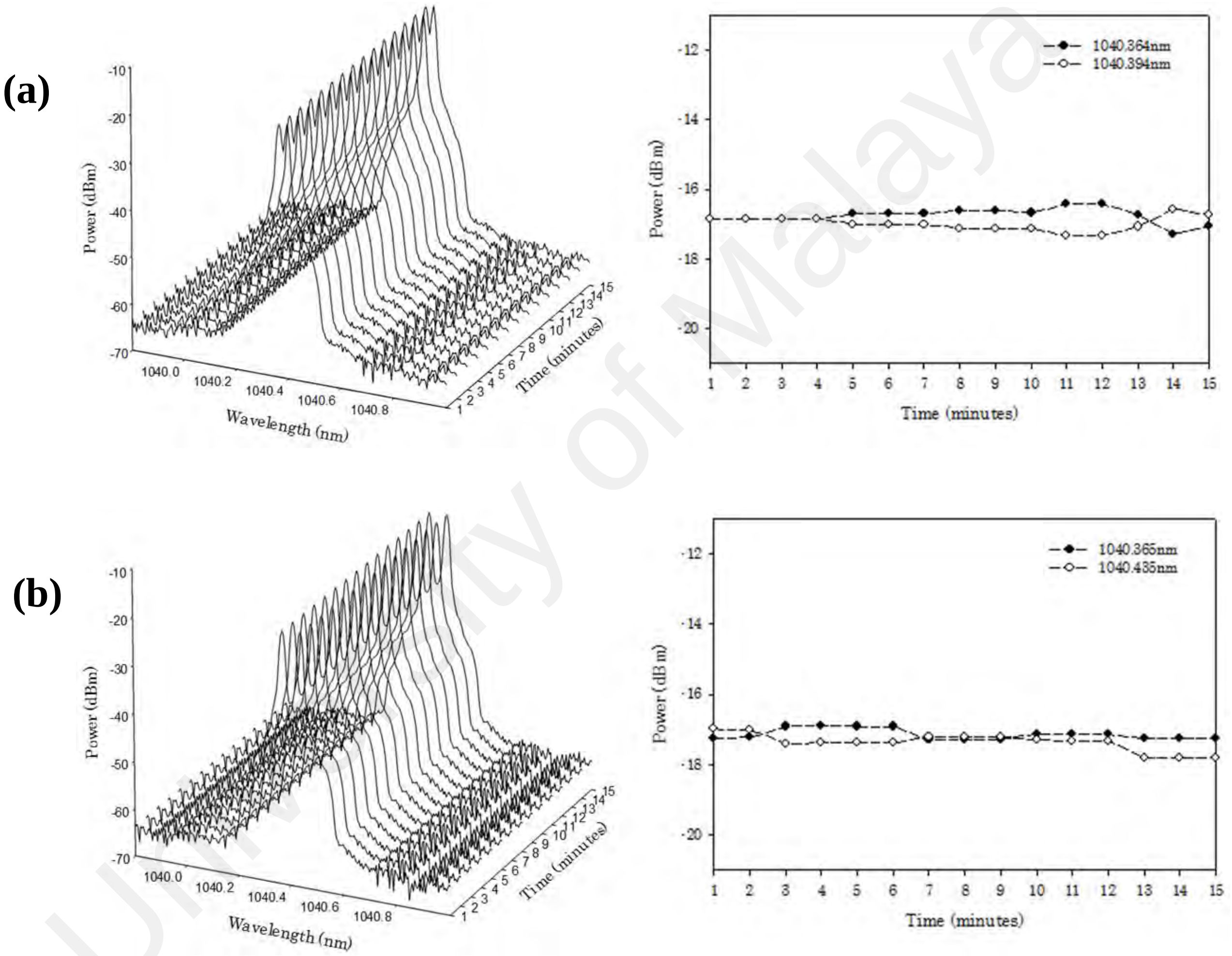

Figure 3.5: Dual wavelength and Peak power stability test with tunable spacing of (a) 0.03nm with λ_1=1040.364nm and λ_2=1040.394nm and (b) 0.07nm with λ_1=1040.365nm and λ_2=1040.435nm

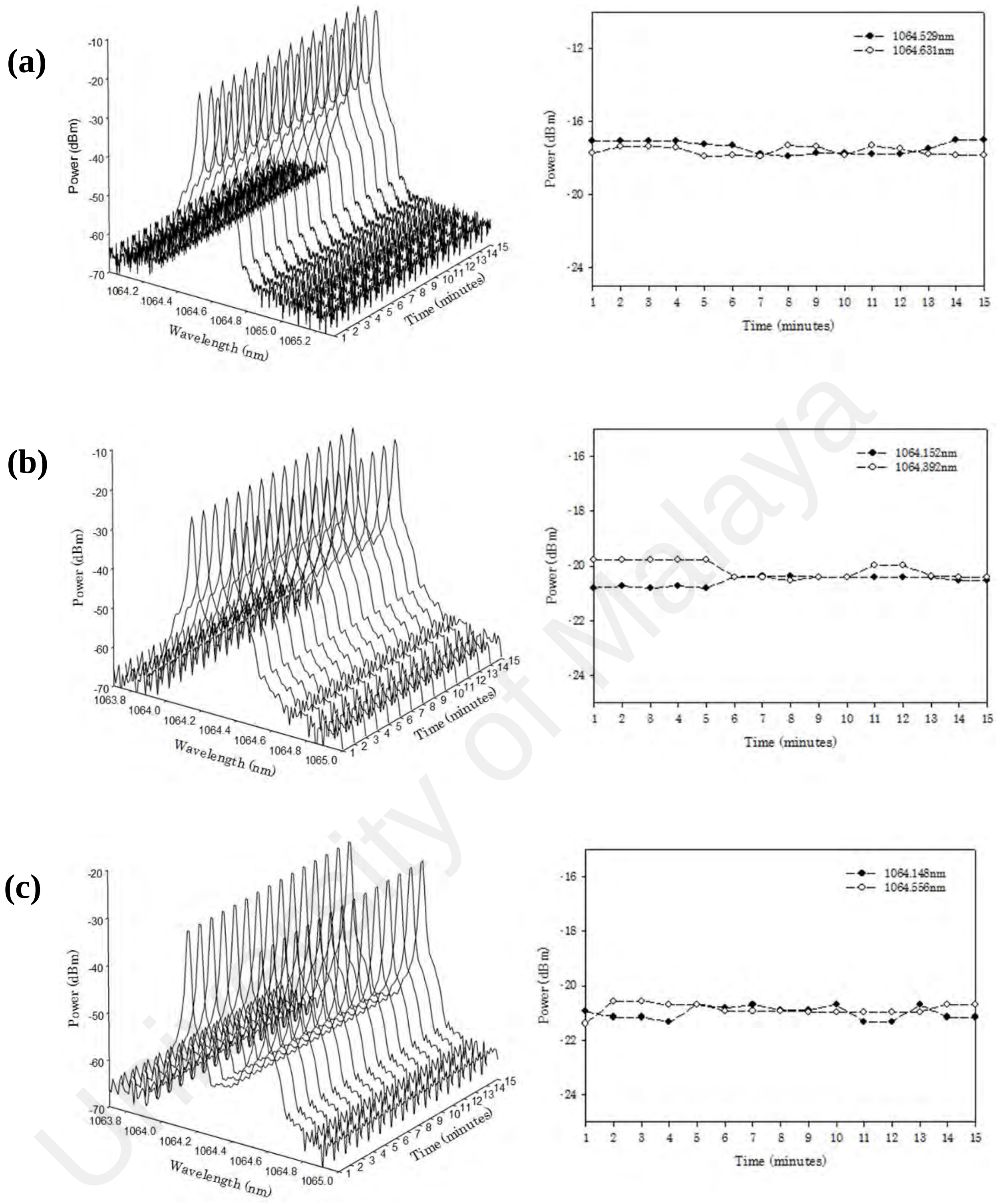

Figure 3.6: Dual wavelength and Peak power stability test with tunable spacing of (a) 0.10nm with λ_1=1064.529nm and λ_2=1064.631nm (b) 0.20nm with λ_1=1064.152nm and λ_2=1064.392nm (c) 0.40nm with λ_1=1064.148nm and λ_2=1064.556nm.

3.3 Dual-Wavelength Fiber Lasers in 1.5 µm region

3.3.1 Dual-Wavelength Fiber Lasers utilizing PCF

In this part, a simple Erbium doped fiber laser (EDFL) with a short length of Photonic Crystal Fiber (PCF) incorporated in a ring cavity configuration is proposed to achieve stable and narrow spacing DWFL utilizing polarization dependent loss (PDL) effect. The setup has advantages of simple structure, adjustable narrow spacing of DWFL, stable and low cost.

3.3.1.1 Experimental Setup

The configuration of the DWFL system based on the PDL controlling is schematically shown in Figure 3.7. The DWFL consists of a 980 nm pump laser diode, a 980/1550 nm wavelength division multiplexing (WDM), a 3 m EDF, a tunable band-pass filter (TBPF) with 1 nm bandwidth, isolators, a polarization controller (PC), a very short length of 10 cm PCF, and a 2:98 fiber based coupler. The 980 nm pump laser is directed into the fiber laser ring cavity through a WDM to provide excitation to the gain medium. TBPF is used to limit or confine the oscillation of dual wavelength laser in a narrow spacing. The isolators are used to assure unidirectional operation of the laser as to achieve a more stable lasing condition. The PC working at C-band region is used to adjust the polarization of light propagating inside the ring cavity. PCF plays the main role in the setup to stabilize the DWFL based on its high nonlinearity and large birefringence coefficient. The micrograph of the HN-PCF cross-section structure is shown in the inset in Figure 3.7. The PCF is a solid core (~4.37 µm diameter) PCF surrounded by air holes with 5.06 µm diameter and separation of 5.52 µm between holes. The 2%:98% fiber based coupler is used to direct part of the laser power out of the laser cavity for measurement, analysis and application.

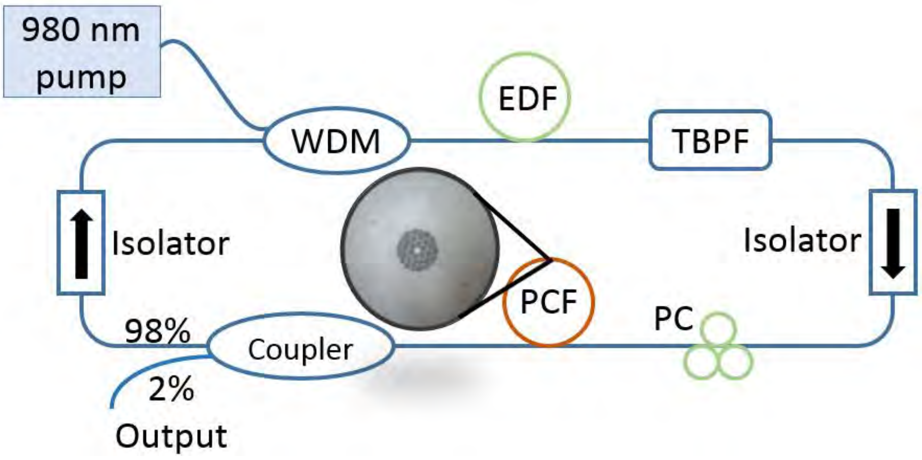

Figure 3.7: Experimental setup of PDL based dual wavelength fiber laser.

3.3.1.2 Experimental results and discussion

The 980 nm pump laser is set at 90.0 mW and the laser output is continuously monitored by Optical Spectrum Analyzer (OSA) from the 2% output of the fiber coupler. PC is tuned to achieve single or dual wavelengths fiber laser from the setup. With similar setup, more lasing wavelengths are achievable by removing the TBPF from the ring laser. However, the current work focuses on narrow spacing DWFL for applications such as microwave generation and radio over fiber. Figure 3.8 shows the experimental result of the DWFL with 81 pm spacing between two wavelengths lasing at 1553.726 nm and 1553.807 nm. Due to the dependence of the lasing wavelength on polarization states, lasing wavelength can be change by fine tuning the PC. The adjustment of the PC will rotates the polarization states of the laser so that the PCF allows to pass by and consequently continuous adjustment of the DWFL within the ring cavity is achieved. By achieving dual wavelengths laser with similar peak powers, a stable DWFL can be obtained. During the experiment, the TBPF is first tuned to a center wavelength of 1553.726 nm to limit laser oscillation within 1553 nm to 1554 nm. The PC is then fine-tuned to obtained dual wavelength laser with almost similar peak powers at -18.8 dBm and -19.0 dBm at 1553.726 nm and 1553.807 nm respectively as shown in Figure 3.8.

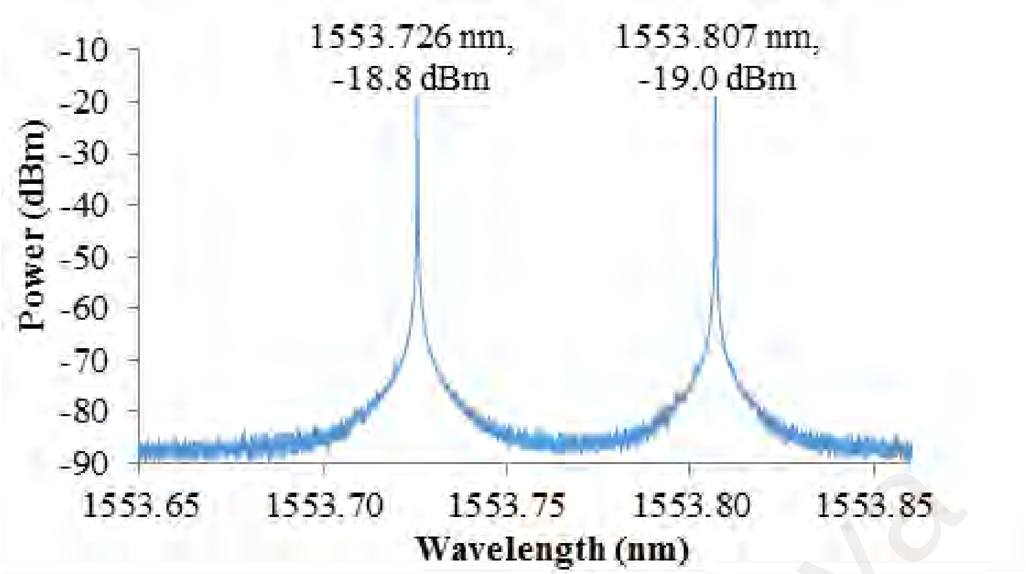

Figure 3.8: Optical spectrum of DWFL lasing at wavelengths 1553.726 nm and 1553.807 nm with peaks power of -18.8 dBm and -19.0 dBm respectively.

Simple design of the DWFL with short ring cavity length of 6 m will minimize the broadening of the lasing and achieve narrow line-width of only 3 pm measured using OSA with spectral resolution of 0.17 pm. Besides that, the DWFL also achieves high signal to noise ratio (SNR) of more than 60 dB as compared to most of the previously reported work that achieved a typical SNR of about 40 dB [10]. The high SNR is basically contributed by two main factors; the first is the function of the TBPF in the ring cavity. The TBPF in the ring cavity allows only spectrum within the 1 nm range to pass through while filtering out other wavelengths, thus reducing the generation of Amplified Spontaneous Emission (ASE) during the lasing period.

The second is the polarization state of both the lasers. Polarization state of the laser output is monitored using a polarization analyzer. When the laser operates under dual wavelength condition, the polarization state of the laser output is a combination of both wavelengths polarization states. To observe the polarization state of each wavelength individually, PC is carefully adjusted so that only a single wavelength is lasing. The polarization state for each wavelength for the DWFL at 1551.736 nm and 1552.040 nm are shown in Figure 3.9 (a) and (b) respectively. The azimuth angle of the polarization state for 1551.736 nm and 1552.040 nm are at 35.311˚ and -49.677˚ respectively. The azimuth angle between both wavelengths is 84.988˚ which means that they are almost perpendicular to each other. Figure 3.9 also shows that the polarization state is in ellipse polarize with ellipticity of 32.213˚ and -23.921˚ which shows that both are in an opposite rotation angle.

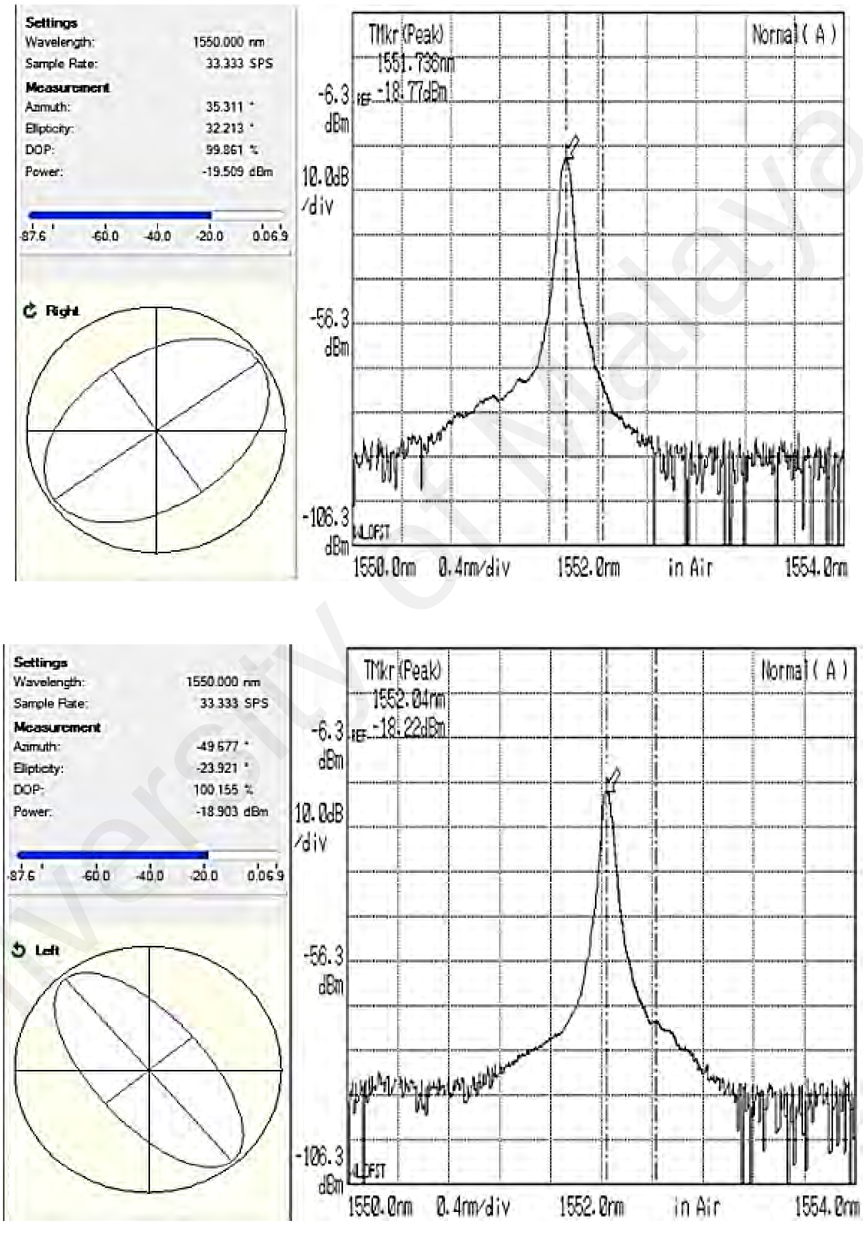

Settings
Wavelength: 1550.000 nm
Sample Rate: 33.333 SPS
Measurement
Azimuth: 35.311 °
Ellipticity: 32.213 °
DOP: 99.861 %
Power: -19.509 dBm

Settings
Wavelength: 1550.000 nm
Sample Rate: 33.333 SPS
Measurement
Azimuth: -49.677 °
Ellipticity: -23.921 °
DOP: 100.155 %
Power: -18.903 dBm

Figure 3.9: Polarization state of each wavelength from dual wavelength fiber laser at (a) 1551.74 nm and (b) 1552.04 nm.

It is known that polarization hole burning (PHB) effect will reduce the SNR due to polarization dependent gain saturation by polarized signal at different wavelength. In the proposed DWFL, the two lasers are elliptically polarized with both polarization state perpendicular to each other. This condition will minimize the polarized saturated signal in the ring laser as the signals are not in the same polarization state. Hence, ASE emission due to the PHB effect will be reduced and leads to high SNR in the DWFL (D. Zhao et al., 2002). In terms of stability of the DWFL, the peak power for both wavelengths is measured at one minute interval for 15 minutes as shown in Figure 3.10. The peak power fluctuation for both wavelengths falls within 0.6 dB with a wavelength shift of less than 10 pm which is considered very stable. Mode competition among wavelength due to the homogeneous broadening effect of the EDF has been suppressed to a very low level.

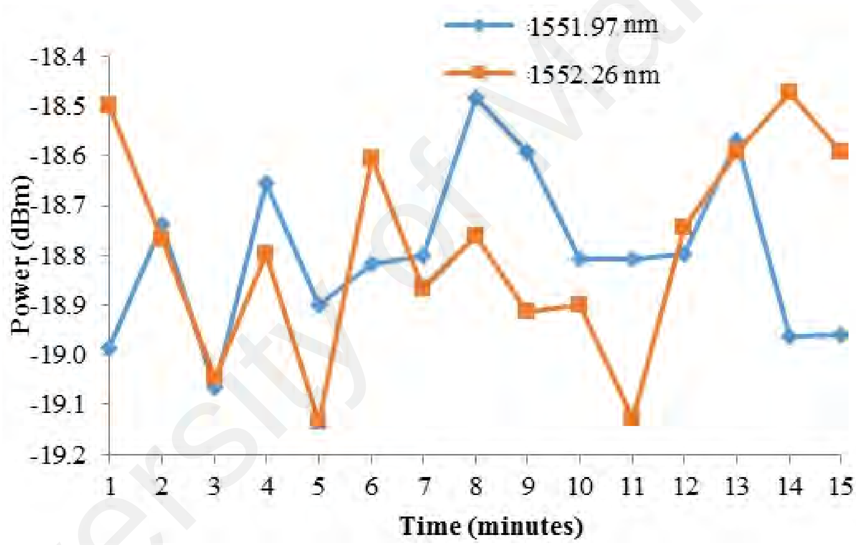

Figure 3.10: Optical power fluctuation of both lasing wavelength at 1551.97 nm and 1552.26 nm for 15 minutes.

One of the advantages of the proposed setup is the capability of adjusting the spacing of the two lasing wavelengths. The flexibility of the TBPF in tuning the laser wavelength will allowed different dual wavelength spacing to be selected. Due to different survival modes in the ring cavity, different combinations of lasing wavelengths are possible at different wavelength region. Figure 3.11 shows the DWFL operating at different wavelength region with different wavelength spacing. Besides the 80 pm spacing shown in Figure 3.8, Figure 3.11 shows different wavelength spacing at 170 pm, 410 pm, 520 pm, and up to 600 pm at different wavelength regions. It is possible to achieve larger wavelength spacing by fine adjustment on the TBPF and PC. Besides that, Figure 3.11 also shows the stability of the DWFL within 15 minutes with one minute scan interval. Most of the DWFL is stable within the fluctuation of 0.6 dB.

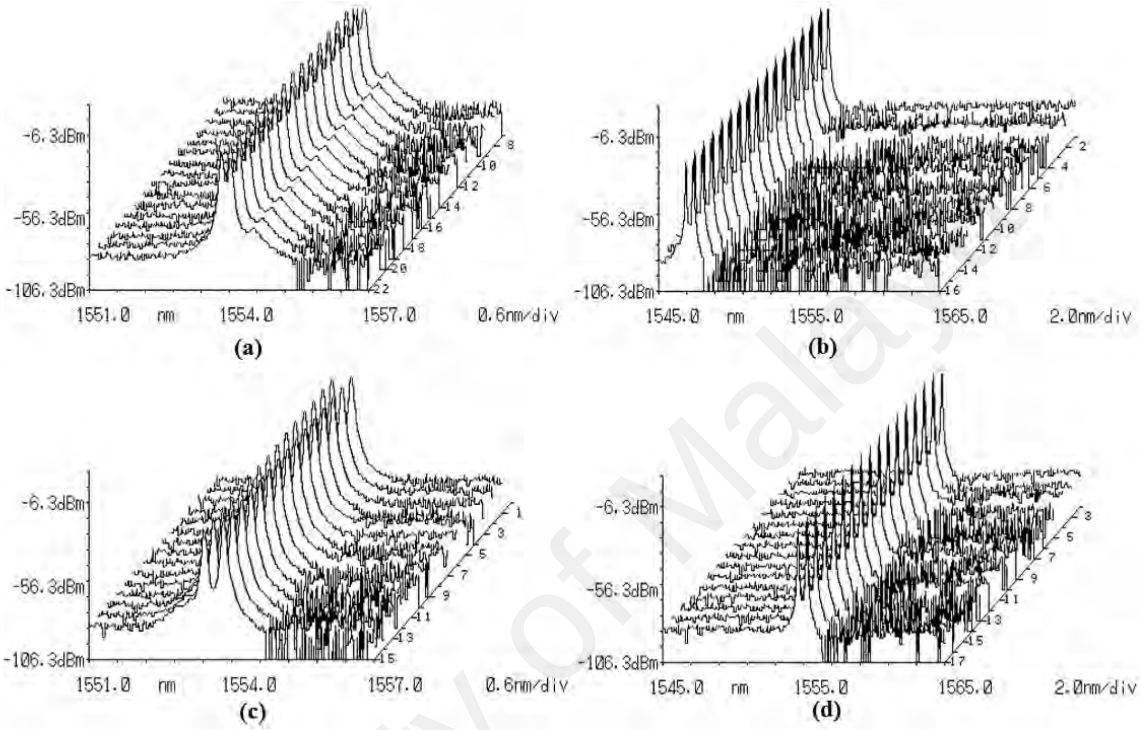

Figure 3.11: Stability of dual-wavelength fiber laser with narrow spacing of (a) 170pm at 1553.85 nm and 1554.02 nm, (b) 410pm at 1553.42 nm and 1553.83 nm, (c) 520pm at 1546.96 nm and 1547.48 nm, and (d) 600 pm at 1554.62 nm and 1555.22 nm over 15 minutes with interval scanning of every 1 minute.

3.3.2 Dual-Wavelength coherent source by splicing a mode-locked laser

In this part, generation of multi-wavelength coherent source operating at 1.5 μm by utilizing micro-ring resonator is investigated and demonstrated both theoretically and experimentally. The generated multi-wavelength has maximum power in its central wavelength at 1560 nm. Subsequently, stable and tunable DW coherent source outputs are obtained from a mode-locked laser spectrum sliced by an add-drop micro-ring resonator with the aid of a tunable band-pass filter (TBPF) and a FBG. The evolution of the theory of mode-locking has been reviewed and some of the salient experiments have been discussed in the context of the theory in the ref (Haus, 2000). Two silicon oxynitride

(SiOxNy) micro-ring resonators with different diameters are used as narrowband filter for the generation of stable tunable dual-wavelength lasers with variable free spectral range (FSR) accordingly. Extraction of DW coherent source signals is demonstrated with side mode suppression of more than 30 dB. The micro-ring resonator can be readily integrated into a photonics integrated chip (PIC) for multifunctional applications as the achieved FSR is in linear relation with the ring resonators' diameter.

3.3.2.1 Experimental setup

Figure 3.12 shows the experimental setup employed for stable tunable dual-wavelength laser generation, in which the fiber laser layout consists of a mode-locked ring laser connected to a single add-drop micro-ring resonator filter. The ring laser utilized a 0.9 m long high concentration erbium-doped fiber (EDF) (Leikki Er80-8/125) as gain medium. The numerical aperture (NA) of the EDF is 0.21, with an absorption coefficient of 84 dB/m at 980 nm and mode field diameter of 5.7 µm at 1550 nm. The EDF was backward-pumped by a Lumics 980 nm laser diode (LD) through a wavelength division multiplexer (WDM). One end of the EDF was connected to the common or signal port of the WDM, while the other end was connected to Isolator 1 to have backward pumping and to ensure unidirectional light propagation in the laser cavity. The Isolator 2 was connected between the WDM and the polarization controller (PC) to prevent unwanted back reflections from the PC towards the gain medium. The PC was subsequently connected to a carbon nanotube (CNT) embedded between two ferrules which acts as the saturable absorber. The output of the embedded CNT was guided towards a 50:50 coupler, which extracts a portion of the signal for analysis. One of the 50% port was connected to Isolator 1, which was then connected to the gain medium. This loop completes the laser cavity.

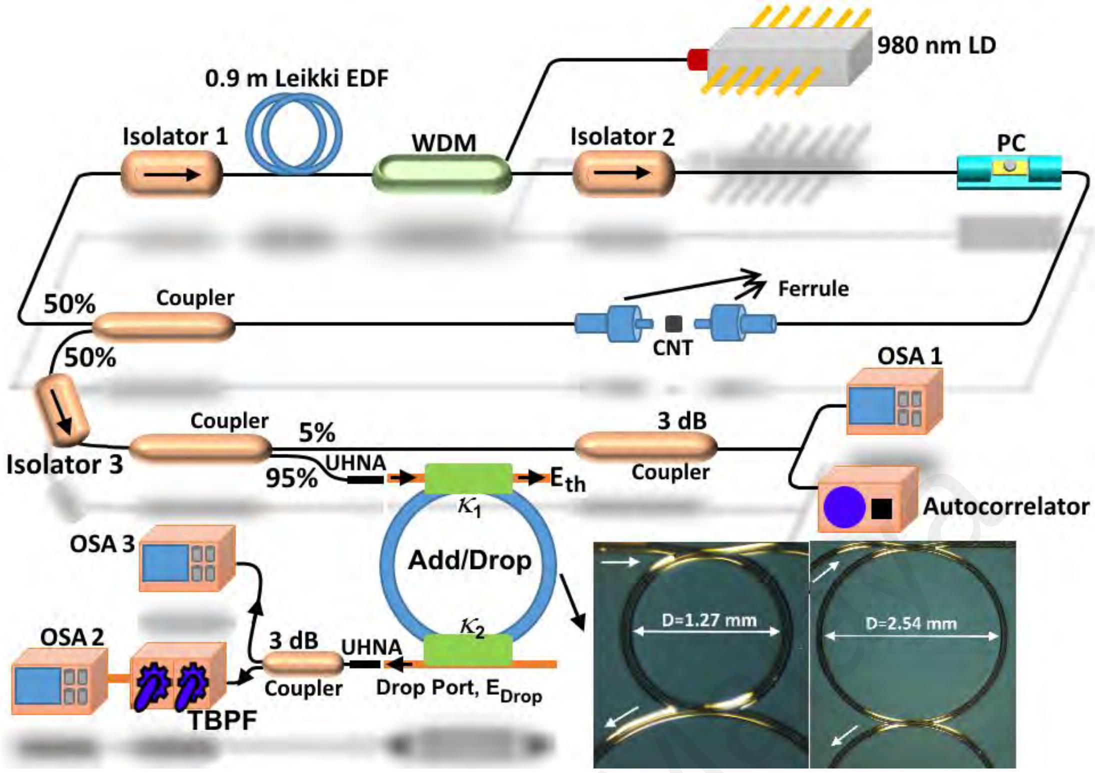

Figure 3.12: Experimental setup to generate stable tunable dual-wavelength

In order to generate the stable tunable dual-wavelength laser, the 50% output port was divided into two portions using a 95:5 coupler through Isolator 3, and the 95% port was spliced to a 10 cm Ultra-high numerical aperture (UHNA) fiber with NA of 0.41 using a fusion splicer (Fujikura 45PM). The UHNA fiber was then aligned with the micro-ring resonators using 3-axis linear alignment stage for the generation of evenly spaced multi-wavelength comb spectrum. The 5% port of the coupler was utilized for monitoring purposes. In order to monitor the extracted output prior to the micro-ring resonator, the generated mode-locked signal from the 5% port was divided into two portions with equal power using a 3 dB coupler; one portion was directed to an optical spectrum analyzer (OSA1) (YOKOGAWA AQ6370B) for spectral analysis while the other portion to an auto-correlator to measure the pulse-width. Output from the micro-ring resonator was coupled to a 3dB coupler through a 10 cm long UHNA fiber. One of the 50% output of the 3dB coupler is then connected to a high resolution OSA2 (APEX AP2051A) via tunable band-pass filter (Yenista xtm-50) with a wavelength resolution of 5 pm and

FWHM of 1 pm to select the desired wavelength pair from the generated multi-wavelength output comb. The OSA3 (YOKOGAWA AQ6370B) was used to monitor the generated multi-wavelength output comb.

Silicon oxynitride (SiO_xN_y) micro-ring resonators were used as the narrow band-pass filter. The SiON film deposited using plasma enhanced chemical vapour deposition (PECVD) has refractive index of 1.513. The film was deposited on a silicon substrate with a 15 μm thick thermal oxide layer as an under cladding buffer. Waveguides are defined through reactive ion etching (RIE) followed by deposition of a boro-phospho-silicate glass (BPSG) layer as the over cladding. The refractive index contrast is 4.5%. The input and output ports of the micro-ring resonators are shown in the inset of Figure 3.12. The SiON micro-ring resonators have a small footprint of 3×5 mm^2. The finesse (F), given by the ratio $FSR/FWHM$, was approximately 15.53. Two micro-rings having diameters of 2.54 and 1.27 mm were used, and their Q factors are 1.2×10^5 and 0.6×10^5 respectively. Using the time-bandwidth product for the case of mode-locked laser or solitons which is 0.32, the minimum pulse duration of laser pulses after micro-ring resonator filtering are approximately 200 and 100 ps for the micro-ring resonators having diameters of 2.54 and 1.27 mm respectively.

3.3.2.2 Experimental results and discussion

Mode-locked fiber laser was generated by incorporating CNT polymer composite as a saturable absorber (SA) in the ring laser cavity. A small piece of CNT composite with an area of 1 mm^2 is placed carefully on the top of a fiber ferrule by using a very thin layer of index matching gel (IMG) on its surface. The ferrule with the CNT layer is then connected to an FC/PC adaptor, and a second fiber ferrule with a clean surface is then connected to this adaptor, thereby sandwiching the CNT layer in between the two ferrules and thus creating the required SA. Mode-locked laser is achieved with a launched pump power of 50 mW, with the laser optical spectrum measured using the OSA 1. The laser spectrum is shown in Figure 3.13 (a).

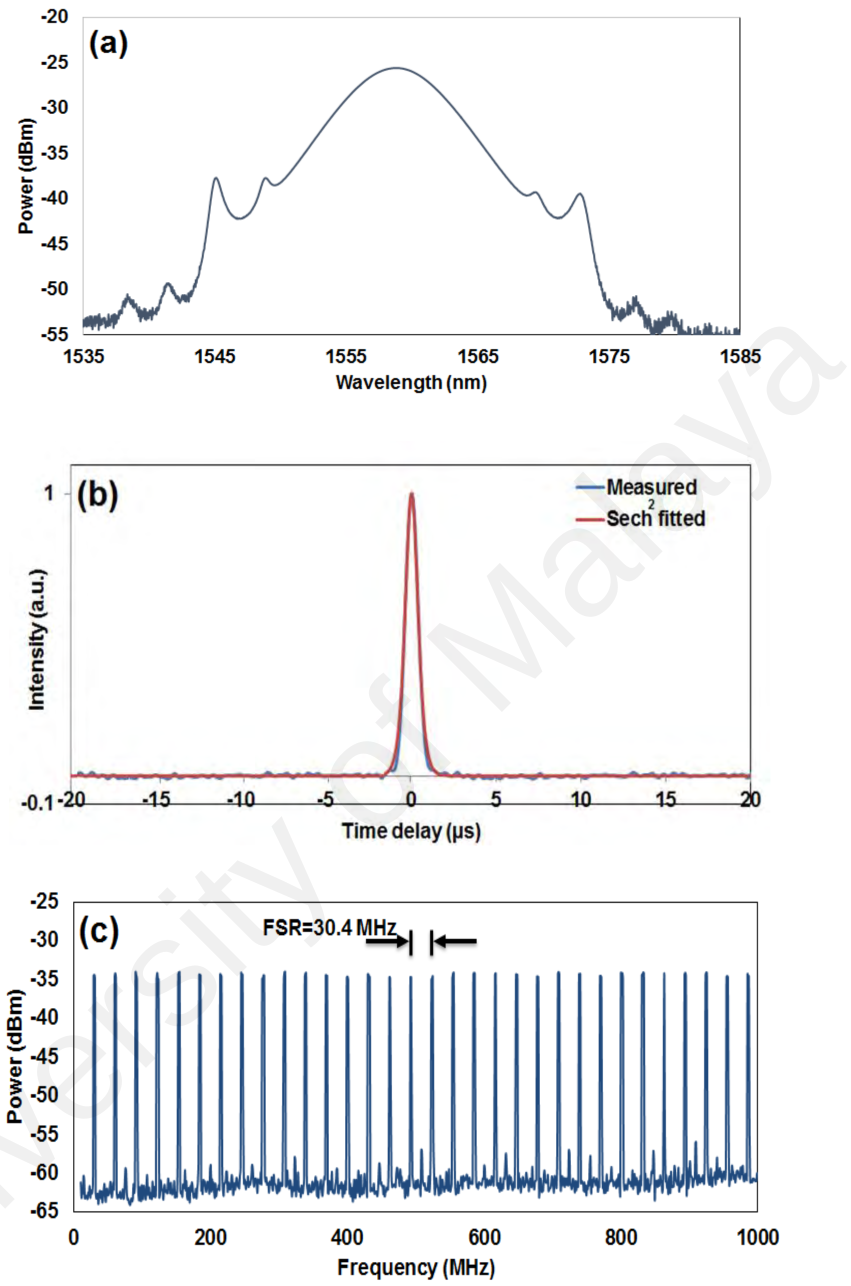

Figure 3.13: (a) Mode-locked laser spectrum taken from OSA 1, (b) Auto-correlator trace of the generated mode-lock and (c) RF spectrum of the generated mode-locked laser with FSR=30.4 MHz.

The corresponding pulse-width of the mode-locked laser measured using an Alnair HAC-200 auto-correlator (including an embedded electrical amplifier) is shown in Figure 3.13 (b). The estimated pulse durations at the full-width at half maximum (FWHM) point is 570 fs. The autocorrelation trace and spectrum are well fitted by a Sech^2

pulse profile, indicating that mode-locked laser is generated. Figure 3.13 (c) shows the RF spectrum of the generated mode-locked laser taken by Anritsu MS2667C RF spectrum analyzer. To obtain this result the RF spectrum analyzer is replaced by the OSA1 in the main configuration setup shown in Figure 3.12. The free spectral range of the optical fiber ring resonator (cavity) is the frequency spacing of its axial (Gaussian-shaped) resonator modes. It is therefore also called axial mode spacing. For an optical fiber ring resonator, the frequency spacing between two successive peaks known as FSR or $\Delta\nu$ is determined by the group index (n_g), rather than by the ordinary refractive index:

$$\Delta\nu = \frac{c}{n_g L} \tag{3.3}$$

where c is the speed of light in vacuum and L is the total length of optical path around the ring. The FSR of 30.4 MHz shown in Figure 3.13 (c) is a result of beating of the adjacent modes generated by mode-locked laser. Introducing a delay line increases the L, the total length of optical path around the ring cavity, and consequently decreases the FSR. Moreover, introducing an optical delay line in the mode-locked laser cavity, by for example adding SMF in the ring cavity, enables fine-tuning of the cavity length, such that the modal spacing could be accurately defined (Ironside et al., 2011).

The generated mode-locked laser is then launched into two different micro-ring resonators independently using fiber butt-coupling technique. To minimize coupling loss between SMF and the micro-ring resonator, short length of UHNA fibers were spliced to the two end of SMF as shown schematically in the Figure 3.12 and the splice loss of 0.5 dB for each side was achieved. Using three 3-axis linear alignment stages to couple the mode-locked laser into and out of the micro-ring resonator, the insertion loss of the micro-ring resonator was measured to be 16 dB. The problem of coupling an optical fiber to a waveguide (or a waveguide to a fiber) is critically important for overall performance of integrated/fiber-optic systems. The most straight forward way of coupling a fiber and a waveguide is the end-fire or butt coupling technique in which the two are aligned end to end and butted into contact. The key factors affecting butt coupling between a fiber and a waveguide are area mismatch between the waveguide cross-sectional area and that of the fiber core, misalignment of the waveguide and fiber axes, and numerical aperture mismatched loss (caused by that part of the waveguide light output profile that lies outside of the fiber's acceptance core or vice versa). In the case of butt coupling of the semiconductor waveguide and a glass laser, reflection at the glass-air-semiconductor interface are also important. The insertion loss problem becomes more important as the refractive-index contrast of the integrated optical waveguides, Δ, which is given by the core refractive index n_{co} and the cladding refractive index n_{cl}, is increased (Lierstuen & Sudbø, 1995):

$$\Delta = \frac{{n_{co}}^2 - {n_{cl}}^2}{2{n_{co}}^2} \approx \frac{n_{co} - n_{cl}}{n_{co}} \qquad 3.4$$

To achieve a good match to optical fibers, silica waveguides are usually designed to have Δ in the range 0.3–0.7%. In considering coupling of light from the fiber into the waveguide, the problems of area mismatch and numerical aperture loss are limiting factors because the core diameter of a single mode fiber is approximately 10 μm and the rectangular waveguide dimensions are about 4 μm. Exact calculation of the coupling efficiency from fiber to waveguide cannot be done until a particular waveguide and optical fiber have been selected and their characteristics known; however, a typical experimentally observed coupling efficiency for this situation would be about 10% (Mentzer, 2011). Robertson et al. (Robertson, Ritchie, & Dayan, 1985) have performed a theoretical analysis of butt coupling between a semiconductor rib waveguide and a single mode fiber, and have designed an optimized waveguide structure with a large (single) mode size for which they calculate a coupling efficiency of 86%. However, no experimental data is available. To obtain efficient coupling between optical fibers and waveguides very accurate alignment of the fiber and waveguide is required. Fiber positioning systems provide repeatable accuracy of 0.1 µm.

The most basic type of optical resonator is the Fabry-Perot cavity resonator, which is the archetype of optical devices. The Fabry-Perot cavity is comprised of two parallel reflective planes separated by a distance L. An important parameter used to measure the resolution of a resonator is the finesse. A Fabry-Perot could have a relatively high finesse intensity transmission but has a low finesse reflection transmission. Subsequently, difficult integration on a chip and low finesse intensity reflection are the two main disadvantages of Fabry-Perot. To improve the integration of a Fabry-Perot resonator on a semiconductor chip is to use a ring resonator, which does not require the use of any cleaved facet. The critical distance in a ring resonator is defined by the circumference of circular waveguide rather than the separation between two reflective planes as in a traditional Fabry-Perot resonator. Although ring resonators establish resonance in a similar manner to the Fabry-Perot resonator, the advantages of a ring resonator over the Fabry-Perot is its ease of integration and higher finesse intensity transmission, but its disadvantage is that it does not reflect back any field. The inherent property of micro-ring resonator as a filter is due to interference of light with itself and consequently excitation of constructive and destructive modes. Evenly spaced modes with equal FSR are selected and passed from the micro-ring resonator. For the add-drop system, the interior electric fields E_a and E_b are expressed as (IS Amiri et al., 2015):

$$E_a = \frac{E_{in} \times j\sqrt{\kappa_1}}{1-\sqrt{1-\kappa_1}\sqrt{1-\kappa_2}\,e^{\frac{-\alpha}{2}L_{ad}-jk_n L_{ad}}} \qquad 3.5$$

$$E_b = \frac{E_{in} \times j\sqrt{\kappa_1}}{1-\sqrt{1-\kappa_1}\sqrt{1-\kappa_2}\,e^{\frac{-\alpha}{2}L_{ad}-jk_n L_{ad}}} \cdot \sqrt{1-\kappa_2}\,e^{\frac{-\alpha}{2}\frac{L_{ad}}{2}-jk_n\frac{L_{ad}}{2}} \qquad 3.6$$

where k_1=0.1 and k_2=0.1 are the coupling coefficients, $L_{ad}=2\pi R_{ad}$, and R_{ad} is the radius of the add-drop micro-ring resonator. $K_n=2\pi n_{eff}/\lambda$ is the wave propagation number in a vacuum and α= 0.5 dBmm^{-1} is the linear absorption coefficient. n_{eff} is the effective index of the waveguide. The waveguide made of SiO_2 with the rectangular shape, 4 µm wide and 3 µm height. The MATLAB modelling uses iterative method to obtain the presented results. The throughput and drop ports electrical fields of the add-drop micro-ring resonator can be expressed as

$$\frac{E_{th}}{E_{in}}=\frac{-\kappa_1\sqrt{1-\kappa_2}\,e^{\frac{-\alpha}{2}L_{ad}-jk_nL_{ad}}+\sqrt{1-\kappa_1}-(1-\kappa_2)\sqrt{1-\kappa_2}\,e^{\frac{-\alpha}{2}L_{ad}-jk_nL_{ad}}}{1-\sqrt{1-\kappa_1}\sqrt{1-\kappa_2}\,e^{\frac{-\alpha}{2}L_{ad}-jk_nL_{ad}}}=\frac{-\sqrt{1-\kappa_2}\,e^{\frac{-\alpha}{2}L_{ad}-jk_nL_{ad}}+\sqrt{1-\kappa_1}}{1-\sqrt{1-\kappa_1}\sqrt{1-\kappa_2}\,e^{\frac{-\alpha}{2}L_{ad}-jk_nL_{ad}}} \qquad 3.7$$

$$\frac{E_{drop}}{E_{in}}=\frac{-\sqrt{\kappa_1.\kappa_2}\,e^{\frac{-\alpha}{2}\frac{L_{ad}}{2}-jk_n\frac{L_{ad}}{2}}}{1-\sqrt{1-\kappa_1}\sqrt{1-\kappa_2}\,e^{\frac{-\alpha}{2}L_{ad}-jk_nL_{ad}}} \qquad 3.8$$

The normalized optical outputs of the micro-ring resonator can be expressed by equations (5) and (6).

$$\frac{|E_{th}|^2}{|E_{in}|^2}=\frac{(1-\kappa_1)-2\sqrt{1-\kappa_1}\cdot\sqrt{1-\kappa_2}\,e^{-\frac{\alpha}{2}L_{ad}}\cos(k_nL_{ad})+(1-\kappa_2)e^{-\alpha L_{ad}}}{1+(1-\kappa_1)(1-\kappa_2)e^{-\alpha L_{ad}}-2\sqrt{1-\kappa_1}\cdot\sqrt{1-\kappa_2}\,e^{-\frac{\alpha}{2}L_{ad}}\cos(k_nL_{ad})} \qquad 3.9$$

$$\frac{|E_{drop}|^2}{|E_{in}|^2}=\frac{\kappa_1\kappa_2 e^{-\frac{\alpha}{2}L_{ad}}}{1+(1-\kappa_1)(1-\kappa_2)e^{-\alpha L_{ad}}-2\sqrt{1-\kappa_1}\cdot\sqrt{1-\kappa_2}\,e^{-\frac{\alpha}{2}L_{ad}}\cos(k_nL_{ad})} \qquad 3.10$$

where $|E_{th}|^2$ and $|E_{drop}|^2$ are the optical output powers of the throughput and drop ports respectively.

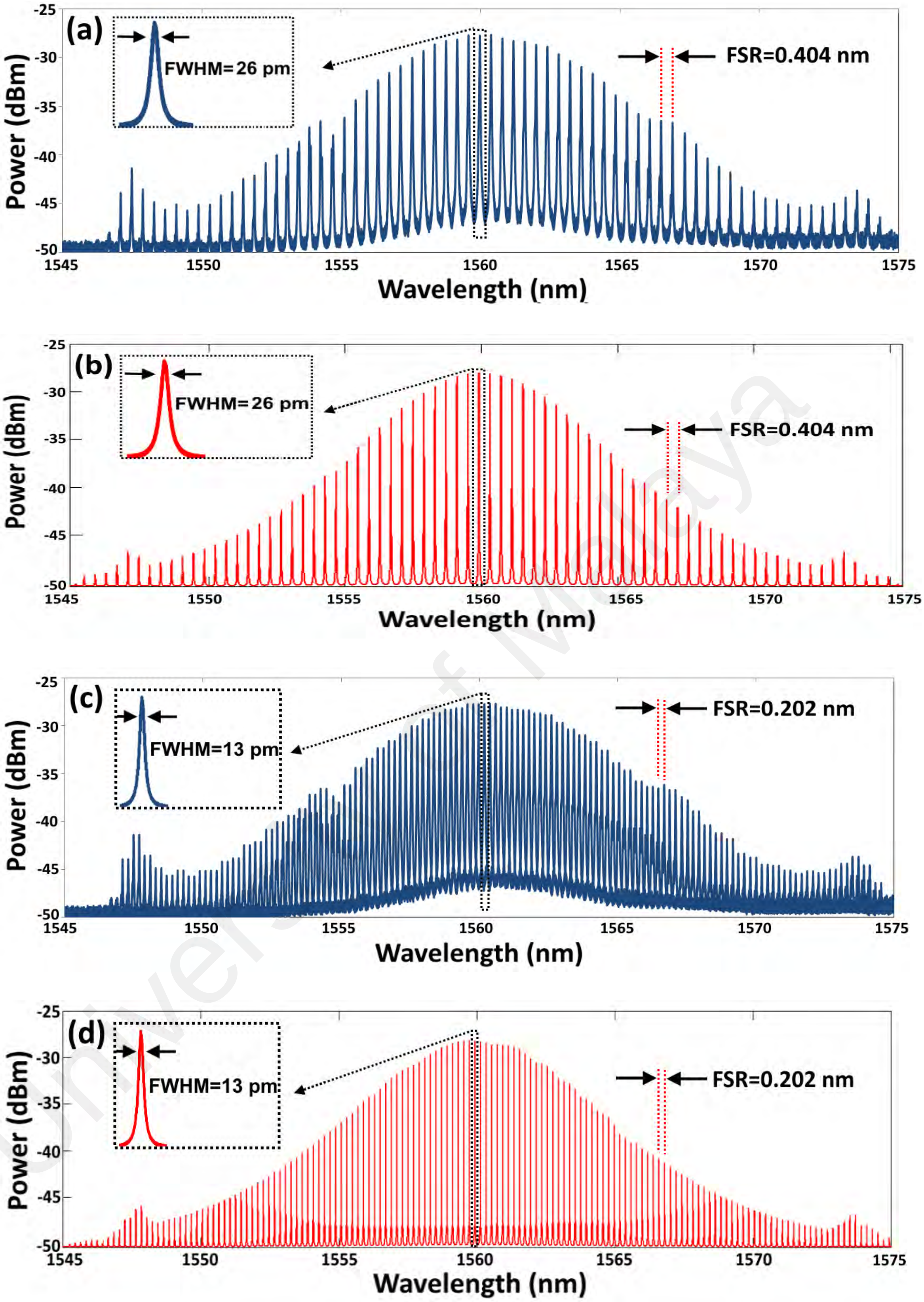

Figure 3.14: (a) output spectrum of micro-ring resonator with D=1.27 mm taken from OSA 3, (b) MATLAB modeling results for micro-ring resonator with D=1.27 mm, (c) output spectrum of micro-ring resonator with D=2.54 mm taken from OSA 3 and (d) MATLAB modeling results for micro-ring resonator with D=2.54 mm.

Figure 3.14 (a) shows the multi-wavelength output spectrum measured using OSA 3 when the micro-ring resonator with the diameter of 1.27 mm was used. The MATLAB modeling for the mentioned configuration is illustrated in Figure 3.14 (b). The MATLAB modeling uses iterative method to obtain the presented results. Achieving same FSR and FWHM of 0.404 nm and 26 pm respectively from the results obtained from OSA3 and MATLAB simulation for the setup utilizing micro-ring resonator with D=1.27 mm is a fidelity confirmation of both experimental and modeling results. The same experiment has been carried out utilizing micro-ring resonator with D=2.54 mm. The experimental and modeling output spectrums are shown in Figure 3.14 (c) and (d) respectively. FSR and FWHM of 0.202 nm and 13 pm were achieved respectively from the results obtained from OSA3 and MATLAB simulation. By fine tuning the bandwidth of high resolution TBPF, desirable dual-wavelength pair from the generated multi-wavelength output was filtered out as shown in Figure 3.15.

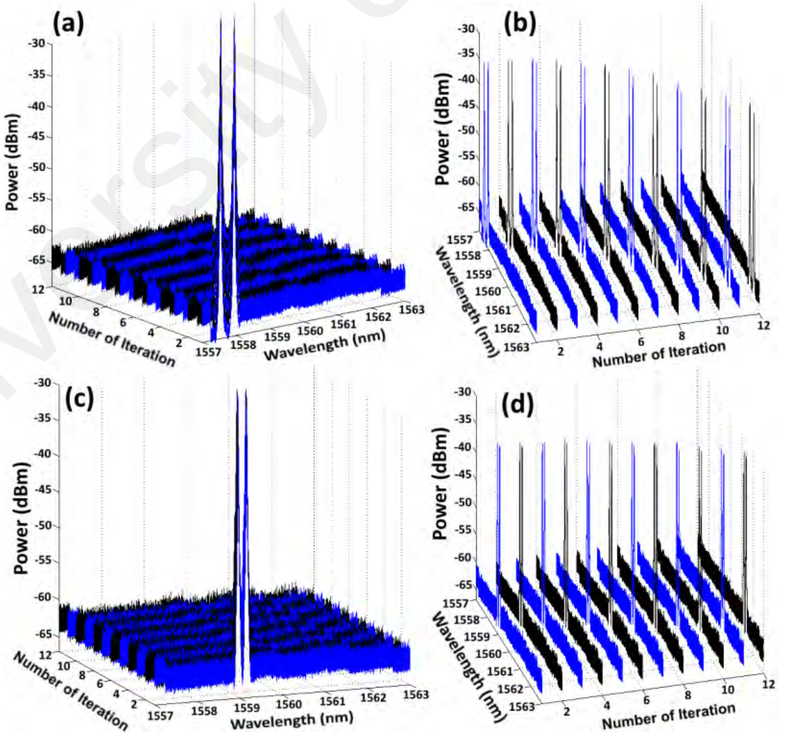

Figure 3.15: (a), (b) tunability of generated dual-wavelength when micro-ring resonator with D=1.27 mm was used, (c) and (d) tunability of generated dual-wavelength when micro-ring resonator with D=2.54 mm was used.

Figures 3.15 (a) and (b) show the tunability of generated DW coherent source vary in the range of 1557 to 1563 nm by varying the TBPF in two different views while the micro-ring resonator with D=1.27 mm was used. Similarly, Figures 3.15 (c) and (d) show the same results when the micro-ring resonator with D=2.54 mm was utilized. The number of iteration corresponds to displacement of the TBPF in each step. The stability of generated DW coherent sources is shown in Figure 3.16. The stability of generated DW coherent source utilizing the micro-ring resonator with D=1.27 mm over 300 minutes with every scan at time interval of 30 minutes is illustrated in Figure 3.16 (a) and (b) in different view. The DW coherent source centre wavelengths were 1559.568 and 1559.972 nm.

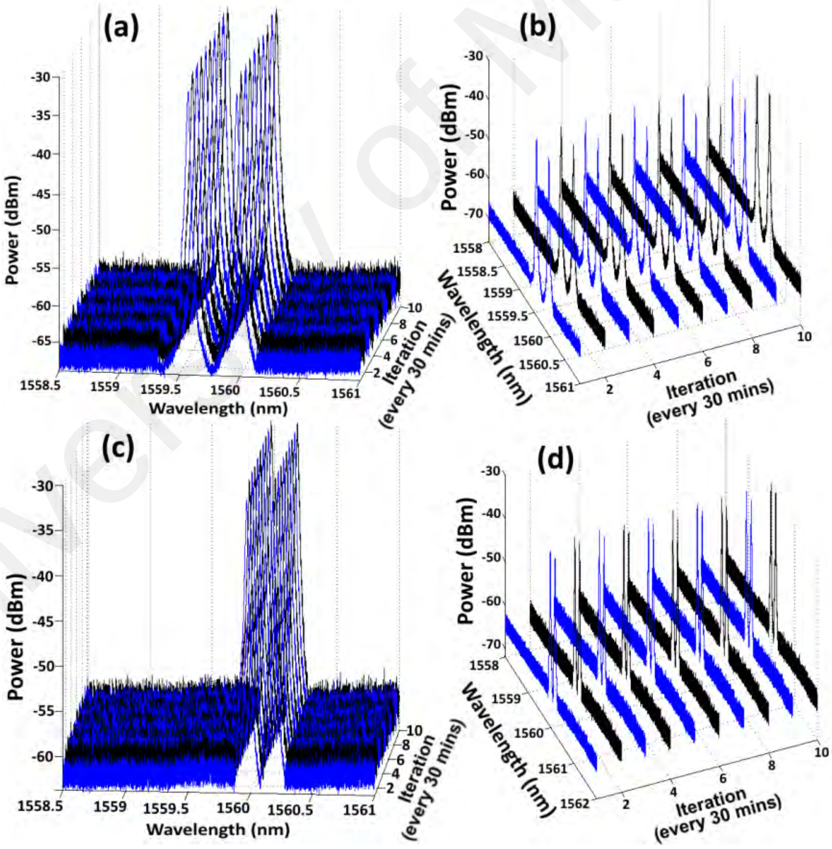

Figure 3.16: (a), (b) Stability of generated DW coherent source at wavelengths of 1559.568 nm and 1559.972 nm over 300 minutes, (c) and (d) stability of generated DW coherent source at wavelengths of 1559.972 nm and 1560.174 nm over 300 minutes.

The stability of generated DW coherent source utilizing micro-ring resonator with D=2.54 mm shown in Figure 3.16 (c) and (d) during 300 minutes with interval scan for every 30 minutes. The DW coherent source centre wavelengths were 1559.972 and 1560.174 nm. Figure 3.17 (a) shows the power fluctuation of the generated DW coherent source utilizing the micro-ring resonator with D=1.27 mm over 300 minutes.

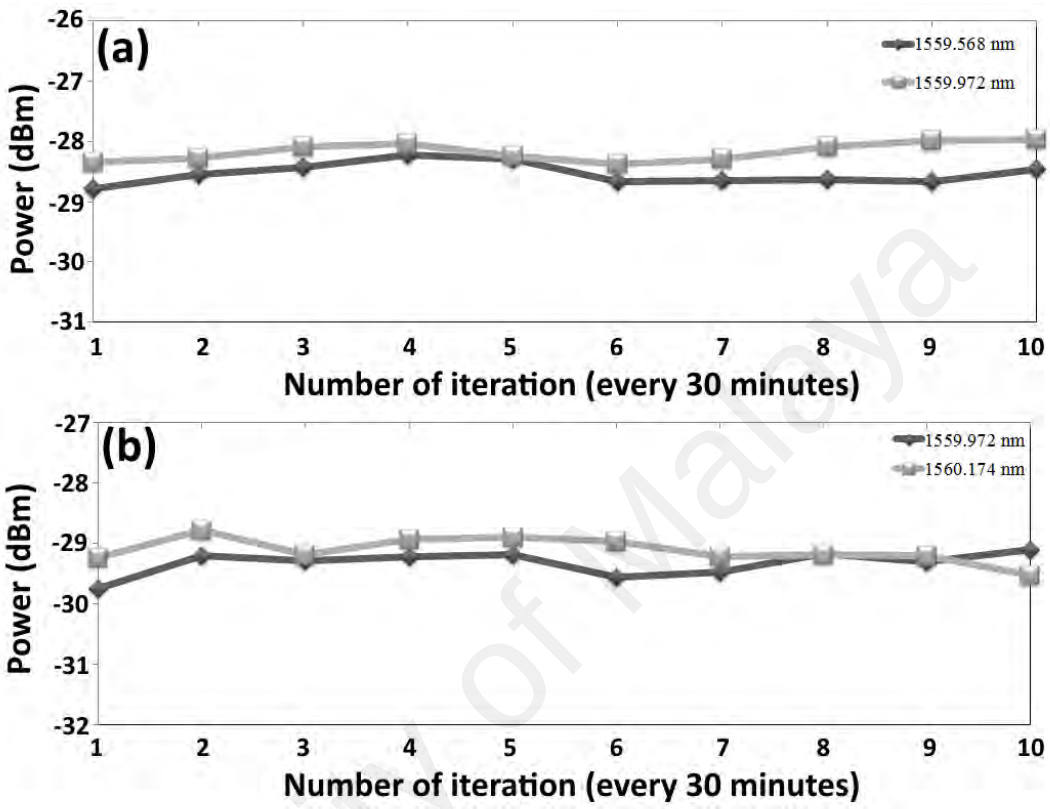

Figure 3.17: The power stability of generated DW coherent source over 300 minutes for the wavelengths of (a) 1559.568 and 1559.972 nm, and (b) 1559.972 and 1560.174 nm.

The power is very stable during the period of experiment at room temperature. Figure 3.17 (b) show the same procedure for the setup utilizing micro-ring resonator with D=2.54 mm. The DW coherent source with different independent FSR were achieved by replacing the module 2 configuration setup shown in Figure 3.18 by the module 1 shown in Figure 3.12 in the main configuration setup. By utilizing module 2 instead of module 1, the generated multi-wavelength is divided in two arms by a 3dB coupler as shown in Figure 3.18. Consequently, the average power of the generated multi-wavelength is decreased by 3dB in each arm. The upper arm contains the high resolution TBPF set the FWHM so that can pass only one wavelength. The lower arm contains a 3-port circulator and a FBG with the center wavelength of 1561.687 nm, FWHM of 0.232 nm and insertion loss of 0.27 dB to filter out the generated wavelength at 1561.558 nm.

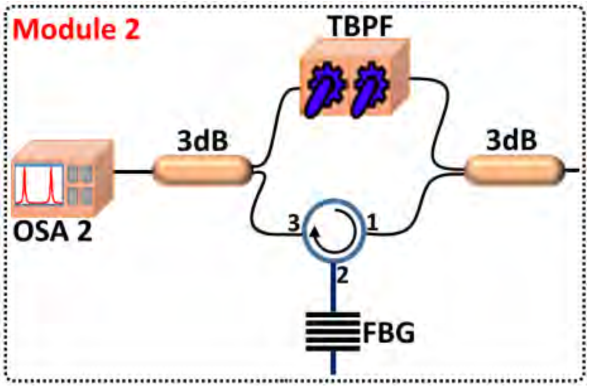

Figure 3.18: Configuration setup as module 2 to place in the main setup instead of module 1to generate tunable DW coherent source with different FSR.

The FBG shown in Fig. 3.18 is a fiber based device with a series of periodic variations of the effective refractive index in the core of an optical fiber, such that a wavelength specific dielectric mirror is generated. This mirror allows the FBG to act as an optical filter or as a wavelength-specific reflector (X. Feng, Tam, Lu, Wai, & Tang, 2007; Keiser, 2003). The length of the periodic variation in the FBG is typically a few millimeters or centimeters. The basic equation that gives the central wavelength of the FBG can be expressed as (Ghatak & Thyagarajan, 1998)

$$\lambda_B = 2\, n_{eff}\, \Lambda \tag{3.11}$$

where λ_B is the central wavelength or the reflected wavelength of the FBG, which is also called Bragg wavelength, n_{eff} is the effective refractive index of the fiber mode and Λ is the grating period. Thus, from this equation, it can be deduced that the central wavelength reflected by the FBG is determined by the grating period Λ of the FBG.

In general, the reflectivity of the FBG is typically between 80% and 99%. The illustration of the FBG with the periodic gratings is shown in Figure 3.19.

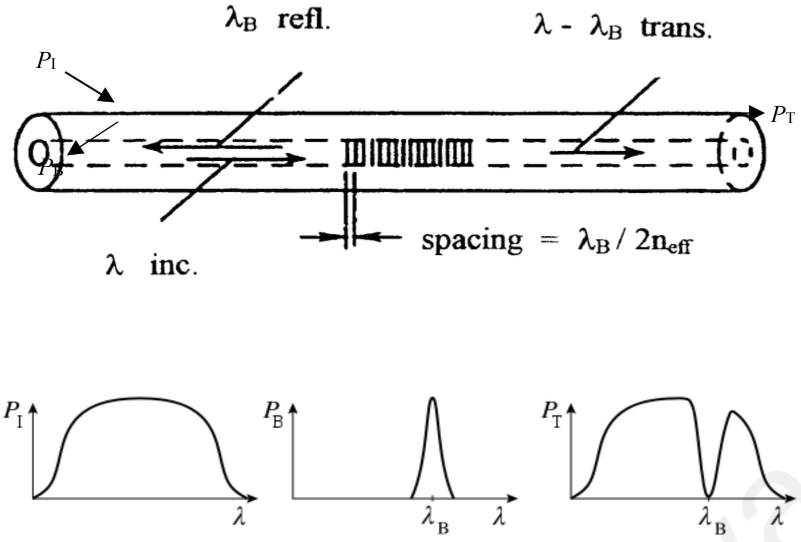

Figure 3.19: Illustration of the gratings inside the FBG (Ghatak & Thyagarajan, 1998)

By fine tuning the TBPF when the micro-ring resonator with D=1.27 mm is used, stable and tunable DW coherent source is achieved as shown in Figure 3.20. The achieved tunable FSR's are integer coefficient of the minimum achieved FSR which is 0.404 nm.

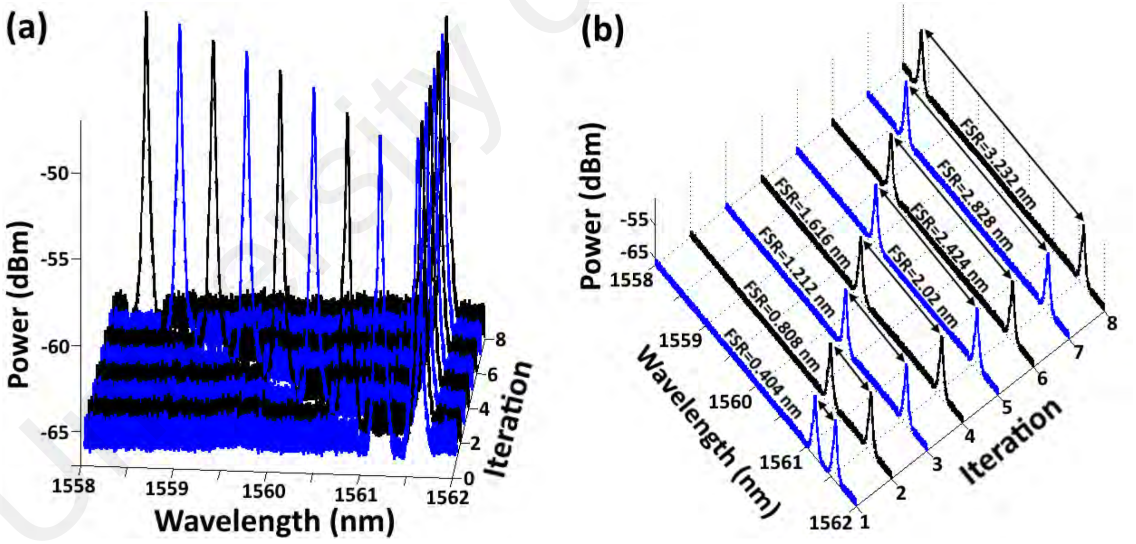

Figure 3.20: (a) and (b) Generation of DW coherent source with different independent FSR in two different views.

Figure 3.20 shows the tunability of achieved FSR from 0.404 to 3.232 nm in two different views. Since the stable DW coherent sources are playing a very important role in applications such as optical spectroscopy, microwaves photonics systems, optical wavelength division multiplexing systems (WDM), CW THz radiation signals, optical component testing and chromatic dispersion measurement, the linear relation between the micro-rings' resonator diameter and FSR of the generated DW coherent source infer to pre-design accurate optics and photonics on chip devices

3.4 Dual-Wavelength Fiber Lasers in 2 μm region

Thulium-doped fiber lasers (TDFLs) have become an increasingly attractive topic in laser research within the past few years due to their useful roles in various applications such as gas detection (De Young & Barnes, 2010), mechanical processing of polymers (Mingareev et al., 2012), optical communication (Z. Li et al., 2013), light detection and ranging (LIDAR), and remote sensing. One major cause for this considerable amount of interest lies in the ability of TDFLs to emit a laser beam in a wavelength region, from 1.9 to 2.1 μm, that poses no damage to eyes. Hence, TDFLs possess a significant advantage for utilization in applications, such as free space optical communication and LIDAR atmospheric water vapor profile measurement (De Young & Barnes, 2010), that involve light propagation in a free space or in the atmosphere. Many researchers have carried out studies on various TDFL configurations that are suitable for particular types of applications. One configuration in which dual-wavelength TDFLs operate at 2μm is considered an attractive proposition for dual-wavelength laser generation, since most dual wavelength fiber lasers previously reported were operating at the 1.0 μm and 1.55 μm bands. Developments relating to this configuration have been further driven by the anticipated applicability to a broad range of purposes such as for ranging systems (L. Liu et al., 2013), communication, microwave photonics (J. Q. Sun, Huang, Li, & Jiang, 2011; T. Wang et al., 2014) and terahertz generation (Q. Sun, Wang, Tong, Luo, & Liu, 2012). Moreover, progress on all-fiber dual wavelength generation from TDFLs has become more feasible due to 2 μm compatible fiber components becoming readily available. Similarly to the case of ytterbium-doped fiber lasers and erbium-doped fiber lasers, which operate at 1.0 μm and 1.55 μm respectively, achieving dual wavelength generation in the

2.0 μm wavelength region with TDFLs is challenging due to strong mode competition caused by homogeneous gain broadening in the gain media. Various approaches for overcoming this setback, such as four wave mixing (M. P. Fok & C. Shu, 2007), polarization hole burning (Mou et al., 2009) and cascaded stimulated Brillouin scattering (Parvizi, Ali, Harun, & Ahmad, 2011), have been reported for erbium-doped fiber lasers, although there has been scant attention in regards to approaches for the comparable case of TDFLs. Zhou et al. have proposed a stable dual-wavelength TDFL based on cascaded fiber Bragg gratings (P. Zhou, Wang, Ma, Han, & Liu, 2011), whereby the laser wavelengths are determined by the fiber Bragg gratings (FBG) and thus the wavelength spacing is fixed by the central wavelength of the FBGs pair. On the other hand, a dual-wavelength laser proposed in (X. W. Ma, Luo, & Chen, 2014) that employs a sagnac loop mirror made by a 145.5 cm polarization maintaining fiber is switchable, tunable, and operates stably at room temperature. Another configuration of tunable dual-wavelength TDFL is demonstrated by (S. Liu et al., 2014), wherein a high birefringence FBG stabilizes the dual-wavelength lasing produced when the polarization state of each wavelength is altered via a polarization controller. A large number of researchers have investigated the distinctive properties of photonic crystal fibers, such as wide range single mode operation, dispersion flexibility, large mode area and its application in multi-wavelength generation (H Ahmad, Soltanian, Alimadad, & Harun, 2014; H. Ahmad, Soltanian, Pua, Alimadad, & Harun, 2014; Russell, 2006; M. Soltanian et al., 2014). In most cases, those properties were proven to be wavelength dependent and equivalent to the behavior of wavelength-selective filters (H. Ahmad, M. R. K. Soltanian, C. H. Pua, M. Z. Zulkifli, & S. W. Harun, 2013; WG Chen et al., 2009).

In this part, a stable dual-wavelength TDFL operating at 1.9 μm is proposed and demonstrated with a short length photonic crystal fiber (PCF) incorporated in our ring cavity setup to obtain sets of stable DWFL output, which are normally achieved using much longer PCF lengths. Therefore, this creates a substantial advantage for the proposed setup, as it now can act as a robust and compact, yet relatively cost effective dual-wavelength source. The use of PCF brings advantages of flexibility and wavelength-dependent characteristics, which make the material almost an ideal choice as a wavelength selective filter for TDFL. This work is synchronous with previous efforts to generate microwave signals from fiber optic elements for use in radio over fiber (ROF) applications, which are mentioned in [16-18] for the 1.5 μm region. The particular interest in the development of the 1.9 μm source is in anticipation of spectroscopic analysis applications of various gases, in particular for high sensitivity trace gas sensing of CO_2, N_2O, H_2CO, and HBr (Ehret et al., 2008).

3.4.1 Laser Configuration

The configuration of the proposed dual-wavelength fiber laser based on polarization dependent loss control is shown in figure 3.21. Components of this laser included a 793/2000 nm wavelength division multiplexer (WDM) that had an attached discrete 793 nm laser diode pump, followed by 2 meters of thulium-doped fiber (TDF), and subsequently a repeated arrangement of WDM and attached pump, a polarization controller, a 10 cm length of photonic crystal fiber, a 10:90 fiber based coupler, and an isolator that closed the fiber laser ring. The 793 nm pump outputs were coupled into the laser cavity by the WDMs in a bidirectional pumping configuration, while the TDF was pumped bi-directionally in the core via the two 793 nm laser diodes.

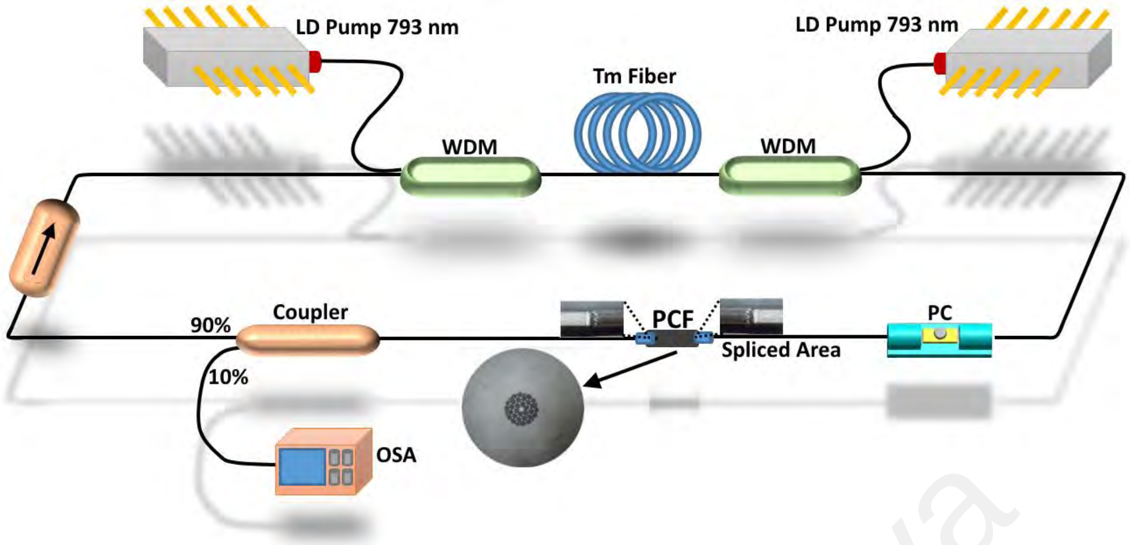

Figure 3.21: Configuration of the dual-wavelength TDFL at 2 μm with photonic crystal fiber based on the Mach Zehnder inter-ferometry effect.

The combination of both laser diodes allowed for approximately 350 mW of pump power. The gain medium used in this setup was a 2 meter single mode TDF manufactured by Nufern Corporation, and had an absorption coefficient of 27 dB/m at 793 nm, core diameter of 9 μm and cutoff wavelength of 1750 nm. In order to obtain a more stable lasing condition, the laser was forced to operate uni-directionally via an isolator. The polarization controller provided a capability to switch the lasing wavelengths' polarization state from one to another, which triggers a polarization dependent loss in the setup and consequent excitation of the dual-wavelength laser. As shown by the micrograph in figure 3.21 (inset), the PCF cross-section structure consisted of a solid core, having diameter of 4.37 μm, and a surrounding ring of air holes each having 5.06 μm diameter and a separation of 5.52 μm between the holes. The internal structure of the PCF was responsible for the separation of incoming light into several modes that subsequently propagated in different paths. The combination of these modes at the other end of the PCF allowed the PCF to perform as a Mach-Zehnder interferometer. In order to measure and analyze the laser output, a 10:90 fused fiber coupler was used to tap 10% of the lasing power from the cavity while feeding back the remaining 90% to the cavity.

3.4.2 Experimental results and discussion

A compact Mach Zehnder interferometer was constructed by fusion splicing a 10 cm long PCF between two segments of single mode fiber as shown in figure 3.22 (a). The schematic diagram depicted in figure 3.22 (b) illustrates the internal structure of the interferometer. Splicing the PCF and single mode fiber manually via a Fujikura 45 PM splicer caused a collapse of the air holes of the PCF. The two spliced points were located in series, and the length of the PCF determined fringe spacing. The splice loss was measured using a Thorlabs tunable laser kit (TLK-L1900M) as a tunable laser source (TLS) that operated from 1870 nm to 1930 nm. The output laser was set at 1900 nm and a Thorlabs power meter (PM100) was used to measure the output power during splicing performed by a Fujikura 45 PM splicer. The minimum splicing loss achieved was 1 dB for each splicing area. The resulting transmission spectrum of the Mach-Zehnder interferometer, as shown in figure 3.23, allowed for measurement of the free spectral range (FSR) as 0.2 nm.

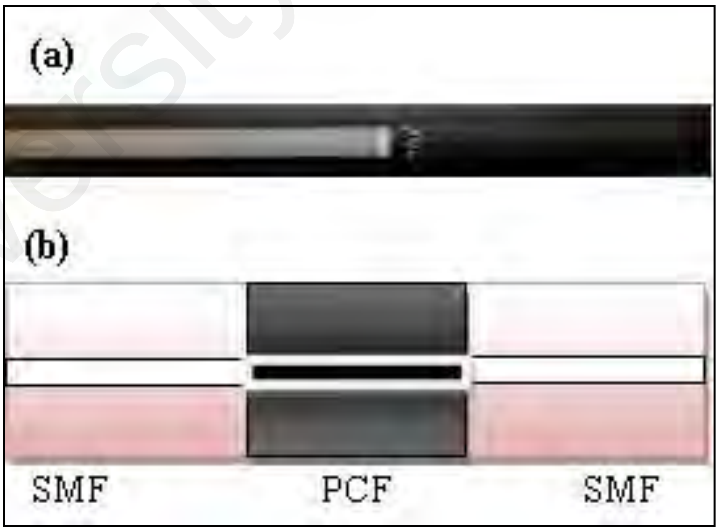

Figure 3.22: (a) Image from the collapsed region after splicing and (b) Schematic diagram of the Mach-Zehnder interferometer filter

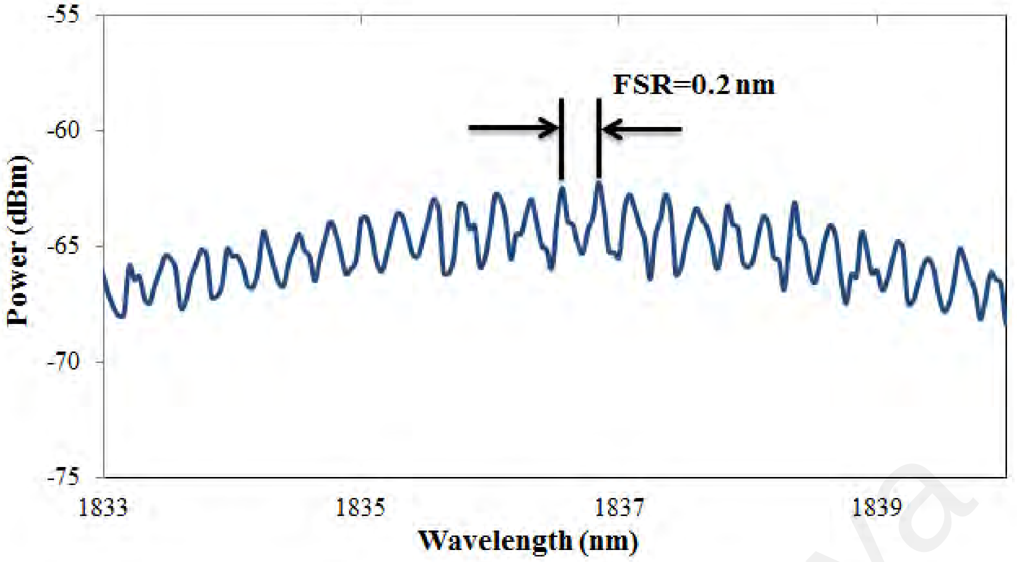

Figure 3.23: Transmission spectrum of the Mach-Zehnder interferometer

The first collapsed region served to diffract the traversing fundamental mode, which resulted in the core and cladding modes becoming excited in the few modes PCF section as shown in figure 3.24 (a), (b), (c) and (d). These four different polarization states images were captured via an Electrophysics Micron Viewer Model 7290A while a single longitudinal mode (SLM) laser lased in 1850 nm wavelength. figure 3.24 (a-1), (a-2), (b-1), (b-2), (c-1), (c-2), (d-1) and (d-2) show the modeling results of the field profiles for the fundamental quasi-TM modes calculated with the vector beam propagation method (BPM). The modeled results are completely in agreement with the experimental results for the modes m=10, 11, 0 and 16 respectively, and these agreed results show that the fundamental mode undergoes diffraction and becomes exited in a few modes. A portion of the fundamental core mode of PCF subsequently could be coupled to a single mode or several cladding modes of the PCF. A variety of optical paths that corresponded to the different arms of Mach-Zehnder interferometer emerged due to the effective refractive index of the cladding being smaller than the core. The fundamental and cladding modes possessed dissimilar phase velocities and hence accumulated a phase difference along the

PCF, whereby the magnitude of this phase difference was dependent on the length of PCF and the wavelength of the guided light.

The phase shifting that occurs within a physical length is equal to the product of different effective refractive indices of core and cladding modes within the length. When the propagating modes reached the subsequent collapsed area of the PCF, the cladding modes became coupled back to the core mode. Since the phase difference and the phase velocities are wavelength dependent, the optical power transmitted by the interferometer is at a minimum at certain wavelengths and maximum at others. The separation between consecutive peaks of a two-mode interferometer is given by $\Delta\lambda = \lambda^2 / L\Delta n_e$, where Δn_{e} is the effective refractive indices difference between the core and cladding modes.

The core and the cladding of the PCF played the role of arms within a Mach–Zehnder interferometer, while the collapsed points acted as couplers splitting or combining light powers at the input and output of the interferometer. Fine-tuning the polarization controller shown in figure 3.21 allowed for a dual-wavelength laser with very similar peak powers of -20.55 dBm and -20.15 dBm at 1851.30 nm and 1853.10 nm respectively, as measured from the 10% port and shown in figure 3.25. Insertion of a polarization controller into the cavity resulted in wavelength-dependent polarization rotation and a consequent diversification of polarization states across multiple wavelengths in the TDFL. If no changes occur in the polarization states, all different wavelengths will remain in approximately identical polarization states in the TDF.

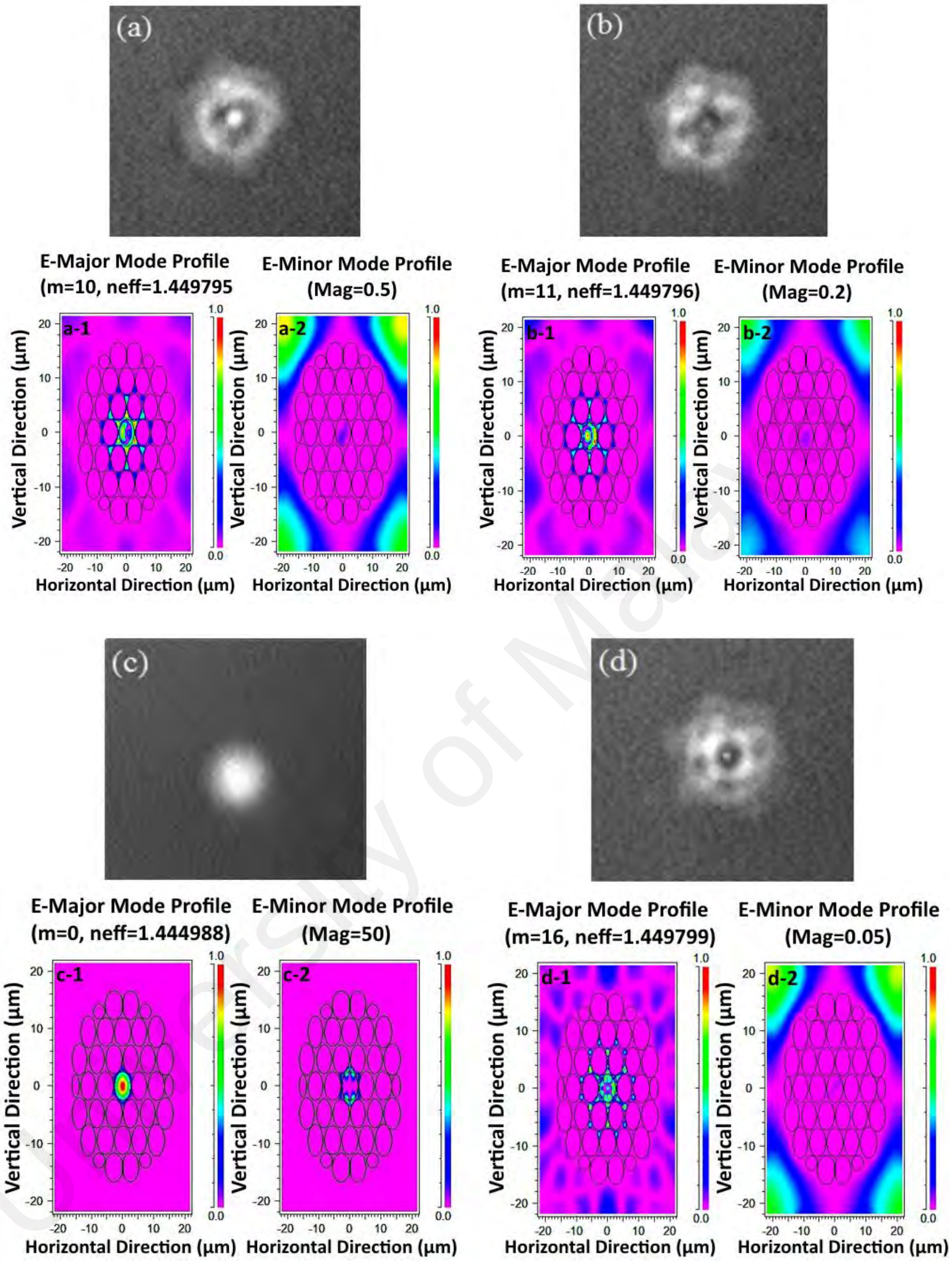

Figure 3.24: (a), (b), (c) and (d) Image captured by Electrophysics Micron Viewer Model 7290A for four different polarization states variations via a PC while a SLM laser source launched in the wavelength of 1850 nm. (a-1), (a-2), (b-1), (b-2), (c-1), (c-2), (d-1) and (d-2) are the modelling results field profiles for the fundamental quasi-TM modes corresponding to the experimental results for the modes m=10, 11, 0 and 16 respectively.

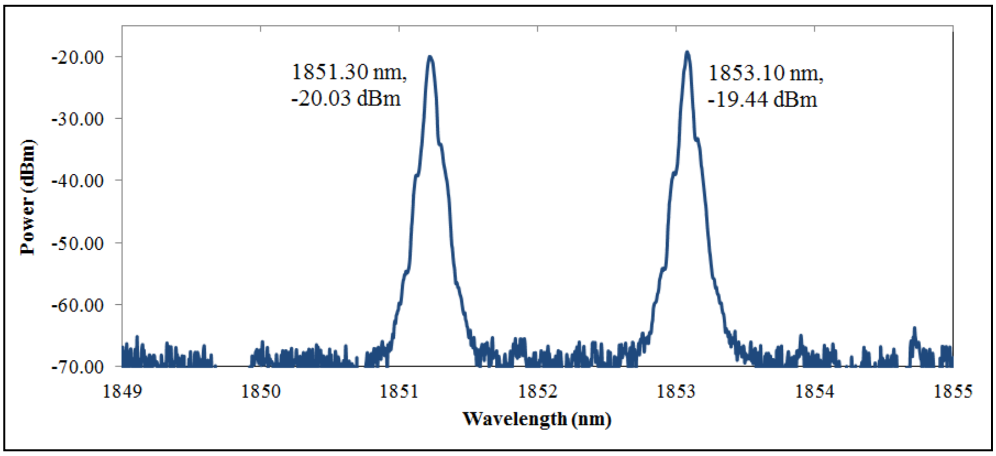

Figure 3.25: Optical spectrum of dual-wavelength fiber laser at wavelengths of 1851.30 nm and 1853.10 nm with peak powers of -20.55 dBm and -20.15 dBm respectively.

Increasing the number of peaks oscillating in the cavity necessitated the use of a polarization hole burning (PHB) technique (Tu et al., 2008). Light entering the TDFL did not have the same polarization state, and this resulted in greatly enhanced PHB and a large reduction in the homogeneous line-width of the TDF. An ensuing suitable adjustment of the polarization controller led to stable dual-wavelength lasing states at room temperature. The distribution of the modes in the PCF is totally dependent on the polarization states of the modes entering the collapsed region created by splicing with SMF fiber. Each mode will be divided into several modes within the core or the cladding of the PCF. The in-fiber PCF-MZI is an in-line, all-fiber, and coupler-free device. In the role of a delay interferometer (DI), this in-fiber PCF has a relative delay governed by the index difference between its core mode and cladding mode. The index difference between the core mode and the cladding mode can be quite large (usually larger than 0.01), which is due to the unique air-hole structure of the PCF, and implies that a short PCF can be used to introduce a large delay while maintaining optical attenuation of the cladding mode at a relatively low level (Jiangbing Du et al., 2010). Hence, the two higher-order modes, whether in the cladding or core, have significantly different propagation constants, which results in these modes having highly dissimilar travel speeds along the PCF and interference between each other in the subsequent collapsed area of the PCF. The simple design of the dual wavelength fiber laser allowed for increased stability of the setup via the short ring cavity of about 6 m, along with high repeatability due to the inclusion of a PC. As can be observed, the wavelength spacing in figure 3.23 may not be the same as that in figure 3.25 and is attributed to the adjustment of the PC, which will either increase or decrease the spacing between the two wavelengths. In this manner, the polarization states of the modes play a key role to generate dual-wavelength fiber laser. Each (l, m, q) mode has two degrees of freedom, corresponding to two independent orthogonal polarizations. These two polarizations are regarded as two independent modes. The two polarization modes of the same l and m have the same spatial distributions. If the resonator and the active medium provide equal gains and losses for both polarizations, regardless of wavelength spacing, the laser will oscillate on the two modes simultaneously, independently, and with the same intensity [22]. Figure 3.26 provides a demonstration of the stability of the generated dual-wavelength over 180 minutes with the interval scanning of every 10 minutes to make sure the dual-wavelength fiber laser generated is stable. It can be observed from this figure that the optical signal-to-noise ratio for both peaks is about 45 dB.

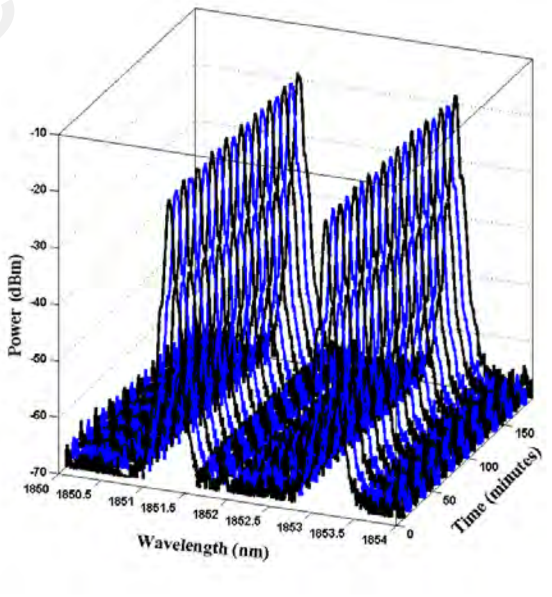

Figure 3.26: Stability of dual-wavelength fiber laser with spacing of 1.8 nm at 1851.30 nm and 1853.10 nm over 180 min with interval scanning of every 10 min.

The power stability of this dual-wavelength was measured and the results shown in figure 3.27. As shown in figure 3.27, the power of the dual-wavelength fiber laser is very stable and the fluctuation is in the range of 1 dB. In general there are several solutions to increase the output power: ensure the cavity is at optimum length, exploit the inherent high absorption characteristics of an incorporated thulium-doped fiber (TDF), increase the pump power, reduce the total loss in the setup e.g. by minimizing splicing loss, and extract a higher portion from the ring laser cavity.

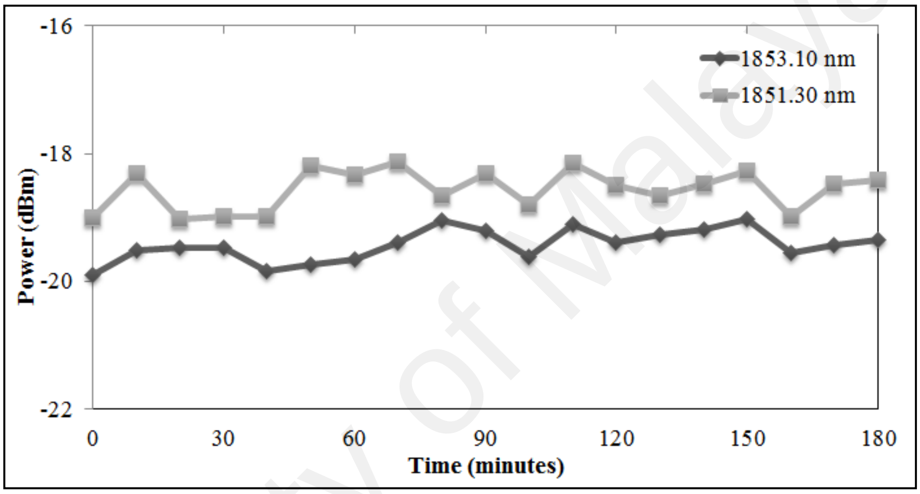

Figure 3.27: Optical power fluctuation for both lasing wavelengths at 1851.30 nm and 1853.10 nm over 180 minutes.

The most appropriate means for increased power is determined by the specific circumstances. For instance, if the output power versus the pump power curve is linear in the highest power region, then increasing the pump power is the simplest way to increase the output power linearly. If the curve is nonlinear, such as the slope reducing as the pump power increases, then the pump output is not fully absorbed and so we should increase the length of the active doped fiber. If there is a limitation to increasing the pump power, then we should seek to improve the laser efficiency and/or the lasing threshold; improvements to both these aspects occur when cavity losses are reduced. The laser output power equation is (Barnard, Myslinski, Chrostowski, & Kavehrad, 1994) :

$$P_{Las} = \eta \left(P_p^{in} - P_p^{th} \right) \qquad 3.12$$

where η is the slope efficiency, P_{Las} is laser output power, P_p^{th} is pump power threshold and P_p^{in} is the input pump power.

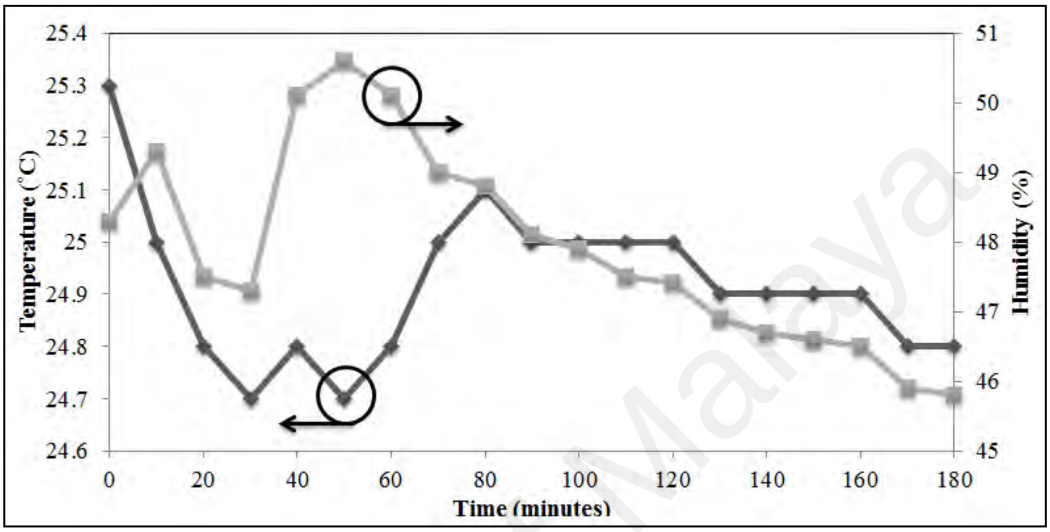

Figure 3.28: Work place temperature and humidity as a function of time over 180 minutes.

Figure 3.28 shows the changing of the temperature and humidity of the environment throughout the experiment, which was performed over a period of 180 minutes. Observation of figure 3.28 shows that the output power of the proposed setup remains relatively stable, and never exceeds a variation beyond 1 dB even with temperature and humidity fluctuations. Such evidence demonstrates that the system is largely stable and unaffected by external influences. That being said, external factors can influence the output power of the system, however in most cases the effect of the external influence is typically too small to have noticeable consequences to the dual-wavelength output of the laser.

In this work, the PCF was used as the means to generate the dual-wavelength output. There have also been demonstrations of using saturable absorbers to generate a dual-wavelength output, such as graphene and graphene oxide. The approach of (Barnard et al., 1994) uses a two-reflection peak fiber Bragg grating as the external cavity mirror together with a saturable absorber to create a Q-switched dual wavelength fiber laser, while the approach of (Harith Ahmad et al., 2013) uses an arrayed waveguide grating to generate the desired tunable dual-wavelength output, which is then stabilized by a graphene based saturable absorber. Graphene oxide can also play the same role, as demonstrated in (Q. Song et al., 2015), in which the graphene saturable absorber is used to stabilize the dual-wavelength output of a Nd:GYSGG laser. Besides this, there has also been a recent demonstration on the use of new materials as saturable absorbers, such as MoS_2 (Juan Du et al., 2014) and black phosphorus (S. Lu et al., 2015). In the case of (Juan Du et al., 2014) MoS_2 is used in the form of a tapered fiber device to generate reasonably high-powered mode-locked pulses through evanescent field interactions. Currently, the interest of this lab would be to investigate MoS_2 as a means of generating a stable dual-wavelength output using a PCF-based fiber laser. Most recently is the discovery of the use of black phosphorous as a saturable absorber, as has been discussed in detail in reference (S. Lu et al., 2015). This finding will spur intense investigation into the development of black phosphorous as a viable alternative to graphene for saturable absorber applications.

CHAPTER 4: DUAL-WAVELENGTH Q-SWITCHED FIBER LASERS

4.1 Introduction

As has been described in earlier, Q-switching is an enabling technique for pulsed laser operation with high output pulse energy; lasing is inhibited in the beginning of the pumping process of the gain medium by a small Q factor, and switching to a high Q factor allows lasing to take place and results in the discharge of the stored energy in the form of pulse output with pulse duration ranging from microseconds to nanoseconds (Popa et al., 2010; Svelto & Hanna, 1976). Q-switching when compared to mode-locking has a relatively much longer pulse duration and much lower repetition rate (usually in the kHz range), which corresponds to the inverse of the time taken between two successive pulses to restore the emitted energy and is dependent on the lifetime of the electron in the excited state inside the gain medium. For instance, the electron lifetime of approximately several milliseconds in erbium-doped fibers is not short enough to yield a high repetition rate in Q-switching, though such a repetition rate can be reached by the mode-locking operation after satisfying specific conditions. Nevertheless, Q-switching has certain advantages over mode-locking in terms of being comparatively easier to accomplish because there is no requirement for a careful design of the cavity parameters in order to attain the equilibrium between the dispersion and nonlinearity of the intra-cavity medium as needed by mode-locking for achieving stable operation. Furthermore, Q-switching is able to produce higher pulse energies, higher operation efficiency, and is more cost effective than mode-locking (Popa et al., 2010). Q-switching laser operation can be realized either actively or passively. Active Q-switching involves the modulation of the Q-factor by external equipment or components applied in the laser cavity such as electro-optic modulators (R. J. Williams, Jovanovic, Marshall, & Withford, 2010), acousto-optic modulators (Q Sun et al., 2010; Villegas et al., 2011) and mechanical rotating choppers.

Passive Q-switching is realized by incorporating a saturable absorber within the laser cavity, whereupon the amount of the photon absorption is determined based on the light intensity passing through the saturable absorber. Generally, passive Q-switching is more difficult to trigger than active Q-switching. In spite of this, the passive Q-switching approach is more desirable and more intensely investigated than active Q-switching due to its advantages of simpler configuration, ease of operation, higher reliability, low cost, and compactness. In contrast, for active Q-switching, the additional mechanisms integrated in the laser cavity will result in a high insertion loss and increase of complexity for the cavity. Thus, compared to active techniques, passively Q-switched fiber lasers are preferable as they are easier to operate and do not require bulky active components.

In conjunction with the need of creating a simple and compact passively Q-switched fiber laser, there has been recent great interest in graphene candidature and topological insulators (TIs) as saturable absorbers (SAs) for passive Q-switching application in fiber laser.

This chapter contains demonstration and presentation of Q-switched DWFL based on different SAs in the region of 1 and 1.5 micron utilizing YDF and EDF respectively as gain medium.

4.2 Passively dual-wavelength Q-switched ytterbium doped fiber laser using Selenium Bismuth as saturable absorber

The generation and manipulation of highly stable optical pulses has become a topic of great interest in the fiber laser research community within the past few years. The main advantage of these optical pulses lies in their wide range of applications, such as in high-speed communication, optical imaging and material processing. The highly compact and stable pulse lasers are also known for their flexibility and low cost deployment (Ancona et al., 2009; Dupriez et al., 2006; Leigh et al., 2007). Passively Q-switched technique has been proven to be very powerful method to generate highly stable optical pulses in fiber laser. A laser ring cavity requires a gain medium such as erbium or ytterbium doped fiber and also a 'Q-switcher' component in order to obtain a stable Q-switching optical pulses. This latter element is usually a fast saturable absorber (SA) such as semiconductor saturable absorber mirrors (SESAMs) (Keller et al., 1996), carbon nanotubes (CNTs) (S Yamashita et al., 2004) and recently graphene (Bao et al., 2009; Hasan et al., 2009).

SESAMs have become a dominant q-switching technology in fiber lasers and deployed widely as a SA within commercial applications within the last decade, although SESAMs are associated with several drawbacks that limit usage with respect to q-switching techniques. Fabrication of SESAMs is expensive and requires clean room facilities, with incorporation into complicated systems being a time-consuming process (Schmidt et al., 2008). Furthermore, integration in fiber ring cavity configuration is not straightforward and restricted to particular types of linear cavity topology due to an inherent reflective property. As a simple alternative, CNTs and graphene have emerged as a promising SA due to their ultrafast recovery time and cost effective production, but the bandgap control complexity of the CNTs limited its saturable absorption of a particular wavelength of light, while graphene has relatively small absorption of only 2.3% at 1550nm and low modulation depth (less than 66.5%) (Bao et al., 2009). More recently, a new SA called topological insulators (TIs) (Bernard, Zhang, Gorza, & Emplit, 2012; P. Tang et al., 2013; C. Zhao, Zhang, et al., 2012; C. Zhao, Zou, et al., 2012) has been discovered and has the potential to replace carbon-based nanomaterial as SA for mode-locking and Q-switching technology. Furthermore, the modulation depth of TIs has been recorded as high as 98% (C. Zhao, Zou, et al., 2012), which make it very interesting and viable solution for fiber laser SA. TI also possesses the ultra-broadband saturable absorption property. For example, the TI:Bi_2Se_3 saturable absorption wavelength range is analyzed to be from ultra-violet to mid-infrared < 4.1 µm (C. Zhao, Zou, et al., 2012). While the TI SA is widely reported in 1.5 micron range of fiber laser) (Bernard et al., 2012; P. Tang et al., 2013; C. Zhao, Zhang, et al., 2012; C. Zhao, Zou, et al., 2012), the only report so far in 1 micron wavelength using ytterbium doped fiber (YDF) with TI:Bi_2Se_3 as SA is available in (H. Ahmad et al., 2013) which generate single wavelength Q-switching fiber laser operation. Therefore, a high level of interest exists for Q-switching operation involving YDF and TI:Bi_2Se_3, especially in dual or multi-wavelength generation due to potential application in optical communication an optical sensing in 1 μm region.

In this part, we report a passively dual-wavelength Q-switched ytterbium doped fiber laser (YDFL) based on a few layer TI:Bi_2Se_3 saturable absorber. The two wavelengths centered at 1037.14 and 1037.69, with spacing of 0.55 nm between them. The work here demonstrates the broadband saturable-absorption nature of TI:Bi_2Se_3 via a simple ring cavity Q-switching operation in 1-micron region.

4.2.1 Experimental Setup

The experimental setup of the proposed dual-wavelength Q-switched YDFL is schematically shown in figure 4.1. The compact linear cavity consists of a 70-cm high-concentration YDF, photonics crystal fiber (PCF) and the Selenium Bismuth (Bi_2Se_3) based SA. The 974 nm centre wavelength laser diode with maximum output power of 600 mW and launch power of 128.8mW (Oclaro Model LC96A74P-20R) was connected through a 980/1060 nm wavelength division multiplexing (WDM) coupler. One port of the WDM was fusion spliced to a gain medium comprising 70 cm YDF (DF1100 Fibercore) that had peak absorption of 1300 dB/m at 977nm, and another port was connected to a 90/10 optical coupler. Output of the YDF amplifier was then fusion-spliced to a polarization insensitive isolator operating at the 1 μm range. This isolator was incorporated into the laser cavity to ensure unidirectional laser ring operation, which was in the clockwise direction in the context of the figure 4.1 layout. The output of the isolator was subsequently connected to a polarization controller (PC) that controlled the cavity state of polarization, and the PC output was attached to the photonic crystal fiber (PCF) based Mach-Zehnder interferometer (MZI). A constructed compact interferometer using an L=10 cm few mode PCF was spliced into two segment of SMF. The PCF played the main function of stabilizing the Dual Wavelength Fiber Laser (DWFL) output based on its birefringence coefficient and nonlinearity (H. Ahmad et al., 2013; Sierra-Hernandez et al., 2013). The PCF was a solid core of 4.37 µm in diameter, and surrounded by air holes with 5.06 µm diameter and separation of 5.52 µm between holes. The cross section of PCF is shown in the inset of figure 4.1 (a). Splicing of PCF and SMF fiber was done using Fujikura 45 PM splicer as depicted in figure 4.1 (b). These two spliced points were located in series and resulted in a simple Mach-Zehnder interferometer, whereby the length of the PCF was directly related to fringe spacing. The schematic depicted in figure 4.1 (c) illustrates the Mach-Zehnder interferometer. The PCF was used to produce dual wavelength by adjusting the PC smoothly. The output of the PCF was subsequently connected to Selenium Bismuth (Bi_2Se_3) based SA (sandwiched between the fiber ferrules), which was in turn, connected to the 90/10 fused bi-conical optical coupler, denoted as OC1. The 10% end of the coupler was then joined to 50/50 optical coupler (denoted as OC2) so that the performance of the dual-wavelength Q-switched YDFL can be monitored simultaneously via optical spectrum analyzer (OSA) YOKOGAWA AQ6373 with a resolution of 0.02 nm and a high-speed photodetector attached to digital oscilloscope (YOKOGAWA DLM2054). Apart from that, the output was also measured using an optical power meter and a radio frequency (RF) spectrum analyzer (Anritsu MS2683A, 9 kHz – 7.8 GHz). The optical deposition technique used to deposit SA on the ferrule.

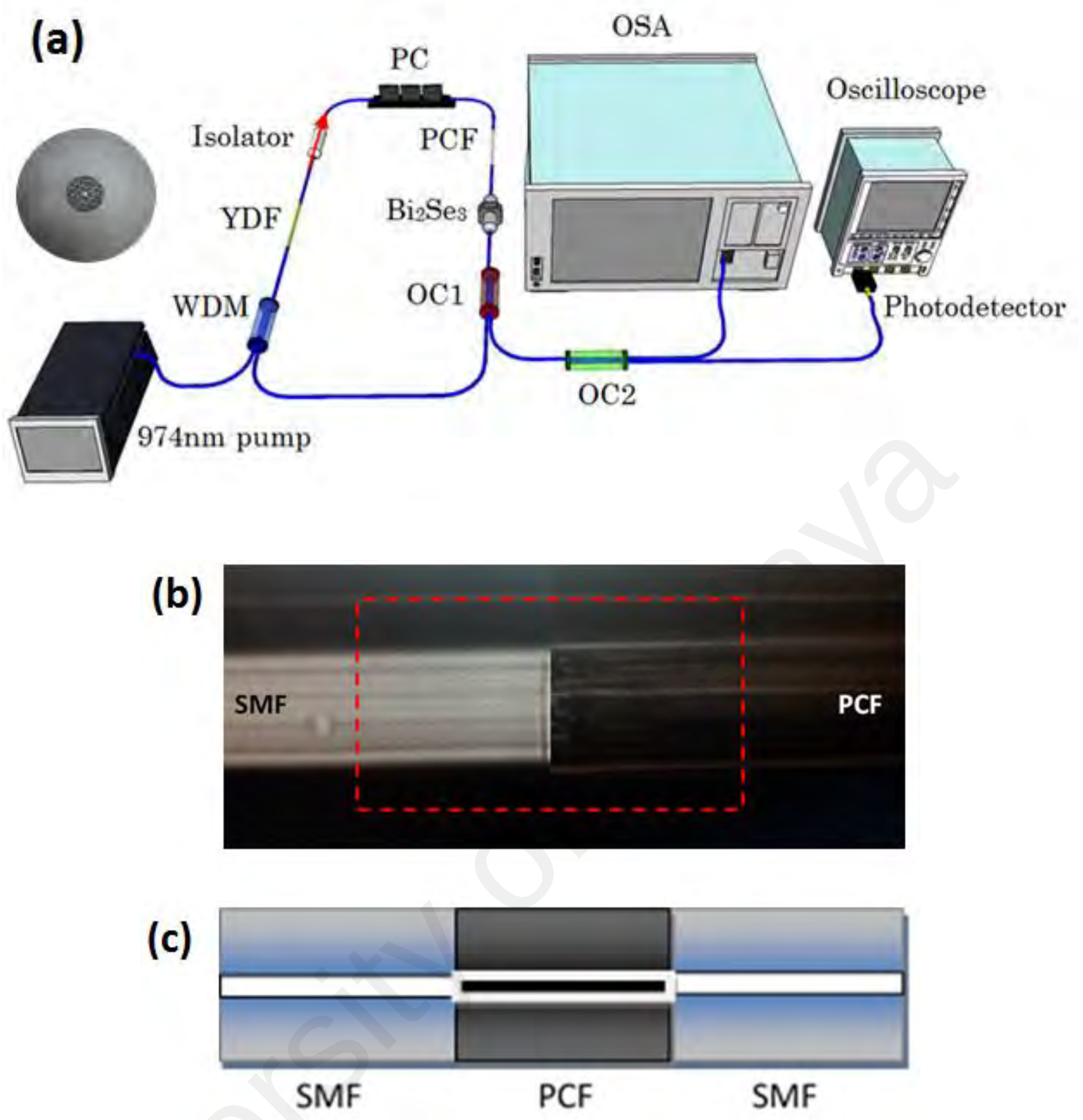

Figure 4.1: (a) Experimental Set up of Selenium Bismuth based passively Q-switched ytterbium doped fiber laser, (b) The Splicing of PCF and SMF fiber and (c) schematic diagram of Mach-Zehnder Interferometer structure.

4.2.2 Experimental results and discussion

In the experiment, the YDFL started its transition to dual-wavelength Q-switching operation at the pump power of 135.5 mW. The output spectrum has two lasing wavelength (1037.14 nm and 1037.69 nm) with output power of -21.40 dBm and -21.22 dBm respectively as shown in figure 4.2 (a). The corresponding pulse train with repetition rate of 15.37 kHz was depicted in figure 4.2 (b). When the pump power was gradually increased from 135.5 mW to 142.1, 148.1 and 155.4 mW, the steady pulse trains with different repetition rates were obtained from the oscilloscope trace, as shown in figure 4.3 (a), (b) and (c) respectively, which is the typical response of passively Q-switching operation.

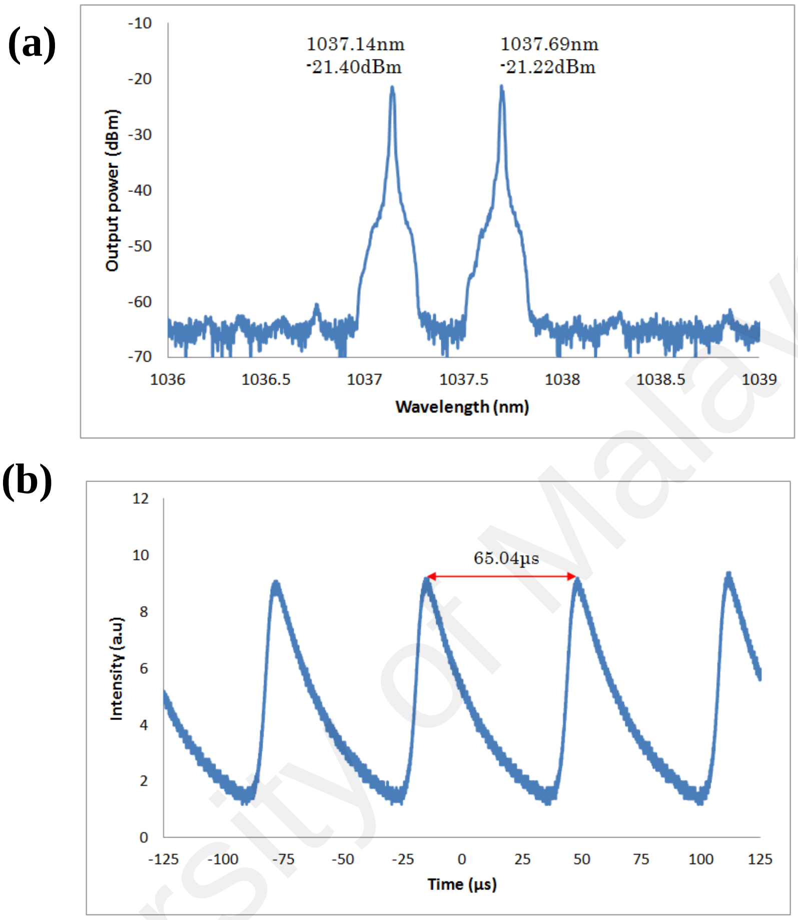

Figure 4.2: (a) The dual wavelength optical spectrum at 1037.14 and 1037.69 nm and (b) corresponding Q-switch pulse train with pump power of 135.5mW and repetition rate of 15.37 kHz.

The pulse train obtained in this experiment is comparable with the Q-switched pulse train of similar cavity configuration using other SAs such as CNTs (D.-P. Zhou, Wei, Dong, & Liu, 2010), SESAM (R Paschotta et al., 1999) and graphene (Cao, Wang, Luo, Luo, & Xu, 2012; Luo et al., 2010; Luo et al., 2011; Popa et al., 2010).

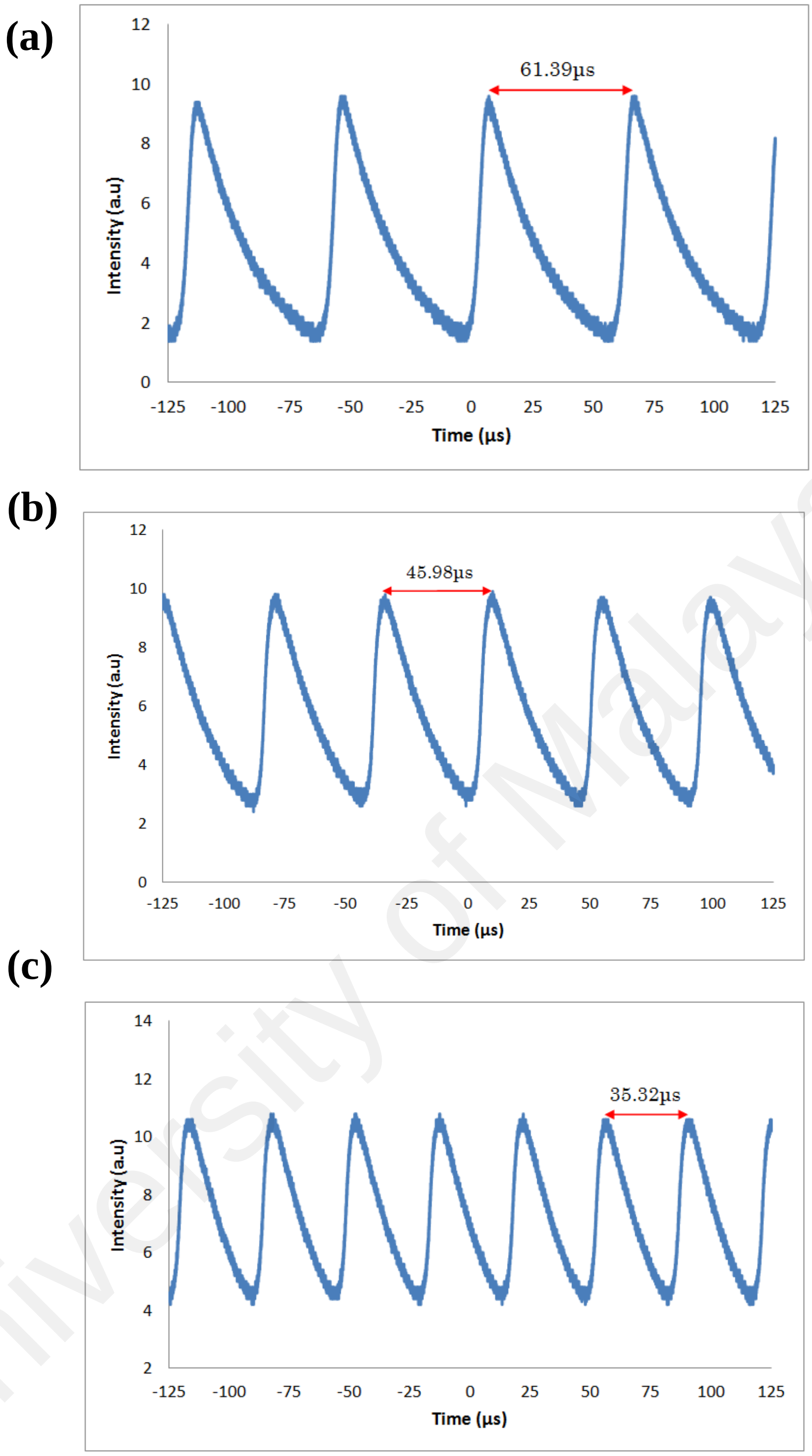

Figure 4.3: The Q-switch pulse train at (a) pump power of 142.1 mW and repetition rate of 16.28 kHz, (b) pump power of 148.1 mW and repetition rate of 21.74 kHz and (c) pump power of 155.4 mW and repetition rate of 28.31 kHz.

Figure 4.4 (a) shows the oscilloscope trace of the Q-switched pulse trains at pump power of 148.1 mW, corresponding to figure 4.3 (b). In this case, the pulse width was 16.41 µs measured from the full-width half-maximum (FWHM). Figure 4.4 (b) shows the output pulse train in frequency domain obtained from the radio frequency spectrum analyzer (RFSA). The spectrum confirms that the fundamental harmonic has a frequency of 21.74 kHz (from the inset) and has a clearly defined pulse with a peak-to-pedestal ratio of 36 dB. Moreover, the broadband RF spectrum in figure 4.4 (b) shows no spectral modulation, indicating the stable repetition rate of the passively q-switching.

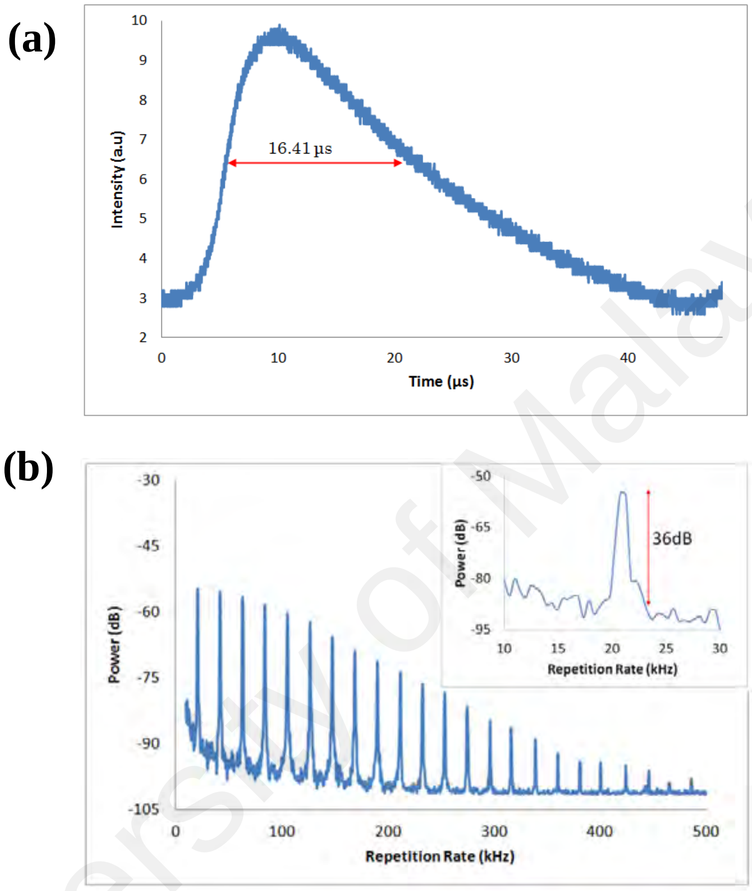

Figure 4.4: The characteristic of Q-switching at 148.1 mW with (a) pulse width and (b) RF output spectrum

Fig. 4.4 (a) shows the pulse width of 16.41 µs. The rise time of the pulse shape, as shown in Fig. 4.4 (a), is proportional to the net gain after the Q-value of the cavity is switched to a high value. The light intensity growth is proportional to $2g_0/T_R$ (Spühler et al., 1999), where g_0 is small signal gain and $T_R = 2L/C_0$ is the roundtrip-time in a linear cavity with optical length $2L$ or a ring cavity with optical length L. An output coupler with transmission T_{out} and output coupling coefficient lout has the definition $T_{out} = 1-exp(-l_{out})$, and a parasitic loss coefficient that is l_p. l_{out} and l_p determine the total nonsaturable loss coefficient per round trip, $l = l_{out} - l_p$. When the gain is depleted, the fall time is mostly dependent on the cavity decay time τ_p. A short cavity length, high gain and a large change in the cavity Q is necessary for short Q-switched pulses. If the Q-switch is not fast, the pulse width can become limited by the speed of the switch. Consequently, for $l < q_0$ the pulses become asymmetric.

Figure 4.5 (a) shows the recorded pulse repetition rate and the pulse duration as a function of pump power. As we increased the pump power from 135.5 mW to 195.3 mW, we can see that the repetition rate of Q-switched pulses were increasing from 15.37 kHz to 59.24 kHz while the pulse width was significantly decreased from 20.88 μs to 8.46 μs. The pulse width could be further narrowed by optimizing the parameters, which includes; 1) shortening the cavity length and 2) improving the modulation depth of the TI: Bi_2Se_3 Q-switcher (D.-P. Zhou et al., 2010). The modulation depth for the TI: Bi_2Se_3 used in this experiment has been measured in (H Ahmad, Soltanian, et al., 2015). In addition, as shown in figure 4.5 (b), we also measured the average output power and corresponding calculated single-pulse energy. The average output power and the pulse energy were linearly increased with the input pump power. At the maximum pump power input of 195.3 mW, the maximum average output power is 0.038 mW, while the maximum pulse energy is 0.65 nJ, comparable to those Q-switched fiber lasers using graphene, CNTs and SESAMs as reported in (Cao et al., 2012; Luo et al., 2010; Luo et al., 2011; R Paschotta et al., 1999; Popa et al., 2010; Zayhowski & Kelley, 1991). The higher pulse energy could be obtained by a using high-gain fiber (e.g. double-clad fiber) with high-performance TI-based SA, and further performance improvement can be achieved by optimizing the cavity designs (e.g. output coupling ratio, cavity loss) (D.-P. Zhou et al., 2010).

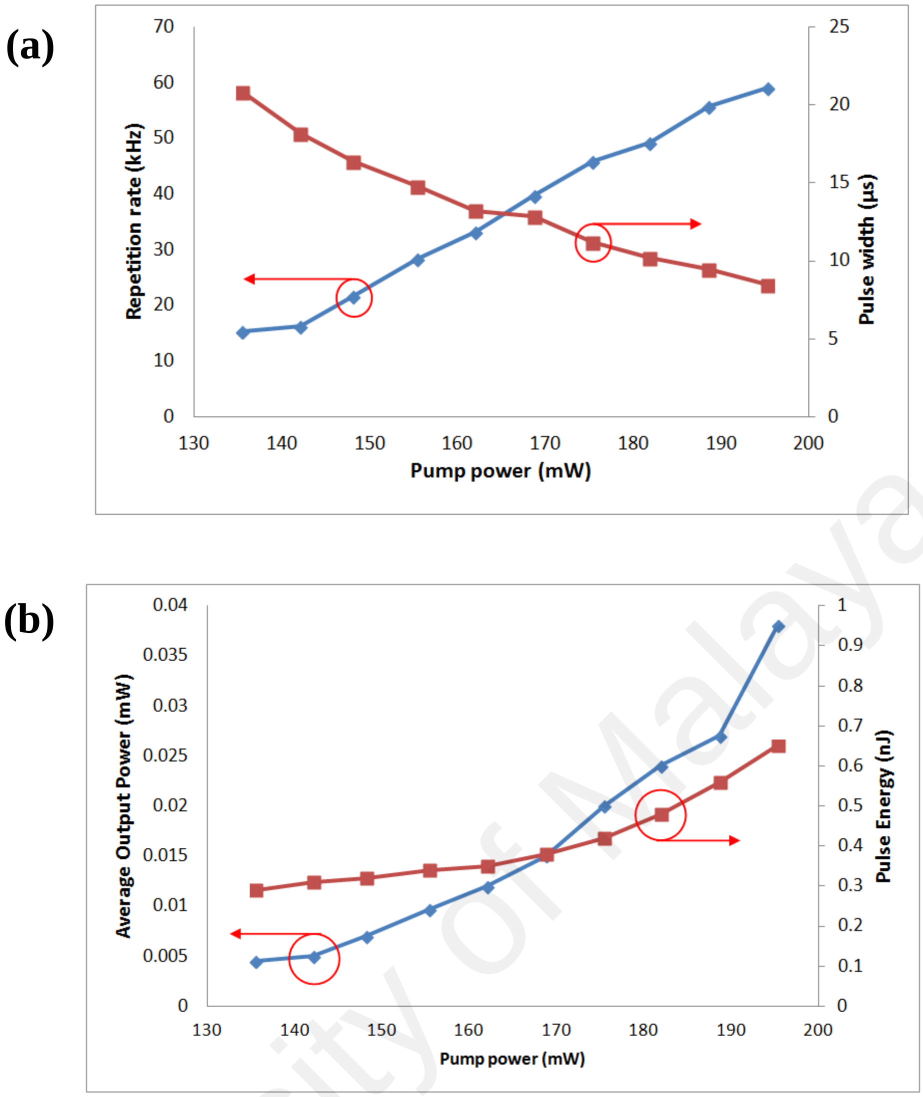

Figure 4.5: (a) The repetition rate and pulse width as a function of pump power, (b) The average output power and pulse energy as a function of pump power

The obtained dual-wavelength set was stability tested over time due to power stability being one of the most important characteristics of dual-wavelength fiber laser. Figure 4.6(a) and 6(b) shows the dual-wavelength stability scan for a period of 20 minutes. Figure 4.6(a) displays a very stable lasing wavelength over the test period and figure 4.6(b) illustrates power fluctuation during the scan, in which the maximum fluctuation is observed as less than 0.8 dB. Such results proved that the wavelength and average power is stable over time and experienced only a very small power fluctuation at room temperature. It should be noted that a test measurement of the dual-wavelength was performed simultaneously with these stability tests, and as such these results confirmed the stability and reliability of the proposed setup.

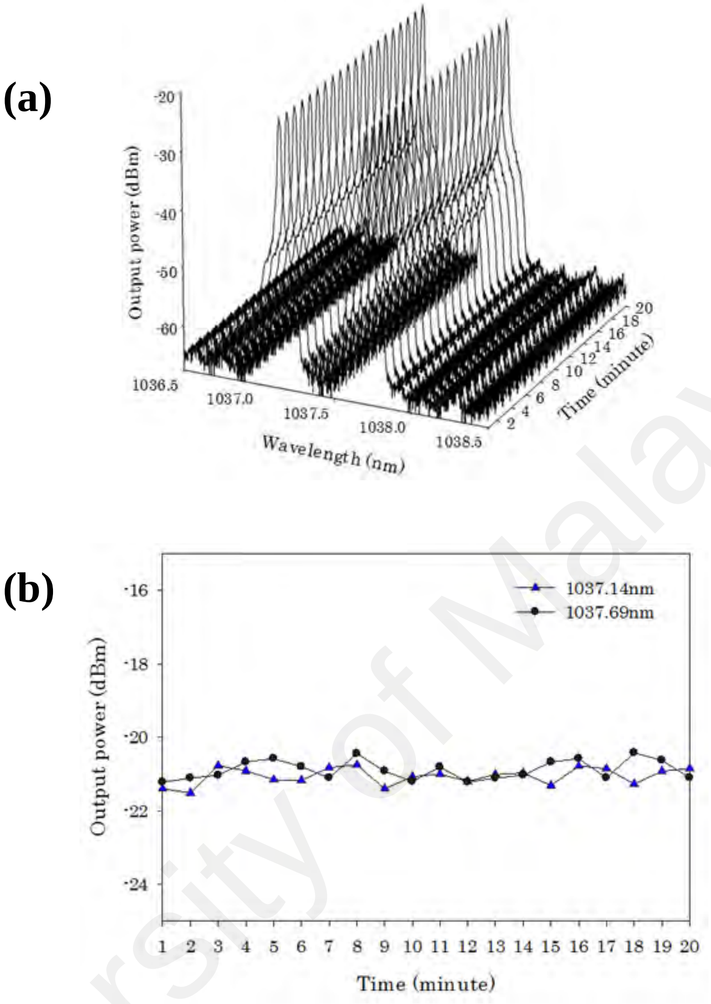

Figure 4.6: (a) dual wavelength output scan, and (b) 20 minutes peak power stability test for spectral spacing of 0.55nm with λ_1=1037.14nm and λ_2=1037.69nm.

4.3 Generation of Dual-Wavelength Passively Q-Switched Ytterbium-Doped Fiber Laser Using Bi_2Te_3 as Saturable Absorber

In this part, we reported a dual-wavelength passively Q-switched YDFL based on a few-layer TI:Bi_2Te_3 SA in a ring cavity setup. The dual-wavelength Q-switched operation was obtained by utilizing short length photonic crystal fiber (PCF) as wavelength selective filter. The two wavelengths were centered at 1042.76 and 1047.0 nm with wavelength spacing of 4.24 nm. The pulse repetition rates obtained from the setup are ranged from 3.79 to 15.63 kHz. The work here demonstrates the saturable absorption nature of TI: Bi_2Te_3 in dual-wavelength Q-switching operation in 1-micron region.

4.3.1 Characterization of few layer Bismuth Telluride SA

In this experiment, the dry oven technique was used to drop few-layer Bi_2Te_3 on the surface of fiber ferrule. The process is illustrated in figure 4.7. The fiber ferrule containing a drop of few-layer Bi_2Te_3 was then placed in the oven (BINDER model FD 53) and heated at 90 degree Celsius for 30 minutes. This process was repeated 3 times until the insertion loss of the fiber ferrule is around 8 dB. This fiber ferrule deposited with Bi_2Te_3 SA was subsequently connected with another ferrule by an optical adaptor to construct a fiber-compatible bismuth telluride Q-switcher.

Figure 4.7: Dry oven technique with few-layer of Bi_2Te_3 drop on the surface of fiber ferrule.

Figure 4.8(a) shows the experimental setup to measure the saturable absorption property of Bi_2Te_3 SA. These measurement systems consist of pulse seed source (Mode locked erbium doped fiber laser (EDFL)) which in this case used CNT to generate homemade femtosecond fiber laser (repetition rate: 27.6 MHz; pulse duration: 0.51 ps), 200m length of single mode fiber (SMF) for dispersion compensation, a variable optical attenuator (VOA), a 3-dB optical coupler and two optical power meter (OPM).

Subsequently the homemade mode locked erbium doped fiber laser (EDFL) generated by CNT where 3 meter erbium doped fiber was pumped by 974nm Laser Diode launch power of 29 mW, (Oclaro Model LC96A74P-20R) through 980/1550 nm wavelength division multiplexing (WDM) coupler. The laser output emerging from the EDF was fusion spliced to the isolator to ensure a unidirectional propagation of the laser inside the cavity. The output of the isolator was subsequently connected to a polarization controller (PC) that controlled the cavity state of polarization. This PC output was then attached to the Carbon Nanotube (CNT) film (sandwiched between the fiber ferrules), which was, in turn connected to a 90/10 fused bi-conical optical coupler denoted as OC1. The pulse signal generated was amplified by using commercial Keopsys EDFA for high peak power to sufficiently saturate the Bi_2Te_3 sample. The mode locked pulse signal is broaden after went through the amplifier therefore SMF was used to compensate the group velocity dispersion (GVD) and reshape pulse signal. The average output power can be amplified up to ~20mW by employed VOA to adjust the input power to Bi_2Te_3 SA. Figure 4.8(b) shows the saturable absorption behavior and well fitted by the following formula:

$$\alpha = \frac{\Delta\alpha}{(1+\frac{I}{I_{sat}})} + \alpha_{linear} \qquad 4.1$$

where $\Delta\alpha$, I_{sat}, α_{linear} represent the modulation depth, saturable optical intensity and non-saturation loss respectively. The modulation depth and saturable intensity were measured to be 67.3% and $0.16 MW/cm^2$ respectively. The modulation depth could be further improved by optimizing Bi_2Te_3 quality and the liquid phase exfoliation processing (Luo et al., 2014).

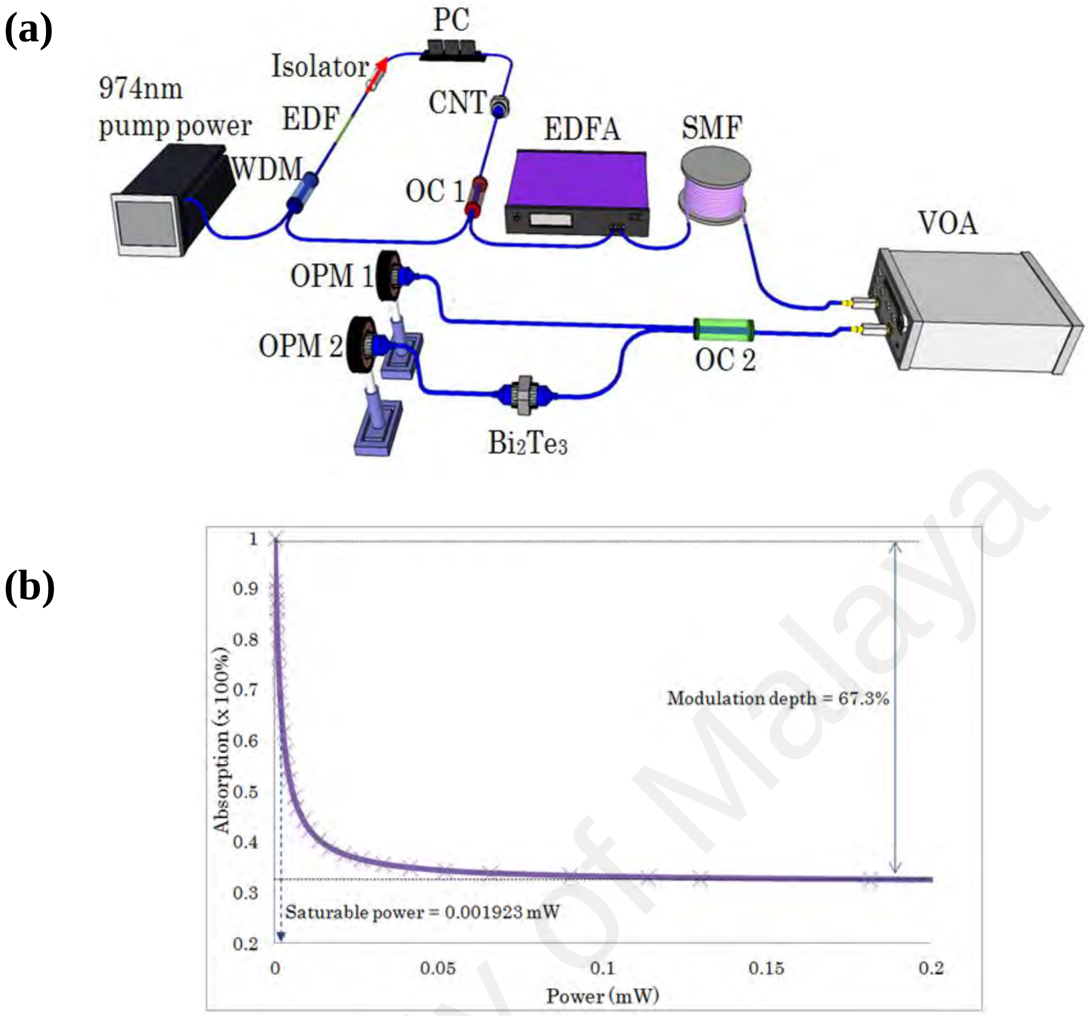

Figure 4.8: (a) The experimental setup for measuring nonlinear absorption of Bi_2Te_3 and (b) The saturable absorption characteristic of the Bi_2Te_3 SA.

4.3.2 Experimental setup

The experimental setup of the proposed dual-wavelength Q-switched YDFL is schematically shown in figure 4.9. The compact linear cavity consists of a 70-cm high-concentration YDF, photonics crystal fiber (PCF) and the Bismuth Telluride (Bi_2Te_3) based SA. The 974 nm center wavelength laser diode with maximum output power of 600 mW and launch power of 132.15mW mW (Oclaro Model LC96A74P-20R) was connected through a 980/1060 nm wavelength division multiplexing (WDM) coupler. One port of the WDM was fusion spliced to a gain medium comprising 70 cm YDF (DF1100 Fibercore) that have peak absorption of 1300 dB/m at 977nm, and another port was connected to a 90/10 optical coupler. Output of the YDF amplifier was then fusion-spliced to a polarization insensitive isolator operating at the 1 μm range. This isolator was incorporated into the laser cavity to ensure unidirectional laser ring operation, which was in the clockwise direction in the context of the figure 4.9 layout. The output of the isolator was subsequently connected to a polarization controller (PC) that controlled the cavity state of polarization, and the PC output was attached to the photonic crystal fiber (PCF) based Mach-Zehnder interferometer (MZI). A constructed compact interferometer using an L=10 cm few mode PCF was spliced into two segment of SMF. The PCF played the main function of stabilizing the Dual Wavelength Fiber Laser (DWFL) output based on its birefringence coefficient and nonlinearity (Bao et al., 2009; C. Zhao, Zhang, et al., 2012). The PCF was a solid core of 4.37 μm in diameter, and surrounded by air holes with 5.06 μm diameter and separation of 5.52 μm between holes. The cross section of PCF is shown in the inset of figure 4.9. Splicing of PCF and SMF fiber was done using Fujikura 45 PM splicer. These two spliced points were located in series and resulted in a simple Mach-Zehnder interferometer, whereby the length of the PCF was directly related to fringe spacing. The PCF was used to produce dual wavelength by adjusting the PC smoothly. The output of the PCF was subsequently connected to Bismuth Telluride (Bi_2Te_3) based SA (sandwiched between the fiber ferrules), which was in turn, connected to the 90/10 fused bi-conical optical coupler, denoted as OC1. The 10% end of the coupler was then joined to 50/50 optical coupler (denoted as OC2) so that the performance of the dual-wavelength q-switched YDFL can be monitored simultaneously via optical spectrum analyzer (OSA) YOKOGAWA AQ6373 with a resolution of 0.02 nm and a high-speed photo-detector attached to digital oscilloscope (YOKOGAWA DLM2054). Apart from that, the output was also measured using an optical power meter and a radio frequency (RF) spectrum analyzer (Anritsu MS2683A, 9 kHz – 7.8 GHz).

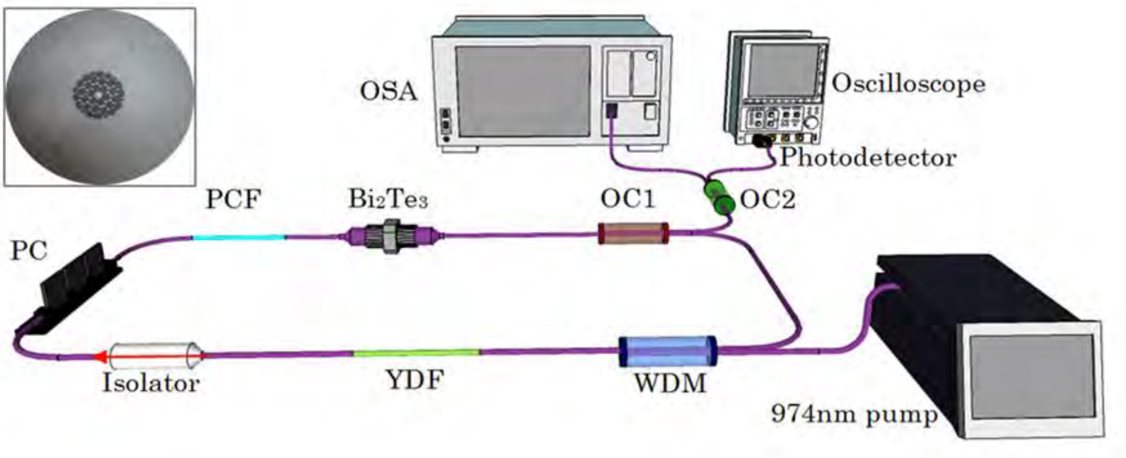

Figure 4.9: Experimental Set up of Bismuth Telluride based passively q-switched ytterbium doped fiber laser, *Inset*: cross section of PCF.

4.3.3 Experimental results and discussion

In the experiment, the YDFL started its Q-switching operation at the pump power of 132.15 mW with repetition rates of 3.79 kHz, as shown in Fig 4.10 (a). When the pump power was gradually increased from 132.15 mW to 138.8, 145.1 and 151.02 mW, a steady pulse trains with different repetition rates were obtained from the oscilloscope trace, as shown in Fig. 4.10 (b)-(d), respectively. The repetition rate was dependent on the pump power to a very high degree, which is the typical response of a passively Q-switching operation. It can also be seen that the pulse width decreased for a corresponding increase in pump power. This effect is due to the gain compression in the Q-switched fiber laser (Herda, Kivistö, & Okhotnikov, 2008).

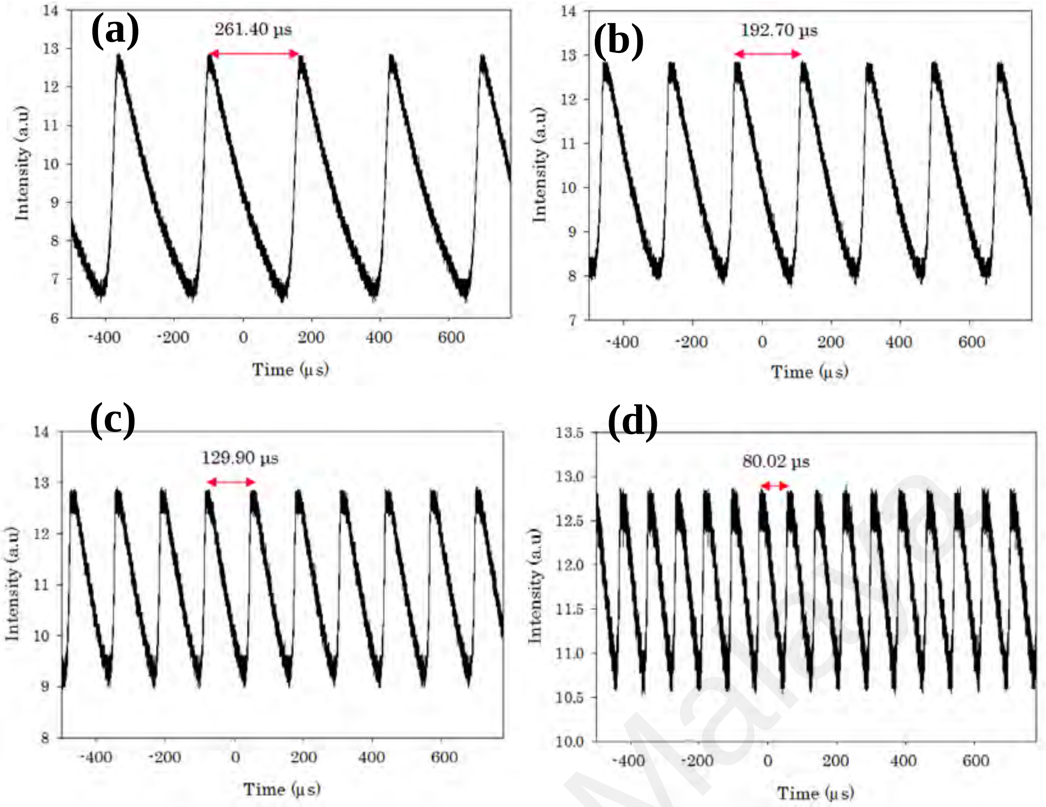

Figure 4.10: The Q-switch pulse train at (a) pump power of 132.15 mW and repetition rate of 3.79 kHz, (b) pump power of 138.8 mW and repetition rate of 5.27 kHz and (c) pump power of 145.1 mW and repetition rate of 7.66 kHz, (d) pump power of 151.02 mW and repetition rate of 12.34 kHz.

Fig. 4.11 (a) shows the output spectrum of two lasing wavelength (1042.76 nm and 1047.00 nm) at pump power of 146.9 mW, taken from the OSA with output power of -17.88 and -17.04 dBm respectively. These two lasing wavelengths can be separated independently by using a wavelength selective filter such as fiber Bragg grating (FBG), tunable band pass filter or any other means. The corresponding Q-switching pulse train with repetition rate of 8.81 kHz was depicted in figure. 4.11 (b) and its pulse width measurement is shown in figure 4.11 (c). In this case, the pulse width was 50.05 µs measured from the full-width half-maximum. Figure 4.11 (d) shows the output pulse train in frequency domain traces obtained from the radio frequency spectrum analyzer (RFSA). The spectrum confirms that the fundamental harmonic has a frequency of 8.81 kHz (from the inset) and has a clearly defined pulse with a peak-to-pedestal ratio of 38 dB. Moreover, the broadband RF spectrum in figure 4.11 (d) shows no spectral modulation, indicating the stable repetition rate of the passively Q-switching.

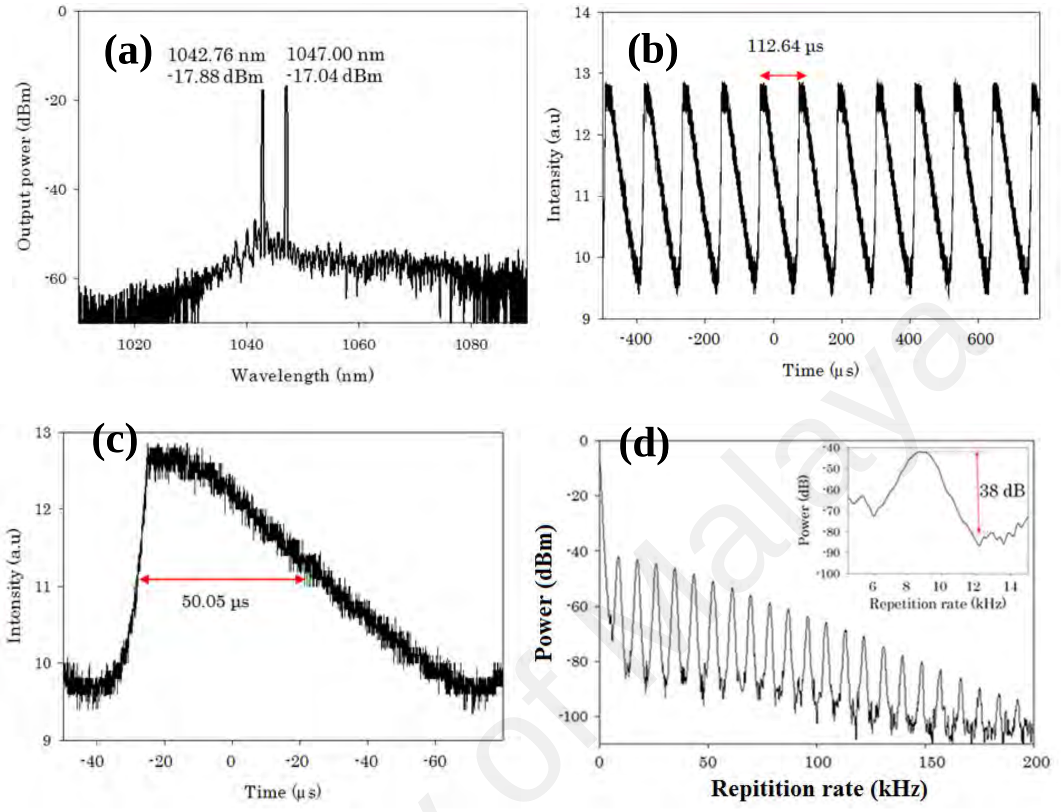

Figure 4.11: The characteristic of q-switching at 146.9 mW with (a) dual wavelength spectrum, (b) pulse duration, (c) pulse width and (d) RF output spectrum.

Figure 4.12 (a) shows the recorded pulse repetition rate and the pulse duration as a function of pump power. As we increased the pump power from 132.15 mW to 153.94 mW, we can see that the repetition rate of Q-switched pulses were increasing from 3.79 kHz to 15.63 kHz while the pulse width was significantly decreased from 96.12 μs to 38.40 μs. The pulse width could be further narrowed by optimizing the parameters, which includes; 1) shortening the cavity length and 2) improving the modulation depth of the TI: Bi_2Te_3 Q-switcher (C. Zhao, Zou, et al., 2012). In addition, as shown in figure 4.12 (b), we also measured the single-pulse energy and corresponding calculated average output power. The pulse energy and the average output power were linearly increased with the input pump power. At the maximum pump power input of 153.94 mW, the maximum average output power is 0.06 mW, while the maximum pulse energy is 3.82

nJ, comparable to those Q-switched fiber lasers using graphene, CNTs and SESAMs as reported in (H Ahmad, Semangun, et al., 2015; Cao et al., 2012; R Paschotta et al., 1999; D.-P. Zhou et al., 2010). The higher pulse energy could be obtained by a using high-gain fiber (e.g. double-clad fiber) with high-performance TI-based SA, and further performance improvement can be achieved by optimizing the cavity designs (e.g. output coupling ratio, cavity loss) (D.-P. Zhou et al., 2010).

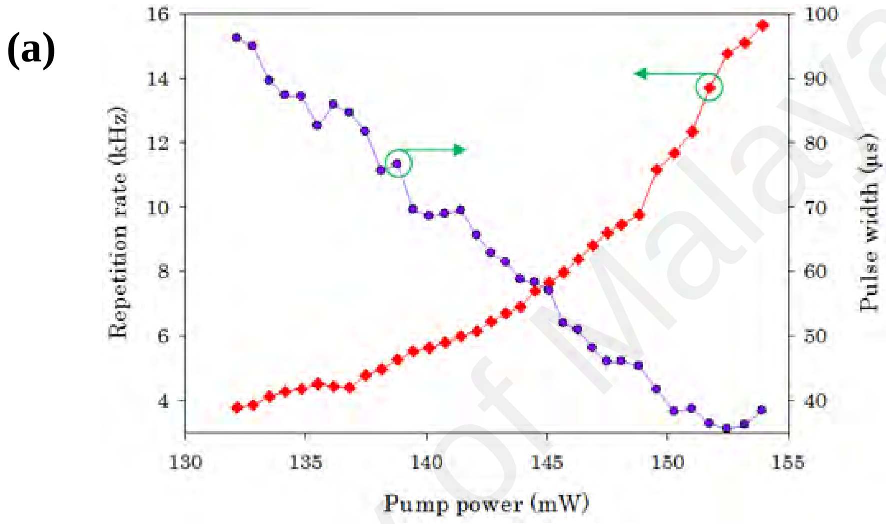

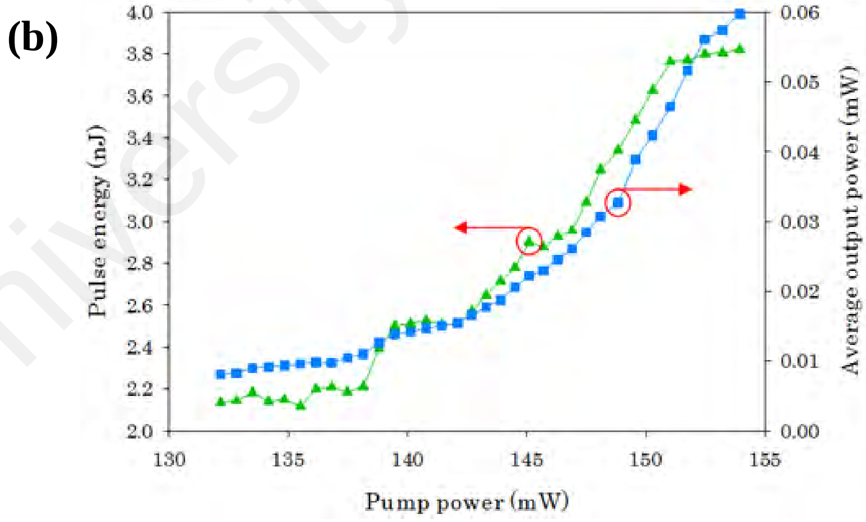

Figure 4.12: (a) The repetition rate and pulse width as a function of pump power, (b) the pulse energy and average output power as a function of pump power.

The obtained dual-wavelength set was stability tested over time due to power stability being one of the most important characteristics of dual-wavelength fiber laser. Figure 4.13 (a) and (b) shows the dual-wavelength stability scan for a period of 20 minutes. Figure 4.13 (a) displays a very stable lasing wavelength over the test period and figure 4.13 (b) illustrates power fluctuation during the scan, in which the maximum fluctuation is observed as less than 0.8 dB. Such results proved that the wavelength and average power is stable over time and experienced only a very small power fluctuation at room temperature. It should be noted that a test measurement of the dual-wavelength was performed simultaneously with these stability tests, and as such these results confirmed the stability and reliability of the proposed setup.

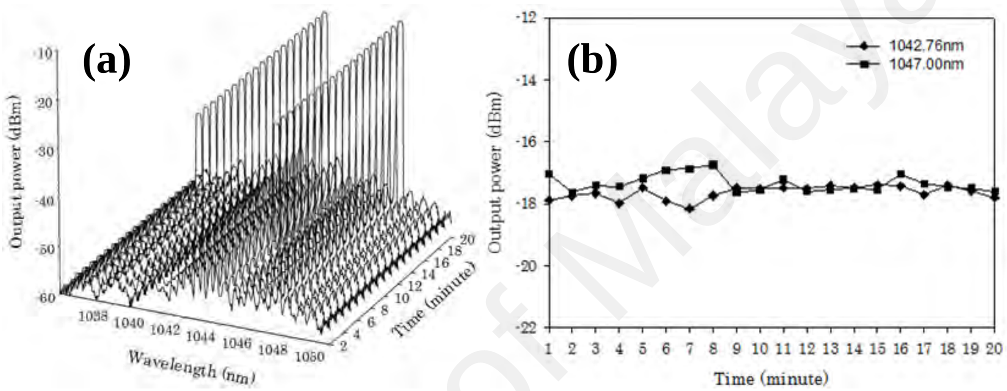

Figure 4.13: (a) dual wavelength output scan, and (b) 20 minutes peak power stability test for spectral spacing of 4.24nm with λ_1=1042.76nm and λ_2=1047.00nm.

4.4 Stable Narrow Spacing Dual-wavelength Q-Switched Graphene-Oxide embedded in Photonic Crystal Fiber

This part proposes, for the first time, a novel approach of using a very short solid core photonics crystal fiber (SCPCF) of approximately 10 cm in length, with approximately 60 μm of GO solution filled inside the PCF's cladding as a saturable absorber (SA) in order to generate an ultra-stable dual-wavelength output. Changing the orientation of Polarization Controllers (PC) within the laser cavity allows specific polarization states to pass through the PCF. In this aspect, the PCF acts as a selective mechanism to accumulate those orthogonal polarization states that will increase the PHB effects in the cavity and also introduce spatial hole burning (SHB) that contributes to reducing the homogeneous line width of the EDF and suppressing unstable mode competition. The PHB effect also greatly enhances the inhomogeneous gain broadening effect in the EDF, and accordingly reduces the mode competition (Qian, Su, & Hong, 2008). The combination of the PCF and embedded GO generate a desired pulsed output while still maintaining the compact form of the system. The proposed laser also allows for continuous tuning between the two wavelengths. This dual-wavelength fiber laser will have significant potential as a seeder pulse for pulsed microwave and terahertz generation.

4.4.1 Experimental setup

The experimental setup of the proposed stable dual-wavelength Q-switched fiber laser is shown in figure 4.14 (a). The laser uses a 0.9 m long highly doped Leikki Er80-8/125 Erbium Doped Fiber (EDF) as the active gain medium. The EDF is pumped backward by a Lumics 980 nm laser diode through a Wavelength Division Multiplexer (WDM). One end of the EDF is connected to the common output of the WDM, while the other end is connected to an isolator to ensure no signals propagate in the opposite direction through the EDF. The isolator connected to the Tunable Band-pass Filter (TBPF) is used to avoid any unwanted back reflection towards the gain medium. The isolator is in turn connected to a TBPF, which is used as a tuning element to define the area of lasing whether single wavelength or dual-wavelength output. The TBPF has a narrow bandwidth of 0.8 nm, high tuning resolution of 0.05 nm, a broad tuning range of 1535–1565 nm and low insertion loss typically around 1.5 dB.

The TBPF is used to determine the operational bandwidth of the fiber laser, while the PC serves to adjust the polarization states of the cavity such that either two wavelengths or only a single wavelength may oscillate in the cavity, thereby giving the desired dual-wavelength output. The output of the TBPF is the connected to a Polarization Controller (PC), and subsequently to a PCF with a zero-dispersion wavelength at about 987 nm and an overall diameter of 124 μm as well as a length of 10 cm. The PCF is held in place by a pair of bare fiber adaptors (BFA), and is used to generate the desired stable dual-wavelength output. The inset of the figure 4.14 (a) shows the cross-section of the PCF.

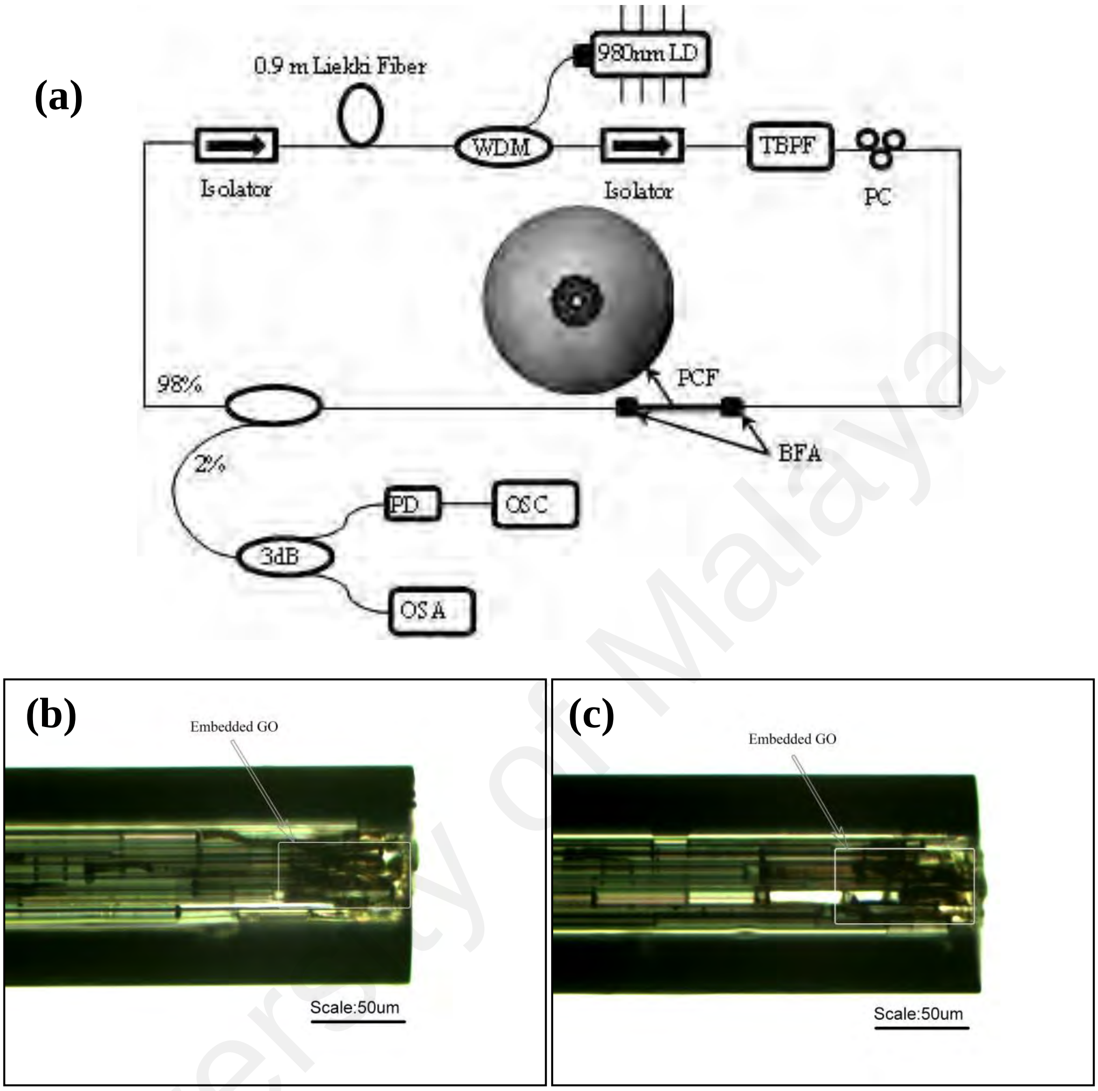

Figure 4.14: (a) Experimental setup of dual-wavelength Q-switched fiber laser and the inset is the cross-section image of the PCF. (b) X-view (c) Y-view of the PCF.

Figure 4.14 (b) and (c) show the embedded GO inside the PCF in X-view and Y-view respectively. The embedded GO is about 60 μm long. The PCF's core structure consists of a solid core of approximately 4.37 μm diameter surrounded by microscopic air-holes, each with an approximate diameter of 5.06 μm and a separation of 5.52 μm between neighboring air-holes. The output of the PCF is guided toward a 98:2 coupler, which extracts a portion of the signal for analysis. The 98% port is connected to the isolator, which is then connected to the gain medium. This completes the laser cavity. The extracted output is divided into two even powered portions using a 3 dB coupler, with one portion being directed to a high resolution Optical Spectrum Analyzer (APEX AP2051A) (OSA) or Anritsu MS9780A while the other spectrum is analyzed separately to obtain the average output power, the spectrum in the time domain, and radio frequency spectrum.

4.4.2 Experimental results and discussion

The dual-wavelength generation in a cavity with PCF has been well explained in reference (W. G. Chen et al., 2009) and (Y.-G. Han, 2010). Typically in a ring laser without the PCF and PC, different wavelengths in almost identical polarization states will be propagating within the laser cavity. Integrating the PCF and PC into the laser cavity results in the polarization states of different wavelengths in the EDFA being dispersed through wavelength dependent polarization rotations that enhance PHB. The narrow-pass filtration of approximately 0.8 nm means over two thousand possible longitudinal modes could pass through the band pass filter in this setup due to the length of the cavity being approximately 6.0 m. The PC then disperses the oscillating modes into one of two possible polarization states, with different spacing that can be adjusted by fine-tuning the PC. The PHB effect comes into play when these modes enter the EDF (which is the active medium of the laser) at different polarization states, and results in lesser mode competition, thus enhancing multi-wavelength generation. The PCF acts as a simple Fabry-Perot cavity that will filter out part of the longitudinal modes, thereby leaving only a few modes oscillating in the cavity. The dual-wavelength output can be realized by fine-adjusting the PC. This operating regime is obtained at a pump power of 90.0 mW, with a launch power into the cavity of about 75.0 mW. The spectrum was monitored using the APEX OSA at the highest resolution of 0.16 pm. The desired dual-wavelength output is obtained by carefully adjusting the PC so as to generate a very stable output. Transmission spectrum of the ring cavity including PCF as a filter with an unpolarized amplified spontaneous emission (ASE) source is depicted in figure 4.15. The insertion loss of the filter is about 6 dB. The fringe spacing is approximately 0.288 nm around 1530 nm. The spectral characteristics were measured by using a YOKOGAWA AQ6370B optical spectrum analyzer (OSA) with 0.02 nm resolution.

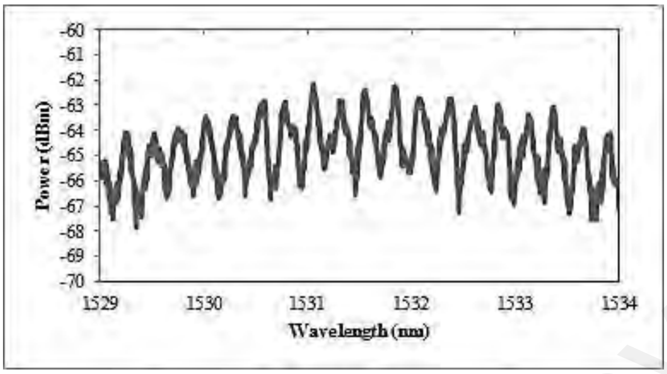

Figure 4.15: Transmission spectrum of the ring cavity including PCF as a filter in a very low pump power of about 15 mW.

A typical result of this dual-wavelength output is shown in the figure 4.16 (a), with a spacing of 0.41 nm between the wavelengths of 1553.42 nm and 1553.83 nm. The corresponding power is -38.09 dBm and -38.08 dBm respectively. Figure 4.16 (b) indicates the stability of this dual-wavelength output over time. The spacing can be tuned by adjusting the TBF together with the PC. Figure 4.16 (c) shows the dual-wavelength output spectrum taken by high resolution OSA being shifted by further adjusting the PC, giving a wavelength spacing of 0.03 nm over the two wavelengths of 1561.64 nm and 1561.67 nm. The corresponding power is -34.32 dBm and -33.12 dBm respectively. The wavelengths are stable and clean, as evidenced by a high Signal to Noise ratio (SNR) of 53.4 dB. The 3 dB linewidth of the output is about 0.6 pm.

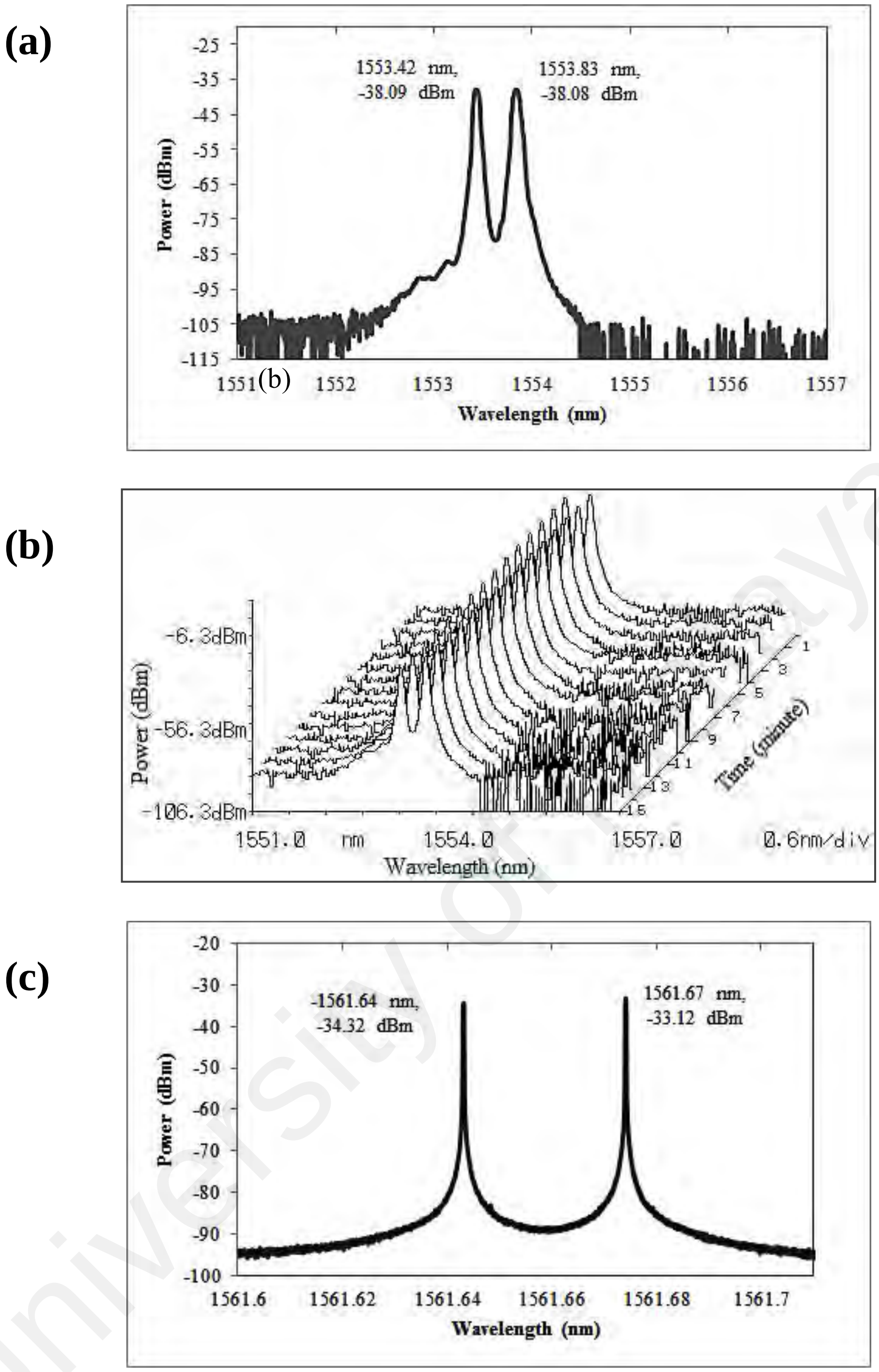

Figure 4.16: (a) Dual-wavelength output spectrum shifted by adjusting the PC, giving a wavelength spacing of 0.41 nm at the wavelength of 1553.42 nm and 1553.83 nm, (b) The stability of switched dual-wavelength laser over time and (c) Dual-wavelength output spectrum shifted by further adjusting the PC, giving a wavelength spacing of 0.03 nm over the two wavelengths of 1561.64 nm and 1561.67 nm.

Figure 4.17 (a) shows the pulse train of the generated pulses from the Q-switched laser. As can be seen in this figure, the pulses obtained are relatively stable, with a pulse repetition rate of approximately 16 kHz. The operating parameters remain unchanged, with the pump power kept constant at 90.0 mW before entering the laser cavity. The pulses are observed by connecting the open port of the 3 dB coupler to a Thorlabs MOBEL D40FC Indium-Galium-Arsenide (InGaAs) photo detector that is in turn connected to a Tektronix TDS 3052C 500 MHz digital oscilloscope (OSC). The pulse repetition rate versus the pump power and pulse energy is shown in figure 4.17(b).

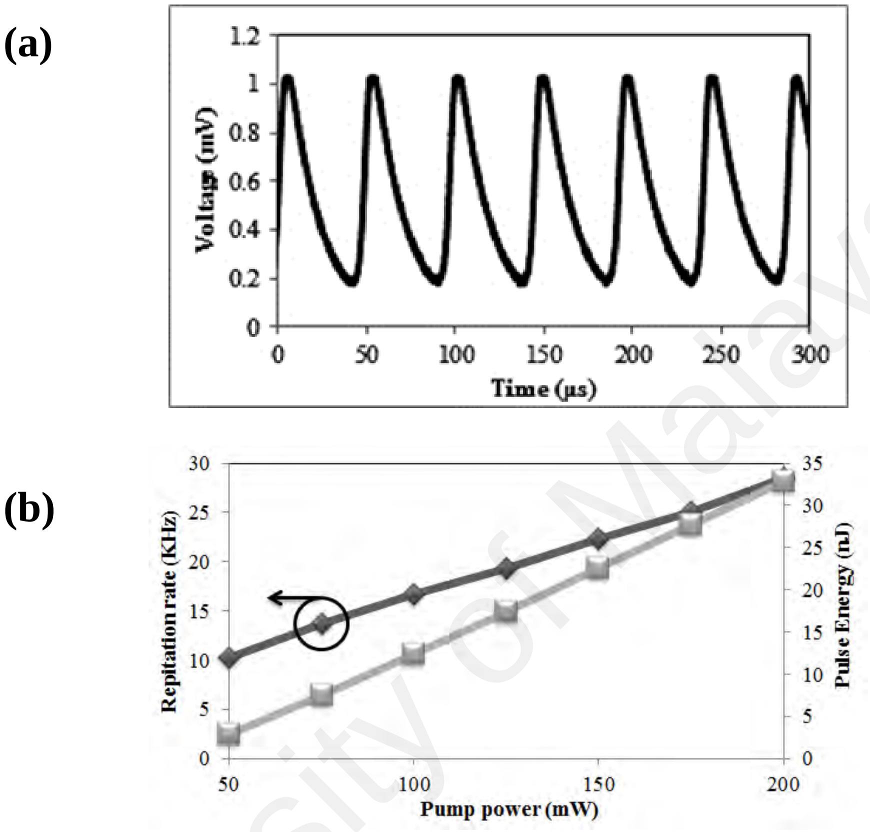

Figure 4.17: (a) Pulse train of the dual-wavelength Q-switched fiber laser pumped at 90 mW. (b) Variation of the repetition rate by changing the pump power.

4.5 Photonic Crystal Fiber based Dual-Wavelength Q-Switched Fiber Laser using Graphene Oxide as a Saturable Absorber

In this part, we propose, for the first time, a novel approach of using a very short Photonics Crystal Fiber (PCF), approximately 10 cm long as a means to generate a dual-wavelength output. The output is made to pulse by incorporating a GO based SA into the laser cavity, which generates the desired pulsed output while still maintaining the compact form of the system. The proposed laser is also tunable, allowing a continuous tuning between the two wavelengths. The proposed dual-wavelength fiber laser will have significant potential as a seeder pulse for pulsed terahertz generation.

4.5.1 Graphene Oxide as Saturable Absorber

The GO based SA used in this work is fabricated by depositing a GO layer on the face of a fiber ferrule. The GO is obtained from Graphene Supermarket Ltd in the form of a GO paper with each disk having an average diameter of 4.0 cm and a thickness of about 10 μm. For the purpose of this experiment, a small piece of the GO paper, about 1 mm x 1mm in area is cut from the GO paper and is placed onto the ferrule, which was prepared with a very thin layer of Index Matching Gel (IMG) on its surface. The ferrule with the GO layer is then connected to an FC/PC adaptor, and a fiber ferrule with a clean surface is then connected to this adaptor, thereby sandwiching the GO layer in between the two ferrules and thus creating the required SA. GO has certain advantages in terms of its mechanical properties, as reported in references (Dikin et al., 2007; S. Park et al., 2008). GO is a low cost and highly attractive alternative to conventional graphene (Harith Ahmad, Zulkifli, Kiat, & Harun, 2014). As it is a precursor for pristine graphene, GO exhibits the same, and in some cases even comparable optical properties of graphene (J. Xu, Liu, Wu, Yang, & Wang, 2012; X. Zhao et al., 2011). The primary advantage of GO however is its ease of fabrication – GO can be easily fabricated from graphite, an inexpensive and easily available raw material. Furthermore, GO is also hydrophilic, thus fulfilling the important criterion of stable aqueous colloids for the easy assembly of macroscopic structures. Figure 4.18 shows the microscopic image of the GO layer on the face of the fiber ferrule.

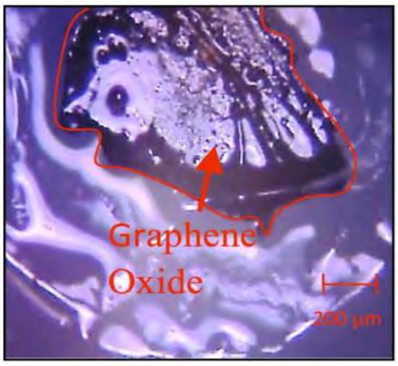

Figure 4.18: Microscopic image of GO layer surrounded by IMG.

It can be seen from the figure that the GO layer is placed in such a way that it falls on the centre of the fiber ferrule, thereby allowing it to completely envelope the propagating beam from the fiber. The GO layer is approximately 1200 µm across its longest length, and is kept in place once the other fiber ferrule has been connected to the FC/PC adaptor. This forms the GO-based SA (GOSA) assembly. Figure 4.19 shows the spectral analysis of the GO paper deposited on the face of the fiber ferrule. The Raman spectroscopy was carried out at a laser output of 50 mW at 532 nm for a period of 10 s.

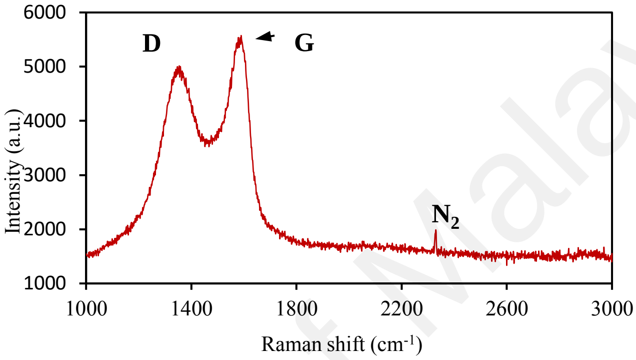

Figure 4.19: Raman spectrum of Graphene Oxide saturable absorber as on the ferrule of the optical connector.

The obtained output spectrum clearly indicates the presence of two peaks at 1353.00 cm^{-1} and 1585.35 cm^{-1} respectively and corresponds to D and G peaks of about similar value as reported in (Haubner et al., 2010). The D intensity is approximately 5000 arbitrary units, while the G intensity is about 5500 arbitrary units. The relatively high D intensity indicates that the edges of the sample form an armchair structure; on the other hand, a low D value would have indicated a predominantly zig-zag edge structure (Casiraghi et al., 2009). The relative intensity ratio of both D and G peaks (I_D/I_G) is computed to be 0.8971 which approximates closely that obtained in reference (L. Chang, Wu, Chen, & Li, 2011). The higher I_D/I_G indicates that there is a higher level of disorder arising from the formation of covalent bonds in the GO layer as a result of the functionalizing material used. A small peak is also observed at 2329.00 cm^{-1}, which is possibly due to the presence of minor amounts of N_2 contaminants present during the characterization process.

4.5.2 Experimental Setup

The experimental setup of the proposed narrowly-spaced dual-wavelength Q-switched fiber laser is shown in figure 4.20. The laser uses a 3 m long Erbium Doped Fiber (EDF) as the active gain medium which has peak absorption of 18.06 dB/m in the wavelength of 980 nm. The EDF is pumped by a Lumics 980 nm laser diode through a Wavelength Division Multiplexer (WDM). One end of the EDF is connected to the common output of the WDM, while the other end is connected to an isolator to ensure no signals propagate in the opposite direction through the EDF. The isolator is in turn connected to a Tunable Bandpass Filter (TBF), which is used as a tuning element to isolate a single wavelength from the dual-wavelength output. The TBF has a bandwidth of 0.8 nm and a tuning resolution of 0.05 nm. The output of the TBF is the connected to a Polarization Controller (PC), and subsequently to a PCF with a zero-dispersion wavelength at about 987 nm and an overall diameter of 124 μm as well as a length of 10 cm. The PCF is held in place by a pair of bare fiber holders, which imposed a total loss of 5 dBm, and is used to generate the desired stable and narrow spacing dual-wavelength output by polarization dependence loss (PDL) and fringe spacing effects. The cross-section of the PCF is shown in the inset of the figure 4.20 and it can be seen that the core structure consists of a solid core approximately 4.37 μm diameter surrounded by microscopic air-holes, each with an approximate diameter of 5.06 μm and a separation of 5.52 μm between neighboring air-holes.

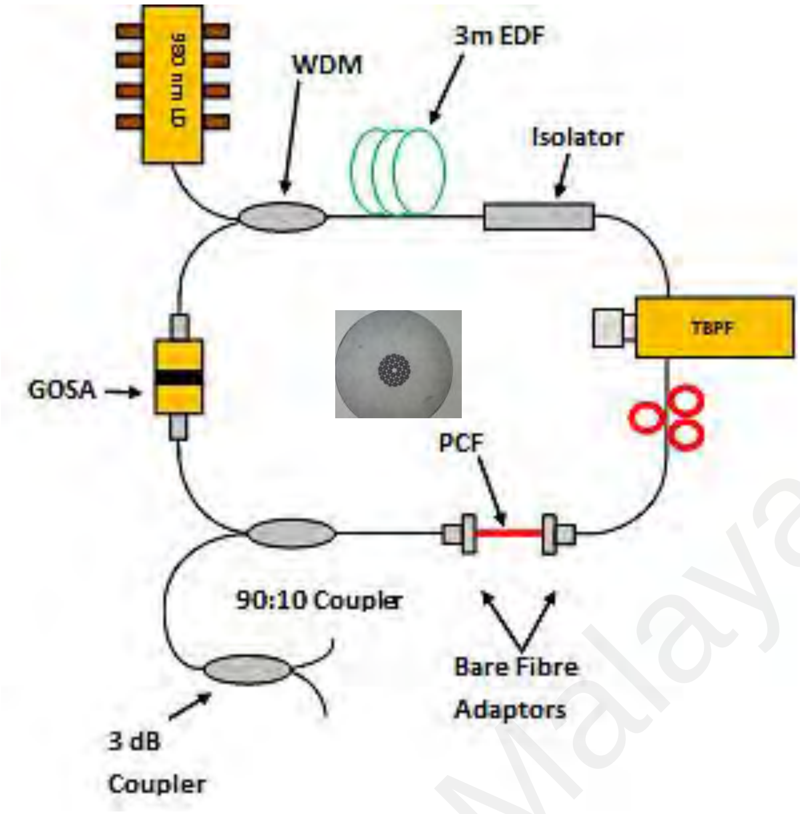

Figure 4.20: Experimental setup of the narrowly-spaced dual-wavelength Q-switched fiber laser and inset is the cross-section image of the PCF.

The output of the PCF is guided towards a 90%:10% coupler, which extracts a portion of the signal for analysis. The 90% port is connected to the GOSA, which is then connected to the signal port (1550 nm port) of the WDM. This completes the laser cavity. The extracted output is divided into two even powered portions using a 3 dB coupler, with one portion being directed to a high resolution Optical Spectrum Analyzer (APEX AP2051A) (OSA) while the other spectrum is analyzed separately to obtain the average output power, the spectrum in the time domain, and radio frequency spectrum. The dual-wavelength output is obtained by the incorporation of the PCF and PC into the cavity, which results in the dispersion of the oscillating modes in the cavity along one of two possible polarization states, with each state being perpendicular to the other. This will result in the Polarization Hole Burning (PHB) effect in the EDF, which results in lower mode competition and as a result enhancing dual-wavelength generation. Furthermore, the 6 folded PCF will doubly degenerates the fundamental modes leading to strong suppression of those modes when they coupling back to the SMF (S. K. Bhadra & A. K. Ghatak, 2013). This will further filter out unwanted longitudinal modes until only a few modes propagate in the cavity. Fine-tuning of the PC now allows a dual-wavelength output to be generated. This mechanism has been explained in reference (WG Chen et al., 2009).

4.5.3 Experimental results and discussion

Figure 4.21(a) shows the dual-wavelength output without the GOSA in the cavity, operating in a Continuous Wavelength (CW) mode. This operating regime is obtained at a pump power of 66.0 mW, with a launch power into the cavity of about 52.4 mW. The spectrum was monitored using the APEX OSA at the highest resolution of 0.16 pm with a span of 0.164 nm. The desired dual-wavelength output is obtained by carefully adjusting the PC so as to generate a very stable output. A typical result of this dual-wavelength output is shown in the figure, with a spacing of about 0.028 nm between the two wavelengths of 1551.845 nm and 1551.873 nm. The spacing can be adjusted or tuned by adjusting the TBF, together with the PC. The wavelengths are stable and relatively ‘clean’, with a high Signal-to-Noise (SNR) ratio of 53.7 dB. The 3 dB linewidth of the output is about 0.6 pm.

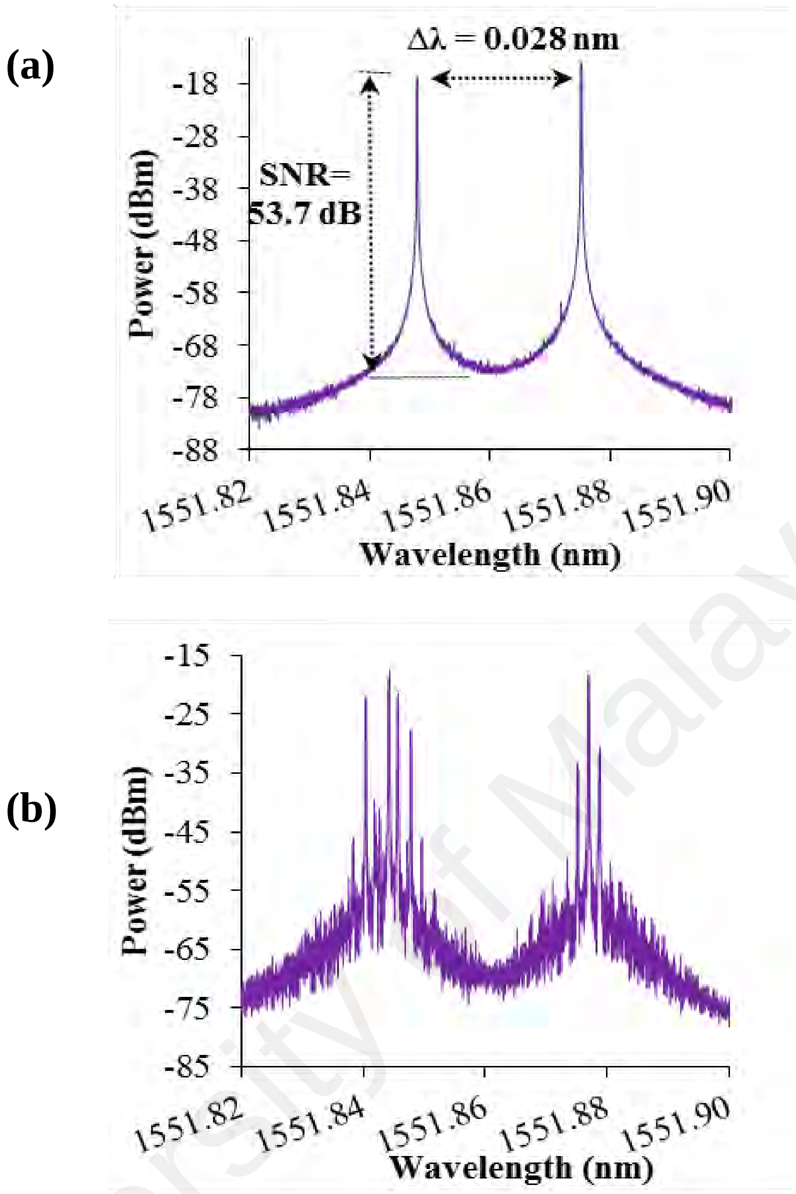

Figure 4.21: Dual-wavelength laser spectra captured using high resolution optical spectrum analyzer with a resolution of 0.16 pm at (a) CW and (b) Q-switching with GOSA assembly is employed in the laser cavity.

On the other hand shows the lasing output of the Q-switched dual-wavelength output, which is obtained by having the GOSA in the cavity. Unlike the spectrum obtained previously, the inclusion of the GOSA generates spikes as observed in the wavelength spectral scan of figure 4.21 (b). Typically, a lower resolution OSA, such as one with a resolution of 0.02 or 0.03 nm would show a ‘cleaner’ spectrum with less spikes. However, the high resolution of 0.16 pm allows for a substantially more detailed spectrum to be observed, and it thus be seen that rather than two output wavelengths with broadened line-widths, the Q-switched laser output in reality consists of a series of spikes around the central wavelength region in the wavelength domain (or frequency domain). Analysis of the output in figure 4.21 (b) gives an average wavelength spacing of 0.032 nm, as well as a slightly lower SNR of about 49.6 dB, as obtained from the two highest peaks of the spectrum.

Overall, the output generated by the system is stable, with little fluctuation in power. For the output generated by the system, a narrow channel output as shown in figure 4.22 is obtained. It can be seen that the output, which has a wavelength spacing of 170 pm between two wavelengths at 1553.85 and 1554.02 nm is highly stable, and shows almost no fluctuation in wavelength or power over a test period of 22 minutes.

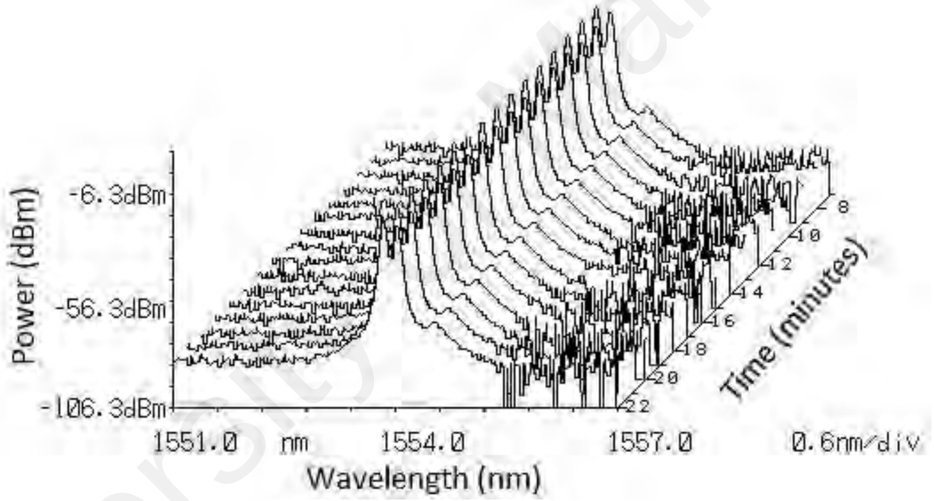

Figure 4.22: Stability of the system with channel spacing of 170 pm

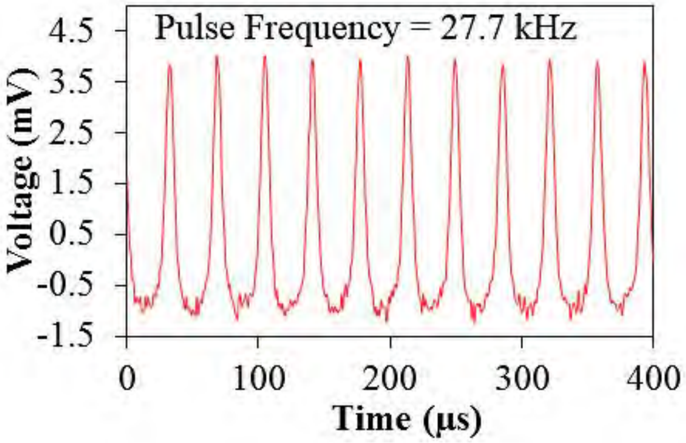

Figure 4.23: Pulse train of the dual-wavelength Q-switched fiber laser pumped at 66 mW measured using digital oscilloscope.

Figure 4.23 shows the pulse train of the generated pulses from the Q-switched laser. As can be seen in figure 4.23, the pulses obtained are relatively stable, with a pulse repetition rate of approximately 27.7 kHz and with average peaks of 3.7 mV. The operating parameters remain unchanged, with the pump power before entering the laser cavity kept constant at 66.0 mW. The pulses are obtained by connecting the open port of the 3 dB coupler to a Thorlabs MOBEL D40FC Indium-Galium-Arsenide (InGaAs) photo-detector which is in turn connected to a LeCroy 500 MHz digital oscilloscope (OSC). Figure 4.24 (a) and (b) provide a detailed analysis on a single pulse which has been extracted from the pulse train. Analysis of a single pulse peak, as shown in figure 4.24 (a), reveals a pulse with an average pulse-width of 8.4 μs. Figure 4.24 (b) on the other hand shows an overlap of 6 consecutive pulses extracted from the same pulse train, approximately 10 seconds apart. From figure 4.24 (b), it can be seen that the pulse-widths of the various pulses are stable and consistent at 8.4 μs. Minor fluctuations in the amplitudes of the pulses are observed, with a deviation of about 0.5 mV from the average amplitude of 3.7 mV. Analysis of the Q-switched pulses is also undertaken by replacing the photodiode and OSC with a (brand) Radio Frequency Spectrum Analyzer (RFSA). Figure 4.25 shows the first harmonic of the pulse train, which is taken at a resolution of 300 Hz and video bandwidth of 1 MHz. A Signal-to-Noise Ratio of about 37 dB is obtained, indicating that the pulse is stable.

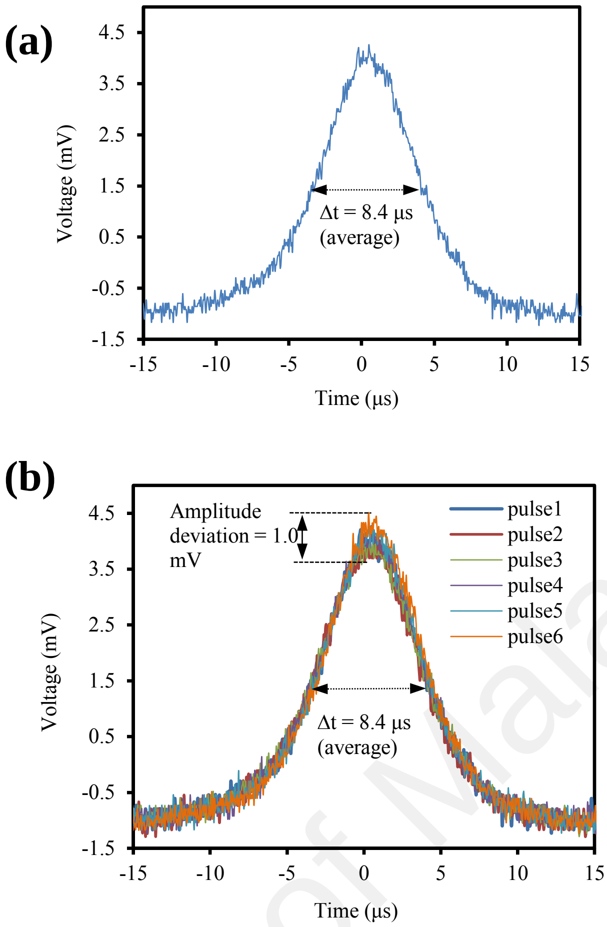

Figure 4.24: (a) Single pulse as obtained from pulse train (b) overlap of 6 consecutive pulses from the same pulse train, with each pulsetaken10 seconds apart.

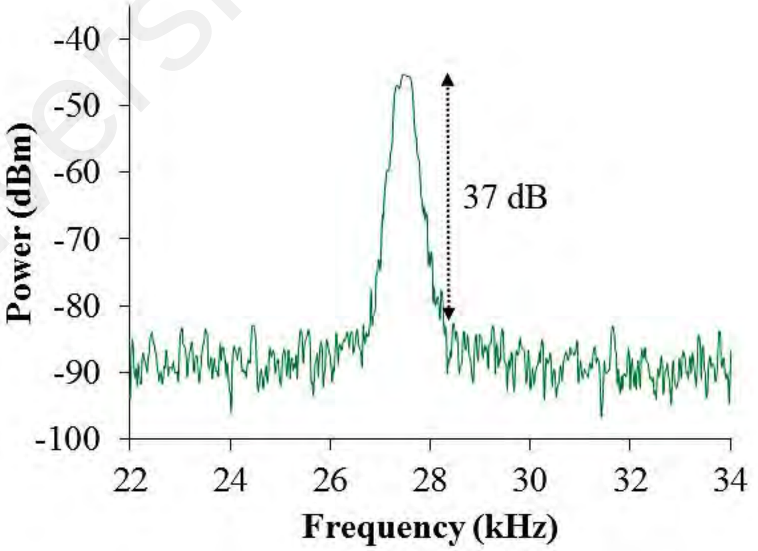

Figure 4.25: First harmonic radio frequency spectrum of the Q-switched DWFL.

Figure 4.26 (a) shows the repetition rate and pulse width of the Q-switched dual-wavelength fiber lasers taken at increasing pump powers. The Q-switching threshold of the laser is determined to be approximately 54 mW. The repetition rate behaves as expected for a Q-switched fiber laser, rising linearly at the threshold power to a maximum repetition rate of 31.0 kHz at a pump power of 72 mW.

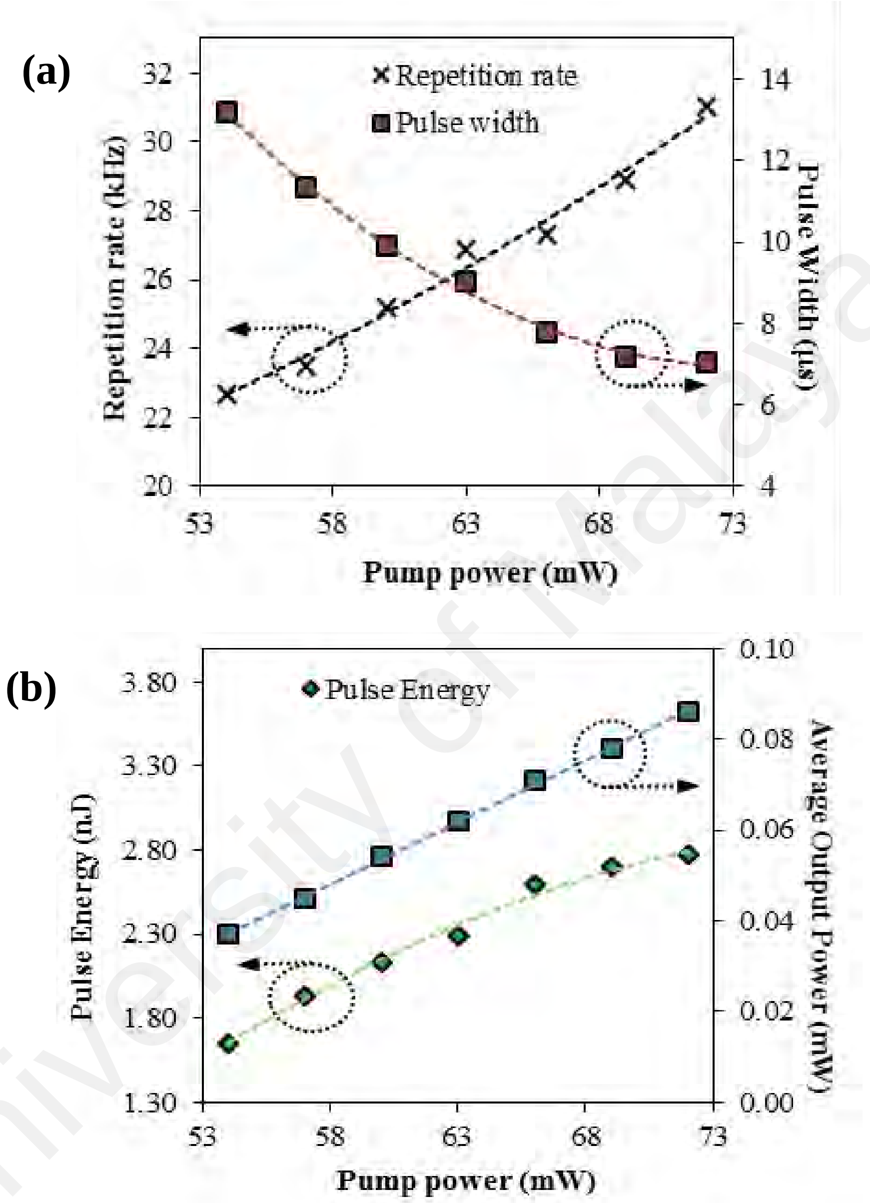

Figure 4.26: (a) Repetition rate and pulse width curves at different pump powers and (b) Pulse energy and average output power curves at different pump powers.

It is important to note that the maximum pump power here is the limitation of the 980 nm LD pump used; an LD with a higher pump would generate a larger repetition rate. The pulse-width on the other hand decreases as the pump power is increased, from 13.2 μs at the threshold power until approximately 7.0 μs at a pump power of 69 mW, after which the pulse width begins to exhibit signs of saturation. Figure 4.26 (b) shows the pulse energy and average output power of the pulses as a function of the pump power. It can be seen that both the pulse energy and average output power increase as the pump power is raised, with the average output power rising from 0.037 mW to 0.086 mW as the pump power increases from 54.0 mW to 72.0 mW. The increase is almost linear, at a uniform rate of 0.0027. The pulse energy on the other initially increases at an almost linear rate, rising from 1.7 nJ to 2.6 nJ as the pump power increases from 54 mW to 66 mW. However, above 66 mW, the rate of increase in the pulse energy becomes shallower, rising from 2.7 to only 2.8 nJ as the pump power increases from 69 mW to 72 mW. The stability of the dual-wavelength output and the narrow channel spacing that can be obtained make the proposed dual-wavelength fiber laser highly suitable for a multitude of applications, in particular those related to sensing microwave and terahertz generation.

CHAPTER 5: APPLICATIONS OF DUAL-WAVELENGTH FIBER LASERS

5.1 Introduction

As has been discussed previously, DWFLs can be used for applications such as sensors and optical instrument testing (D. Liu et al., 2007; Shengchun Liu et al., 2009; Shimose et al., 1991) which requires high precision, and therefore normally sophisticated measurement. DWFLs are also applicable for Terahertz generation (Jeon, Kim, et al., 2010b; Jeon, Kim, Shin, Lee, et al., 2010; M. Tang & Wang, 2010; Taniuchi, Shikata, & Ito, 2000), iron concentration measurement (G. Lu, 1999); and for microwave and millimeter-wave generation (X. Chen et al., 2006; Villanueva et al., 2009; Yao et al., 2006; J. Zhou, Xia, Cheng, Dong, & Shum, 2008).

Additionally, dual-wavelength fiber lasers can also be applied in the communication systems as a wavelength converter by employing four waves mixing (Chow, Shu, Mak, & Tsang, 2001; Hsu et al., 2003) effects. This is achieved by converting the signal from one communication band to another without the use of any active devices to allow for an optical-electrical-optical conversion, thus effectively fulfilling the communication demand with a low cost borne by the network providers.

This chapter focuses on the potential applications of the DWFLs. It has to be noted that despite the fact that there are a number of applications for the DWFL, each of the application requires certain changes in the design of the DWFL in order to meet the unique demand of each application. Particularly, the majority of the DWFLs will need to be in single longitudinal mode (SLM) operations, which is a condition whereby the laser sources are free of noise or mode fluctuations.

5.2 Tunable microwave output over a wide RF region generated by optical dual-wavelength fiber laser

5.2.1 Introduction

The generation of microwave signals from optical sources has long been a substantial area of interest due to its large potential for a variety of applications encompassing communications, sensors, and testing (Enming, Xinliang, Lina, Yu, & Dexiu, 2009; Shupei et al., 2013; Siyu et al., 2013; E.-M. Xu, Zhang, Zhou, Zhang, & Huang, 2009; X. P. Yang, Gan, Xu, & Yang, 2013). Microwave signals of high frequency and little phase noise can easily be generated from optical sources by beating two optical signals that have consistent wavelength spacing. The advantage of such signals is that they can be potentially distributed over single mode optical fibers, resulting in very low transmission losses and so preserve the overall power of the system.

One method of generating microwave signals lies in exploiting beat frequency outputs at a photo detector from two laser beams from two different sources (Fan & Dagenais, 1997; Genest, Chamberland, Tremblay, & Têtu, 1997). This method allows generation of a beat signal without a reference microwave source, although an appropriate phase-locking technique is required. Alternatively, microwave signals can be created using external modulators, such as electro optic intensifier or phase modulator (O'reilly, Lane, Heidemann, & Hofstetter, 1992).

Both approaches, while capable of generating the desired output, suffer from a limitation in that the required phase matching is very difficult to achieve and typically requires a reference source for signal stability and low noise. As such, a laser source capable of generating a single wavelength with dual longitudinal modes (Hyodo, Tani, Matsuura, Onodera, & Sakai, 1996; Siyu et al., 2013), or two wavelengths with each in the single longitudinal mode (SLM) (Brunel et al., 2004), would be highly attractive. Multi-wavelength fiber lasers are inexpensive, stable and highly compatible with existing fiber systems, and thus have substantial opportunities for the optical generation of microwave signals. Research attention is most often directed to the wavelength selectable filter since the filtering scheme is of critical importance to the operating characteristics of a multi-wavelength fiber laser. The quality of the microwave signals generated by the beating of two wavelengths from a single laser source is subject to a number of requirements: both wavelengths must operate in single longitudinal mode (SLM), possess consistent spacing between the two wavelengths, exhibit no mode hopping, and have an insignificant relative phase fluctuation. The best approach to achieve this result is the use of active fibers such as erbium-doped fiber (EDF) to generate a broad-spectrum output that can then be sliced into the desired dual-wavelength output. Wavelength selection can be accomplished via devices such as fiber Bragg gratings (FBGs) (Alvarez-Chavez, Martinez-Rios, Torres-Gomez, & Offerhaus, 2007; Bao et al., 2009; S. Feng, Xu, et al., 2008; Y.-G. Han, Van Anh Tran, & Lee, 2006; M. Lin, Zexin, Yanhui, & Shuisheng, 2014; Moon, Paek, & Chung, 2005). Alternatively, a PCF in a Sagnac loop configuration together with a broadband FBG has been demonstrated to generate a dual-wavelength output via mode suppression and inhibiting mode competition through Spectral Hole Burning (SHB) and Polarization Hole Burning (PHB) (Weiguo Chen et al., 2009). The flexibility afforded by the PCF permits a number of applications, such as sensor equipment, that are otherwise unattainable by other methods of suppressing mode competition.

This part demonstrates a switchable stable dual-wavelength fiber laser by means of introducing a segment of highly nonlinear PCF into an optical circuit loop. The PCF in question is of a short length with the zero dispersion wavelengths at 987 nm and the wavelength dependent loss of 670 dB/km in 1400 nm. Specific polarization states can pass through the PCF by changing the orientation of Polarization Controllers (PC) within the laser cavity. PCF connected with SMF at the fiber end will act as a simple Mach-Zehnder interferometer cavity that further filters out part of the longitudinal modes that contributes to a reduction of the homogeneous line width of the EDF and suppressing unstable mode competition. The PHB effect also greatly enhances the inhomogeneous gain broadening effect in the EDF, and accordingly reduces the mode competition (Jeon, Kim, et al., 2010a). The configuration proposed in this paper overcomes such limitations by allowing dual-wavelength output over a wide region of the microwave wavelength, and hence permits applications within these newly accessible regions. Two approaches are explored, namely the generation of a dual-wavelength output based on a single branch method (Module 1) or the generation of two single-wavelength outputs based on a dual branches method that allows for a wider tuning range (Module 2).

5.2.2 Microwave generation using a single branch Dual-wavelength output from an EDF-PCF based fiber laser

The experimental setup of the proposed fiber laser for both Modules is shown in Figure 5.1. Module 1 and Module 2 are configured in a black box condition such that either of them can replace the other easily. In the first approach with Module 1 implemented, the fiber laser is configured to provide a dual-wavelength output from a single branch. The proposed laser uses a Fibercore Ltd (M-12 (980/80) EDF as the active gain medium. The EDF has a Numerical Aperture (NA) of 0.21 to 0.24 as well as a mode field diameter of 5.7 - 6.6 μm at 1550 nm and absorption coefficient of 16.0 - 20.0 dB/m at 1531 nm and 11.0 - 13.0 dB/m at 980 nm. The EDF is pumped in the backward configuration using a 980 nm laser diode operating at 90 mW, with the EDF placed before the WDM as shown in figure 5.1. Two optical isolators, isolator 1 and isolator 2, are used to contain the EDF and ensure unidirectional travel of all signals through the cavity in a clockwise direction. Taking a backward pumping approach allows the EDF to be pumped high enough that it is fully excited, to the extent that it can be over-pumped if required without having the pump signal leaking into the cavity. The common output of the WDM is connected to the EDF, while its 1550 nm port is connected to one end of isolator 2.

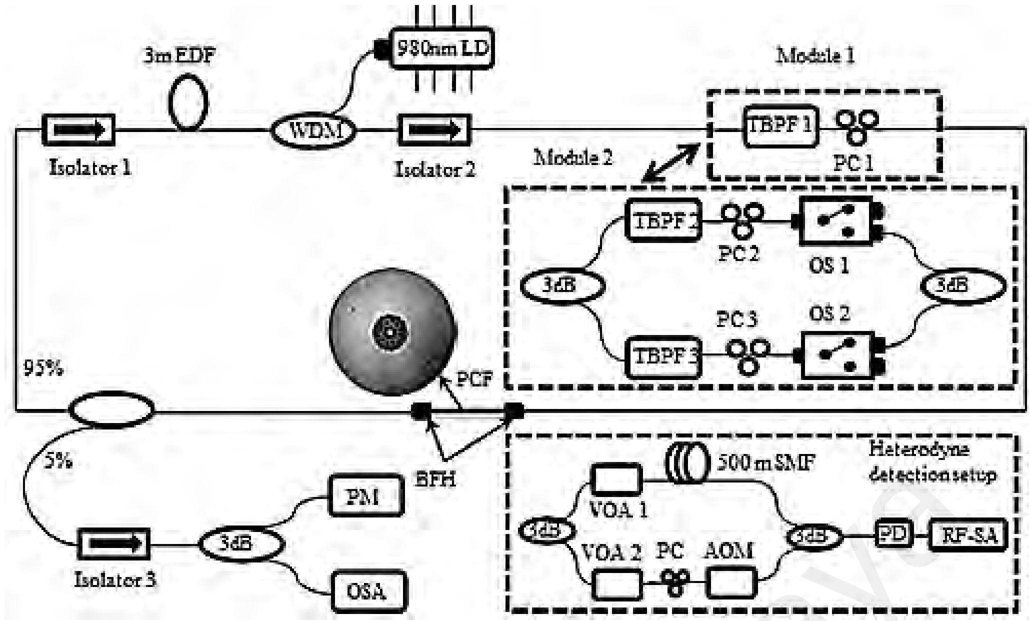

Figure 5.1: Experimental setup of the dual wavelength fiber laser configuration based on either single branch (Module 1) or dual branch (Module 2).

Subsequently, isolator 2 is now connected to the wavelength-tuning element of the system, designated Module 1 in this setup. Module 1 consists simply of a tunable band pass filter (TBPF) and PC. The TBPF has a narrow bandwidth of 0.8 nm, high tuning resolution of 0.05 nm, a broad tuning range of 1535–1565 nm and low insertion loss typically around 1.5 dB. The TBPF is used to determine the operational bandwidth of the fiber laser, while the PC serves to adjust the polarization states of the cavity such that either single wavelengths or multiple wavelengths may oscillate in the cavity and thereby provide the possibility of producing dual wavelengths output for microwave generation.

The output of Module 1 is next connected to a short PCF of about 10 cm long, which has a solid core diameter of about 4.37 μm, and surrounded by air holes with 5.06 μm diameter and a separation of 5.52 μm between holes. The PCF can be considered the primary component of the setup as it is responsible for generating the desired stable dual-wavelength output in a mechanism similar to that employed in refs (H. Ahmad, M. Soltanian, C. Pua, M. Zulkifli, & S. Harun, 2013b) and (Y.-G. Han, 2010). The PCF is not spliced to the setup in order to preserve the PCF structural integrity, and is held in place using two bare fiber holders (BFHs). The output end of the PCF is connected to the input port of the 95:5 coupler so that a portion of the signal can be extracted for further analysis. The 95% port of the coupler connects to isolator 1, which in turn attaches to the other end of the EDF and thus completes the laser cavity. The extracted signal is channeled through an isolator 3 before being split into two even portions using a 3 dB coupler, which is in turn connected to a high-resolution APEX technology AP2051A optical spectrum analyzer (OSA) with 0.16 pm resolution and a Thor labs TXP 5004 polarimeter (PM). This configuration allows for the optical spectrum and the polarization state of the laser signal propagating through the setup to be monitored simultaneously and in real-time.

In order to validate that the output generated by the fiber laser does indeed operate in the SLM regime, a self-heterodyning setup is used to measure the phase shift beating frequency following the isolator 3 as shown in Figure 5.1. This setup consists of a 3 dB coupler to create two parallel branches. One branch comprises a variable optical attenuator (VOA) followed by a single mode fiber of length 500 m, while the other branch includes a VOA, PC and acousto-optic modulator (AOM) in series. These branches are combined at another 3 dB coupler that leads to a photodiode and finally a radio frequency-spectrum analyzer (RF-SA).

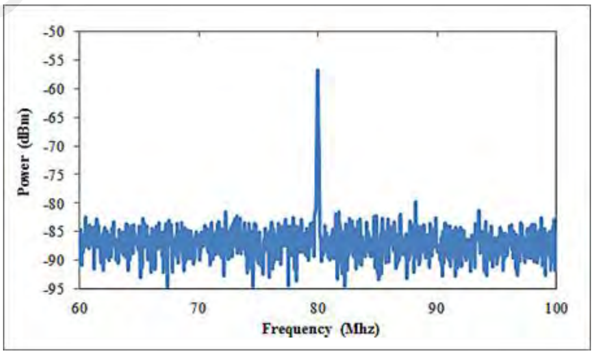

Figure 5.2: RFSA spectrum of fiber laser under SLM operation with beating frequency around 80 MHz.

A delayed self-heterodyning occurs as a result of this additional branch, and the resulting line-width measurements are used as to confirm the ring cavity operates in the SLM regime. Observation of the spectrum via the RF-SA with the AOM deactivated shows a line at 0 Hz. Activating the AOM allows the output generated by the beating of the two signals to display a spectrum at the same frequency as the applied frequency of the AOM.

During the verification, the PC is first fine-tuned to obtain a single wavelength lasing condition before measurement occurs via the RFSA. Figure 5.2 shows the RFSA spectrum of the laser beating frequency, which appears to be single frequency beating at 80 MHz. This single peak validates the SLM operation in the optical cavity. SLM operation validations of different wavelength have been completed across a broad bandwidth with the assistance of TBPF from 1540 nm up to 1565 nm.

Fine-tuning the PC can change the lasing wavelength due to dependence of the lasing wavelength on polarization states. The adjustment of the PC will rotate the polarization states and leads to a changing of lasing wavelength and gain of the lasing wavelengths. A stable DWFL can be obtained by achieving dual-wavelength laser with similar peak powers. From figure 5. 3 (a1), it can be seen that the proposed system is capable of generating a wavelength spacing of less than 0.001 nm (the higher resolution cannot be achieved due to OSA resolution constraint) between two wavelengths lasing at 1561.603 nm and 1561.604 nm at powers of -10.06 dBm and -10.16 dBm respectively.

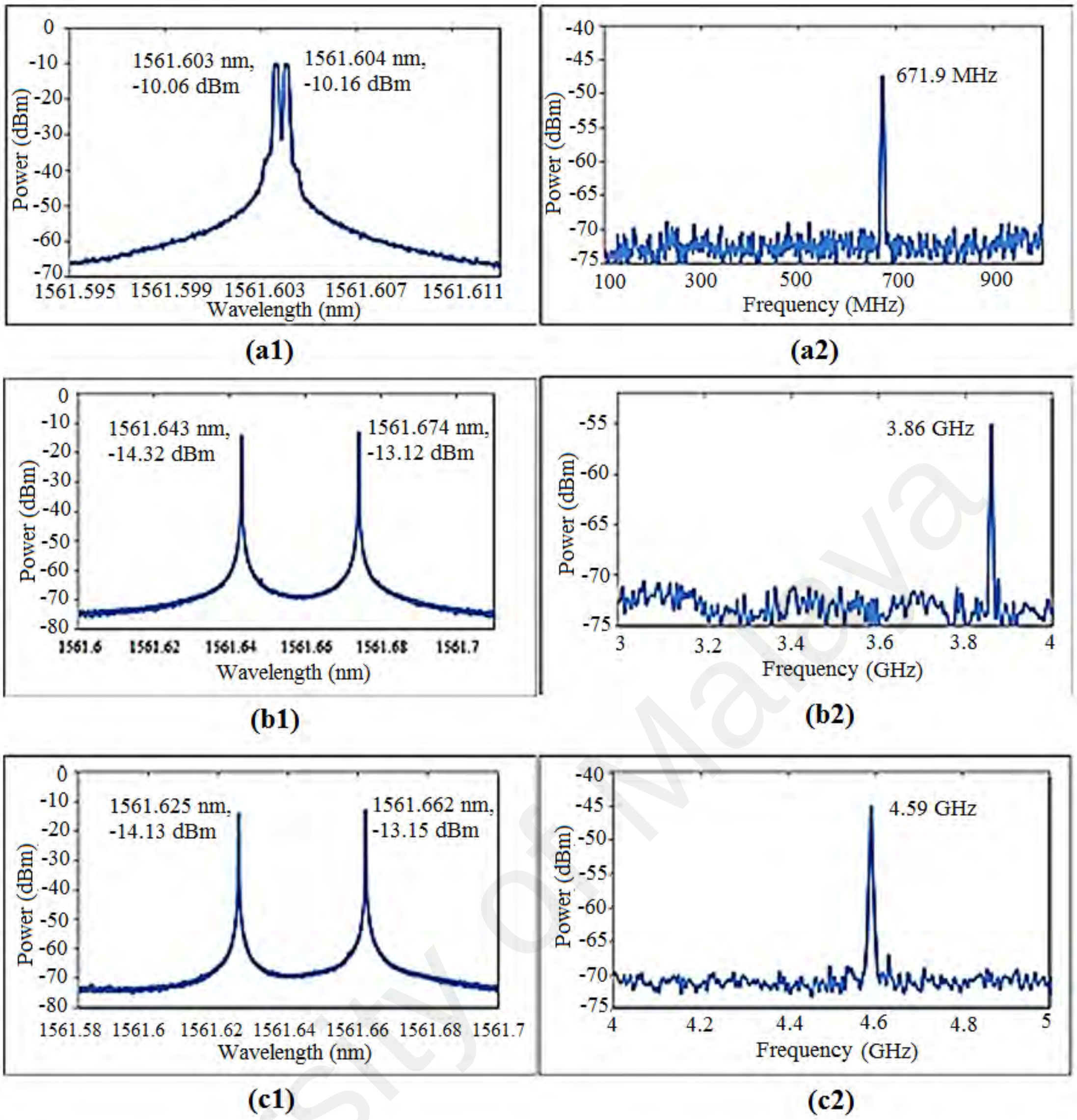

Figure 5.3: Dual-wavelength output spectrum at (a1) 1561.60364 nm and 1561.60407 nm, (b1) 1561.64312 nm and 1561.67413 nm, and (c1) 1561.62590 nm and 1561.66221 nm; with microwave frequency output at (a2) 671.9 MHz, (b2) 3.86 GHz, and (c2) 4.59 GHz respectively.

The dual wavelength generation in a cavity with PCF has been explained in reference (WG Chen et al., 2009). Typically in a ring laser without the PCF and PC, different wavelengths in almost identical polarization states will be propagating within the laser cavity. Integrating the PCF and PC into the laser cavity results in the polarization states of different wavelengths in the EDFA being dispersed through wavelength dependent polarization rotations that enhance PHB. Over two thousand possible longitudinal modes could pass through the band pass filter in this setup due to the length of the cavity around 6.0 m and narrow-pass filtration of approximately 0.8 nm. The PC then disperses the oscillating modes into one of two possible polarization states, with different spacing that can be adjusted by fine-tuning the PC. The PHB effect appears when these modes enter the EDF (which is the active medium of the laser) at different polarization states, which results in lesser mode competition and thus enhances multi-wavelength generation. A filtering out of a portion of the longitudinal modes, via the PCF connected with SMF at the fiber end acting as a simple Mach-Zehnder interferometer cavity, leaves only a few modes oscillating in the cavity. The dual-wavelength output can be realized by fine-adjusting the PC.

The microwave generation is subsequently determined by connecting the dual-wavelength output to the photo detector and taking measurements with the RFSA. The RF spectrum is shown in figure 5.3 (a2) as having a frequency of 671.9 MHz. This frequency is one of the shortest microwave frequency reported thus far; such outputs are mostly reported above 10 GHz. Adjusting the PC allows a tuning of the laser wavelengths in order to achieve different wavelengths. Figure 5.3 (b1) displays a wider wavelength spacing of 0.031 nm at the wavelength of 1561.643 nm and 1561.674 nm, with corresponding power of -14.32 dBm and -13.12 dBm respectively. Resultant microwave frequency is generated at 3.86 GHz as shown in figure 5.3 (b2). The widest spacing achieved using the current Module 1 setup is 0.036 nm at wavelengths 1561.625 nm and 1561.662 nm as seen in figure 5.3 (c1), with the microwave frequency at 4.59 GHz shown in figure 5.3 (c2). From these results it can be inferred that the usage of Module 1 allows tuning from the region of 671.9 MHz to 4.59 GHz. It is prudent to note that this is not restrictive and can be tuned discretely to generate microwave outputs above this range.

5.2.3 Microwave generation using a two branch Dual-wavelength output from an EDF-PCF based fiber laser

Another approach towards generating a dual-wavelength output with a wider spacing is to use a dual branch method by replacing Module 1 with Module 2. This dual branch is able to generate microwaves of substantially higher frequencies that even extend into the Terahertz region. In Module 2, the input into the Module is split into two equal parts using a 3 dB coupler, with each portion channeled to a TBPF that is in turn connected to a PC and an optical switch (OS). The TBPFs are used to determine the operating range of the SLM wavelengths, while the PCs (PC2 and PC3) are used to ensure that only a single wavelength can propagate through each branch.

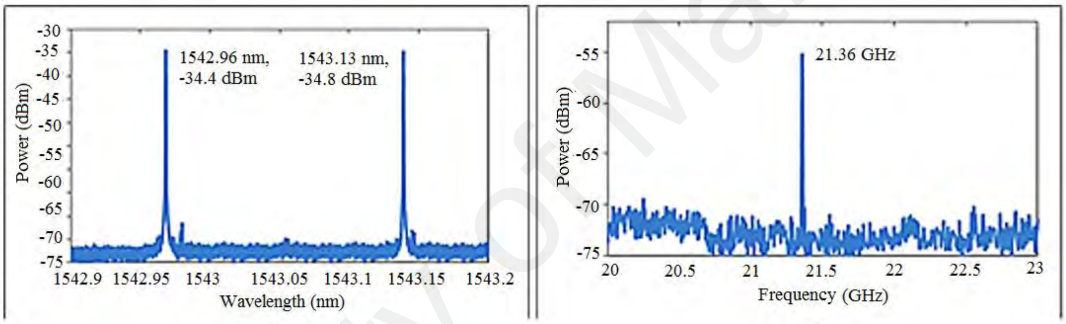

(a) (b)

Figure 5.4: (a) Overlapping of the two TBPF over wavelengths of 1542.9683 nm and 1543.1392 nm to give wavelength spacing of 0.1709 nm, and (b) shows the beating frequency of 21.36 GHz in the RFSA.

Although a user is able to determine the tuning range of each TBPF in an essentially unrestricted manner, this experiment uses the upper TBPF (TBPF1) and PC2 to obtain the shorter SLM wavelength, while the lower TBPF (TBPF2) and PC3 is used to obtain a longer SLM wavelength. The two independent signals are recombined using another 3 dB coupler prior to re-entering the cavity. The advantage of this approach is that the system can quickly switch between each wavelength or combine both wavelengths as needed. These wider frequencies that extend into the Terahertz region can be detected using a LTG-InGaAs photomixer, EFDA and bolometer configuration as described in (Jeon, Kim, et al., 2010c) figure 5.4 (a) shows the dual wavelength output at

1542.9683 nm and 1543.1392 nm with powers of -34.6 dBm and -34.8 dBm respectively, while figure 5.4 (b) indicates the resulting microwave signal of 21.36 GHz.

Figure 5.5 (a), (b), (c), and (d) demonstrate the capability of the experimental setup to generate a wide range of wavelength spacing via PC adjustments and varying the TBPFs. The advantage of a setup containing the dual branch method lies in the wavelength tuning being almost continuous and accurately controlled by the TBPF. However, a problem arises in that the lasing power is low due to losses caused by the two 3 dB coupler and extra components in the setup. Overall, it can be inferred that although the second approach may be slightly more complex in terms of deployment, this disadvantage is by far offset by the ability of the system to generate a much larger range of microwave signals.

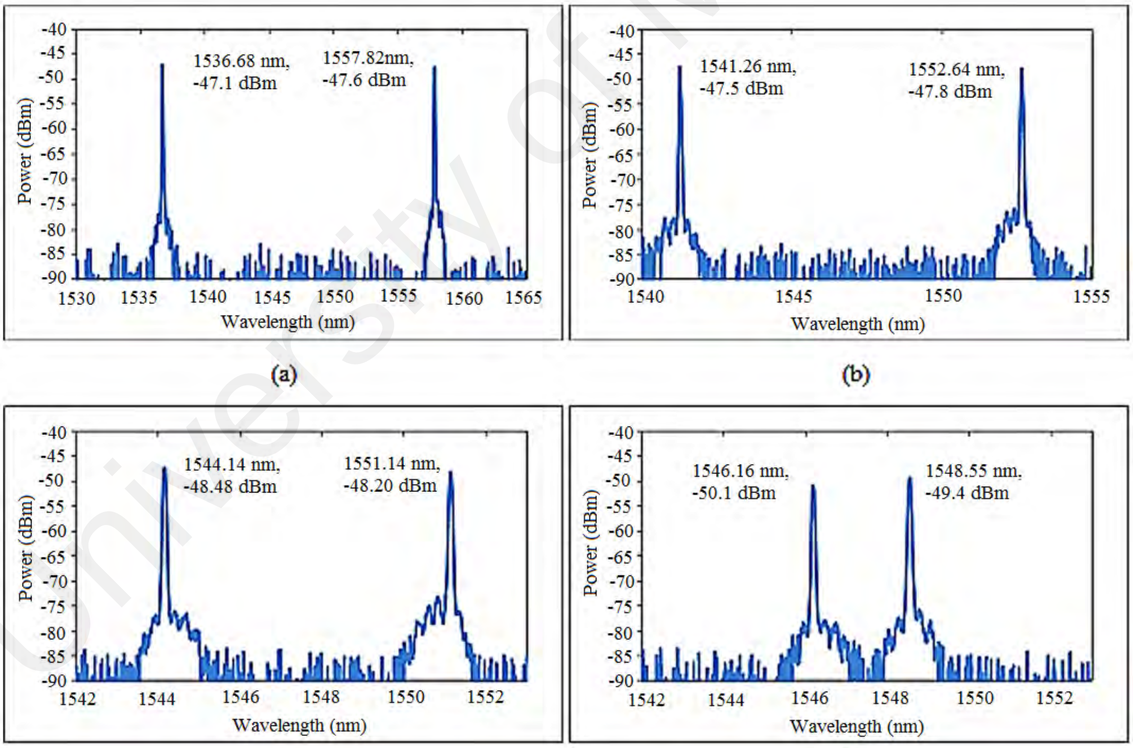

(a) (b)

(c) (d)

Figure 5.5: (a) Wavelength spacing of 21.14 nm, (b) Wavelength spacing of 11.38 nm, (c) Wavelength spacing of 7 nm, and (d) wavelength spacing of 2.39 nm.

5.2.4 Output stability

Dual wavelength laser stability is verified by monitoring multiple scanning of the optical spectrum for 22 minutes continuously, with interval scan period of 1 minute.

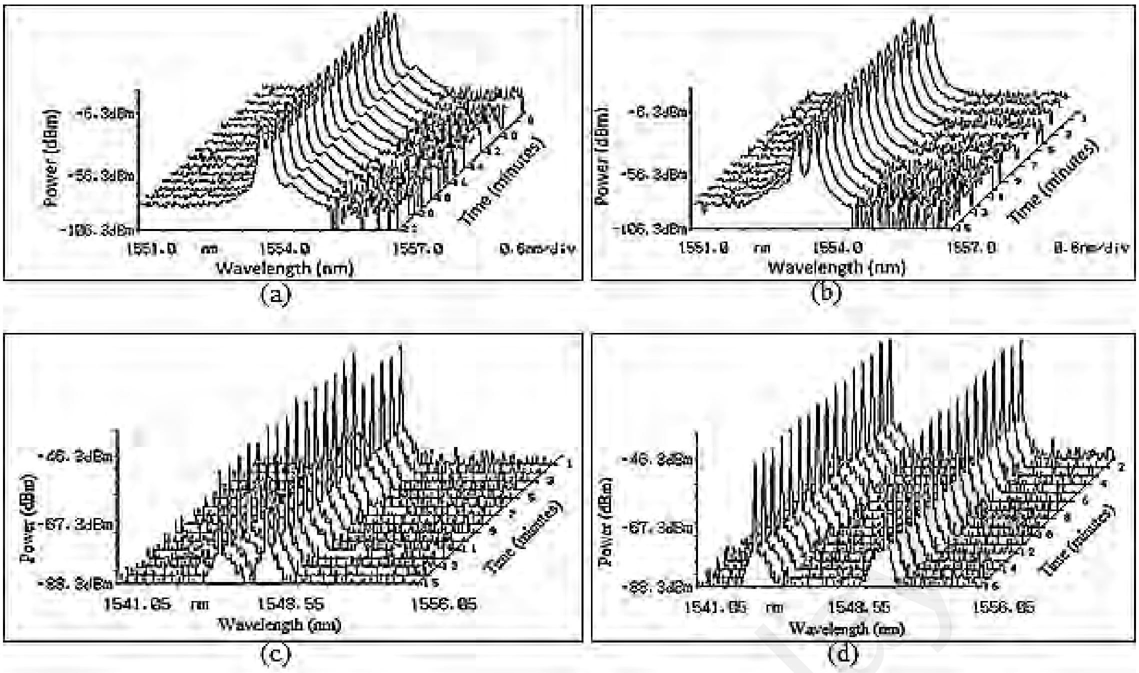

Figure 5.6: Stability of the system with channel spacing of (a) 170 pm, (b) 410 pm, (c) 2.39 nm, and (d) 7 nm.

Overall, the laser output generated by the system is stable for both Module 1 and Module 2 in terms of power and wavelength, with fluctuation less than 0.5 dB. Figure 5.6 (a) to (d) illustrate that the system is highly stable and consistent, and combined with its compact and robust platform, can act as a viable source for the generation of microwave signals in the field.

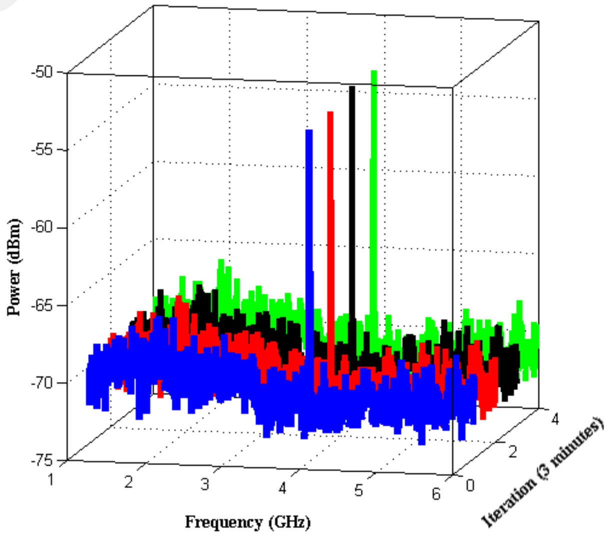

Figure 5.7: Stability of RFSA spectrum output from dual wavelength fiber laser for a period of 12 minutes with scanning interval of 3 minutes.

Further evidence of the stability of microwave generation is acquired by measuring the RFSA spectrum of the output for the dual wavelength fiber laser lasing at 1561.64312 nm and 1561.67413 nm as shown in figure 5.3 (b1). The microwave is generated at frequency of 3.86 GHz and periodic scans allow the stability of the microwave generated by the dual wavelength fiber laser to be monitored as shown in figure 5.7. The microwave frequency generated is stable at 3.86 GHz for a period of 12 minutes with an interval scan of 3 minutes, while the peak power fluctuates at a range of 0.5 dB.

5.3 Dual-Wavelength Erbium-Doped Fiber Laser to Generate Terahertz Radiation Using Photonic Crystal Fiber

5.3.1 Introduction

Terahertz (THz) radiation sources have attracted considerable interest in the past few years, and have applicability within communications, agriculture environmental monitoring, spectroscopy, medicine, and security scanning (Ferguson & Zhang, 2002; Hosako et al., 2007; Tonouchi, 2007). Continuous wave (CW) THz radiation emerges through the beating of two stable single longitudinal modes (SLM) from an optical source launched into a photo-mixer such as an organic ionic salt, 4-dimethylamino-*N*-methyl-4-stilbazolium-tosylate (DAST) crystal. This CW THz radiation can be subject to frequency tunability via fine-tuning the spacing between the two optical SLM wavelengths. THz radiation emission has been reported from a variety of nonlinear materials such as lithium niobate ($LiNbO_3$) (K. Yang, Richards, & Shen, 1971; X. C. Zhang, Jin, & Ma, 1992), lithium tantalate ($LiTaO_3$) (Hu, Zhang, Auston, & Smith, 1990; X. C. Zhang, Jin, et al., 1992), zinc telluride (ZnTe) (Nahata, Weling, & Heinz, 1996), indium phosphide (InP) (Rice et al., 1994), gallium arsenide (GaAs) (Nagai et al., 2004), gallium selenide (GaSe) (Shi, Ding, Fernelius, & Vodopyanov, 2002), cadmium telluride (CdTe) (Xie, Xu, & Zhang, 2006), cadmium zinc telluride (CdZnTe) (K. Liu, Kang, Kim, & Zhang, 2002), DAST (X. C. Zhang, Ma, et al., 1992), and metals (Kadlec, Kužel, & Coutaz, 2004). The performance of THz emitters based on these materials in terms of bandwidth and signal strength of the emitted THz radiation has been summarized in section 2.3 of ref (Wilke & Sengupta, 2008). Zhang and coworkers (X. C. Zhang, Ma, et al., 1992) reported that use of a 180-mW optical pump beam focused to a 200-μm diameter spot enabled a DAST organic electro-optic crystals sample to provide a detected THz electric field that was 185 times larger than that obtained from an $LiTaO_3$ crystal and 42 times larger than from GaAs and InP crystals under the same experimental conditions. DAST has also been shown to perform well at higher frequencies, with an observable bandwidth up to 20 THz from a 100-μm DAST crystal showing a six-fold increase over that reported from a 30-μm ZnTe crystal under similar experimental conditions (P. Han, Tani, Pan, & Zhang, 2000). The frequency spectrum of DAST shows a characteristic strong absorption line at 1.1 THz (from transverse optical (TO) phonon resonance) along with some additional absorption lines between 3 and 5 THz. These latter lines (with the exception of the line at 5 THz) are significantly weaker than the absorption line at 1.1 THz, although the THz amplitude at these frequencies is still well above the noise level (A. Schneider & Guenter, 2005). The optical beat sources are typically obtained using two distributed Bragg reflector (DBR) laser diodes (LDs) or tunable distribution feedback (DFB) devices for dissimilar operating wavelengths (Jeon, Kim, et al., 2010c; Klehr et al., 2008). The most challenging aspect is to stabilize the frequencies and spatially match the two laser beams in order to achieve mode matching.

Dual-wavelength fiber lasers (DWFLs) can perform suitably as compact and inexpensive optical beat sources that generate CW THz radiation over a wide tuning range (Kleine-Ostmann, Knobloch, Caspary, Hofmann, & Koch, 2002). Recently, DWFLs have also been demonstrated through the use of dual-wavelength vertical external cavity surface emitting laser (VECSEL) for intra-cavity difference frequency generation (DFG) mixing in a nonlinear crystal (Scheller et al., 2010). However, this approach may have limited applications, as the proposed system requires the use of a very high power pump laser operating at 808 nm with an output of approximately 50 W in order to obtain the desired dual-wavelength output at 1030 nm from the VECSEL, therefore making this approach highly unsuited for laboratory environments. A comparable case can be seen in the proposed setups described by M. Wichmann *et al.* (Wichmann et al., 2013), which while performing admirably, also required a high power to pump the VECSEL. Other research efforts have also explored alternative approaches towards generating THz radiation, such as using photoconductors and p-i-n diode-based devices, which have the benefit of a large bandwidth source (Preu, 2014). Recent research efforts have now identified multi-wavelength fiber lasers as a possible and highly attractive means of generating THz radiation. Generation of THz radiation output from a fiber based laser was also theoretically investigated and reported recently (Suizu & Kawase, 2007), and this method promises lower sensitivity and higher robustness in relation to the operating environment as compared to free-space sources. Early attempts at THz generation from fiber lasers had a high measure of success (D Chen, Fu, Liu, Wei, & He, 2008; S. Feng, Xu, et al., 2008; S. Pan, Zhao, & Lou, 2008a), yet further developments were limited due to the general reliance on erbium-doped fiber (EDF) as a gain medium. The reason behind this stagnation lies in the inherent characteristics of the EDF, whereby the erbium ions within the glass matrix of the fiber exhibit homogenous broadening characteristics. This feature makes the EDF highly suitable for generating high-powered single wavelength outputs, but limits the generation of stable, dual- or multi wavelength outputs from the same laser. Many methods have been brought forward to resolve this issue, including cooling the EDF in liquid-nitrogen (N. Park & Wysocki, 1996), exploiting the polarization hole burning effect (S. Feng, Xu, et al., 2008), and using a hybrid gain medium (S. Pan et al., 2008a). While successful in eliminating the gain competition effects of the EDF that arise from homogenous broadening, these approaches are very elaborate and not practical outside of a laboratory setting. A viable solution to this problem lies in the use of photonics crystal fiber (PCF). This is a highly specialized optical fiber that can behave as a Mach-Zehnder interferometer (MZI) by exploiting the polarization dependent loss (PDL) effect (H. Ahmad, M. Soltanian, C. Pua, M. Zulkifli, & S. Harun, 2013a) in order to generate a stable, high power dual lasing output. Such output can be used to generate a stable source for THz radiation generation. Multi-wavelength fiber ring lasers with switchable wavelength outputs have been demonstrated by Chen *et al.* (WG Chen et al., 2009) via a compact in-fiber Mach-Zehnder interferometer together with a PCF. Hae Young Choi *et al*. made a pioneering proposal for all-fiber Mach-Zehnder type interferometers formed in photonic crystal fiber (PCF) (Choi et al., 2007), in which the interference between the core and the cladding modes of a PCF was exploited. In this work, the generation of THz radiation from a PCF based multi-wavelength source is demonstrated. This approach is a detailed and comprehensive extension of the work described in (M. Soltanian et al., 2014), and provides a means to generate a stable DWFL with large inter-spacings in order to obtain highly stable CW THz radiation.

5.3.2 Experimental Setup

Figure 5.8 is an overview of the configuration setup used to generate THz radiation. The experimental design utilizes a 10 cm length of PCF, which has a structure comprising a 4.37-µm diameter solid core surrounded by an air-silica clad of 5.06-µm d diameter air holes with a 5.52-µm pitch. The role of this PCF is to enable the generation of stable dual-wavelength output as detailed in (H Ahmad et al., 2013a) and similarly in (Young-Geun Han, 2010), and is manually spliced to a single mode fiber (SMF) via a Fujikura 45 PM splicer. Additionally, a 0.9 m Leikki EDF gain medium possessing an NA of 0.21 to 0.24, mode field diameter of 5.7 - 6.6 µm at 1550 nm, and absorption coefficient of 84 dB/m at 980 nm is used as a gain medium and pumped via an Oclaro

LC96 series 980nm pump laser diode operating at approximately 80 mW. The incorporated tunable band pass filters (TBPFs) causes the dual-wavelength output to be widely spaced, and has specifications of 0.8 nm narrow bandwidth, 0.05 nm high tuning resolution, a broad tuning range of 1535–1565 nm, and a low insertion loss of typically around 1.5 dB. Each TBPF is tuned to one of the desired wavelength peaks.

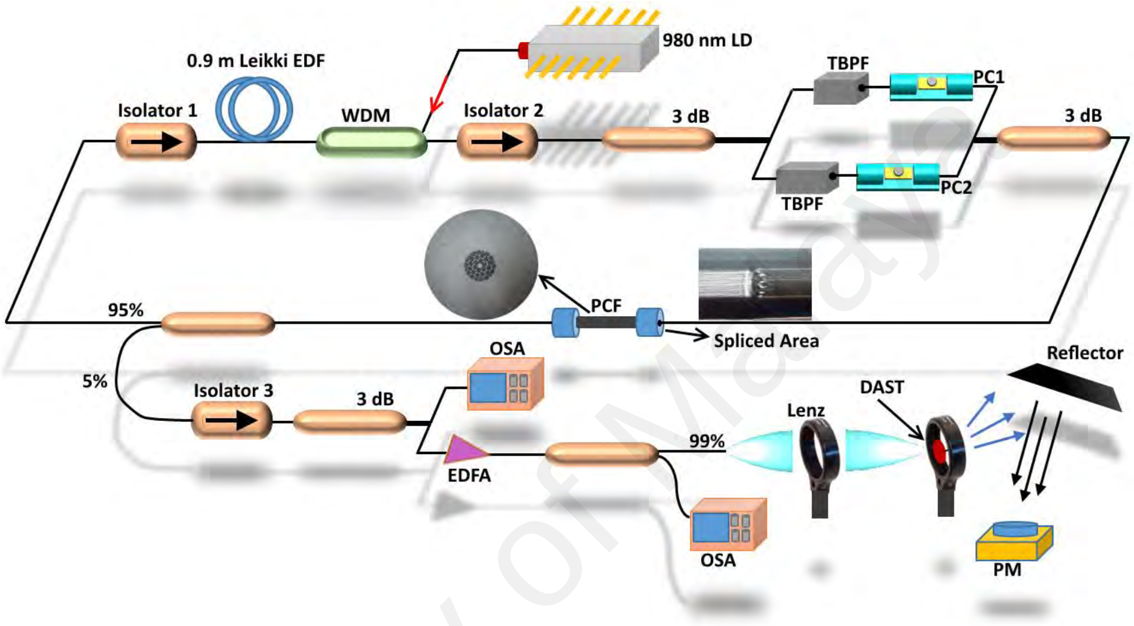

Figure 5.8: Experimental setup for generating terahertz radiation.

A copper plate is used as a metal reflector to reflect the majority of the generated terahertz radiation power from the DAST organic electro-optic crystals to an Ophir high sensitivity thermal sensor model 3A-P-THz, which is designed to measure THz light sources from a low power of 15 µW up to a high power of 3 W with a power accuracy of ±3%. The sensor detects short pulses or CW laser output in the 0.1 to 10 THz wavelength range. The reflectivity of copper in the THz region has been investigated as reported in (Tan et al., 2012), in which the relative reflection amplitudes from the mirrors were tested in the range of 50 to 700 cm^{-1}, corresponding to a frequency of 1.5 THz to 21 THz. The research revealed that the copper-based mirror has a reflectivity that is almost similar to that exhibited by gold-, silver-, and aluminum-based mirrors. This shared feature is advantageous since copper-based mirrors are relatively inexpensive and easily obtained.

5.3.3 SLM Properties of Cavity

The process of validating that the fiber laser output was within the SLM regime involved a self-heterodyning setup, whereby the phase shift beating frequency could be measured for output in the circuit branch containing isolator 3 (refer to figure 5.8). This setup, as shown in figure 5.9 (a), began with a 3 dB coupler for the purpose of creating two parallel branches. One branch consisted of a variable optical attenuator (VOA) and subsequent single mode fiber of 500 m in length, while the other branch contained a VOA, PC and acousto-optic modulator (AOM) in sequence. Both branches were combined at a second 3 dB coupler, the other end of which led to a photodiode and terminated with a radio frequency-spectrum analyzer (RF-SA). Horak *et al.* (Horak & Loh, 2006) and Dawson *et al*. (Dawson, Park, & Vahala, 1992) used an 11 km length of delay fiber to achieve a resolution of about 0.6 KHz, while Dennis Derickson (Fischer, 1998) used an interferometer with a delay, τ_0 , of 3.5 μs in his experiment, which corresponded to about 715 m of spooled fiber. Since achieving a higher resolution is not a main focus of this research, the interferometer illustrated in figure 5.9 (a) and possessing a delay, τ_0, of 2.5 μs, corresponding to about 500 m of spooled fiber, was used to measure the line-width and provide proof of SLM. Delayed self-heterodyning occurred while this setup was in operation, and the resulting line-width measurements constituted evidence of the ring cavity operating in the SLM regime. Prior to the spectrum measurement via the RF-SA, the PC was fine-tuned to a single wavelength lasing condition.

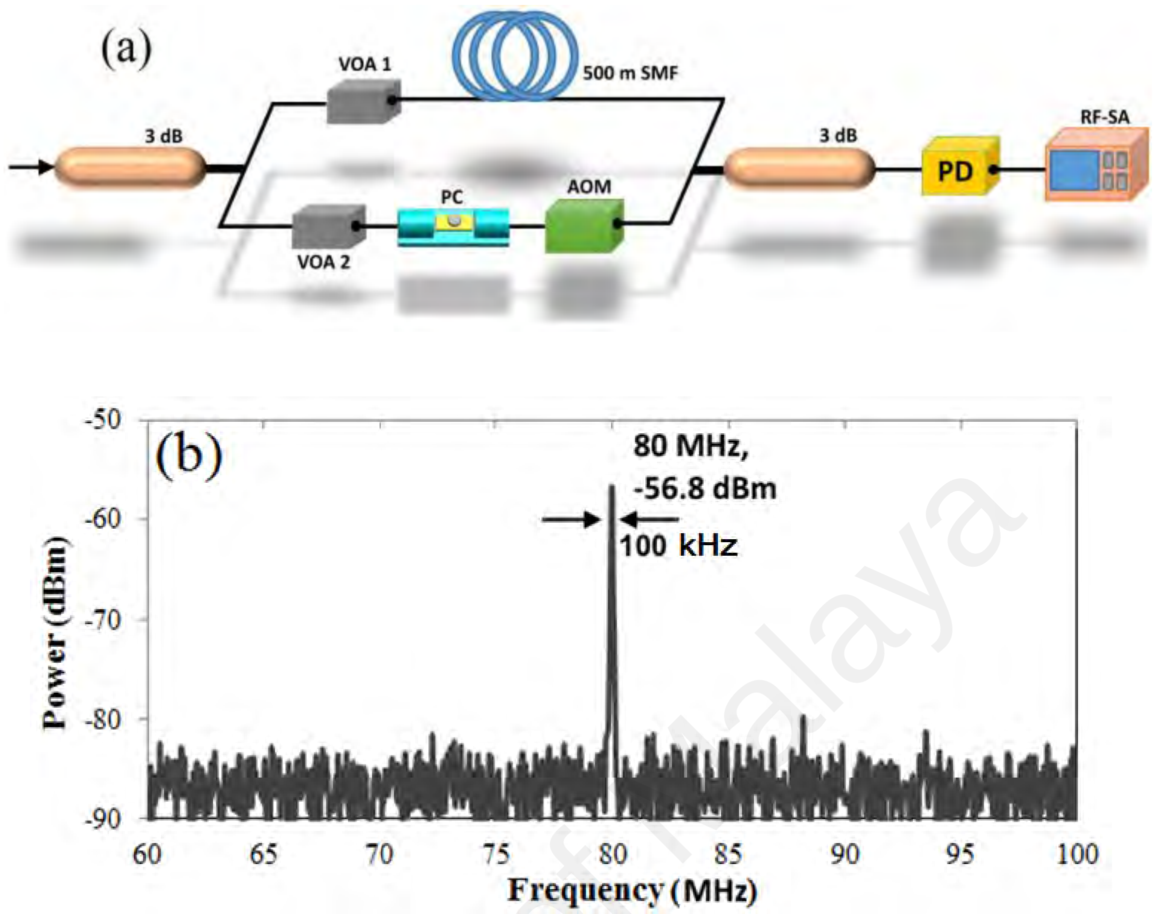

Figure 5.9: (a) SLM validation using self-heterodyning setup, and (b) the RFSA spectrum of the laser with beating frequency at 80 MHz and line-width of 100 kHz.

A line at 0 Hz was observed in the spectrum via the RF-SA while the AOM was disabled. Activation of the AOM caused the output generated by the beating of the two signals to possess a spectrum at the same frequency as the applied frequency of the AOM. Figure 5.9 (b) shows the RF-SA spectrum of the laser beating frequency, which appears to be a single frequency beating at 80 MHz. This result provides validation of SLM operation in the optical cavity.

5.3.4 Stable DWFL output generation to generate THz radiation

Inserting a PC into the cavity triggered a wavelength-dependent polarization rotation that resulted in a variation of polarization states emerging across multiple wavelengths in the EDFA. If polarization states were to remain unchanged, all wavelengths would retain nearly identical polarization states in the EDF. Increasing the number of peaks oscillating in the cavity necessitates the exploitation of polarization hole burning (PHB) (Tu et al., 2008). As the relative polarization states of the signal changes (due to polarization mode dispersion), the magnitude of the differential gain changes. Fiber lasers can simultaneously emit on two wavelengths of orthogonal polarization states (S. Zhang & Holzapfel, 2013). The effect of orthogonality of polarization states to generate DWFL has been investigated and demonstrated in (H Ahmad et al., 2013a; S. Feng, Li, et al., 2008; S. Feng, Xu, et al., 2008; L. Wang, Yan, Mao, Jian, & Jian, 2009). This condition will minimize the polarized saturated signal in the ring laser as the signals are not in the same polarization state and the PHB effect in the cavity is greatly enhanced. The only two modes that can exist in the cavity are those in which the polarization states are perpendicular to each other, whether within the range of one or both TBPFs. The two TBPFs are used for coarse wavelength selection as in a regular ring-cavity single or multi-wavelength laser. Then the PCF-MZI allows for a set of modes (0.2 nm spacing) to be transmitted inside the 0.8 nm bandwidth of the TBPF. Tuning the polarization of each of the two wavelengths will change the MZI mode spacing, location and transmission amplitude. Thanks to mode competition in the gain medium (EDFA), only one of the MZI modes will lase (in a stable way) at each of the two wavelengths. By fine-tuning the PCs, we could achieve two orthogonally polarized lasers so that one is lasing in the range of TBPF-1 and another is lasing in the range of TBPF-2. In fact, PCF-MZI together with PC acts not only as a filter in order to filter out the two wavelengths of orthogonal polarization states, but also enhances the PHB in the cavity.

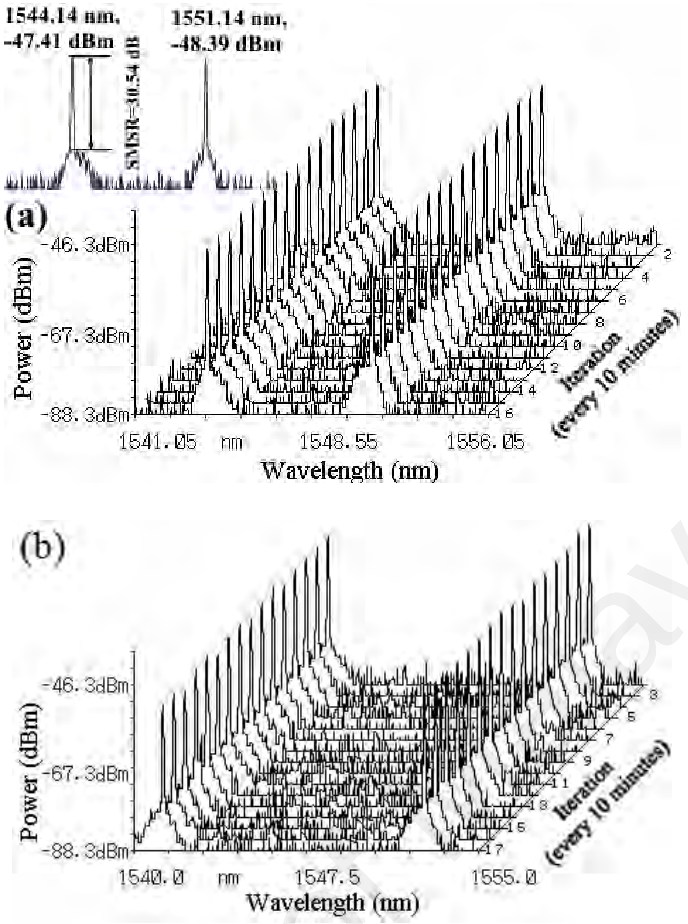

Figure 5.10: Optical spectrum revealing high tunability and stability for DWFL lasing at wavelengths (a) 1544.14 nm and 1551.14 nm (spacing of 7nm), inset shows the SMSR of generated DWFL which are 30.54 dB, and (b) 1541.2 nm and 1552.6 nm (spacing of 11.4 nm) over 160 minutes.

Consequently, it reduced the homogeneous gain broadening of EDF and then reduced the wavelength competition. In such cases at room temperature, adjusting the PC will result in stable dual-wavelength lasing states. Fine-tuning the TBPFs and the PCs, which were illustrated in the configuration of figure 5.8, during dual-wavelength lasing facilitated the variety of measurement results shown in figure 5.10. These measurements were taken from the 5% port for lasing at 1544.14 nm and 1551.14 nm with spacing of 7 nm as shown in figure 5.10 (a). The inset of figure 5.10 (a) shows the SMSR of the generated DWFL, which is 30.54 dB. The lasing output at 1541.2 nm and 1552.6 nm with the spacing of 11.4 nm is shown in figure 5.10 (b). This simple design of DWFL means that the stability of the setup is increased via the utilized short ring cavity with a length of 6 m, while the incorporated PCs allow for a means to achieve high repeatability. The stability of generated dual-wavelength output over 160 minutes with interval scanning of every 10 minutes before and after amplification via EDFA is shown in figure 5.11 (a) and (b) respectively, and it can be seen from these figures that the output is stable.

The power stability measurements of this dual-wavelength output are shown in figure 5.12, in which the power of the dual-wavelength fiber laser is observed to be very stable and the fluctuation is in the range of 0.5 dB. In general, several solutions exist to increase the output power: ensure the cavity is at optimum length, exploit the inherent high absorption characteristics of an incorporated EDF, increase the pump power, reduce the total loss in the setup e.g. by minimizing splicing loss, and extract a higher portion from the ring laser cavity.

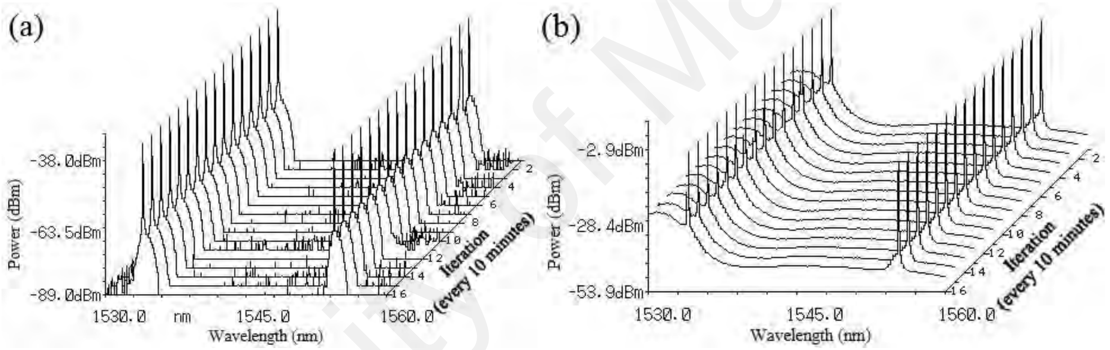

Figure 5.11: Optical spectrum revealing stability for DWFL, with spacing of 21.2 nm at 1534.10 nm and 1555.30 nm, over 160 min with interval scanning every 10 minutes (a) before amplification, and (b) after amplification.

The DWFL can be generated with FSR ranging from 0.2 nm to 21.2 nm, corresponding to a frequency span from 25 GHz to 2.66 THz. However, in regards to the optical properties of DAST in the THz range (Cunningham & Hayden, 2010), the main idea to generate DWFL with spacing of 7, 11.4 and 21.2 nm is for the purpose of avoiding effects due to the radiation absorption frequency of the DAST crystal. The optical power fluctuation for both lasing wavelengths at 1534.10 nm and 1555.30 nm over 160 minutes is shown before amplification by EDFA in figure 5.12 (a). Figure 5.12 (b) shows the DWFL results scaled to the optical power fluctuations of the 99% output port of the coupler.

In order to obtain THz generation, the dual-wavelength achieved should be amplified through an EDFA, as shown within figure 5.8, and launched into a DAST photo-mixer. The dual-wavelength was used as a THz optical beat source. The amplified dual-wavelength was then focused onto the DAST crystal photo-mixer through a free space lens system. The DAST crystal was mounted within a collimating lens arrangement.

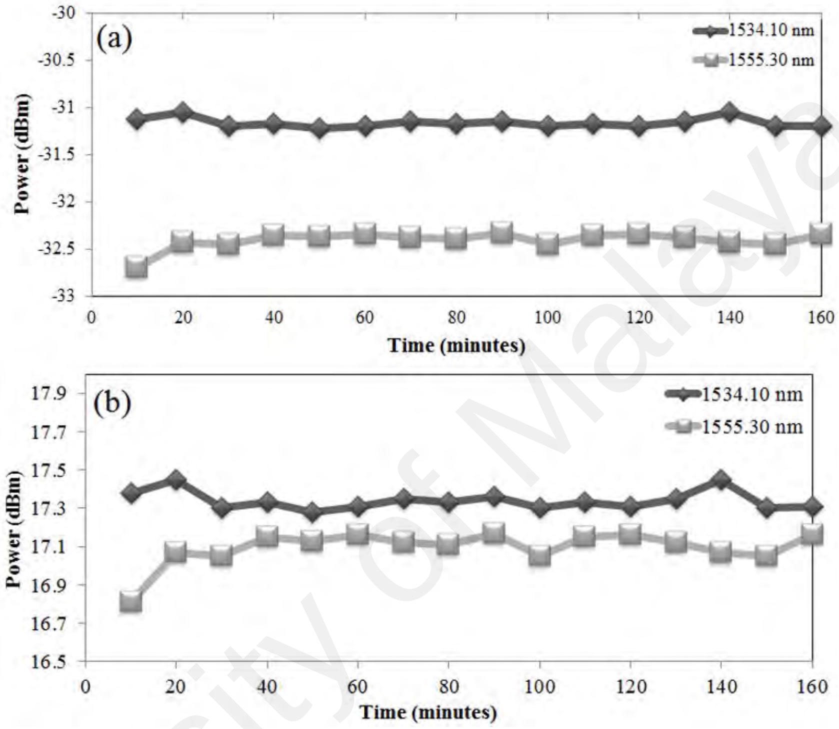

Figure 5.12: Optical power fluctuation for lasing wavelengths at 1534.10 nm and 1555.30 nm over 160 minutes (a) before EDFA and (b) scaled to the actual optical power fluctuations from 99% output port while the OSA attenuator was turned on (the OSA attenuates the signal by 13 dB).

An Ophir High Sensitivity Thermal Sensor model 3A-P-THz was calibrated for terahertz radiation, whereby the frequency was set to about 0.9, 1.4 and 2.6 THz, corresponding to DWFL with FSR of 7, 11.4 and 21.2 nm respectively, to match the expected radiation product of beating of the SLM dual-wavelength, and was used to measure the THz emission radiation.

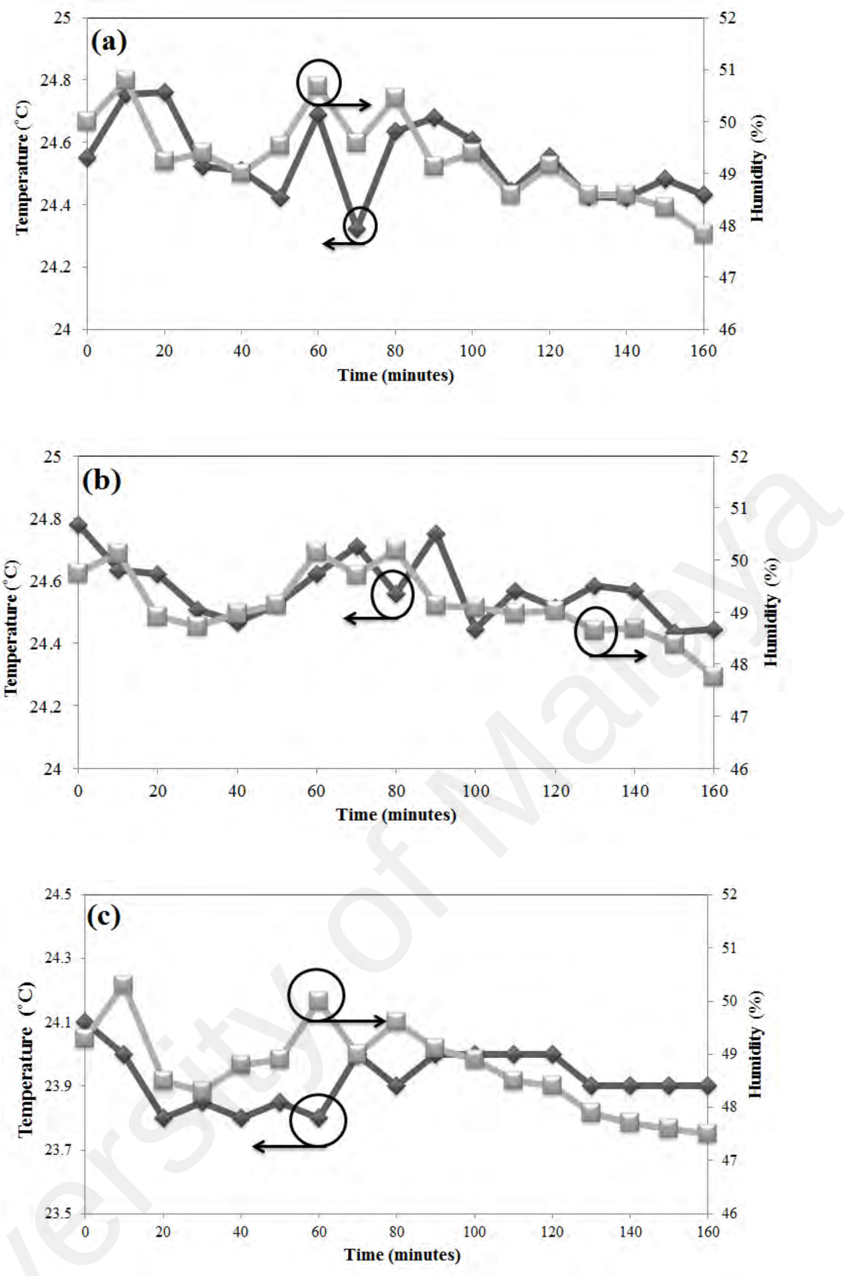

Figure 5.13: Ambient temperature and humidity as a function of time over 160 minutes for (a) 0.9 THz, (b) 1.4 THz and (c) 2.66 THz.

To minimize the redundant power from the ASE, a copper plate covered by a tiny black tape was used as a terahertz reflector to absorb the redundant power and reflect only the THz radiation power. Figure 5.13 shows the variation of the temperature and humidity of the environment throughout the 160 minutes duration of the experiment. Attempts were made to keep the room temperature stable during this time. Figure 5.14 shows the detected power corresponding to 0.9, 1.4 and 2.66 THz over 160 minutes.

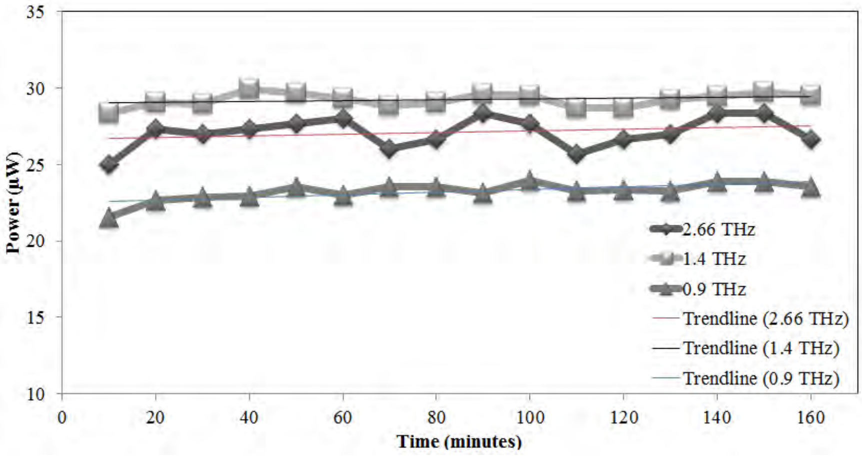

Figure 5.14: Received power corresponding to 0.9, 1.4 and 2.66 THz detected over a 160 minutes period by an Ophir High Sensitivity Thermal Sensor model 3A-P-THz calibrated for terahertz radiation.

Observation shows that the output power of the proposed setup remained relatively stable, and the power of the dual-wavelength laser and generated THz radiation never exceeded a fluctuation above 0.5 dB and 10 % respectively even when exposed to sharp and sudden fluctuations of temperature and humidity.

The terahertz emission at 2.66 THz shown in figure 5.14 is less stable than the others due to increase in the output power difference of the amplified DWFL. Although EDFA can provide gains over an entire band of 40 nm, the gain spectrum is, in general, not flat, that is, the gain dependents on the signal wavelength. Thus, if multiple wavelength signals with the same power are input into the amplifier, then their output powers will be different (S. Bhadra & A. Ghatak, 2013). As such, the more increase in the spacing of the generated DWFL, the more potential to amplify the generated DWFL with different power. Consequently, the THz radiation result of beating of these two wavelengths with longer spacing is less stable than the other two results from beating the generated DWFL with shorter spacing. More stable THz radiation output can be achieved if a gain flattening filter (GFF) is utilized to minimize the difference of the output powers of generated DWFL.

Maintaining a very stable polarization state throughout lasing was a chief factor in the high stability of the dual-wavelength output. The observed instability of the polarization state of the laser in the ring laser cavity could be attributed to variations in the environmental temperature and humidity. Minimizing fluctuations of the environmental temperature and humidity is therefore crucial for ensuring that the polarization state of lasing remains stable.

Although several investigations have been reported to measure line-width of THz radiation (Kosterev et al., 1999; Totschnig, Winter, Pustogov, Faist, & Müller, 2002; R. M. Williams et al., 1999), no line-width measurement were done here, but there are different options to perform such measurements in the future. M. Ravaro *et al.* exploited a technique based on an electro-optic modulator that allows the generation of a heterodyne beatnote between the emission frequency of a THz and a harmonic of the repetition rate of a near-IR laser comb (Ravaro et al., 2012). The frequency fluctuations of such beatnote are then converted into a voltage signal using a voltage controlled oscillator (VCO) that tracks the beatnote frequency. Hua *et al.* used an optical self-mixing method to characterize the line-width enhancement factor (LEF) of terahertz (J.-H. Xu, 2007). In this technique, external optical feedback is produced by reflecting a part of the light output from one of the laser facets back onto this facet. This is done using a mirror which is movable along the optical axis. By moving the mirror, the phase of the reflected light incident on the facet is changed and so the level of the external optical feedback changes with consequent changes in the output level of the laser.

5.4 Towards 5G: A photonic based millimeter wave signal generation for applying in 5G access fronthaul

5.4.1 Introduction

Due to fast revolution in mobile technology, wireless technology has been evolving from 1G to 4G. Seamless integration of cellular networks such as GSM and 3G, WLAN and Bluetooth was the main focus of 4G systems (Hui & Yeung, 2003) and now

4G technology is also reaching maturity. Currently researchers are working on defining next generation of wireless communication, i.e., 5G. Emphasizing on small cell concepts, network speed and capacity enhancement and introducing new communications technologies are among the most important announcements about future 5G (Andrews et al., 2014). Improving the speed and capacity is required to make the communication for potentially billions of wireless devices feasible. Wireless access network (WAN) at millimeter wave bands (30-300GHz) has large bandwidth which offer an alternative for high speed indoor/hotspot communication to be utilized for 5G.

To support the combination of small cells and mm-wave radio for future 5G access, fiber-optic communication plays an important role in both the backhaul and fronthaul networks. According to (Cheng, Zhu, Gul, Ma, & Chang, 2014) optical access network (OAN) is required to be scalable to support the expected 5G deployment goals by 2020: 1-10Gb/s at the user terminal; 100Gb/s for the backhaul truck; 1Tb/s for metro transport and 1Pb/s for the core transport. Here, the view of the next-generation 5G which is the integration of high speed WAN-OAN is illustrated in figure 5.15.

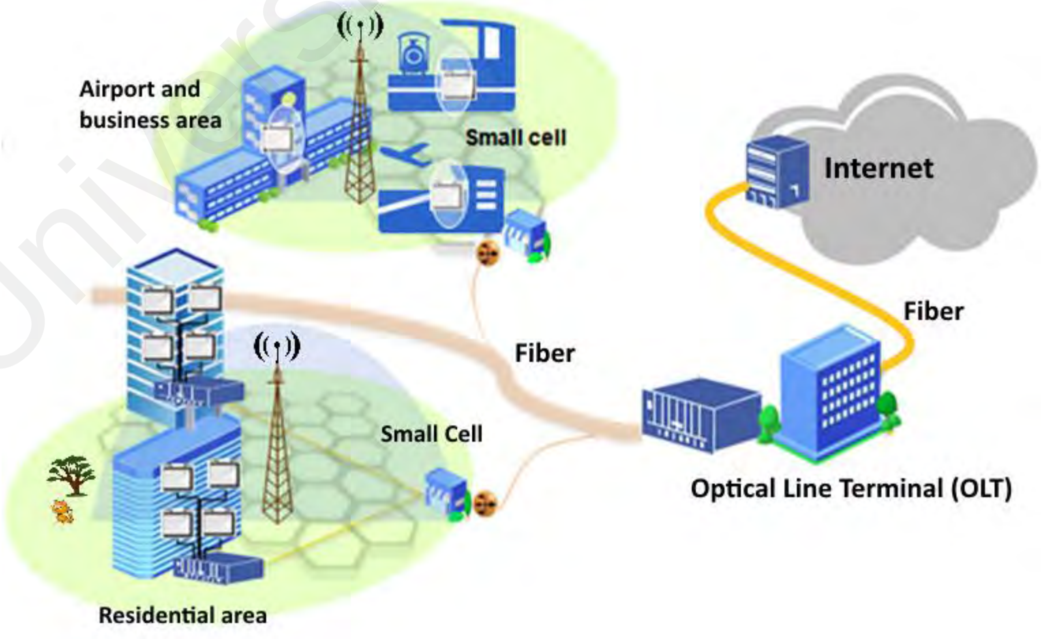

Figure 5.15: Next-generation converged optical-wireless access networks in 5G

As can be seen from figure 5.15, to make an end-to-end transport network all different types of WAN are connected to the fiber optic. In one hand, OAN provide very-high-speed Internet access for fiber to the x (FTTX) applications through optical line terminal (OLT). On the other hand, high-speed and convenient mm-wave and small cell WAN is utilized. For the high speed WAN many bands including the local multipoint distribution service at 28–30 GHz, the license-free band at 60 GHz, and the E-band at 71–76 GHz, 81–86 GHz, and 92–95 GHz are become available for 5G (Boccardi, Heath, Lozano, Marzetta, & Popovski, 2014; G.-k. Chang & Liu, 2013; Osseiran et al., 2014). For generating the high-frequency mm-wave electrical signals, using conventional electronics becomes less financially attractive; therefore, there is a high concern to directly generate mm-wave signals in the optical domain. As a consequence in this work, the photonic generation, modulation and distribution of 60 GHz frequency band signals to be applied in 5G have been suggested and demonstrated. Essentially, a photonics based mm-wave is a laser beam consisting of two or more coherent longitudinal modes with frequency spacing equal to the wanted mm-wave. As the longitudinal modes beat with each other in the photodiode, the required electrical mm-wave could be generated.

The generation of microwave signals from optical sources has long been a substantial area of interest due to its large potential for a variety of applications in communications (Enming et al., 2009; Shupei et al., 2013; Siyu et al., 2013; E.-M. Xu et al., 2009; X. P. Yang et al., 2013). A wide variety of techniques have been demonstrated for optically mm-wave generation, e.g., based on dual-mode laser (C. Kim et al., 2005), dual lasers with different wavelengths locked by optical phase locking and/or injection phase locking (Fukushima, Ohno, & Yoshino, 2001; Y. Li, Bystrom, Yoo, Goldwasser, & Herczfeld, 2005), mode locked lasers (Kuri & Kitayama, 1999), on optical external modulation(Y. Chen, Wen, & Shang, 2010; Jia et al., 2008; Jianjun et al., 2006; C.-T. Lin et al., 2009; J. Ma et al., 2010; Mohamed, Zhang, Hraimel, & Wu, 2008; Vegas Olmos, Kuri, &

Kitayama, 2007) optical heterodyning techniques (Georges, Cutrer, Solgaard, & Lau, 1995) (Jing Li et al., 2010) or on approaches based on nonlinear properties including four-wave mixing (FWM) (M. Li, Chen, Yin, Chen, & Xie, 2009; Shih et al., 2010; Q. Wang, Rideout, Zeng, & Yao, 2006), and stimulated Brillouin scattering (Jiang Li, Lee, & Vahala, 2013; T. Schneider, Junker, & Lauterbach, 2006). There is also some methods based on an optical frequency combs (OFC) that is generated by i.e. gain switching a distributed feedback laser (DFB) (Martin et al., 2014). This comb generation technique offers flexibility as the FSR of the optical combs possess tunability within a 20 GHz range and provides excellent signal to noise ratio.

Since the two longitudinal modes generated by a dual-mode laser or two separate lasers have low coherency, the mm-wave generated by their beating has poor spectral purity (Johansson & Seeds, 2000; Tao et al., 2012). While mode locked lasers can generate a wide bandwidth frequency comb, they suffer from cavity complexity and lack tunability of the free spectral range (FSR) due to a fixed cavity length. Moreover, the optical linewidth of the individual comb lines may be relatively large and the imperfect phase coherence between two optical tones can cause significant phase noise on the generated mm-wave signal (Brendel et al., 2011). The longitudinal modes generated by the nonlinear effects have higher coherency, but higher pump powers are required and their conversion efficiencies are low(Jia, Yu, Ellinas, & Chang, 2007). Moreover, since the Brillouin frequency shift is fixed in the fiber, the generated optical mm-wave is frequency limited. While a number of methods based on the external modulation technique have been proposed, modulators have large insertion losses particularly when cascaded. Coupled with the modulation efficiency and the instability induced by bias drift, the use of the external modulation technique can be complex(Weiß et al., 2008). Dual wavelength fiber laser (DWFL) is one of the interesting approach to generate radio frequency (RF) signals at mm-wave frequencies (Liang, Jin, Cheng, & Guan, 2014; M. Soltanian et al.,

2014) and terahertz sources (Jeon, Kim, et al., 2010b; Taniuchi et al., 2000). Erbium doped fiber (EDF) is the most commonly used gain medium in fiber laser setup in regions of 1.5 micron including multi-wavelength laser. However, strong mode competition induced by the homogeneous broadening (Becker et al., 1999) has become the main challenge to achieve stable multi-wavelength oscillation in room temperature. Achieving dual wavelength generation in the 1.5 µm wavelength region with EDFL is challenging due to strong mode competition caused by homogeneous gain broadening in the gain media. Various approaches for overcoming this setback, such as four wave mixing (M. P. Fok & C. Shu, 2007), polarization hole burning (Mou et al., 2009) and cascaded stimulated Brillouin scattering (Parvizi et al., 2011), have been reported for Thulium-doped fiber laser (TDFL), Ytterbium-doped fiber (YDF) and EDF. Various methods have been proposed to realize the multi-wavelength operation at room temperature by reducing cross-gain saturation and suppressing mode competition. These include polarization hole burning effect (Qian et al., 2008), frequency-shifted feedback (S. K. Kim, Chu, & Lee, 2001), cascaded stimulated Brillouin scattering (Ali, Anyi, Arof, & Harun, 2014), four wave mixing (P. Wang et al., 2013), etc. Recently, the authors have demonstrated a tunable spacing dual wavelength using a photonic crystal fiber (PCF) as a Mach-Zehnder interferometer utilizing a polarization dependent loss (PDL) effect (H Ahmad et al., 2013a). This DWFL shows high power stability with a very narrow line-width. The use of PCF brings advantages of flexibility and wavelength-dependent characteristics, which make the material almost an ideal choice as a wavelength selective filter for EDF (WG Chen et al., 2009). Furthermore, the RF generated by DWFL using PCF has been demonstrated as being highly stable (M. Soltanian et al., 2014). The work that is described in this paper had the central principle of generating stable DWFL with specific inter-spacing in order to obtain CW 60 GHz radiation of high quality and stability.

For the purpose of wireless transmission of the generated mm-wave signal in 60 GHz spectrum it is required to utilize the antenna suitable for 5G applications. The authors in (Haraz, Elboushi, Alshebeili, & Sebak, 2014) proposed a new four-element dense dielectric patch array antenna at 28 GHz for future 5G short-range wireless communications with relatively large size, complex structure, good impedance bandwidth and 16 dBi gain using EBG and dielectric superstrate. In this work an appropriate antenna to be utilized in 60 GHz is designed to be utilized in our proposed 5G system. Moreover, the generated DWFL provides comparative outputs using only a very short-length of PCF (only 10 cm long). Furthermore, the proposed generated DWFL not only utilizes a very simple and compact ring laser cavity, but also generates coherent and tuneable DWFL. Consequently, the RF signal generated by the proposed setup is tuneable, simple, and more stable compared to the other discussed methods. This has not been reported before, and this information would be of substantial benefit to the scientific and engineering community in the sense that it would allow for the development of a compact and robust dual-wavelength source that can be easily and safely used to generate RF radiation in real-world settings.

5.4.2 Experimental setup for generating 60 GHz RF signal

The configuration of the DWFL system in 1.5 micron region is schematically shown in figure 5.16. The DWFL consists of a 980 nm pump laser diode (LD), a 980/1550 nm wavelength division multiplexing (WDM), a 0.9 m Likkie EDF, a tunable band-pass filter (TBPF) with 1 nm bandwidth, isolators, a polarization controller (PC), a very short length of 10 cm PCF, and a 5:95 fiber based coupler.

The LD is directed into the fiber laser ring cavity through a WDM to provide excitation to the gain medium. TBPF is used to limit or confine the oscillation of dual wavelength laser in a narrow spacing. The isolators are used to assure unidirectional operation of the laser as to achieve a more stable lasing condition. The PC is inevitably exploited to adjust the polarization of light propagating inside the ring cavity. PCF plays the main role in the setup to stabilize the DWFL. The micrograph of the PCF cross-section structure is shown in the inset in figure 5.16. The PCF surrounded by air holes with 5.06 μm diameter and separation of 5.52 μm between holes. The coupler is used to direct part of the laser power out of the laser cavity for measurement, analysis and application.

The output end of the PCF was connected to the input port of coupler, with the 95% output port then connected to isolator 1. This isolator was further linked to the Leikki EDF gain medium that possessed an NA of 0.21 to 0.24, mode field diameter of 5.7 - 6.6 at 1550 nm, and absorption coefficient of 84 dB/m at 980 nm. The other end of the EDF was subsequently connected to a WDM fused coupler. Thereafter the 980 nm port was coupled to a LD operating at approximately 80 mW. The signal port of the WDM was connected to another isolator, labeled as isolator 2 which is attached to TBPF in series with a PC. The TBPF acted as a window to tune the generated dual wavelength output and had specifications of 0.8 nm narrow bandwidth, 0.05 nm high tuning resolution, a broad tuning range of 1535–1565 nm, and a low insertion loss typically around 1.5 dB. Laser output was continuously monitored by means of an optical spectrum analyzer (OSA) connected to a 3 dB coupler that was linked, by way of an isolator labeled isolator 3, to a fiber coupler on the main optical ring. This main circuit coupler was responsible for diverting 5% of the laser output towards isolator 3. Another branch of the 3 dB coupler with one port linked to the OSA was then connected to an oscilloscope (OSC) through a photodiode to show RF spectrum generated by beating of the DWFL.

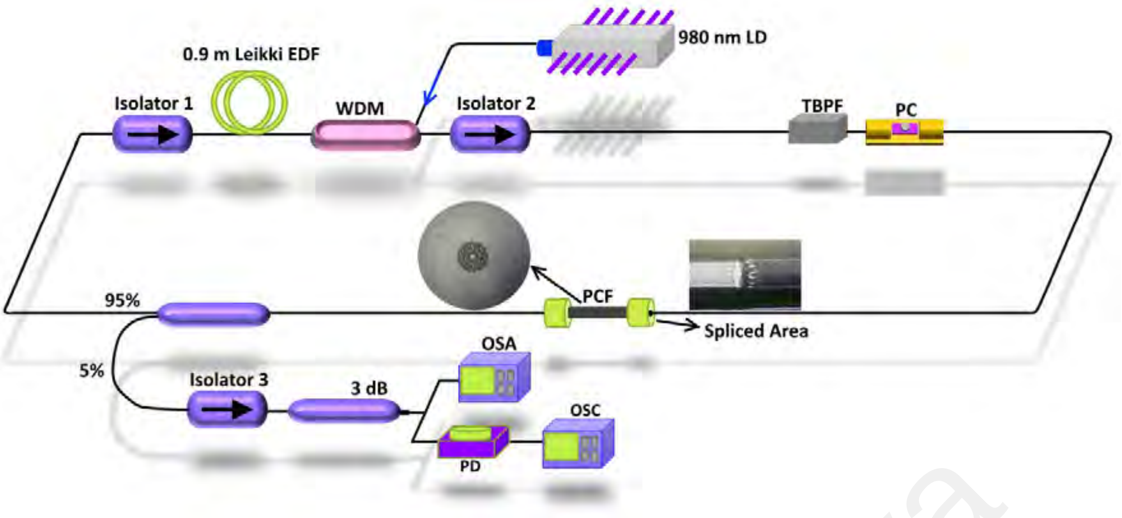

Figure 5.16: Experimental setup to generate stable dual-wavelength fiber laser

Figure 5.17 (a) shows the experimental result of the DWFL with 0.52 nm spacing between two wavelengths lasing at wavelengths 1546.96 nm and 1547.48 nm. The stability of the achieved DWFL over 160 minutes is shown in figure 5.17 (b) with the interval scan of 10 minutes. The displacement of the output lasing can be achieved by fine tuning of the PC due to the polarization dependence of the laser inside the ring cavity. The adjustment of the PC will rotates the polarization states and allows continuous adjustment of the birefringence within the ring cavity to balance the gain and loss of the lasing wavelengths. By achieving dual wavelengths laser with similar peak powers, a stable DWFL can be obtained. The PC is then fine-tuned to obtained dual wavelength laser with almost similar peak powers at -22.22 dBm and -21.21 dBm at wavelengths 1546.96 nm and 1547.48 nm respectively as shown in Fig. 5.17.

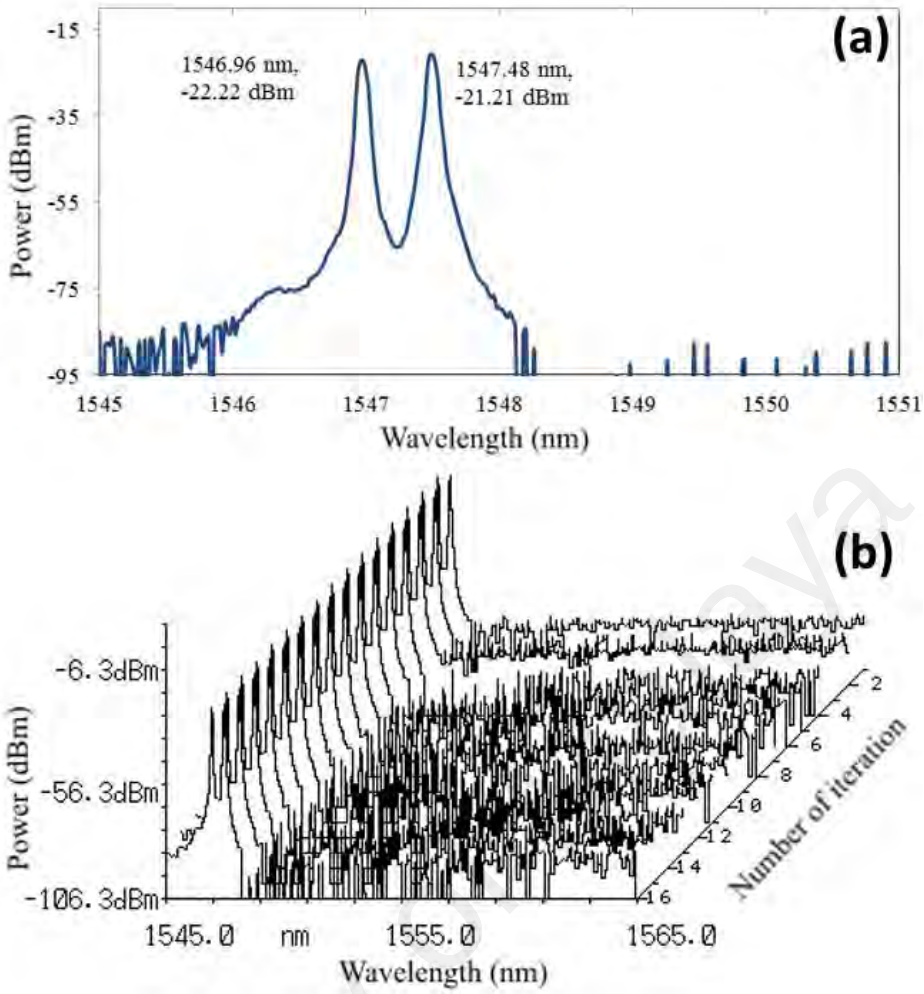

Figure 5.17: (a) Optical spectrum of DWFL lasing at wavelengths 1546.96 nm and 1547.48 nm and (b) the stability of achieved DWFL over 160 minutes with the interval scan of every 10 minutes.

5.4.3 Experiment results for 60 GHz signal generation

The unique properties of PCF, such as wide range single mode operation, dispersion flexibility and large mode area, have been investigated recently (Russell, 2006), and the inherent flexibility in particular puts PCF in contention for use as an interferometer. Interferometers employing PCF also can be wavelength-selective filters (WG Chen et al., 2009) due to the wavelength-dependent characteristics afforded by PCF. A constructed compact interferometer using a 10 cm length of few-mode PCF spliced on each end to SMF, as shown for one side in the image labeled “spliced area” in figure 5.16. Manually splicing the PCF and SMF fiber at two points in series led to an inevitable collapse of the PCF air holes and creation of a very simple Mach-Zehnder interferometer.

The first collapsed region served to diffract the traversing fundamental mode, and consequently allow core and cladding modes to become excited within the few modes PCF section. A portion of the fundamental core mode can be coupled to a single or several cladding modes in the PCF. Phase shifting within a physical length, L, of the PCF is a product of dissimilar effective refractive indices of core and cladding modes. As the effective refractive index of the cladding is smaller than that of the core, separate optical paths that correspond to arms of the Mach-Zehnder interferometer can be achieved. The fundamental and cladding modes accumulate a phase difference along the PCF due to different phase velocities, and this phase difference depends on the length of PCF and the wavelength of the guided light. Cladding modes recouple to the core mode upon reaching the second collapsed area of the PCF. Since the phase difference and the phase velocities are wavelength dependent, the optical power transmitted by the interferometer will be minimum at certain wavelengths and maximum at the others. The separation between consecutive peaks of a two-mode interferometer is given by $\Delta\lambda=\lambda^2/L\Delta n_e$, where λ represents the source wavelength, L is the length of the PCF between the two splices, and Δn_e symbolizes the effective refractive indices difference between the core and cladding modes. The optical paths established via the core and the cladding modes behavior within the PCF play the role of arms of a Mach–Zehnder interferometer, and the collapsed points perform as couplers that split or combine light in the interferometer arms.

The microwave generation is subsequently determined by connecting the dual-wavelength output to the photo detector and taking measurements with the RFSA. The RF spectrum is shown in figure 5.18. (a) as having a frequency of 65.12 GHz. As described earlier, the 60 GHz frequency band has the potential to support very high data rate wireless communication applications. Considering the limited data rates offered by current wireless LAN (802.11a, 11b, etc) and mobile networking systems, it is anticipated that future higher data rate wireless LAN and mobile networking technology could occur in the 60 GHz band. Furthermore, in the UK these millimeter wave bands are expected to relieve congestion and reduce demand for spectrum in frequency bands below 20 GHz (Burns, 1994) that would further attract commercial interest. The frequency drift associated with these transceiver devices is an important factor in specifying frequency band requirements. According to several test reports on 60 GHz equipment available on the Federal Communications Commission's website, the worst case frequency deviation was recorded to be 57 MHz from the nominal frequency when the transmitter was operated between -20°C to 50°C. Noting the above, there is a need to avoid interference being caused to adjacent frequency bands due to frequency drift of equipment operating in the 59.3 - 64 GHz bands. It is therefore proposed to introduce 100 MHz guard bands to protect adjacent band services from excessive drift in operating millimeter wave transceiver (MWT) equipment. The frequency tolerance of a crystal or oscillator is defined as the initial deviation of the crystal or oscillator frequency as compared to the absolute at 25°C. The frequency stability over temperature is defined as the frequency deviation compared to the measured frequency at 25°C over the defined operating temperature range (i.e. 0°C to +70°C). For instance in 60-GHz radio regulation in Japan, allowable frequency deviation is limited by +/-500 ppm which is corresponding to frequency deviation of +/- 30 MHz.

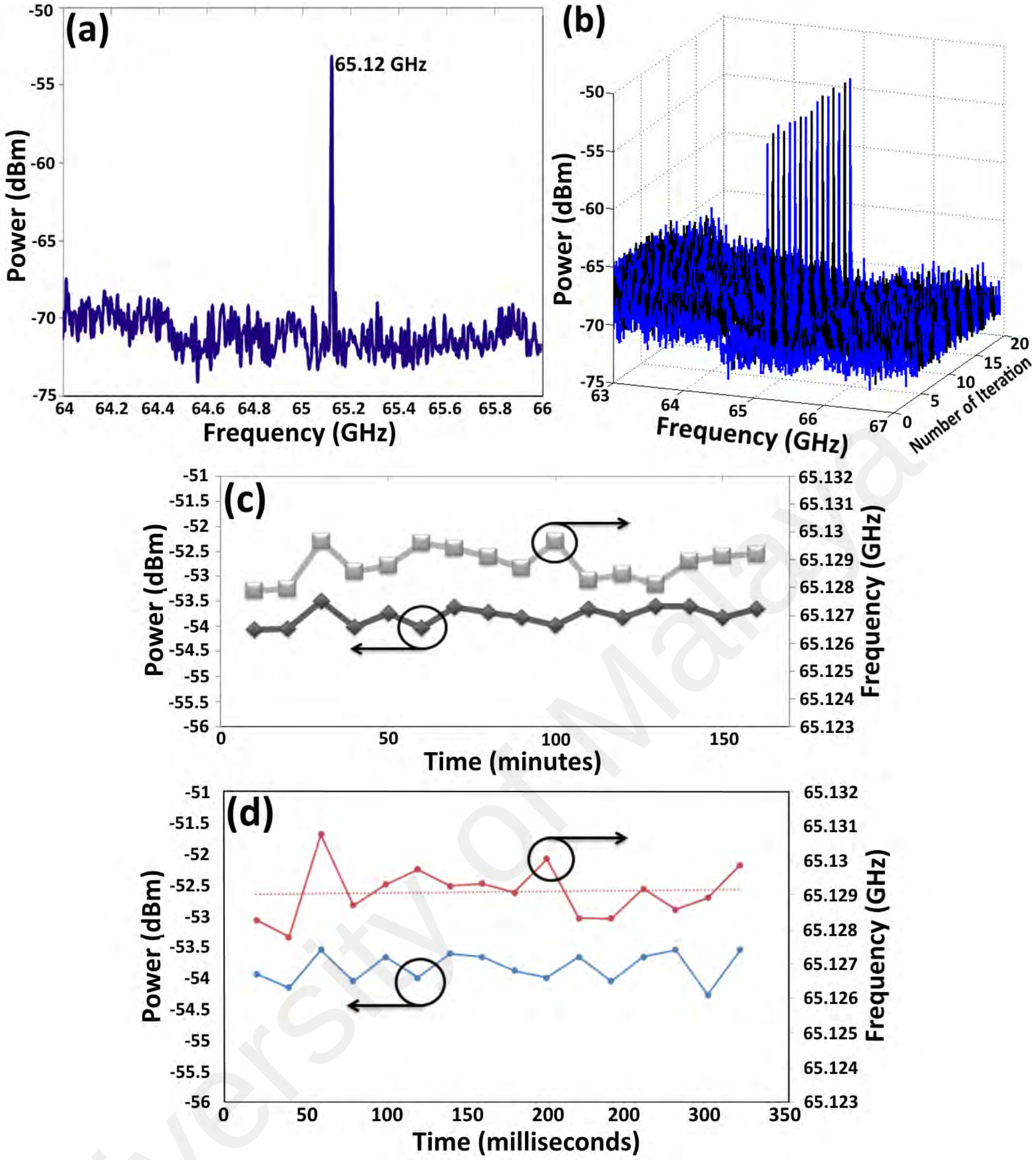

Figure 5.18: (a) The beating frequency of 65.12 GHz in the RFSA, (b) the stability of generated RF over 160 minutes with the scan interval of 10 minutes, (c) power and frequency fluctuation of the generated RF as a function of time recorded in 160 minutes and (d) 320 ms in the scan interval of every 20 ms.

Therefore, here, the signal stability is investigated by scanning the RF spectrum for every ten minutes. The RF power and frequency stabilities are recorded as shown in figure 5.18 (c). It is found that the frequency drifts between 65.1265 GHz and 65.1274 GHz with 0.00077% maximum deviation from the average. Figure 5.18 (d) provides the RF power and frequency stabilities during 320 ms in the scan interval of every 20 ms. The carrier frequency can be further stabilized by placing the fiber spool in a temperature controller or using polarization maintaining fiber (PMF). RF power stability is important in the implementation of oscillators and carriers. The measured average peak power is at −52.55 dBm and its peak power fluctuation is ± 0.49 dB. Fluctuations in the millimeter wave power can only be reduced with the enhancement of laser stability. The measured power is low due to the bandwidth limitation of the photodetector.

5.4.4 60 GHz antenna design

Microstrip Comb Array Antenna (MCAA) has been designed to operate at 60GHz for 5G application. The MCAA shows broader impedance bandwidth and lower cross-polarized radiation as compared with the conventional microstrip grid array antennas. The MCAA is designed not as a travelling-wave, but a standing-wave antenna. As a result, the match load and the reflection-cancelling structure can be avoided, which is important, especially in the millimeter-wave frequencies. The structure of designed antenna is presented in figure 5.19. In this work, the Ansoft-HFSS software is used for different analysis and parametric simulations. ANSYS HFSS software is the industry standard for simulating 3-D, full-wave, electromagnetic fields. Its gold-standard accuracy, advanced solvers and high-performance computing technologies make it an essential tool for engineers tasked with executing accurate and rapid design in high-frequency and high-speed electronic devices and platforms. HFSS offers state-of the-art solver technologies based on finite element, integral equation, asymptotic and advanced hybrid methods to solve a wide range of microwave, RF and high-speed digital applications. In all designs, a single-layer Rogers RT/duroid 5880 substrate ($\varepsilon_r = 2.2$, $h = 0.787$ mm & $\tan\delta = 0.001$) is used. Dimensions are optimized by using parallel parametric studies and tabulated in Table 5.1.

Table 5.1: Optimized antenna dimensions for the proposed antenna

Parameter	L	w_1	w_2	h
Value	3.01mm	0.4mm	0.6mm	1.505mm

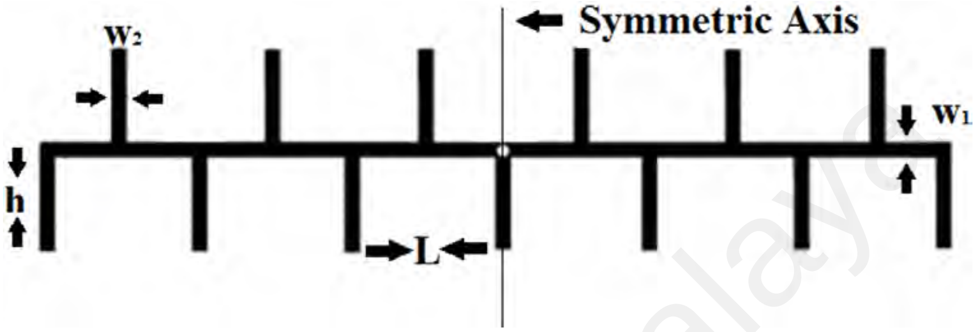

Figure 5.19: Schematic of the proposed antenna

Proposed antenna has a gain of 23.6 dB at 60GHz which is greater than 5G antenna's gain requirement (Rappaport et al., 2013). In this design not only high gain with an acceptable bandwidth around 7.8GHz has been obtained but also the side lobe level is below -20dB. Measured $|S_{11}|$ versus frequency is shown in figure 5.20 (a). As can be seen clearly from this figure the proposed MCAA achieves -10dB impedance bandwidth of 7.8GHz from 54.43 to 62.23GHz and proves that the bandwidth is more than enough bandwidth has been covered by the proposed antenna for 5G application as 1GHz bandwidth is enough for 5G application (Schmogrow et al., 2012).

Figure 5.20 (b) and (c) show the co-polar radiation patterns of the proposed antenna in the *H* and *E* planes at 60 GHz, respectively. It must be noted that a narrow beam in the *H*- plane with the 3-dB beamwidth of 20° and a broad beam in the *E*- plane with 3-dB beamwidth of 90° has been observed.

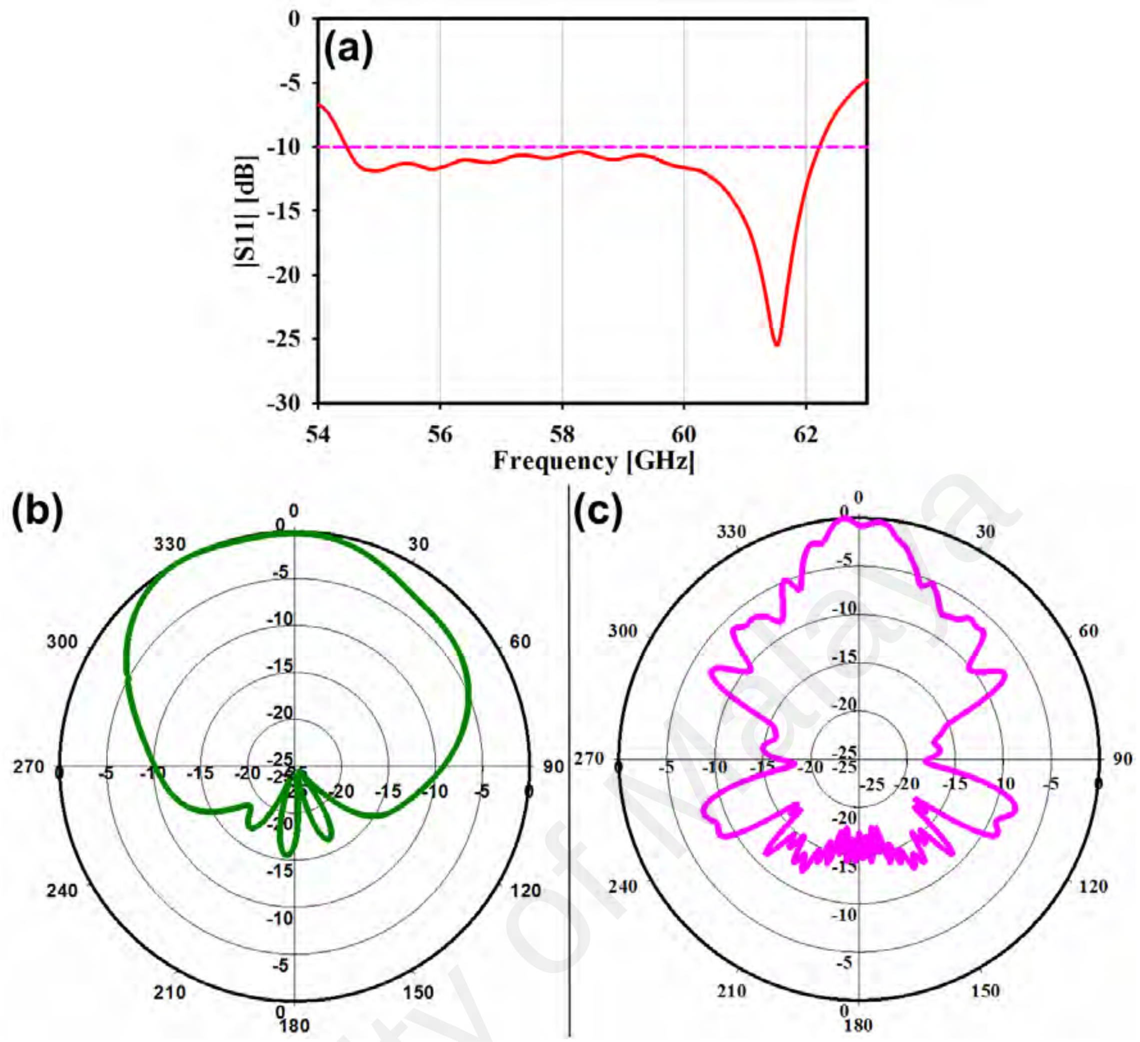

Figure 5.20: (a) Measured $|S_{11}|$ of the proposed antenna for 5G application (b) E-plane & (c) H-plane radiation patterns of the proposed antenna at 60GHz.

5.4.5 System setup

Figure 5.21 shows the system design. First, using the proposed DWFL system discussed in Section 2 the dual wavelength signal with 65.12 GHz frequency distance between each wavelength is generated.

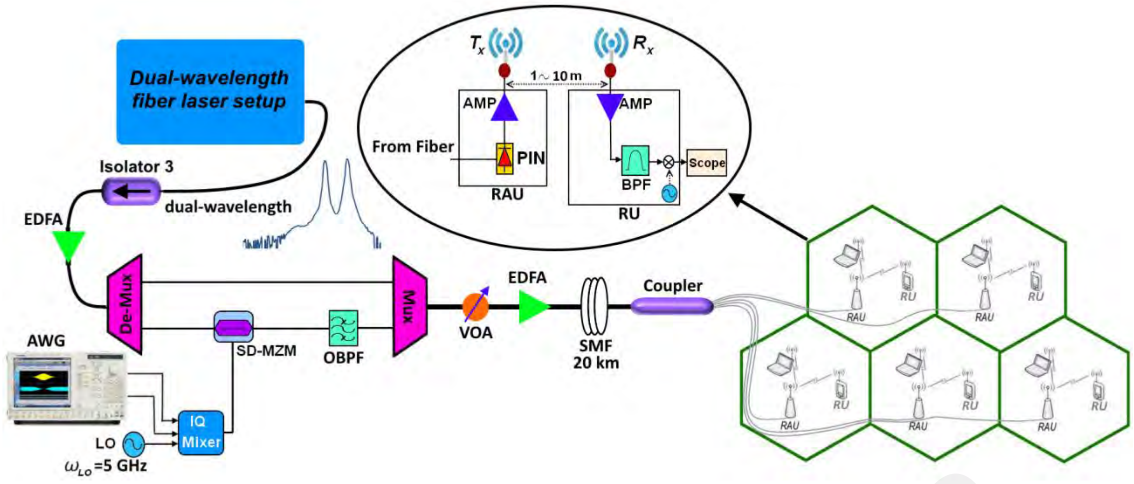

Figure 5.21: System setup

Then in order to utilize the generated carriers in 5G application we used the OFDM signal to be transmitted in a 5G small cell. For this purpose the OFDM signal is generated using arbitrary waveform generator (AWG) and it was up-converted to IF region using the I/Q mixer with local oscillator of f_{LO}=5GHz. The OFDM signal parameters are listed in Table 2.

Table 5.2: OFDM signal parameters

AWG	**Parameters**
Tektronix AWG7122C	F_s=12 GHz
	FFT_size = 512,
	Enabled carriers = 426
	$OFDM_{BW}$= 5GHz
	CP Length = 1/16 frame

As shown in figure 5.22 the lower carrier from DWFL system was modulated by the OFDM signal using double side band techniques with an single-electrode Mach–Zehnder modulator (SD-MZM) while the upper carrier is kept unmodulated. The optical filter with a centre frequency of 193.86 THz and 15 GHz bandwidth is used to remove the lower carrier and the lower side band of the OFDM (LSB-OFDM); therefore, only the upper side band of the OFDM (USB-OFDM) is multiplexed by the unmodulated upper carrier they are 60.12 GHz apart from each other.

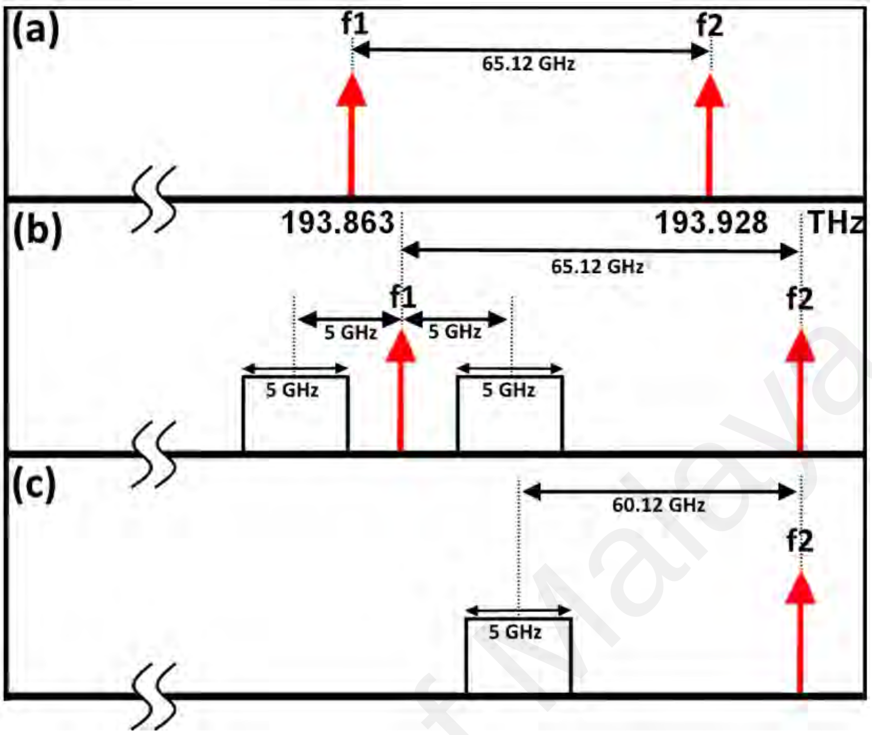

Figure 5.22: Wireless RF signal generation for 5G

Next, the multiplexed signal is amplified by an erbium-doped fiber amplifier (EDFA) and transmitted over an SMF link. In the remote antenna unit (RAU), the modulated OFDM signal and unmodulated carrier that are 60.12 GHz apart are beaten to photo-detector; therefore, after photo-detection, the 60.12-GHz mm-wave OFDM signal is amplified using a low noise amplifier (LNA) and then transmitted to the 5G antenna with 23-dBi gain designed in previous section. Increasing the number of channels in optical communication systems will eventually result in the usage of optical signal de-multiplexing components with greater values of optical attenuation. Additionally to this, when transmitted over long distances, the optical signal is highly attenuated, and therefore, to restore the optical power budget it is necessary to implement optical signal amplification. At the choice of signal amplification method for the wavelength division multiplexing (WDM) systems the preference is given to the class of (EDFAs). Therefore, due to the low power of the generated DWFL, the use of the EDFAs is necessary in order to accommodate the power budget. These amplifiers are low-noise, almost insensitive to polarization of the signal and can be relatively simply realized (Dutta, Dutta, & Fujiwara, 2003). Besides providing gain at 1550 nm, in the low-loss window of a silica fiber such amplifier allows achieving such gain in wider RF band. To ensure the required level of amplification over the frequency band used for transmission it is highly important to choose the optimal configuration of the EDFAs, as the flatness and the level of the obtained amplification, and the amount of EDFA produced noise are highly dependent on each of the many parameters of the amplifier. Moreover, to achieve a stable RF frequency resulted from beating of the generated DWFL, EDFA decreases the power fluctuation of DWFL and provides more stable RF signal.

After wireless transmission, the OFDM signal is received by a second 5G antenna with 23 dBi gain. Subsequently, at the receiver unit (RU), the received signal is amplified using LNA (57-64 GHz), and then, electrical down-conversion is performed in the 60 GHz-band. The down-converted signal is further amplified in the frequency range of 0.7–12 GHz and then captured by Oscilloscope operated at a sampling rate of 50–100 GS/s. Baseband digital signal processing including one-tap equalization, demodulation, demapping, and error vector magnitude (EVM) computation are performed offline. The EVM is defined as follows:

$$\%EVM = 100 \times \left[\sum_{l=1}^{N} \frac{\left| \overline{d}_r - d_l \right|^2}{N} \right]^{\frac{1}{2}} / \, d_{\max} \qquad 5.1$$

where $\overline{d}_r$ and d_l are the received and ideal symbols, respectively, and $d_{\max}$ is the maximum symbol vector in the constellation. Here, N is the number of 16-QAM symbols (Schmogrow et al., 2012).

5.4.6 System performance

First, the system EVM performance was tested based on the variation of the optical link length for a fixed wireless distance (5 m). Second, the EVM of the system based on the variation of the wireless link distance between 1–10 m over a 20-km SMF was calculated. Figure 5.23 shows the EVM performances of 16-QAM OFDM signals for different lengths of the SMF transmission link and different wireless channels. The optical power is fixed at 0dB using variable optical attenuator (VOA). The constellations for 10 km and 20 km for wireless channel (2) also shows a successful transmission for 5 m wireless link at the threshold EVM of 10% (Schmogrow et al., 2012).

In the second case shown in figure 5.24, the dependence of system performance on the wireless distance was investigated. Here, for fiber length of 20km the received optical power was varied from -3 to 5 dBm, and for three different wireless distances (10, 5 and 2 meters) the EVM was calculated. With an increase in the wireless distance, the free-space path loss causes degradation of the EVM performance. It can be seen that the system can support a maximum wireless transmission distance of 10 m for the power penalty of 0.7dBm. The eye diagrams also show the successful transmission for two wireless distances of 2 and 5 m.

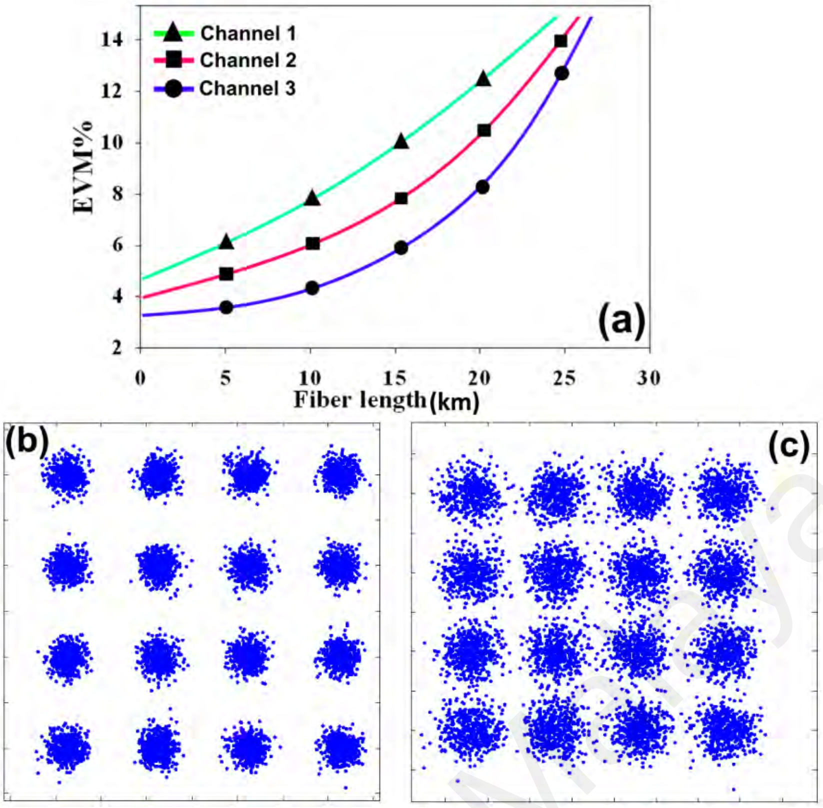

Figure 5.23: EVM performance and constellation diagram related to different optical link lengths and 6m wireless link.

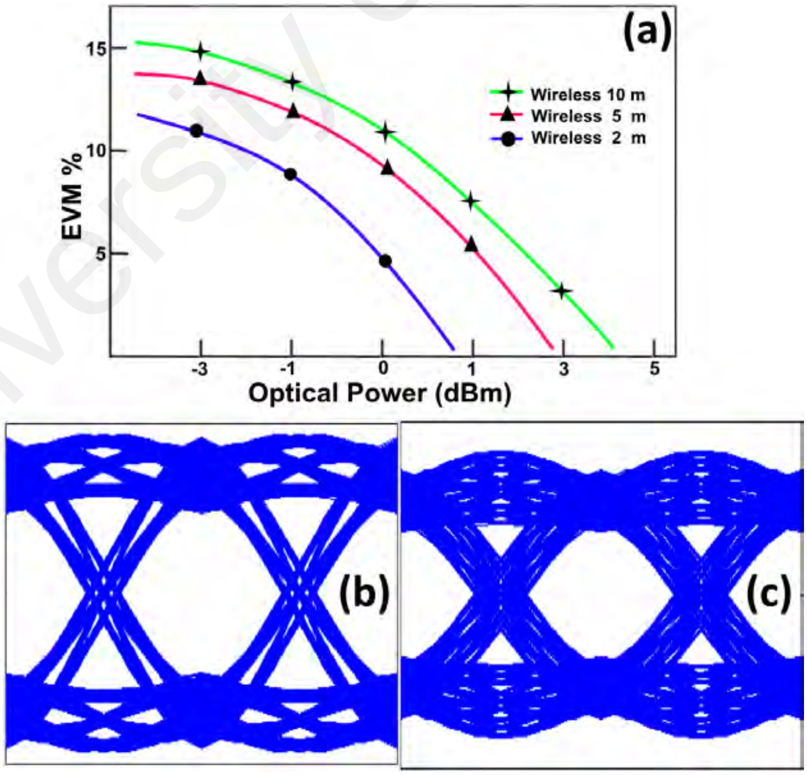

Figure 5.24: (a) EVM performance for different wireless link distances, (b) eye diagrams for 2 meters wireless distance, (c) eye diagrams for 5 meters wireless distance

CHAPTER 6: CONCLUSION AND FUTURE OUTLOOK

In this final chapter, we will summarize and conclude what has been demonstrated and future outlook will be discussed.

6.1 Introduction

In conclusion, all the objectives set in this research work were achieved. The first objective is to generate and characterize tunable dual-wavelength fiber lasers by using the three different homogeneous broadening gain media in the regions of 1, 1.5 and 2 micrometer. It was solved successfully by using the mode competition issues emit by the gain media. Applications for the DWFL design form the second objective. The two objectives are briefly presented in this chapter.

6.2 The generation of Dual-Wavelength Fiber Lasers

The first motivation of the thesis is to design the tunable dual-wavelength fiber lasers which have been successfully done in the research work. It is known that YDF, EDF and TDF are suitable amplifier in the 1, 1.5 and 2 micron regions respectively. However, they have their own limitation of difficulty to provide dual-wavelength or multi-wavelength outputs due to near homogeneous broadening effects emit by the gain media, mentioned previously. A novel approach of using the PHB and SHB are reported in this thesis as an alternative way to solve the mode competition issue. The design is effective to overcome the limitation of mode competition inherit in the homogeneous gain media to provide a balance dual-wavelength output power source. In this thesis, the generations of dual-wavelength fiber lasers are set forth by using a very short length PCF as a selective element. The maximum SMSR of more than 50, 60 and 40 dB were achieved when YDF, EDF and TDF gain media utilized in the configuration setup respectively as shown in figure 3.4, figure 3.8 and figure 3.25.

In section 3.2, we demonstrated the narrow spacing dual-wavelength fiber laser on the Ytterbium doped fiber using a photonic crystal fiber based Mach Zehnder Interferometer fiber. The dual-wavelength narrow spacing tuning range for our proposed setup is between 0.03nm, 0.07nm, 0.1nm, 0.2nm and 0.40nm. The observed SMSR of our proposed experiment is 50dB for spacing wavelength below 0.1nm and increasing to 49 dB with decreasing of spacing wavelength of 0.1nm. We achieved a highly stable set of dual-wavelength output with power fluctuation of ~0.8 dB over a period of 15 minutes and wavelength fluctuation less than 0.01 nm. By using the tunable band-pass filter, our setup has the capability of adjusting the narrow spacing between dual-wavelength outputs. Moreover, our proposed setup is simple and inexpensive, and offers flexibility in dual-wavelength laser application.

In section 3.3.1, The dual-wavelength Erbium doped photonic crystal fiber ring laser utilizing the polarization dependent loss was demonstrated. The short ring cavity setup generated DWFL with 3 pm narrow line-width at full wave half maximum. Utilizing the birefringence of the photonic crystal fiber and polarization controller, high signal to noise ratio of more than 60 dB is achieved with the proposed setup. The polarization of each laser in the DWFL is studied and analyzed. The flexibility of the proposed setup in selecting different spacing between the two lasing wavelength with proper adjustment of the tunable band pass filter and polarization controller to achieved stable dual wavelength fiber laser with peak power fluctuation that less than 0.6 dB and wavelength fluctuation of less than 10 pm is demonstrated. The wavelength spacing tuning range of the DWFL is between 80 pm and 600 pm.

In section 3.3.2, a tunable stable DW coherent source have been studied and demonstrated experimentally by launching mode-locked laser pulses with FWHM pulse duration of 570 fs into a micro-ring resonator. Moreover, generation of multi-wavelength coherent source operating at 1.5 μm by utilizing micro-ring resonator is investigated and demonstrated both theoretically and experimentally. The experimental results were in agreement with the MATLAB modeling results. The SiO_xN_y micro-ring resonators have a small footprint of 3×5 mm^2. The finesse (F), given by the ratio FSR/FWHM, was approximately 15.53, where the Q factors of the two micro-ring resonators having diameters of 2.54 and 1.27 mm are 1.2×10^5 and 0.6×10^5 respectively. Regarding the time-bandwidth product which is 0.32 for the case of mode-locked laser or solitons, the minimum pulse duration calculated are 200 and 100 ps for the micro-ring resonators having diameters of 2.54 and 1.27 mm respectively. The FSR of 0.202 and 0.404 nm and FWHM of 13 and 26 pm were achieved by the setup utilizing add-drop micro-ring resonator with D=2.54 and D=1.27 mm respectively. Obtaining higher FSR as integer coefficient of the minimum achieved FSR results from utilizing FBG and TBPF together. The dual wavelength fiber laser showed stable operation at room temperature with both wavelength and power. It has more than 30 dB optical signal-to-noise-ratio. The authors anticipate the success of the design described here will spur further research efforts and application in this area.

In section 3.4, a stable dual wavelength laser operating at 1.9 μm and based on thulium-doped fiber as the gain medium has been proposed and demonstrated. The laser made use of the principle of polarization-dependent loss control to realize a dual-wavelength operation, and attained stability by utilization of a 10 cm long photonic crystal fiber. This photonic crystal fiber effectively acted as a Mach-Zehnder interferometer with a free spectral range of 0.2 nm. The dual wavelength thulium-doped fiber laser operated stably at room temperature in regards to both wavelength and power, and had a 45 dB optical signal-to-noise-ratio. The authors anticipate the success of the design described here will spur further research efforts and application in this area.

6.3 The applications of Dual-Wavelength Fiber Lasers

The main motivation of the thesis is on the application of DWFL by the virtue of new findings that have been successfully done and explained in Chapter 4 and 5. A few applications demonstrated in this research are considered as new and novel, since it is developed using the new and innovative design of the DWFL. They are tunable dual-wavelength single longitudinal mode fiber laser, dual-wavelength for generating microwave signals, DWFL for future generation of mobile networks, the Q-switch DWFLs, the DWFL application for the generation of terahertz signals. Initially, the generation of tunable dual-wavelength single longitudinal mode fiber laser was presented.

In section 4.1, we have proposed and experimentally demonstrated the dual-wavelength Q-switched ytterbium doped fiber laser using Selenium Bismuth (Bi_2Se_3) as saturable absorber. Using the optical deposition method, the few-layer Bi_2Se_3 in the suspension was well deposited onto a fiber ferrule to fabricate the fiber-compatible Selenium Bismuth based q-switcher. Our stable dual-wavelength Q-switching operation was successfully achieved with maximum pulse energy of 0.65 nJ, shortest pulse duration of 8.46 μs and pulse repetition rate from 15.37 to 59.24 kHz. These results mean that the proposed setup relative to similar reported approaches has key advantages of simpler setup, lower cost deployment, and highly stable operation under room temperature for the 1 μm wavelength region.

In section 4.2, we have proposed and demonstrated the dual-wavelength Q-switched ytterbium doped fiber laser using Bismuth Telluride (Bi_2Te_3) as saturable absorber. Using the dry oven method, the few-layer Bi_2Te_3 was well deposited onto a fiber ferrule to fabricate the fiber-compatible Bismuth Telluride based q-switcher. Our dual-wavelength Q-switching was successfully achieved with two lasing wavelength of 1042.76 and 1047 nm, with maximum pulse energy of 3.82 nJ and pulse repetition rate from 3.79 to 15.63 kHz. Results indicated that TI:Bi_2Te_3 was compatible with the 1 μm waveband, and hence could be considered a potential broadband SA for passively Q-switched optical fiber lasers.

In section 4.3, a Q-switched fiber laser with dual-wavelength output by utilizing embedded graphene oxide solution into short length PCF is proposed and demonstrated. The dual-wavelength output generated overcomes the mode-competition in the EDF gain medium. The PCF has a zero-dispersion wavelength of about 987 nm and a solid core approximately 4.37 μm in diameter surrounded by microscopic air holes with an approximate diameter of 5.06 μm each and separation of 5.52 μm. The pulsed output is obtained using about 60 μm embedded GO based SA inside the PCF. The channel spacing of the output can be tuned by polarization controller. At the maximum pump power of 206 mW, pulses with a repetition rate of 24.0 kHz, average output power and pulse energy of 0.167 mW and 8.98 nJ respectively are obtained.

In section 4.4, a Q-switched fiber laser with a narrowly spaced dual-wavelength output is proposed and demonstrated. The dual-wavelength output is generated using a short, 10 cm long PCF as to overcome the mode-competition in the EDF gain medium. The PCF has a zero-dispersion wavelength of about 987 nm and a solid core approximately 4.37 μm in diameter surrounded by microscopic air-holes with an approximate diameter of 5.06 μm each and separation of 5.52 μm. The pulsed output is obtained using a GO based SA, whereby a GO paper with an average diameter of 4.0 cm and a thickness of about 10 μm is sandwiched between two fiber ferrules. The channel spacing of the output can be tuned, with each pulse having an average 3 dB linewidth of 0.6 pm. At the maximum pump power, pulses with a repetition rate, pulse-width, average output power and pulse energy of 31.0 kHz, 7.0 μs, 0.086 mW and 2.8 nJ respectively are obtained. The proposed dual-wavelength fiber laser has high potential for applications such as sensing microwave and terahertz radiation generation.

In section 5.1, the results demonstrated the capability of a dual-wavelength fiber laser with tunable SLM outputs to be used in the optical generation of microwave emissions. The proposed configurations discussed here are based on a ring fiber laser using an EDF with an absorption coefficient of 16.0 - 20.0 dB/m at 1531 nm and 11.0 - 13.0 dB/m at 980 nm. A 10 cm long PCF with a solid core diameter of 4.37 μm surrounded by air holes of 5.06 μm diameter and separated by 5.52 μm acts to generate the desired dual-wavelength output, while a TBPF with a narrow bandwidth of 0.8 nm and a PC acts as a tuning element. Channel spacing of as narrow as 0.00043 nm spacing are obtained, giving a microwave emission of 671.9 MHz, to spacing as large as 0.03631 nm, giving a microwave emission of 4.59 GHz can be realized with this system. The output is stable and, combined with the compact form factor and robust build of such fiber lasers, provides new avenues of application, particularly in fields such as sensing and monitoring.

In section 5.2, optical generation of THz emissions of satisfactory quality via a DWFL outputting in SLM has been described and demonstrated with a series of results in this paper. The facilitating configurations were based on a ring fiber laser using an EDF with an absorption coefficient of 84 dB/m at 980 nm. A PCF of 10 cm length assisted in the generation of the desired dual-wavelength output. An incorporated tuning element comprised a TBPF with a narrow bandwidth of 0.8 nm and a PC. The system was capable to generate variable and tunable dual-wavelength output with channel spacing of 7, 11.4 and 21.2 nm corresponding to 0.9, 1.4 and 2.66 THz emission respectively. This CW THz output was subsequently verified as stable. In combination with consideration of the compact form factor and robust build of such fiber lasers, the successful work described here provides a basis for new avenues of application and further research in this area.

In section 5.3, a DWFL system has been demonstrated through detailed discussions of the mm-wave signal generation system for 5G applications. Data transmissions are achieved using a 5 GHz bandwidth OFDM signal centred on 60 GHz.

For the purpose of wireless transmission in 5G small cell network a 60 GHz antenna was designed and fabricated. The efficiency of the system was evaluated using EVM measurement curve. Based on the results it can be concluded that the system with a 16-QAM OFDM signal can be received by the end user with acceptable EVM over a 20 km optical fibre and a 10-m wireless link with an optical power penalty of 0.7dBm.

6.4 Future Works

Up to this point in time, the objective of producing tunable dual-wavelength fiber lasers has been fulfilled. However, many other avenues in which this research could be continued and explored. One of them is to generate a high quality output beam, in terms of its output power, as most of the design presented in the research works operating in the -30 dBm until 0 dBm of output power which is quite good especially to be used as a seeding signal for further amplification. Another factor to be considered is in the SMSR values. They can be improved by solving the noise level problem inside the laser cavity. Another area of future work is in the tunability range characteristic for the DWFL as the tunability represents the capability of the design to be used for many kinds of applications without having any wavelength range limitation problem. All of the suggested improvements are important for the output laser in order to match the ITU and IEEE standards.

The other key focus for future research is to improve the output wavelengths by generating multi-wavelength fiber lasers. In this research outline, the DWFL was successfully presented by using a homogeneous gain media. Subsequently, this study can be extended to find an alternative way to improve the current design to generate multi-wavelength fiber lasers. These multi-wavelength fiber lasers using the cavity loss control method is not applicable in this matter, as the design would be complicated since power for each wavelength has to be controlled to obtain multi-wavelength fiber laser with a balance output power. This subsequently leads to the construction of a complicated setup and may be found to be challenging in real applications, hence the need for a further design improvement.

Despite the improvements in the design to produce better laser output, DWFL has still greater potential applications in Terahertz and microwaves generations. Further research should include the Terahertz generation for the applications into the field of sensors, gyroscope and inter-ferometry. A few techniques such as using the saturable absorbers are required to improve the performance of a single longitudinal mode laser operation with a simpler cavity design. The same contention also applies for the microwaves generations. The DWFL for wireless temperature sensor is also one of the promising research works that could be done in the future. The design should capable to detect very low fluctuations of temperature change and at the same time can be translated to the microwave region. These two fields can be merged together for a thorough experimental investigation for wireless temperature sensors that can be used for much kind of purposes in the future.

REFERENCES

Adachi, S. (1982). Material parameters of $In_{1-x}Ga_xAs_yP_{1-y}$ and related binaries. *Journal of Applied Physics, 53*(12), 8775-8792.

Adachi, S. (1989). Optical dispersion relations for GaP, GaAs, GaSb, InP, InAs, InSb, $Al_xGa_{1-x}As$, and $In_{1-x}Ga_xAs_yP_{1-y}$. *Journal of Applied Physics, 66*(12), 6030-6040.

Adachi, S., Kawaguchi, H., Takahei, K., & Noguchi, Y. (1981). InGaAsP/InP buried-heterostructure lasers (λ= 1.5 μm) with chemically etched mirrors. *Journal of Applied Physics, 52*(9), 5843-5845.

Agger, S., Povlsen, J. H., & Varming, P. (2004). Single-frequency thulium-doped distributed-feedback fiber laser. *Optics Letters, 29*(13), 1503-1505.

Agrawal, G. P. (2012). *Fiber-optic communication systems* (Vol. 222): John Wiley & Sons.

Ahmad, H., Latif, A. A., Abdul Khudus, M. I. M., Zulkifli, A. Z., Zulkifli, M. Z., Thambiratnam, K., & Harun, S. W. (2013). Highly stable graphene-assisted tunable dual-wavelength erbium-doped fiber laser. *Applied Optics, 52*(4), 818-823.

Ahmad, H., Semangun, J. M., Azzuhri, S. R., Zulkifli, M., Awang, N., & Harun, S. W., (2015). Passively mode-locked laser using an entirely centred erbium-doped fiber. *Laser Physics, 25*(4), 045105.

Ahmad, H., Soltanian, M., Alimadad, M., & Harun, S. W., (2014). Stable narrow spacing dual-wavelength Q-switched graphene oxide embedded in a photonic crystal fiber. *Laser Physics, 24*(10), 105101.

Ahmad, H., Soltanian, M., Narimani, L., Amiri, I., Khodaei, A., & Harun, S. W., (2015). Tunable S-Band Q-Switched Fiber Laser Using Bi 2 Se 3 as the Saturable Absorber. *IEEE Photonics Journal, 7*(3), 1-8.

Ahmad, H., Soltanian, M., Pua, C., Zulkifli, M., & Harun, S. W. (2013a). Narrow Spacing Dual-Wavelength Fiber Laser Based on Polarization Dependent Loss Control. *Photonics Journal, IEEE, 5*(6), 1502706-1502706.

Ahmad, H., Soltanian, M. R. K., Pua, C. H., Alimadad, M., & Harun, S. W. (2014). Photonic crystal fiber based dual-wavelength Q-switched fiber laser using graphene oxide as a saturable absorber. *Applied Optics, 53*(16), 3581-3586. doi:10.1364/AO.53.003581

Ahmad, H., Soltanian, M. R. K., Pua, C. H., Zulkifli, M. Z., & Harun, S. W. (2013). Narrow spacing dual-wavelength fiber laser based on polarization dependent loss control. *Photonics Journal, IEEE, 5*(6), 1502706-1502706. doi:10.1109/JPHOT.2013.2293613

Ahmad, H., Zulkifli, A. Z., Kiat, Y. Y., & Harun, S. W. (2014). Q-switched fibre laser using 21cm Bismuth-erbium doped fibre and graphene oxide as saturable absorber. *Optics communications, 310*, 53-57.

Ali, N., Anyi, C., Arof, H., & Harun, S. W. (2014). Q-switched multi-wavelength Brillouin erbium fiber laser. *Journal of Nonlinear Optical Physics & Materials, 23*(01), 1450010.

Alouini, M., Brunel, M., Bretenaker, F., Vallet, M., & Le Floch, A. (1998). Dual tunable wavelength Er, Yb: glass laser for terahertz beat frequency generation. *Photonics Technology Letters, IEEE, 10*(11), 1554-1556.

Alvarez-Chavez, J., Martinez-Rios, A., Torres-Gomez, I., & Offerhaus, H. (2007). Wide wavelength-tuning of a double-clad Yb^{3+}-doped fiber laser based on a fiber Bragg grating array. *Laser Physics Letters, 4*(12), 880.

Amiri, IS, Alavi, ES, Soltanian, MRK, Fisal, N, Supa'at, ASM, & Ahmad, H. (2015). Increment of Access Points in Integrated System of Wavelength Division Multiplexed Passive Optical Network Radio over Fiber. *Scientific Reports, 5*. doi:10.1038/srep11897

Ancona, A., Döring, S., Jauregui, C., Röser, F., Limpert, J., Nolte, S., & Tünnermann, A. (2009). Femtosecond and picosecond laser drilling of metals at high repetition rates and average powers. *Optics Letters, 34*(21), 3304-3306.

Andrews, J. G., Buzzi, S., Choi, W., Hanly, S. V., Lozano, A., Soong, A. C., & Zhang, J. C. (2014). What will 5G be? *Selected Areas in Communications, IEEE Journal on, 32*(6), 1065-1082.

Bao, Q., Zhang, H., Wang, Y., Ni, Z., Yan, Y., Shen, Z. X., Tang, D. Y. (2009). Atomic-layer graphene as a saturable absorber for ultrafast pulsed lasers. *Advanced Functional Materials, 19*(19), 3077-3083.

Barnard, C., Myslinski, P., Chrostowski, J., & Kavehrad, M. (1994). Analytical model for rare-earth-doped fiber amplifiers and lasers. *Quantum Electronics, IEEE Journal of, 30*(8), 1817-1830.

Becker, P. M., Olsson, A. A., & Simpson, J. R. (1999). *Erbium-doped fiber amplifiers: fundamentals and technology*: Academic press.

Bellemare, A. (2003). Continuous-wave silica-based erbium-doped fibre lasers. *Progress in Quantum Electronics, 27*(4), 211-266.

Bellemare, A., Rochette, M., & LaRochelle, S. (2000). Room temperature multifrequency erbium-doped fiber lasers anchored on the ITU frequency grid. *Journal of lightwave technology, 18*(6), 825.

Bernard, F., Zhang, H., Gorza, S.-P., & Emplit, P. (2012). *Towards mode-locked fiber laser using topological insulators.* Paper presented at the Nonlinear Photonics.

Bhadra, S., & Ghatak, A. (2013). *Guided Wave Optics and Photonic Devices*: CRC Press.

Boccardi, F., Heath, R. W., Lozano, A., Marzetta, T. L., & Popovski, P. (2014). Five disruptive technology directions for 5G. *Communications Magazine, IEEE, 52*(2), 74-80.

Bolognini, G., Soto, M. A., & Pasquale, F. D. (2009). Fiber-optic distributed sensor based on hybrid Raman and Brillouin scattering employing multiwavelength Fabry–Pérot lasers. *Photonics Technology Letters, IEEE, 21*(20), 1523-1525.

Brendel, F., Poëtte, J., Cabon, B., Zwick, T., Van Dijk, F., Lelarge, F., & Accard, A. (2011). Chromatic dispersion in 60 GHz radio-over-fiber networks based on mode-locked lasers. *Journal of Lightwave Technology , 29*(24), 3810-3816.

Broberg, B., & Lindgren, S. (1984). Refractive index of $In_{1-x}Ga_xAs_yP_{1-y}$ layers and InP in the transparent wavelength region. *Journal of Applied Physics, 55*(9), 3376-3381.

Brunel, M., Lai, N. D., Vallet, M., Le Floch, A., Bretenaker, F., Morvan, L., Merlet, T. (2004). *Generation of tunable high-purity microwave and terahertz signals by two-frequency solid state lasers.* Paper presented at the Photonics Europe.

Burns, J. (1994). *The application of millimetre wave technology for personal communication networks in the United Kingdom and Europe: A technical and regulatory overview.* Paper presented at the Microwave Symposium Digest, 1994., IEEE MTT-S International.

Cao, W., Wang, H., Luo, A., Luo, Z., & Xu, W. (2012). Graphene-based, 50 nm wide-band tunable passively Q-switched fiber laser. *Laser Physics Letters, 9*(1), 54.

Capmany, J., Ortega, B., Martinez, A., Pastor, D., Popov, M., & Fonjallaz, P.-Y. (2005). Multiwavelength single sideband modulation for WDM radio-over-fiber systems using a fiber grating array tandem device. *Photonics Technology Letters, IEEE, 17*(2), 471-473.

Casiraghi, C., Hartschuh, A., Qian, H., Piscanec, S., Georgi, C., Fasoli, A., Ferrari, A. (2009). Raman spectroscopy of graphene edges. *Nano Letters, 9*(4), 1433-1441.

Chang, G.-k., & Liu, C. (2013). *1–100GHz microwave photonics link technologies for next-generation WiFi and 5G wireless communications.* Paper presented at the Microwave Photonics (MWP), 2013 International Topical Meeting on.

Chang, L., Wu, S., Chen, S., & Li, X. (2011). Preparation of graphene oxide–molecularly imprinted polymer composites via atom transfer radical polymerization. *Journal of materials science, 46*(7), 2024-2029.

Chen, D., Fu, H., Liu, W., Wei, Y., & He, S. (2008). Dual-wavelength single-longitudinal-mode erbium-doped fibre laser based on fibre Bragg grating pair and its application in microwave signal generation. *Electronics Letters, 44*(7), 459-461.

Chen, D., Qin, S., & He, S. (2007). Channel-spacing-tunable multi-wavelength fiber ring laser with hybrid Raman and Erbium-doped fiber gains. *Optics Express, 15*(3), 930-935.

Chen, W. G., Lou, S., Feng, S., Wang, L., Li, H., Guo, T., & Jian, S. (2009). *Switchable dual-wavelength fiber laser based on PCF Sagnac loop and broadband FBG.* Paper presented at the Asia Communications and Photonics.

Chen, W. G., Lou, S. Q., Feng, S. C., Wang, L. W., Li, H. L., Guo, T. Y., & Jian, S. S. (2009). Switchable multi-wavelength fiber ring laser based on a compact in-fiber Mach-Zehnder interferometer with photonic crystal fiber. *Laser Physics, 19*(11), 2115-2119. doi:10.1134/S1054660X09210026

Chen, X., Deng, Z., & Yao, J. (2006). Photonic generation of microwave signal using a dual-wavelength single-longitudinal-mode fiber ring laser. *Microwave Theory and Techniques, IEEE Transactions on, 54*(2), 804-809.

Chen, Y., Wen, A., & Shang, L. (2010). Analysis of an optical mm-wave generation scheme with frequency octupling using two cascaded Mach–Zehnder modulators. *Optics communications, 283*(24), 4933-4941.

Cheng, L., Zhu, M., Gul, M. M. U., Ma, X., & Chang, G.-K. (2014). Adaptive Photonics-Aided Coordinated Multipoint Transmissions for Next-Generation Mobile Fronthaul. *Journal of Lightwave Technology , 32*(10), 1907-1914.

Choi, H. Y., Kim, M. J., & Lee, B. H. (2007). All-fiber Mach-Zehnder type interferometers formed in photonic crystal fiber. *Optics Express, 15*(9), 5711-5720.

Chow, K., Shu, C., Mak, M., & Tsang, H. (2001). *Widely tunable wavelength converter using a double-ring fiber laser incorporating a semiconductor optical amplifier.* Paper presented at the Lasers and Electro-Optics Society, 2001. LEOS 2001. The 14th Annual Meeting of the IEEE.

Connelly, M. J. (2007). *Semiconductor optical amplifiers*: Springer Science & Business Media.

Cregan, R., Mangan, B., Knight, J., Birks, T., Russell, P. S. J., Roberts, P., & Allan, D. (1999). Single-mode photonic band gap guidance of light in air. *science, 285*(5433), 1537-1539.

Cunningham, P. D., & Hayden, L. M. (2010). Optical properties of DAST in the THz range. *Optics Express, 18*(23), 23620-23625.

Das, G., & Lit, J. (2002). L-band multiwavelength fiber laser using an elliptical fiber. *Photonics Technology Letters, IEEE, 14*(5), 606-608.

Dawson, J. W., Park, N., & Vahala, K. J. (1992). An improved delayed self-heterodyne interferometer for linewidth measurements. *Photonics Technology Letters, IEEE, 4*(9), 1063-1066.

De Young, R. J., & Barnes, N. P. (2010). Profiling atmospheric water vapor using a fiber laser lidar system. *Applied Optics, 49*(4), 562-567. doi:Doi 10.1364/Ao.49.000562

Desurvire, E., Giles, C. R., Simpson, J. R., & Zyskind, J. L. (1991). Erbium-doped fiber amplifier: Google Patents.

Dikin, D. A., Stankovich, S., Zimney, E. J., Piner, R. D., Dommett, G. H., Evmenenko, G., Ruoff, R. S. (2007). Preparation and characterization of graphene oxide paper. *Nature, 448*(7152), 457-460.

Du, J., Dai, Y., Lei, G. K., Tong, W., & Shu, C. (2010). Photonic crystal fiber based Mach-Zehnder interferometer for DPSK signal demodulation. *Optics Express, 18*(8), 7917-7922.

Du, J., Wang, Q., Jiang, G., Xu, C., Zhao, C., Xiang, Y., Zhang, H. (2014). Ytterbium-doped fiber laser passively mode locked by few-layer Molybdenum Disulfide (MoS2) saturable absorber functioned with evanescent field interaction. *Scientific Reports, 4*.

Dudley, J. M., & Taylor, J. R. (2010). *Supercontinuum generation in optical fibers*: Cambridge University Press.

Dupriez, P., Finot, C., Malinowski, A., Sahu, J. K., Nilsson, J., Richardson, D. J., Tropper, A. C. (2006). High-power, high repetition rate picosecond and femtosecond sources based on Yb-doped fiber amplification of VECSELs. *Optics Express, 14*(21), 9611-9616.

Dutta, A. K., Dutta, N. K., & Fujiwara, M. (2003). *WDM Technologies: Passive Optical Components: Passive Optical Components* (Vol. 2): Academic press.

Ebendorff-Heidepriem, H., Warren-Smith, S. C., & Monro, T. M. (2009). Suspended nanowires: fabrication, design and characterization of fibers with nanoscale cores. *Optics Express, 17*(4), 2646-2657.

Ehret, G., Kiemle, C., Wirth, M., Amediek, A., Fix, A., & Houweling, S. (2008). Space-borne remote sensing of CO_2, CH_4, and N_2O by integrated path differential absorption lidar: a sensitivity analysis. *Applied Physics B, 90*(3-4), 593-608.

Emsley, J. (2011). *Nature's building blocks: an AZ guide to the elements*: Oxford University Press.

Enming, X., Xinliang, Z., Lina, Z., Yu, Z., & Dexiu, H. (2009). A simple microwave photonic notch filter based on a semiconductor optical amplifier. *Journal of Optics A: Pure and Applied Optics, 11*(8), 085405.

Esterowitz, L. (1990). Diode-pumped holmium, thulium, and erbium lasers between 2 and 3 m operating cw at room temperature. *Opt. Eng, 29*(6), 676-680.

Fan, F., & Dagenais, M. (1997). Optical generation of a megahertz-linewidth microwave signal using semiconductor lasers and a discriminator-aided phase-locked loop. *Microwave Theory and Techniques, IEEE Transactions on, 45*(8), 1296-1300.

Feng, S., Li, H., Xu, O., Lu, S., Mao, X., Ning, T., & Jian, S. (2008). *Dual-wavelength erbium-doped fiber ring laser based on one polarization maintaining fiber Bragg grating in a Sagnac loop interferometer.* Paper presented at the Asia Pacific Optical Communications.

Feng, S., Xu, O., Lu, S., Mao, X., Ning, T., & Jian, S. (2008). Single-polarization, switchable dual-wavelength erbium-doped fiber laser with two polarization-maintaining fiber Bragg gratings. *Optics Express, 16*(16), 11830-11835.

Feng, S., Xu, O., Lu, S., Mao, X., Ning, T., & Jian, S. (2009). Switchable dual-wavelength erbium-doped fiber-ring laser based on one polarization maintaining fiber Bragg grating in a Sagnac loop interferometer. *Optics & Laser Technology, 41*(3), 264-267.

Feng, S., Xu, O., Lu, S., Ning, T., & Jian, S. (2009). Switchable single-longitudinal-mode dual-wavelength erbium-doped fiber ring laser based on one polarization-maintaining fiber Bragg grating incorporating saturable absorber and feedback fiber loop. *Optics communications, 282*(11), 2165-2168.

Feng, X., Li, J., Dong, Y., Li, Z., Cheng, L., & Guan, B.-o. (2011). *WDM-PON using Fabry-Pérot laser diodes injection locked by multiwavelength erbium-doped fiber laser.* Paper presented at the 16th Opto-Electronics and Communications Conference.

Feng, X., Tam, H., Lu, C., Wai, P., & Tang, D. (2007). Multiwavelength Erbium-Doped Fiber Laser Based on a Nonlinear Hi-Bi Fiber Loop Mirror. *ECOC 2007*.

Feng, X., Wai, P., Tam, H., Lu, C., & Guan, B.-o. (2011). Switchable multiwavelength erbium-doped fiber laser employing wavelength-dependent loss. *Optical Fiber Technology, 17*(2), 138-140.

Ferguson, B., & Zhang, X.-C. (2002). Materials for terahertz science and technology. *Nature materials, 1*(1), 26-33.

Fiedler, F., & Schlachetzki, A. (1987). Optical parameters of InP-based waveguides. *Solid-state electronics, 30*(1), 73-83.

Fischer, G. L. (1998). Fiber optic test and measurement, by Dennis Derickson. *Optics & Photonics News, 9*, 67.

Fok, M. P., & Shu, C. (2007). Tunable dual-wavelength erbium-doped fiber laser stabilized by four-wave mixing in a 35-cm highly nonlinear bismuth-oxide fiber. *Optics Express, 15*(10), 5925-5930.

Fok, M. P., & Shu, C. (2007). Tunable dual-wavelength erbium-doped fiber laser stabilized by four-wave mixing in a 35-cm highly nonlinear bismuth-oxide fiber. *Optics Express, 15*(10), 5925-5930.

Frenkel, A., & Lin, C. (1989). Angle-tuned etalon filters for optical channel selection in high density wavelength division multiplexed systems. *Journal of Lightwave Technology , 7*(4), 615-624.

Fukushima, S., Ohno, T., & Yoshino, K. (2001). Frequency stabilization of millimeter-wave subcarrier using laser heterodyne source and optical delay line. *Photonics Technology Letters, IEEE, 13*(9), 1002-1004.

Gandy, H., Ginther, R., & Weller, J. (1967). Stimulated emission of Tm^{3+} radiation in silicate glass. *Journal of Applied Physics, 38*(7), 3030-3031.

Genest, J., Chamberland, M., Tremblay, P., & Têtu, M. (1997). Microwave signals generated by optical heterodyne between injection-locked semiconductor lasers. *Quantum Electronics, IEEE Journal of, 33*(6), 989-998.

Geng, J., Spiegelberg, C., & Jiang, S. (2005). Narrow linewidth fiber laser for 100-km optical frequency domain reflectometry. *Photonics Technology Letters, IEEE, 17*(9), 1827-1829.

Georges, J. B., Cutrer, D. M., Solgaard, O., & Lau, K. Y. (1995). Optical transmission of narrowband millimeter-wave signals. *Microwave Theory and Techniques, IEEE Transactions on, 43*(9), 2229-2240.

Ghatak, A., & Thyagarajan, K. (1998). *An introduction to fiber optics*: Cambridge university press.

Gong, Y., Luo, B., Hao, J., Ng, J., Paulose, V., & Xia, L. (2007). *Tunable Terahertz Difference Frequency generation with 1550nm fiber laser.* Paper presented at the 2007 Joint 32nd International Conference on Infrared and Millimeter Waves and the 15th International Conference on Terahertz Electronics.

Gong, Y., Tang, M., Shum, P., Lu, C., Wu, J., & Xu, K. (2005). Dual-wavelength 10-GHz actively mode-locked erbium fiber laser incorporating highly nonlinear fibers. *Photonics Technology Letters, IEEE, 17*(12), 2547-2549.

Guan, W., & Marciante, J. (2007). Dual-frequency operation in a short-cavity ytterbium-doped fiber laser. *Photonics Technology Letters, IEEE, 19*(5), 261-263.

Han, H., Park, H., Cho, M., & Kim, J. (2002). Terahertz pulse propagation in a plastic photonic crystal fiber. *Applied Physics Letters, 80*(15), 2634-2636.

Han, P., Tani, M., Pan, F., & Zhang, X.-C. (2000). Use of the organic crystal DAST for terahertz beam applications. *Optics Letters, 25*(9), 675-677.

Han, Y.-G. (2010). Triple-wavelength Switchable Multiwavelength Erbium-doped Fiber Laser Based on a Highly Nonlinear Photonic Crystal Fiber. *Journal of the Korean Physical Society, 56*, 1251-1255.

Han, Y.-G., Tran, T., Kim, S.-H., & Lee, S. B. (2005). Multiwavelength Raman-fiber-laser-based long-distance remote sensor for simultaneous measurement of strain and temperature. *Optics Letters, 30*(11), 1282-1284.

Han, Y.-G., Van Anh Tran, T., & Lee, S. B. (2006). Wavelength-spacing tunable multiwavelength erbium-doped fiber laser based on four-wave mixing of dispersion-shifted fiber. *Optics Letters, 31*(6), 697-699.

Hanna, D., Percival, R., Perry, I., Smart, R., Suni, P., Townsend, J., & Tropper, A. (1988). Continuous-wave oscillation of a monomode ytterbium-doped fibre laser. *Electronics Letters, 24*(17), 1111-1113.

Hanna, D., Percival, R., Smart, R., & Tropper, A. (1990). Efficient and tunable operation of a Tm-doped fibre laser. *Optics communications, 75*(3), 283-286.

Haraz, O. M., Elboushi, A., Alshebeili, S. A., & Sebak, A.-R. (2014). Dense Dielectric Patch Array Antenna with Improved Radiation Characteristics Using EBG Ground Structure and Dielectric Superstrate for Future 5G Cellular Networks. *Access, IEEE, 2*, 909-913.

Hasan, T., Sun, Z., Wang, F., Bonaccorso, F., Tan, P. H., Rozhin, A. G., & Ferrari, A. C. (2009). Nanotube-polymer composites for ultrafast photonics. *Adv. Mater, 21*(38-39), 3874-3899.

Haubner, K., Murawski, J., Olk, P., Eng, L. M., Ziegler, C., Adolphi, B., & Jaehne, E. (2010). The route to functional graphene oxide. *ChemPhysChem, 11*(10), 2131-2139.

Haus, H. A. (2000). Mode-locking of lasers. *IEEE Journal of Selected Topics in Quantum Electronics, 6*(6), 1173-1185.

Hecht, J. (2015). *Understanding fiber optics*: Jeff Hecht.

Henderson, S. W., Suni, P. J., Hale, C. P., Hannon, S., Magee, J. R., Bruns, D. L., & Yuen, E. H. (1993). Coherent laser radar at 2 μm using solid-state lasers. *Geoscience and Remote Sensing, IEEE Transactions on, 31*(1), 4-15.

Henry, C. H., Johnson, L. F., Logan, R. A., & Clarke, D. (1985). Determination of the refractive index of InGaAsP epitaxial layers by mode line luminescence spectroscopy. *Quantum Electronics, IEEE Journal of, 21*(12), 1887-1892.

Herda, R., Kivistö, S., & Okhotnikov, O. G. (2008). Dynamic gain induced pulse shortening in Q-switched lasers. *Optics Letters, 33*(9), 1011-1013.

Horak, P., & Loh, W. H. (2006). On the delayed self-heterodyne interferometric technique for determining the linewidth of fiber lasers. *Optics Express, 14*(9), 3923-3928.

Hosako, I., Sekine, N., Patrashin, M., Saito, S., Fukunaga, K., Kasai, Y., Ochiai, S. (2007). At the dawn of a new era in terahertz technology. *Proceedings of the IEEE, 95*(8), 1611-1623.

Hsu, D.-Z., Gong, P.-M., Lin, Y.-M., Lee, S.-L., Lee, S.-L., & Yuang, M. C. (2003). *High-efficiency and wideband SOA-based wavelength converters by using four-wave-mixing with orthogonal pumps and an assisted beam.* Paper presented at the Lasers and Electro-Optics, 2003. CLEO/Pacific Rim 2003. The 5th Pacific Rim Conference on.

Hu, B., Zhang, X. C., Auston, D., & Smith, P. (1990). Free-space radiation from electro-optic crystals. *Applied Physics Letters, 56*(6), 506-508.

Hui, S. Y., & Yeung, K. H. (2003). Challenges in the migration to 4G mobile systems. *Communications Magazine, IEEE, 41*(12), 54-59.

Hyodo, M., Tani, M., Matsuura, S., Onodera, N., & Sakai, K. (1996). Generation of millimetre-wave radiation using a dual-longitudinal-mode microchip laser. *Electronics Letters, 32*(17), 1589-1591.

Inoue, K., Nakanishi, K., Oda, K., & Toba, H. (1994). Crosstalk and power penalty due to fiber four-wave mixing in multichannel transmissions. *Journal of Lightwave Technology , 12*(8), 1423-1439.

Ironside, C., Haji, M., Hou, L., Akbar, J., Kelly, A. E., Seunarine, K., Figueiredo, J. M. (2011). *Review of optoelectronic oscillators based on modelocked lasers and* *resonant tunneling diode optoelectronics.* Paper presented at the International Conference on Applications of Optics and Photonics.

Ito, H., Nakata, T., Sakaki, K., Ohtsu, M., Lee, K., & Jhe, W. (1996). Laser spectroscopy of atoms guided by evanescent waves in micron-sized hollow optical fibers. *Physical Review Letters, 76*(24), 4500.

Jeon, M. Y., Kim, N., Shin, J., Jeong, J. S., Han, S.-P., Lee, C. W., Park, K. H. (2010b). Widely tunable dual-wavelength Er $^{3+}$-doped fiber laser for tunable continuous-wave terahertz radiation. *Optics Express, 18*(12), 12291-12297.

Jeon, M. Y., Kim, N., Shin, J., Lee, C. W., Han, S.-P., Leem, Y. A., Park, K. H. (2010). *Continuous terahertz wave emission using tunable dual-wavelength erbium-doped fiber laser.* Paper presented at the 35th International Conference on Infrared, Millimeter, and Terahertz Waves.

Jia-Ming, L. (2005). Photonic devices. *Cambridge university text*.

Jia, Z., Yu, J., Ellinas, G., & Chang, G.-K. (2007). Key enabling technologies for optical–wireless networks: optical millimeter-wave generation, wavelength reuse, and architecture. *Journal of Lightwave Technology, 25*(11), 3452-3471.

Jia, Z., Yu, J., Hsueh, Y.-T., Chowdhury, A., Chien, H.-C., Buck, J., & Chang, G.-K. (2008). Multiband signal generation and dispersion-tolerant transmission based on photonic frequency tripling technology for 60-GHz radio-over-fiber systems. *Photonics Technology Letters, IEEE, 20*(17), 1470-1472.

Jiang, M., Shum, P. P., Lin, B., Tjin, S. C., & Jiang, Y. (2011). *A stable dual-wavelength single-longitudinal-mode fiber laser with a tunable wavelength spacing based on a chirped phase-shifted grating filter.* Paper presented at the Asia Communications and Photonics Conference and Exhibition.

Jianjun, Y., Zhensheng, J., Lilin, Y., Yikai, S., Gee-Kung, C., & Ting, W. (2006). Optical millimeter-wave generation or up-conversion using external modulators. *Photonics Technology Letters, IEEE, 18*(1), 265-267. doi:10.1109/LPT.2005.862006

Johansson, L., & Seeds, A. (2000). Millimeter-wave radio-over-fiber transmission using an optical injection phase-lock loop source. *PSC 802 BOX 14 FPO 09499-0200*, 129.

Kadlec, F., Kužel, P., & Coutaz, J.-L. (2004). Optical rectification at metal surfaces. *Optics Letters, 29*(22), 2674-2676.

Kaman, V., & Bowers, J. (2000). 120 Gbit/s OTDM system using electroabsorption transmitter and demultiplexer operating at 30 GHz. *Electronics Letters, 36*(17), 1477-1479.

Kaminow, I., Li, T., & Willner, A. E. (2010). *Optical fiber telecommunications VB: systems and networks*: Academic press.

Kao, K., & Hockham, G. A. (1966). *Dielectric-fibre surface waveguides for optical frequencies.* Paper presented at the Proceedings of the Institution of Electrical Engineers. 113.7 (1966): 1151-1158.

Kashyap, R. (1999). *Fiber Bragg gratings*: Academic press.

Kato, T., Hirano, M., Onishi, M., & Nishimura, M. (1999). Ultra-low nonlinearity low-loss pure silica core fibre for long-haul WDM transmission. *Electronics Letters, 35*(19), 1615-1617.

Kawanishi, S., Takara, H., Morioka, T., Kamatani, O., Takiguchi, K., Kitoh, T., & Saruwatari, M. (1996). *400 Gbit/s TDM transmission of 0.98 ps pulses over 40 km employing dispersion slope compensation.* Paper presented at the Conf. Optic. Fiber Commun.(OFC'96).

Keiser, G. (2003). *Optical fiber communications*: Wiley Online Library.

Keller, U., Weingarten, K. J., Kärtner, F. X., Kopf, D., Braun, B., Jung, I. D., Au, J. A. d. (1996). Semiconductor saturable absorber mirrors (SESAM's) for femtosecond to nanosecond pulse generation in solid-state lasers. *Selected Topics in Quantum Electronics, IEEE Journal of, 2*(3), 435-453.

Kim, C., Kim, I., GUIFANG, L., Lange, M. R., Dimmick, T. E., Langlois, P., & Reid, B. (2005). Optical microwave/millimeter-wave links using direct modulation of two-section gain-coupled DFB lasers. *IEEE Photonics Technology Letters, 17*(8), 1734-1736.

Kim, S. K., Chu, M. J., & Lee, J. H. (2001). Wideband multiwavelength erbium-doped fiber ring laser with frequency shifted feedback. *Optics communications, 190*(1), 291-302.

Klehr, A., Fricke, J., Knauer, A., Erbert, G., Walther, M., Wilk, R., Koch, M. (2008). High-power monolithic two-mode DFB laser diodes for the generation of THz radiation. *Selected Topics in Quantum Electronics, IEEE Journal of, 14*(2), 289-294.

Kleine-Ostmann, T., Knobloch, P., Caspary, R., Hofmann, M., & Koch, M. (2002). Dual-wavelength fibre laser. *Electronics Letters, 38*(7), 309-310. doi:10.1049/el:20020211

Knight, J., Birks, T., Russell, P. S. J., & Atkin, D. (1996). All-silica single-mode optical fiber with photonic crystal cladding. *Optics Letters, 21*(19), 1547-1549.

Koroshetz, J. E. (2005). *Fiber lasers for lidar.* Paper presented at the Optical Fiber Communication Conference.

Kosterev, A., Curl, R., Tittel, F., Gmachl, C., Capasso, F., Sivco, D., Cho, A. (1999). Methane concentration and isotopic composition measurements with a mid-infrared quantum-cascade laser. *Optics Letters, 24*(23), 1762-1764.

Kumar, V., George, A., Reeves, W., Knight, J., Russell, P., Omenetto, F., & Taylor, A. (2002). Extruded soft glass photonic crystal fiber for ultrabroad supercontinuum generation. *Optics Express, 10*(25), 1520-1525.

Kuri, T., & Kitayama, K.-i. (1999). Long-term stabilized millimeter-wave generation using a high-power mode-locked laser diode module. *Microwave Theory and Techniques, IEEE Transactions on, 47*(5), 570-574.

Leigh, M., Shi, W., Zong, J., Wang, J., Jiang, S., & Peyghambarian, N. (2007). Compact, single-frequency all-fiber Q-switched laser at 1 μm. *Optics Letters, 32*(8), 897-899.

Li, E. H. (2000). Material parameters of InGaAsP and InAlGaAs systems for use in quantum well structures at low and room temperatures. *Physica E: Low-dimensional systems and Nanostructures, 5*(4), 215-273.

Li, J., Lee, H., & Vahala, K. J. (2013). Microwave synthesizer using an on-chip Brillouin oscillator. *Nature communications, 4*.

Li, J., Ning, T., Pei, L., Qi, C., Zhou, Q., Hu, X., & Gao, S. (2010). 60 GHz millimeter-wave generator based on a frequency-quadrupling feed-forward modulation technique. *Optics Letters, 35*(21), 3619-3621.

Li, M., Chen, H., Yin, F., Chen, M., & Xie, S. (2009). Full-duplex 60-GHz RoF system with optical local oscillating carrier distribution scheme based on FWM effect in SOA. *Photonics Technology Letters, IEEE, 21*(22), 1716-1718.

Li, Y., Bystrom, M., Yoo, D., Goldwasser, S. M., & Herczfeld, P. R. (2005). Coherent optical vector modulation for fiber radio using electrooptic microchip lasers. *Microwave Theory and Techniques, IEEE Transactions on, 53*(10), 3121-3129.

Li, Z., Heidt, A. M., Daniel, J. M. O., Jung, Y., Alam, S. U., & Richardson, D. J. (2013). Thulium-doped fiber amplifier for optical communications at 2 μm. *Optics Express, 21*(8), 9289-9297. doi:Doi 10.1364/Oe.21.009289

Liang, Y., Jin, L., Cheng, L., & Guan, B.-O. (2014). Stabilization of microwave signal generated by a dual-polarization DBR fiber laser via optical feedback. *Optics Express, 22*(24), 29356-29362.

Lierstuen, L. O., & Sudbø, A. S. (1995). Coupling losses between standard single-mode fibers and rectangular waveguides for integrated optics. *Applied Optics, 34*(6), 1024-1028.

Lin, B., Tjin, S. C., Zhang, H., Tang, D., Hao, J., Dong, B., & Liang, S. (2010). Switchable dual-wavelength single-longitudinal-mode erbium-doped fiber laser using an inverse-Gaussian apodized fiber Bragg grating filter and a low-gain semiconductor optical amplifier. *Applied Optics, 49*(36), 6855-6860.

Lin, C.-T., Shih, P.-T., Jiang Jr, W., Chen, J. J., Peng, P.-C., & Chi, S. (2009). A continuously tunable and filterless optical millimeter-wave generation via frequency octupling. *Optics Express, 17*(22), 19749-19756.

Lin, M., Zexin, K., Yanhui, Q., & Shuisheng, J. (2014). Tunable dual-wavelength fiber laser based on an MMI filter in a cascaded Sagnac loop interferometer. *Laser Physics, 24*(4), 045102.

Liu, D., Ngo, N. Q., Tjin, S. C., & Dong, X. (2007). A dual-wavelength fiber laser sensor system for measurement of temperature and strain. *Photonics Technology Letters, IEEE, 19*(15), 1148-1150.

Liu, G., & Jacquier, B. (2006). *Spectroscopic properties of rare earths in optical materials* (Vol. 83): Springer Science & Business Media.

Liu, K., Kang, H.-S., Kim, T.-K., & Zhang, X.-C. (2002). Study of ZnCdTe crystals as terahertz wave emitters and detectors. *Applied Physics Letters, 81*(22), 4115-4117.

Liu, L., Zhao, X., Wang, Q., Gong, Z., Liu, J. S., & Zheng, Z. (2013). Fast, Asynchronous Sampling Distance Ranging Using an SOA Gate and a Dual-Wavelength Mode-Locked Fiber Laser. *2013 Conference on Lasers and Electro-Optics Pacific Rim (Cleo-Pr)*.

Liu, S., Yan, F. P., Peng, W. J., Feng, T., Dong, Z., & Chang, G. K. (2014). Tunable Dual-Wavelength Thulium-Doped Fiber Laser by Employing a HB-FBG. *IEEE Photonics Technology Letters, 26*(18), 1809-1812. doi:Doi 10.1109/Lpt.2014.2336654

Liu, S., Yin, Z., Zhang, L., & Chen, X. (2009). *A dual-wavelength DBR fiber laser strain sensor.* Paper presented at the 2009 14th OptoElectronics and Communications Conference.

Liu, X., & Lu, C. (2005). Self-stabilizing effect of four-wave mixing and its applications on multiwavelength erbium-doped fiber lasers. *Photonics Technology Letters, IEEE, 17*(12), 2541-2543.

Lu, G. (1999). A dual-wavelength method using the BDJ detector and its application to iron concentration measurement. *Measurement Science and Technology, 10*(4), 312.

Lu, S., Miao, L., Guo, Z., Qi, X., Zhao, C., Zhang, H., Fan, D. (2015). Broadband nonlinear optical response in multi-layer black phosphorus: an emerging infrared and mid-infrared optical material. *Optics Express, 23*(9), 11183-11194.

Luo, Z., Huang, Y., Zhong, M., Li, Y., Wu, J., Xu, B., Weng, J. (2014). 1-, 1.5-, and 2-μm fiber lasers Q-switched by a broadband few-layer MoS 2 saturable absorber. *Journal of lightwave technology, 32*(24), 4077-4084.

Luo, Z., Zhou, M., Weng, J., Huang, G., Xu, H., Ye, C., & Cai, Z. (2010). Graphene-based passively Q-switched dual-wavelength erbium-doped fiber laser. *Optics Letters, 35*(21), 3709-3711.

Luo, Z., Zhou, M., Wu, D., Ye, C., Weng, J., Dong, J., Chen, L. (2011). Graphene-induced nonlinear four-wave-mixing and its application to multiwavelength Q-switched rare-earth-doped fiber lasers. *Journal of Lightwave Technology, 29*(18), 2732-2739.

Ma, J., Yu, J., Yu, C., Xin, X., Sang, X., & Zhang, Q. (2010). 64GHz optical millimeter-wave generation by octupling 8GHz local oscillator via a nested LiNbO 3 modulator. *Optics & Laser Technology, 42*(2), 264-268.

Ma, X. W., Luo, S. J., & Chen, D. R. (2014). Switchable and tunable thulium-doped fiber laser incorporating a Sagnac loop mirror. *Applied Optics, 53*(20), 4382-4385. doi:Doi 10.1364/Ao.53.004382

Mabrouki, A., Gadonna, M., & Le Naour, R. (1996). Polarization characterization of a Mach–Zehnder interferometer. *Applied Optics, 35*(19), 3591-3596.

Maddaloni, P., Bellini, M., & De Natale, P. (2013). *Laser-Based Measurements for Time and Frequency Domain Applications: A Handbook*: CRC Press.

Mahad, F. D., Supa'at, M., & Sahmah, A. (2009). EDFA gain optimization for WDM system. *Elektrika, 11*(1), 34-37.

Maran, J.-N., Slavík, R., LaRochelle, S., & Karásek, M. (2004). Chromatic dispersion measurement using a multiwavelength frequency-shifted feedback fiber laser. *Instrumentation and Measurement, IEEE Transactions on, 53*(1), 67-71.

Marcenac, D., Ellis, A., & Moodie, D. (1998). 80 Gbit/s OTDM using electroabsorption modulators. *Electronics Letters, 34*(1), 101-103.

Marshall, J., Stewart, G., & Whitenett, G. (2006). Design of a tunable L-band multi-wavelength laser system for application to gas spectroscopy. *Measurement Science and Technology, 17*(5), 1023.

Martin, E. P., Shao, T., Vujicic, V., Anandarajah, P. M., Browning, C., Llorente, R., & Barry, L. P. (2014). 25-Gb/s OFDM 60-GHz Radio Over Fiber System Based on a Gain Switched Laser. *Journal of lightwave technology, 33*(8), 1635-1643.

Mentzer, M. A. (2011). *Applied Optics Fundamentals and Device Applications: Nano, MOEMS, and Biotechnology*: CRC Press.

Mims III, F. M. (1980). Alexander Graham Bell and the Photophone: The Centennial of the Invention of Light-Wave Communications, 1880–1980. *Optics News, 6*(1), 8-16.

Mingareev, I., Weirauch, F., Olowinsky, A., Shah, L., Kadwani, P., & Richardson, M. (2012). Welding of polymers using a 2 mu m thulium fiber laser. *Optics and Laser Technology, 44*(7), 2095-2099. doi:Doi 10.1016/J.Optlastec.2012.03.020

Miya, T., Terunuma, Y., Hosaka, T., & Miyashita, T. (1979). Ultimate low-loss single-mode fibre at 1.55 µm. *Electronics Letters, 15*(4), 106-108.

Mohamed, M., Zhang, X., Hraimel, B., & Wu, K. (2008). Analysis of frequency quadrupling using a single Mach-Zehnder modulator for millimeter-wave generation and distribution over fiber systems. *Optics Express, 16*(14), 10786-10802.

Moodie, D., Ellis, A., Thurlow, A., Harlow, M., Lealman, I., Perrin, S., Robertson, M. (1995). Multiquantum well electroabsorption modulators for 80 Gbit/s OTDM systems. *Electronics Letters, 31*(16), 1370-1371.

Moon, D., Paek, U.-C., & Chung, Y. (2005). Polarization controlled multi-wavelength Er-doped fiber laser using fiber Bragg grating written in few-mode side-hole fiber with an elliptical core. *Optics Express, 13*(14), 5574-5579.

Mou, C., Saffari, P., Fu, H., Zhou, K., Zhang, L., & Bennion, I. (2009). Single- and dual-wavelength switchable erbium-doped fiber ring laser based on intracavity polarization selective tilted fiber gratings. *Appl Opt, 48*(18), 3455-3459.

Murata, H., & Inagaki, N. (1981). Low-loss single-mode fiber development and splicing research in Japan. *Quantum Electronics, IEEE Journal of, 17*(6), 835-849.

Mynbaev, D. K., & Scheiner, L. L. (2001). *Fiber-optic communications technology*: Prentice Hall.

Myslinski, P., Pan, X., Barnard, C. W., Chrostowski, J., Sullivan, B. T., & Bayon, J.-F. (1993). Q-switched thulium-doped fiber laser. *Optical engineering, 32*(9), 2025-2030.

Nagai, M., Tanaka, K., Ohtake, H., Bessho, T., Sugiura, T., Hirosumi, T., & Yoshida, M. (2004). Generation and detection of terahertz radiation by electro-optical process in GaAs using 1.56 mum fiber laser pulses. *Applied Physics Letters, 85*, 3974.

Nahata, A., Weling, A. S., & Heinz, T. F. (1996). A wideband coherent terahertz spectroscopy system using optical rectification and electro-optic sampling. *Applied Physics Letters, 69*(16), 2321-2323.

Nakazawa, M., Yoshida, E., Yamamoto, T., Yamada, E., & Sahara, A. (1998). TDM single channel 640 Gbit/s transmission experiment over 60 km using 400 fs pulse train and walk-off free, dispersion flattened nonlinear optical loop mirror. *Electronics Letters, 34*(9), 907-908.

O'reilly, J., Lane, P., Heidemann, R., & Hofstetter, R. (1992). Optical generation of very narrow linewidth millimetre wave signals. *Electronics Letters, 28*(25), 2309-2311.

Oh, K., Morse, T., Weber, P., Kilian, A., & Reinhart, L. (1994). Continuous-wave oscillation of thulium-sensitized holmium-doped silica fiber laser. *Optics Letters, 19*(4), 278-280.

Oraevsky, A. A., Jacques, S. L., & Esenaliev, R. O. (1998). Optoacoustic imaging for medical diagnosis: Google Patents.

Osseiran, A., Boccardi, F., Braun, V., Kusume, K., Marsch, P., Maternia, M., Taoka, H. (2014). Scenarios for 5G mobile and wireless communications: the vision of the METIS project. *Communications Magazine, IEEE, 52*(5), 26-35.

Pan, J. (1993). *Multiwavelength photonic communications.* Paper presented at the Telesystems Conference, 1993.'Commercial Applications and Dual-Use Technology', Conference Proceedings., National.

Pan, L., Utkin, I., & Fedosejevs, R. (2009). Two-wavelength ytterbium-doped fiber laser with sustained relaxation oscillation. *Applied Optics, 48*(29), 5484-5489.

Pan, S., & Yao, J. (2009). A wavelength-switchable single-longitudinal-mode dual-wavelength erbium-doped fiber laser for switchable microwave generation. *Optics Express, 17*(7), 5414-5419.

Pan, S., Zhao, X., & Lou, C. (2008a). Switchable single-longitudinal-mode dual-wavelength erbium-doped fiber ring laser incorporating a semiconductor optical amplifier. *Optics Letters, 33*(8), 764-766.

Pan, S., Zhao, X., & Lou, C. (2008b). *Switchable single-longitudinal-mode dual-wavelength fiber ring laser using hybrid gain medium.* Paper presented at the Conference on Lasers and Electro-Optics.

Park, N., & Wysocki, P. F. (1996). 24-line multiwavelength operation of erbium-doped fiber-ring laser. *Photonics Technology Letters, IEEE, 8*(11), 1459-1461.

Park, S., Lee, K.-S., Bozoklu, G., Cai, W., Nguyen, S. T., & Ruoff, R. S. (2008). Graphene oxide papers modified by divalent ions—enhancing mechanical properties via chemical cross-linking. *ACS nano, 2*(3), 572-578.

Parvizi, R., Ali, N. M., Harun, S. W., & Ahmad, H. (2011). Architecture of a Dual-Wavelength Brillouin Fibre Laser Based on a Photonic Crystal Fibre with Dual-Pass Amplification Configuration. *Lasers in Engineering, 21*(3-4), 209-216.

Paschotta, R., Häring, R., Gini, E., Melchior, H., Keller, U., Offerhaus, H., & Richardson, D. (1999). Passively Q-switched 0.1-mJ fiber laser system at 1.53 µm. *Optics Letters, 24*(6), 388-390.

Paschotta, R., Nilsson, J., Tropper, A. C., & Hanna, D. C. (1997). Ytterbium-doped fibre amplifiers. *IEEE Journal of quantum electronics, 33*(7), 1049-1056.

Peng, P.-C., Tseng, H.-Y., & Chi, S. (2004). Long-distance FBG sensor system using a linear-cavity fiber Raman laser scheme. *Photonics Technology Letters, IEEE, 16*(2), 575-577.

Peng, W., Yan, F., Li, Q., Liu, S., Feng, T., & Tan, S. (2013). A 1.97 µm multiwavelength thulium-doped silica fiber laser based on a nonlinear amplifier loop mirror. *Laser Physics Letters, 10*(11), 115102.

Perram, G. P., Marciniak, M. A., & Goda, M. (2004). *High-energy laser weapons: technology overview.* Paper presented at the Defense and Security.

Pinto, A., Frazão, O., Santos, J., Lopez-Amo, M., Kobelke, J., & Schuster, K. (2010). Interrogation of a suspended-core Fabry–Perot temperature sensor through a dual wavelength Raman fiber laser. *Journal of lightwave technology, 28*(21), 3149-3155.

Piprek, J., Hutchinson, J. M., Henness, J. A., Masanovic, M. L., & Coldren, L. A. (2004). *Saturation analysis of a monolithic wavelength converter.* Paper presented at the Optics East.

Popa, D., Sun, Z., Hasan, T., Torrisi, F., Wang, F., & Ferrari, A. (2010). Graphene Q-switched, tunable fiber laser. *Applied Physics Letters, 98, 073106 (2011), DOI:http://dx.doi.org/10.1063/1.3552684.*

Pradhan, S., Town, G. E., & Grant, K. J. (2006). Microwave frequency generation using a dual-wavelength DBR fiber laser. *Optical Fibre Technology/Australian Optical Society, 2006. ACOFT/AOS 2006. Australian Conference on*, Melbourne, VIC, 2006, pp. 104-105.

Preu, S. (2014). A Unified Derivation of the Terahertz Spectra Generated by Photoconductors and Diodes. *Journal of Infrared, Millimeter, and Terahertz Waves, 35*(12), 998-1010.

Pua, C. H., Ahmad, H., Harun, S. W., & De La Rue, R. M. (2012). Study of dual-wavelength mode competition in an erbium-doped fiber laser (EDFL) produced by acoustic waves. *Quantum Electronics, IEEE Journal of, 48*(12), 1499-1504.

Qian, J.-r., Su, J., & Hong, L. (2008). A widely tunable dual-wavelength erbium-doped fiber ring laser operating in single longitudinal mode. *Optics communications, 281*(17), 4432-4434. doi:http://dx.doi.org/10.1016/j.optcom.2008.05.017

Qureshi, K. K., Wang, S.-H., Wai, P., Tam, H. Y., Lu, C., & Sugimoto, N. (2007). Width-tunable pulse generation using four-wave mixing in bismuth based highly nonlinear fiber. *Optics communications, 275*(1), 223-229.

Rappaport, T. S., Sun, S., Mayzus, R., Zhao, H., Azar, Y., Wang, K., Gutierrez, F. (2013). Millimeter wave mobile communications for 5G cellular: It will work! *Access, IEEE, 1*, 335-349.

Ravaro, M., Barbieri, S., Santarelli, G., Jagtap, V., Manquest, C., Sirtori, C., Linfield, E. (2012). Measurement of the intrinsic linewidth of terahertz quantum cascade lasers using a near-infrared frequency comb. *Optics Express, 20*(23), 25654-25661.

Raybon, G., Mikkelsen, B., Essiambre, R.-J., Stentz, A., Nielsen, T., Peckham, D., Johnson, J. (2000). *320 Gbit/s single-channel pseudo-linear transmission over 200 km of nonzero-dispersion fiber.* Paper presented at the Optical Fiber Communication Conference.

Rice, A., Jin, Y., Ma, X., Zhang, X. C., Bliss, D., Larkin, J., & Alexander, M. (1994). Terahertz optical rectification from< 110> zinc-blende crystals. *Applied Physics Letters, 64*(11), 1324-1326.

Robertson, M., Ritchie, S., & Dayan, P. (1985). *Semiconductor waveguides: Analysis of coupling between rib waveguides and optical fibres.* Paper presented at the 1985 Cambridge Symposium.

Roeloffzen, C. G., Zhuang, L., Taddei, C., Leinse, A., Heideman, R. G., van Dijk, P. W., Boller, K.-J. (2013). Silicon nitride microwave photonic circuits. *Optics Express, 21*(19), 22937-22961.

Russell, P. S. J. (2006). Photonic-crystal fibers. *Journal of lightwave technology, 24*(12), 4729-4749.

Saleh, B. E., Teich, M. C., (1991). *Fundamentals of photonics* (Vol. 22): Wiley New York.

Sanders, S. (2002). Wavelength-agile fiber laser using group-velocity dispersion of pulsed super-continua and application to broadband absorption spectroscopy. *Applied Physics B, 75*(6-7), 799-802.

Scheller, M., Yarborough, J. M., Moloney, J. V., Fallahi, M., Koch, M., & Koch, S. W. (2010). Room temperature continuous wave milliwatt terahertz source. *Optics Express, 18*(26), 27112-27117.

Schmidt, A., Rivier, S., Steinmeyer, G., Yim, J. H., Cho, W. B., Lee, S., Aguiló, M. (2008). Passive mode locking of Yb: KLuW using a single-walled carbon nanotube saturable absorber. *Optics Letters, 33*(7), 729-731.

Schmogrow, R., Nebendahl, B., Winter, M., Josten, A., Hillerkuss, D., Koenig, S., Koos, C. (2012). Error vector magnitude as a performance measure for advanced modulation formats. *Photonics Technology Letters, IEEE, 24*(1), 61-63.

Schneider, A., & Guenter, P. (2005). Spectrum of terahertz pulses from organic DAST crystals. *Ferroelectrics, 318*(1), 83-88.

Schneider, T., Junker, M., & Lauterbach, K.-U. (2006). Theoretical and experimental investigation of Brillouin scattering for the generation of millimeter waves. *JOSA B, 23*(6), 1012-1019.

Shi, W., Ding, Y. J., Fernelius, N., & Vodopyanov, K. (2002). Efficient, tunable, and coherent 0.18–5.27-THz source based on GaSe crystal. *Optics Letters, 27*(16), 1454-1456.

Shih, P.-T., Chen, J. J., Lin, C.-T., Jiang Jr, W., Huang, H.-S., Peng, P.-C., & Chi, S. (2010). Optical millimeter-wave signal generation via frequency 12-tupling. *Journal of lightwave technology, 28*(1), 71-78.

Shimose, Y., Okamoto, T., Maruyama, A., Aizawa, M., & Nagai, H. (1991). Remote sensing of methane gas by differential absorption measurement using a wavelength tunable DFB LD. *Photonics Technology Letters, IEEE, 3*(1), 86-87.

Shupei, M., Zhouming, F., Shanhui, X., Weinan, Z., Dongdan, C., Tong, Y., Zhongmin, Y. (2013). Photonic generation of tunable microwave signals from a dual-wavelength distributed-Bragg-reflector highly Er 3+ /Yb 3+ co-doped phosphate fiber laser. *Laser Physics Letters, 10*(12), 125107.

Siegman, A. Lasers. 1986, Mill Valley. *University Science Books. Chapters, 10*, 26.

Sierra-Hernandez, J., Rojas-Laguna, R., Vargas-Rodriguez, E., Estudillo-Ayala, J., Mata-Chavez, R., Jauregui-Vazquez, D., Gutierrez-Gutierrez, J. (2013). A tunable multi-wavelength laser based on a Mach–Zehnder interferometer with photonic crystal fiber. *Laser Physics, 23*(5), 055105.

Siyu, T., Fengping, Y., Qi, L., Wanjing, P., Shuo, L., Ting, F., & Fei, C. (2013). A stable single-longitudinal-mode dual-wavelength erbium-doped fiber ring laser with superimposed FBG and an in-line two-taper MZI filter. *Laser Physics, 23*(7), 075112.

Smith, S., Zarinetchi, F., & Ezekiel, S. (1991). Narrow-linewidth stimulated Brillouin fiber laser and applications. *Optics Letters, 16*(6), 393-395.

Snitzer, E. (1961). Optical maser action of Nd+ 3 in a barium crown glass. *Physical Review Letters, 7*(12), 444.

Soltanian, M., Ahmad, H., Pua, C., & Harun, S. W. (2014). Tunable microwave output over a wide RF region generated by an optical dual-wavelength fiber laser. *Laser Physics, 24*(10), 105116.

Soltanian, M. R. K., Sadegh Amiri, I., Alavi, S. E., & Ahmad, H. (2015). Dual-Wavelength Erbium-Doped Fiber Laser to Generate Terahertz Radiation Using Photonic Crystal Fiber. *Journal of Lightwave Technology , 33*(24), 5038-5046. doi:10.1109/JLT.2015.2495255

Song, Q., Wang, G., Zhang, B., Zhang, Q., Wang, W., Wang, M., Peng, Q. (2015). Passively Q-switched mode-locked dual-wavelength Nd: GYSGG laser using graphene oxide saturable absorber. *Optics communications, 347*, 64-67.

Song, W., Zhao, Y., Bao, Y., Li, S., Zhang, Z., & Xu, T. (2007). Numerical simulation and analysis on mode property of photonic crystal fiber with high birefringence by fast multipole method. *PIERS online, 3*(6), 836-841.

Sorokina, I. T., & Vodopyanov, K. L. (2003). *Solid-state mid-infrared laser sources* (Vol. 89): Springer Science & Business Media.

Spühler, G., Paschotta, R., Fluck, R., Braun, B., Moser, M., Zhang, G., Keller, U. (1999). Experimentally confirmed design guidelines for passively Q-switched microchip lasers using semiconductor saturable absorbers. *JOSA B, 16*(3), 376-388.

Steen, W., Watkins, K. G., & Mazumder, J. (2010). *Laser material processing*: Springer Science & Business Media.

Stoneman, R., & Esterowitz, L. (1990). Efficient, broadly tunable, laser-pumped Tm: YAG and Tm: YSGG cw lasers. *Optics Letters, 15*(9), 486-488.

Suizu, K., & Kawase, K. (2007). Terahertz-wave generation in a conventional optical fiber. *Optics Letters, 32*(20), 2990-2992.

Sun, J., Dai, Y., Chen, X., Zhang, Y., & Xie, S. (2006). Stable dual-wavelength DFB fiber laser with separate resonant cavities and its application in tunable microwave generation. *Photonics Technology Letters, IEEE, 18*(24), 2587-2589.

Sun, J., Qiu, J., & Huang, D. (2000). Multiwavelength erbium-doped fiber lasers exploiting polarization hole burning. *Optics communications, 182*(1), 193-197.

Sun, J. Q., Huang, Y. X., Li, H., & Jiang, C. (2011). Photonic generation of microwave signals using dual-wavelength single-longitudinal-mode fiber lasers. *Optik, 122*(9), 764-768. doi:Doi 10.1016/J.Ijleo.2010.05.019

Sun, Q., Mao, Q., Chen, X., Feng, S., Liu, W., & Lit, J. (2010). Influences of ASE on the performances of Q-switched ytterbium-doped fiber lasers. *Laser Physics, 20*(6), 1438-1448.

Sun, Q., Wang, J., Tong, W., Luo, J., & Liu, D. (2012). Channel-switchable single-/dual-wavelength single-longitudinal-mode laser and THz beat frequency generation up to 3.6 THz. *Applied Physics B-Lasers and Optics, 106*(2), 373-377. doi:Doi 10.1007/S00340-011-4780-0

Svelto, O., & Hanna, D. C. (1976). *Principles of lasers*: Springer.

Talaverano, L., Abad, S., Jarabo, S., & Lopez-Amo, M. (2001). Multiwavelength fiber laser sources with Bragg-grating sensor multiplexing capability. *Journal of lightwave technology, 19*(4), 553.

Tan, P., Fu, Q., Li, Y., Xiong, Y., Qin, B., Fan, T. Y. M., & Li, D. (2012). Effects of Metal Mirrors Reflectivity and Aberrations on the THz FEL Radiation Performance. *Proceedings of IPAC*, 1729-1731.

Tanaka, S., Inamoto, K., Yokosuka, H., Somatomo, H., & Takahashi, N. (2007). *Multi-wavelength tunable fiber laser using SOA: application to fiber Bragg grating vibration sensor array.* Paper presented at the Sensors, 2007 IEEE.

Tang, M., Minamide, H., Wang, Y., Notake, T., Ohno, S., & Ito, H. (2011). Tunable terahertz-wave generation from DAST crystal pumped by a monolithic dual-wavelength fiber laser. *Optics Express, 19*(2), 779-786.

Tang, M., & Wang, Y. (2010). *Tunable narrow linewidth THz-wave generation using dual-wavelength fiber ring laser and organic DAST crystal.* Paper presented at the 35th International Conference on Infrared, Millimeter, and Terahertz Waves.

Tang, P., Zhang, X., Zhao, C., Wang, Y., Zhang, H., Shen, D., Fan, D. (2013). Topological insulator: saturable absorber for the passive Q-switching operation of an in-band pumped 1645-nm Er: YAG ceramic laser. *Photonics Journal, IEEE, 5*(2), 1500707-1500707.

Taniuchi, T., Shikata, J., & Ito, H. (2000). Tunable terahertz-wave generation in DAST crystal with dual-wavelength KTP optical parametric oscillator. *Electronics Letters, 36*(16), 1414-1416.

Tao, L., Dong, Z., Yu, J., Chi, N., Zhang, J., Li, X., Chang, G.-K. (2012). Experimental demonstration of 48-Gb/s PDM-QPSK radio-over-fiber system over 40-GHz mm-wave MIMO wireless transmission. *Photonics Technology Letters, IEEE, 24*(24), 2276-2279.

Tearney, G., Boppart, S. A., Bouma, B. E., Brezinski, M., Swanson, E. A., & Fujimoto, J. G. (2000). Method and apparatus for performing optical measurements using a fiber optic imaging guidewire, catheter or endoscope: Google Patents.

Toliver, P., Deng, K. L., Glesk, I., & Prucnal, P. R. (1999). Simultaneous optical compression and decompression of 100-Gb/s OTDM packets using a single bidirectional optical delay line lattice. *IEEE Photonics Technology Letters, 11*(9), 1183-1185.

Tomkos, I., Zacharopoulos, I., Roditi, E., Syvridis, D., Girardin, F., Occhi, L., & Uskov, A. (1998). *Highly performing wavelength converter based on dual pump wave mixing in semiconductor optical amplifier.* Paper presented at the Lasers and Electro-Optics Society Annual Meeting, 1998. LEOS'98. IEEE.

Tonouchi, M. (2007). Cutting-edge terahertz technology. *Nature photonics, 1*(2), 97-105.

Totschnig, G., Winter, F., Pustogov, V., Faist, J., & Müller, A. (2002). Mid-infrared external-cavity quantum-cascade laser. *Optics Letters, 27*(20), 1788-1790.

Tu, C., Guo, W., Li, Y., Zhang, S., Zhu, H., & Lu, F. (2008). Multiwavelength YB-doped fiber ring laser based on a Mach-Zehnder interferometer. *Microwave and Optical Technology Letters, 50*(3), 723-725.

Uchida, A., Takeoka, M., Nakata, T., & Kannari, F. (1998). Wide-range all-optical wavelength conversion using dual-wavelength-pumped fiber Raman converter. *Journal of Lightwave Technology , 16*(1), 92-99.

Vegas Olmos, J. J., Kuri, T., & Kitayama, K.-i. (2007). Dynamic reconfigurable WDM 60-GHz millimeter-waveband radio-over-fiber access network: architectural considerations and experiment. *Journal of lightwave technology, 25*(11), 3374-3380.

Villanueva, G. E., Pérez-Millán, P., Palací, J., Martí, J., Cruz, J. L., & Andrés, M. V. (2009). *Tunable microwave signal generation using dual-wavelength DFB erbium-doped fiber laser.* Paper presented at the Microwave Photonics, 2009. MWP'09. International Topical Meeting on.

Villegas, I., Cuadrado-Laborde, C., Díez, A., Cruz, J., Martínez-Gámez, M., & Andrés, M. (2011). Yb-doped strictly all-fiber laser actively Q-switched by intermodal acousto-optic modulation. *Laser Physics, 21*(9), 1650-1655.

Vlachos, K., Bintjas, C., Pleros, N., & Avramopoulos, H. (2004). Ultrafast semiconductor-based fiber laser sources. *Selected Topics in Quantum Electronics, IEEE Journal of, 10*(1), 147-154.

Wang, F., Zhang, X., Zhang, Y., & Xu, E. (2010). *A tunable and switchable single-longitudinal-mode dual-wavelength fiber laser for microwave generation.* Paper presented at the Asia Communications and Photonics Conference and Exhibition.

Wang, L., Yan, F., Mao, X., Jian, W., & Jian, S. (2009). *An orthogonal-polarization dual-wavelength fiber laser with stable output.* Paper presented at the Communications and Mobile Computing, 2009. CMC'09. WRI International Conference on.

Wang, P., Weng, D., Li, K., Liu, Y., Yu, X., & Zhou, X. (2013). Multi-wavelength Erbium-doped fiber laser based on four-wave-mixing effect in single mode fiber and high nonlinear fiber. *Optics Express, 21*(10), 12570-12578.

Wang, Q., Rideout, H., Zeng, F., & Yao, J. (2006). Millimeter-wave frequency tripling based on four-wave mixing in a semiconductor optical amplifier. *Photonics Technology Letters, IEEE, 18*(23), 2460-2462.

Wang, T., Sang, X. Z., Yan, B. B., Ai, Q., Li, Y., Chen, X., Alameh, K. (2014). Tunable microwave signal generation based on an Opto-DMD processor and a photonic crystal fiber. *Chinese Physics B, 23*(6). doi:Artn 064217

Doi 10.1088/1674-1056/23/6/064217

Wang, X., Zhu, Y., Zhou, P., Wang, X., Xiao, H., & Si, L. (2013). Tunable, multiwavelength Tm-doped fiber laser based on polarization rotation and four-wave-mixing effect. *Optics Express, 21*(22), 25977-25984.

Weiß, M., Huchard, M., Stöhr, A., Charbonnier, B., Fedderwitz, S., & Jäger, D. S. (2008). 60-GHz photonic millimeter-wave link for short-to medium-range wireless transmission up to 12.5 Gb/s. *Journal of lightwave technology, 26*(15), 2424-2429.

White, T., McPhedran, R., de Sterke, C. M., Botten, L., & Steel, M. (2001). Confinement losses in microstructured optical fibers. *Optics Letters, 26*(21), 1660-1662.

Wichmann, M., Shakfa, M. K., Zhang, F., Heinen, B., Scheller, M., Rahimi-Iman, A., Koch, M. (2013). Evolution of multi-mode operation in vertical-external-cavity surface-emitting lasers. *Optics Express, 21*(26), 31940-31950.

Wilke, I., & Sengupta, S. (2008). Nonlinear optical techniques for terahertz pulse generation and detection—optical rectification and electrooptic sampling. *Terahertz Spectroscopy: Principles and Applications, Optical Science and Engineering, 131*, 41.

Williams, R. J., Jovanovic, N., Marshall, G. D., & Withford, M. J. (2010). All-optical, actively Q-switched fiber laser. *Optics Express, 18*(8), 7714-7723.

Williams, R. M., Kelly, J. F., Hartman, J. S., Sharpe, S. W., Taubman, M. S., Hall, J. L., Baillargeon, J. N. (1999). Kilohertz linewidth from frequency-stabilized mid-infrared quantum cascade lasers. *Optics Letters, 24*(24), 1844-1846.

Xie, X., Xu, J., & Zhang, X.-C. (2006). Terahertz wave generation and detection from a CdTe crystal characterized by different excitation wavelengths. *Optics Letters, 31*(7), 978-980.

Xu, E.-M., Zhang, X.-L., Zhou, L.-N., Zhang, Y., & Huang, D.-X. (2009). Hybrid Active-Passive Microwave Photonic Filter with High Quality Factor. *Chinese Physics Letters, 26*(9), 094208.

Xu, J.-H. (2007). *Linewidth enhancement factor of a THz quantum cascade laser.* Paper presented at the 2007 Joint 32nd International Conference on Infrared and Millimeter Waves and the 15th International Conference on Terahertz Electronics.

Xu, J., Liu, J., Wu, S., Yang, Q.-H., & Wang, P. (2012). Graphene oxide mode-locked femtosecond erbium-doped fiber lasers. *Optics Express, 20*(14), 15474-15480.

Yamashita, S., & Hotate, K. (1996). Multiwavelength erbium-doped fibre laser using intracavity etalon and cooled by liquid nitrogen. *Electronics Letters, 32*(14), 1298-1299.

Yamashita, S., Inoue, Y., Maruyama, S., Murakami, Y., Yaguchi, H., Jablonski, M., & Set, S. (2004). Saturable absorbers incorporating carbon nanotubes directly synthesized onto substrates and fibers and their application to mode-locked fiber lasers. *Optics Letters, 29*(14), 1581-1583.

Yang, C. (2007). Carrier Dynamics of Quantum-Dot, Quantum-Dash, and Quantum-Well Semiconductor Optical Amplifiers Operating at 1.55$\ mu {\ hbox {m}} $. *IEEE Journal of quantum electronics, 43*(11), 982-991.

Yang, K., Richards, P., & Shen, Y. (1971). Generation of Far-Infrared Radiation by Picosecond Light Pulses in LiNbO3. *Applied Physics Letters, 19*(9), 320-323.

Yang, X. P., Gan, J. L., Xu, S. H., & Yang, Z. M. (2013). Temperature sensing based on a Brillouin fiber microwave generator. *Laser Physics, 23*(4), 045104.

Yao, Y., Chen, X., Dai, Y., & Xie, S. (2006). Dual-wavelength erbium-doped fiber laser with a simple linear cavity and its application in microwave generation. *Photonics Technology Letters, IEEE, 18*(1), 187-189.

Yeh, C.-H., Chow, C.-W., Shih, F.-Y., Wang, C.-H., Wu, Y.-F., & Chi, S. (2009). Tunable dual-wavelength fiber laser using optical-injection Fabry–Pérot laser. *Photonics Technology Letters, IEEE, 21*(3), 125-127.

Yeh, C.-H., Shih, F.-Y., Chen, C.-T., Lee, C.-N., & Chi, S. (2007). Stabilized dual-wavelength erbium-doped dual-ring fiber laser. *Optics Express, 15*(21), 13844-13848.

Yeh, C., Chow, C., Wu, Y., Shih, F., Wang, C., & Chi, S. (2009). Multiwavelength erbium-doped fiber ring laser employing Fabry–Perot etalon inside cavity operating in room temperature. *Optical Fiber Technology, 15*(4), 344-347.

Zayhowski, J., & Kelley, P. (1991). Optimization of Q-switched lasers. *Quantum Electronics, IEEE Journal of, 27*(9), 2220-2225.

Zhang, S., & Holzapfel, W. (2013). *Orthogonal Polarization in Lasers: Physical Phenomena and Engineering Applications*: John Wiley & Sons.

Zhang, X. C., Jin, Y., & Ma, X. (1992). Coherent measurement of THz optical rectification from electro-optic crystals. *Applied Physics Letters, 61*(23), 2764-2766.

Zhang, X. C., Ma, X., Jin, Y., Lu, T. M., Boden, E., Phelps, P., Yakymyshyn, C. (1992). Terahertz optical rectification from a nonlinear organic crystal. *Applied Physics Letters, 61*(26), 3080-3082.

Zhao, C., Zhang, H., Qi, X., Chen, Y., Wang, Z., Wen, S., & Tang, D. (2012). Ultra-short pulse generation by a topological insulator based saturable absorber. *Applied Physics Letters, 101*(21), 211106.

Zhao, C., Zou, Y., Chen, Y., Wang, Z., Lu, S., Zhang, H., Tang, D. (2012). Wavelength-tunable picosecond soliton fiber laser with topological insulator: Bi 2 Se 3 as a mode locker. *Optics Express, 20*(25), 27888-27895.

Zhao, D., Shu, X., Zhang, W., Lai, Y., Zhang, L., & Bennion, I. (2002). *Stable dual-wavelength oscillation of an erbium-doped fiber ring laser at room temperature.* Paper presented at the Photonics Asia 2002.

Zhao, X., Liu, Z.-B., Yan, W.-B., Wu, Y., Zhang, X.-L., Chen, Y., & Tian, J.-G. (2011). Ultrafast carrier dynamics and saturable absorption of solution-processable few-layered graphene oxide. *Applied Physics Letters, 98*(12), 121905-121905-121903.

Zhou, D.-P., Wei, L., Dong, B., & Liu, W.-K. (2010). Tunable passively-switched erbium-doped fiber laser with carbon nanotubes as a saturable absorber. *Photonics Technology Letters, IEEE, 22*(1), 9-11.

Zhou, J., Xia, L., Cheng, X., Dong, X., & Shum, P. (2008). Photonic generation of tunable microwave signals by beating a dual-wavelength single longitudinal mode fiber ring laser. *Applied Physics B, 91*(1), 99-103.

Zhou, P., Wang, X. L., Ma, Y. X., Han, K., & Liu, Z. J. (2011). Stable all-fiber dual-wavelength thulium-doped fiber laser and its coherent beam combination. *Laser Physics, 21*(1), 184-187. doi:Doi 10.1134/S1054660x10230192

Zilkie, A. J., Meier, J., Mojahedi, M., Poole, P. J., Barrios, P., Poitras, D., Malloy, K. J. (2007). Carrier dynamics of quantum-dot, quantum-dash, and quantum-well semiconductor optical amplifiers operating at 1.55 µm. *Quantum Electronics, IEEE Journal of, 43*(11), 982-991.

Zongjiu, Z., & Liu, Y. (2010). *Multiwavelength oscillations of Ytterbium-doped fiber laser.* Paper presented at the Signals Systems and Electronics (ISSSE), 2010 International Symposium on.